EFFECTS OF DIE DESIGN, MANUFACTURING AND PROCESS PARAMETERS ON CHEVRON AND SURFACE CRACKING OF COPPER WIRE DURING WIRE DRAWING

by

Floyd Banda
(MSc. in Manufacturing Engineering)

A thesis submitted in fulfilment of the requirements of the degree of Doctor of Philosophy in Production Engineering and Management.

The University of Zambia

Lusaka

2018

DECLARATION

I **Floyd Banda** do declare that this thesis is my own work, and that it has not been previously submitted for a degree or other qualification at this or another University.

Signature: ....

Date: 20-11-2018

Signature: ....
(Prof. L. Siaminwe - Principal Supervisor)

Date: 20-11-2018

COPYRIGHT

APPROVAL

This thesis of **Floyd Banda** has been approved as fulfilment of the requirements for the award of the degree of Doctor of Philosophy in Production Engineering and Management by the University of Zambia.

NAME	**SIGNATURE**	**DATE**
DR. J. PHIRI **Internal Examiner 1**		20/11/2018
Dr C.G. Chizyuka **Internal Examiner 2**		21-11-2018
S.S. VIRDY **External Examiner**		21/11/2018
Prof Mundia Muya **Board of Examiners Chairperson**		21.11.2018

ABSTRACT

The practice of copper wire drawing has faced problems regarding process, quality and manufacturing cost and satisfying world market demand of drawn wires. Of great importance to the practitioner are problems due to the interaction of process parameters during wire drawing.

The present research study on the “Effects of Die Design, Manufacturing and Process Parameters on Chevron and Surface Cracking of Copper Wire during Wire Drawing” is based on multi-pass copper wire drawing studies from the industry and the application of a scientific approach using the finite element method (FEM). A 2-dimensional axisymmetric model of multi-pass copper wire drawing was developed using ABAQUS 6.14 to model and simulate the major factors contributing to and influencing the development of both internal (chevron) and surface cracks during copper wire drawing, with an emphasis on die bearing length variation. Drawn wire scanning electron micrographs were used to validate the effects of bearing length variation during copper wire drawing.

Studies showed that a good selection and application of die geometrical and process parameters participating as an integral unit in copper wire drawing leads to the production of a defect-free copper wire. Models showed that, except the exit angle, all other die geometrical parameters influenced ductile damage.

Studies from the simulations and drawn wire micrographs showed that the Cockroft and Latham damage criterion was not met in all the multi-pass stages for the internal centerline nodes, whereas the criterion was met during the second and third multi-pass stages for the surface nodes. The models showed that internal centreline damage is minimised when using bearing length values between 30% and 40% while surface damage is lower when using bearing lengths of 30%.

DEDICATION

I humbly and sincerely thank my family, in particular my wife Namonje Nakapizye and the children Madalitso, Kondwelani and Pyelanji, and all the relatives and friends who gave me support during the research period. To my recently departed friend and colleague Eng. Coster Mwaba, thank you for all the help and support you rendered to me, and may the Lord grant you everlasting mercies.

Above all, I am grateful to the good Lord for according me good health and making everything possible during the course of my research work.

ACKNOWLEDGEMENTS

My heartfelt gratitude and thanks go to all members of staff of the Department of Mechanical Engineering in particular and the School of Engineering in general for their support, patience and encouragement offered to me during my research period. In particular, I express my gratitude and thanks to my supervisors Prof. L. Siaminwe and Dr. H.M.Mwenda for their unwavering professional guidance throughout the research and production of this thesis.

I would like to thank the Dean, Prof M. Muya and the Head of Mechanical Engineering Department, Mr G.M. Munakaampe for their assistance in ensuring that all the necessary requirements and logistics to carry out my research work were executed on time. This made my academic life easier.

I also thank the following for their insights and co-operation during my data collection from industry: Messiers Chad Hakamangwe, Hussein Hussein and Sundar Singh at Zalco Limited; Brigadier General Musonda, Mr P. Sinkala and Mr Mwenda at Mupepetwe Engineering and Contracting Company.

Many thanks go to my two sponsors, the Copperbelt University and the National Science and Technology Council for their financial support during my research activities. Thanks also go to Mr G. Mitchell and Mr H. Bowles at Finite Element Analysis Services (PTY) Limited, South Africa for the technical guidance in finite element and ABAQUS applications.

TABLE OF CONTENTS

LIST OF FIGURES

LIST OF TABLES

LIST OF APPENDICES

ABBREVIATIONS

AAS	-	Atomic Absorption Spectrophotometry
ASM	-	American Society of Metals
ASTM	-	American Society of Testing and Measurements
FEM	-	Finite Element Method
CAE	-	Computer Aided Engineering
CBN	-	Cubic Boron Nitride
DUCTCRT	-	Ductile Criterion
EDM	-	Electrical Discharge Machining
ETP	-	Electrolytic Tough Pitch
HSS	-	High Speed Steel
IACS	-	International Annealed Copper Standard
IEC	-	International Electrotechnical Commission
MECCO	-	Mupepetwe Engineering and Contracting Company
PCD	-	Polycrystalline Diamond
PEEQ	-	Equivalent Plastic Strain
P/M	-	Powder Metallurgy
SDEG	-	Stiffness Degradation
SEM	-	Scanning Electron Microscope
TRIAX	-	Stress Triaxiality
UNS	-	Unified Numbering System
UTM	-	Universal Tensile Machine
UTS	-	Ultimate Tensile Strength
WC	-	Tungsten Carbide
ZABS	-	Zambia Bureau of Standards
ZALCO	-	Zambia Aluminium and Copper Ores

DEFINITION OF TERMS AND CONCEPTS

Anisotropy	- characteristic of exhibiting different physical properties in different directions in a body of material.
Annealing	- a process of heat treatment allowing recrystallisation to take place with consequent softening of work hardened materials.
Chevron Cracking	- progressive damage caused by pores which link up along the wire centre-line. Terms such as "arrowhead cracks", "centerline burst", "cuppy core" and "crow's foot" are also used to mean the same.
Crack	- a line of fracture without complete separation and a form of volume defect.
Crystalline	- a state in which the constituent atoms or molecules of a substance are arranged in a regular, repetitive and symmetrical pattern.
Defect	- a discontinuity whose size, shape, orientation, or location makes it detrimental to the useful service of the part in which it occurs. Also called a "flaw".
Draw die	- a tool, usually containing a cavity that imparts shape to the wire being drawn.
Drawability	- the degree to which rod or wire can be reduced in cross section by drawing through successive draw dies of practical design.
Finite Element Method	- a numerical method seeking an approximated solution of the distribution of field variables in the problem domain that is difficult to obtain analytically.
Fractography	- descriptive treatment of fracture of materials, with specific reference to photographs of the fracture surface. Macrofractography involves photographs at low magnification (< 25x); microfractography,

photographs at high magnification (> 25x).

Homogeneous - state of a material being composed of the same or similar particles.

Inclusion - a physical and mechanical discontinuity occurring within a material or part, usually consisting of either a solid, encapsulated foreign material.

Isotropic - state of a material possessing the same properties in all directions.

Microstructure - the structure of an object, organism, or material as revealed by a microscope at magnifications greater than 25x.

Recrystallisation - the formation of a new, strainfree grain structure from that existing in coldworked metal, usually accomplished by heating.

Rod - wire raw material stock that is cast or rolled prior to drawing, with dimensions ranging from 3 mm to 10 mm in diameter.

Strain - the proportional deformation produced in a material under the influence of stress, and is a dimensionless number.

Strain (or work) hardening - an increase in hardness and strength of metals caused by plastic deformation at temperatures below the recrystallisation range, accompanied by a decrease in ductility and an increase in electrical resistivity of the material .

Strain rate - the time rate of straining for the usual tensile test, measured in reciprocal time.

Stress - the intensity of the internally distributed forces or components of forces that resist a change in the volume or shape of a material that is or has been subjected to external forces, expressed in force per unit area.

Wear	- damage to a solid surface, generally involving progressive loss of material, due to a relative motion between that surface and a contacting surface or substance.
Wire drawing	- a manufacturing process involving pulling wire or rod repeatedly through a die or dies with the sole purpose of decreasing the cross-sectional area.
Wire	- product from rod or other wire with dimensions from 0.01 mm to 3 mm.
Workability	- the degree to which a material may be plastically deformed prior to fracture.

(Source: John, 1992; Higgins, 1994; Hosford and Caddell, 1983; Liu and Quek, 2003; Wright, 2011):

CHAPTER 1: INTRODUCTION

1.1 Background

The production of copper and copper alloy semis has increased from less than nine million metric tonnes in the 1980's to over thirty million metric tonnes in 2015 (International Copper Study Group, 2016). Refined copper is consumed by semi fabricators or "first users" such as wire rod plants among others. Copper is the best metal conductor of electricity as it encounters much less resistance compared with other commonly used metals and is an essential component of energy efficient generators, motors, transformers, renewable energy production systems, power cables, domestic subscriber lines, wide and local area networks, mobile phones and personal computers. In addition, copper's exceptional strength, ductility and resistance to creeping and corrosion makes it the preferred and safest conductor for commercial and residential building wiring (International Copper Study Group, 2016).

Copper sets the standard to which other conductors are compared. Copper and copper-based products are manufactured using extrusion, drawing, rolling, forging, electrolysis or atomization, welding, to form wire, rod, tube, sheet, plate, strip, castings, powder and other shapes. Wire drawing is a cold working, net shape manufacturing process and produces long wires using dies with different profiles. In comparison to other processes mentioned, wire drawing produces good surface finish, uses low-to-moderate dies, equipment, and labour costs and requires low-to-moderate operator skills (Kalpakjian and Schmid, 2010). Cold drawn wire products equally have high strengths and very close tolerances.

In manufacturing using bulk deformation, more components are rolled and extruded than they are wire drawn. However, in comparison to rolling, wire drawing offers better dimensional control, lower capital equipment cost, and extension to small cross sections. In comparison to extrusion, wire drawing offers continuous processing, lower capital equipment costs, and extension to small sections (Wright, 2011).

Depending on the workpiece material condition, die material and its manufacturing accuracy, and wire drawing process variables, drawn products can develop several types of defects that can significantly affect their strength and product quality. Of particular interest is the presence of chevron cracks (or center bursting) and surface cracks in copper wire drawing which are prevalent and deteriorate the quality and functionality of the drawn copper wire (Chia and Patel, 1996). Center bursting in wire drawing is aligned along the wire axis, thereby reducing the wire tensile resistance and eventually leading either to process failure, disruption of production or delayed rupture later on, even in the absence of a load (Zompì and Levi, 2008). Chevron cracking has been encountered in conditions of small reductions, large die angles, and low frictions and after severe cold working of the billet (Ahmadi and Farzin, 2008).

Processing of copper into wire involves the technology of wire drawing. The wire drawing process reduces the cross section of the initial rod using dies into wires of different cross sections depending on the number of stages or passes of reduction (i.e number of dies). This is a crucial and value addition stage for wire production. The wire drawing processing of both ferrous and non-ferrous metals is beset with numerous challenges which include:

- development of metal forming fluids to improve lubrication in the die-workpiece interface (Canter, 2009; Kalpakjian and Schmid, 2010). This is due to lubricant breakdown under severe drawing conditions and the quest for affordable, easily available and biodegrable lubricants (Solomon, *et al*., 2010).
- development of solutions for variation in strain and residual stresses (Kalpakjian and Schmid, 2010). This is attributed to different semi angles and area reductions which are also affected by wear of the die.
- design and manufacturing accuracy of draw die geometry (Conoptica, 2007; Kalpakjian and Schmid, 2010). Draw die geometrical parameters have an effect on wire drawing forces (Kabayama, *et al*., 2009) and manifestation of cracks (Norasethasopon, 2003).
- inclusion reduction (Norasethasopon, 2003). Inclusions lead to wire breakage during processing.

The Finite Element Method (FEM) can be used to analyse the complex wire drawing process. This tool is equally useful in the prediction of occurrence of defects in the drawn wire. FEM would also supplement the lower capital costs for equipment installation and running, thus save the organizations involved in wire drawing practice from unprecedented costs at design and implementation stages. A simple simulator used in wire drawing is shown in Figure 1.1.

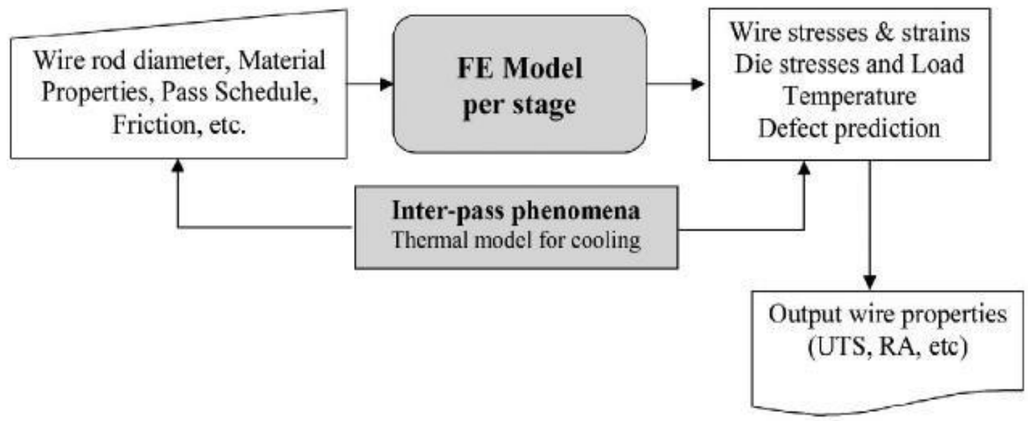

Figure 1.1: Schematic Diagram of a Wire Drawing Simulator.
(Source: Singh, *et al*., 2007)

Die design and manufacturing has an effect on wire drawing performance. Consistency and performance in wire drawing applications depend on two main characteristics of a diamond die blank: excellent sinter quality and a perfectly homogenic distribution of pore sizes within the polycrystalline diamond structure (Diamond Innovations, 2004). This provides the die manufacturer with the capability to generate a high quality polished surface in minimal cycle time and a consistent long die life. Realisation of accurate geometries on a die therefore becomes important for attaining longer die life during wire drawing (Ibid).

As the draw die is a major factor in wire drawing practice, the optimisation of die design parameters becomes important in sustaining die life (Ibid). The choice of die material and its influence on die life thus becomes equally an important characteristic during wire drawing practice. Relative costs for different die materials and sizes are shown in Figure 1.2.

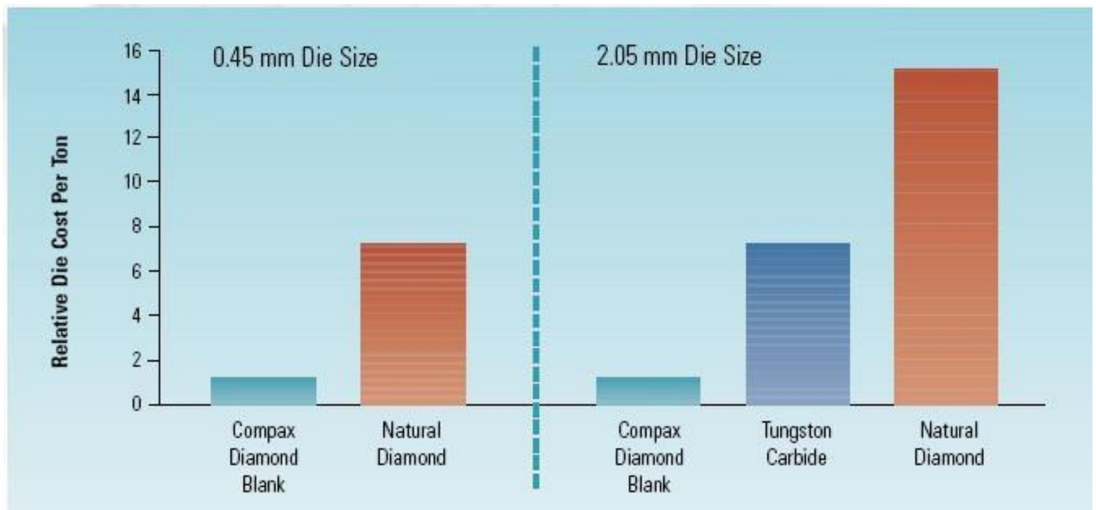

Figure 1.2: Comparative Die Costs (in US $) for Drawing Copper Wire. (Source: Diamond Innovations, 2004)

The end-users have preferred the use of natural diamond dies during drawing of fine and ultra-fine copper wire. Dies made from natural diamond have a higher wear resistance (Figure 1.3), though this comes at a greater cost as can be seen from Figure 1.2. Polycrystalline diamond (PCD), such as compax diamond, have a relatively shorter wear resistance to natural diamond but they are readily affordable. For a wire drawing practitioner, the obvious choice of using PCD or cemented carbides has been influenced mainly by cost, and this has brought the complex problems faced during wire drawing practice, mainly resulting in the occurrence of defects in the wire product.

This thesis establishes the causes of copper wire defects, namely chevron and surface cracking during wire drawing as a result of the interaction of the wire and the die. The research details the changes or additions to die design and manufacturing practices and wire drawing process conditions that result in the reduction of the mentioned wire defects.

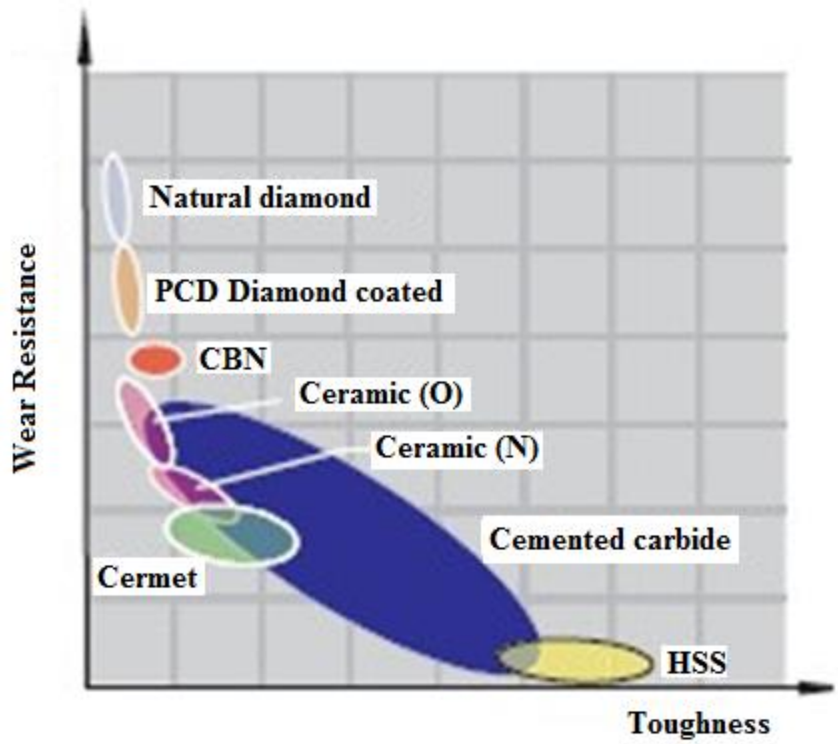

Figure 1.3: Wear and Toughness Ranges for Different Die Materials.
(Source: Ceratizit, www.ceratizit.com)

1.2 Statement of the Problem

Presently, most of the countries around the world have been challenged by the increasing demand for energy due to increased industrial activity while depleting resources. Conservation of this energy has been emphasized through employment of value-adding concepts. Efficient production of copper cables for such industries through wire drawing demands the usage of good raw copper with minimal adverse inclusions and its transformation with minimal defects. During copper wire drawing, defects due to chevron and surface cracking account for more than 13% of the total defects possible during production (Norasethasopon, 2003).

Most of the researchers have tried to address individual components of die geometry (mainly semi angle) parameters in conjunction with other variables (strain, stress, temperature and lubrication). However, the optimisation of both the die geometry parameters (with consistent manufacturing accuracy) and wire drawing process parameters in order to eliminate cracks (chevron and surface) is still outstanding.

Further, the combined effect of die geometrical parameters (semi angle, bearing land, blending radius and back-relief radius) and process parameters on elimination of cracks during wire drawing has not been addressed. Equally the impact of die design and manufacturing methods on die wear under different temperature and lubrication regimes and the combined effects on process and geometrical parameters during wire drawing leading to crack formation in wire drawing demands attention.

1.3 Objectives of the Investigation

1.3.1 General Objective

The general objective of the research was to develop a copper wire drawing model to reduce chevron and surface crack formations during the wire drawing process.

1.3.2 Specific Objectives

The specific objectives of the research were:

(i) To establish die design and manufacturing aspects influencing accuracy of die geometry

(ii) To determine the Δ-parameter values, die geometrical parameters and process conditions leading to the manifestation of surface and chevron cracks during wire drawing

(iii) To develop an integrated model for die geometry and process parameters for multi-pass copper wire drawing

(iv) To validate the developed models using industry-based copper wire drawing process setup

1.4 Delineation and Limitations

The current study examined defects arising from the copper wire's interaction with the die, and not as a result of other means. The use of more than two dies during modelling presented flow problems, hence all multi-pass stages were based on sequences using two dies. Equally, models of die and wire temperatures which had an impact on die wear and die life were not done. The effects of process and modifying conditions leading to wear and die life were not part of the modelling or industrial experiments.

Surface roughness aspects could not be investigated due to the dies being outsourced and lack of appropriate fixtures for copper wire clamping. Local manufacture of dies and their consequent maintenance through re-cutting and re-polishing were not possible due to lack of equipment and necessary instruments. Equally, wire defects due to wear of the die and other means were not part of this study.

1.5 Significance of Study

A major concern facing the wire industry is the extremely high quantity of surface defects that are generated during wire drawing by abrasive or delamination wear (Pops, 1997). High manufacturing costs associated with production of superfine wires has been attributed to the breakage of wires during processing (Norasethasopon and Yoshida, 2003). Wire drawing practice is faced with many challenges, notable of which is the elimination of defects in form of cracks in metallic products and the development and production of draw dies to accurate designs (Conoptica, 2007; Kalpakjian and Schmid, 2010).

This study is important in that global manufacturing companies involved in copper wire drawing are finding it difficult and costly to improve the quality of products and increase production levels significantly, hence failing to cope with the high global demand for copper wire products (Zompì and Levi, 2008; Norasethasopon and Yoshida, 2003). Copper-based manufacturing companies also need to adopt technologies and strategies to cope with the global demand for quality drawn copper wire.

Design of drawing dies and their manufacturing has an effect on the die quality. Improved die quality will reduce the amount of rejected dies, reduce wire production halts, and possibly help increase wire drawing speed (Conoptica, 2007).

Potential values obtainable from the study include:

- Potential of replicating improvement techniques to similar manufacturing industries involved in copper value addition
- Potential for improved productivity and competitiveness of companies
- Reduced defective copper wires used in domestic electrical wiring systems, with a potential to abate fires in homes and industries
- Potential for manufacturing companies continued growth and employment provision

1.6 General Structure of the Thesis

The thesis is divided into eight chapters and begins with the current chapter which is the **Introduction.** The Introduction highlights the rationale for undertaking the study, thereby laying a foundation for the thesis. The general and specific terms used in the thesis are explained, including the significance of the research study.

Chapter Two is the **Literature Review** in which the scope and structure of the study is reviewed. The chapter also details the general theory base and the theory for study focus. The identified gaps in the literature are also presented. Chapter Three presents the **Conceptual Framework** which highlights the interaction of research variables used during the study. The **Methodology** section is presented in Chapter Four in which the research design and methodology of data acquisition are undertaken. The chapter also outlines the limitations encountered, including the consideration of ethical issues.

Chapter Five is the **Modelling and Simulation** chapter which presents the theory and results of copper wire drawing modeling and simulation. The **Experimental Design and Procedures** section of the thesis are given in Chapter Six which presents experimental procedures, equipment and instrumentation used, and the results pertaining to experimental procedures.

Chapter Seven is the **Results Analysis and Discussion** section of the thesis and presents an analysis and discussions of the results from simulations and experimental procedures. Chapter Eight is the **Conclusions and Recommendations** section and gives a summary of the conclusions, contributions and recommendations for further research.

CHAPTER 2: LITERATURE REVIEW

2.1 Introduction

Wire drawing practice has been going on since the 1800's, though the practice has not seen much modernisation. The current wire drawing equipment being used globally is the exact replica of the ancient methods, with improvement being seen in draw die materials, lubrication methods and the powering of the equipment using modern power systems.

Major studies concerning wire drawing have focused on improved draw die materials, lubrication methods, optimization of drawing velocities, drawing forces and the draw die semi angle prediction. The finite element method (FEM) has been applied extensively in the study for prediction of optimized die design and process parameters. This chapter presents a review of theoretical and experimental studies undertaken by various scholars and researchers.

The chapter is divided into five sections. The first section presents the theory of wire drawing and gives details regarding die design and manufacturing, including materials and process parameters involved in the wire drawing process. The second section outlines the theory behind crack initiation and propagation mechanisms during wire drawing.

The third section looks at the application of FEM in wire drawing processes while the fourth section gives a literature review of the research so far undertaken in copper wire drawing. The last section discusses the research gaps concerning wire drawing research and presents the contributions this study makes to the body of knowledge.

2.2 Theory of Wire Drawing

2.2.1 Wire Drawing Process

The process of wire drawing involves reducing or changing the cross section of a long wire by pulling it through a draw die as shown in Figure 2.1. Wire products include electrical wiring, cables, springs, paper clips, spokes for bicycle wheels, and stringed instruments (Kalpakjian and Schmid, 2010).

The applied drawing force is used for homogeneous deformation, overcoming frictional forces and internal distortions. Frictional work per unit volume is consumed at the interface between the deforming metal and the tool faces that constrain the metal. Internal shearing causes distortion of plane sections as they pass through the deformation zone. As a consequence, the metal experiences a strain greater than that based upon the ideal shape changes; this causes the end product to be harder, stronger, and less ductile than it would be if the deformation were truly homogeneous (Hosford and Caddell, 1983).

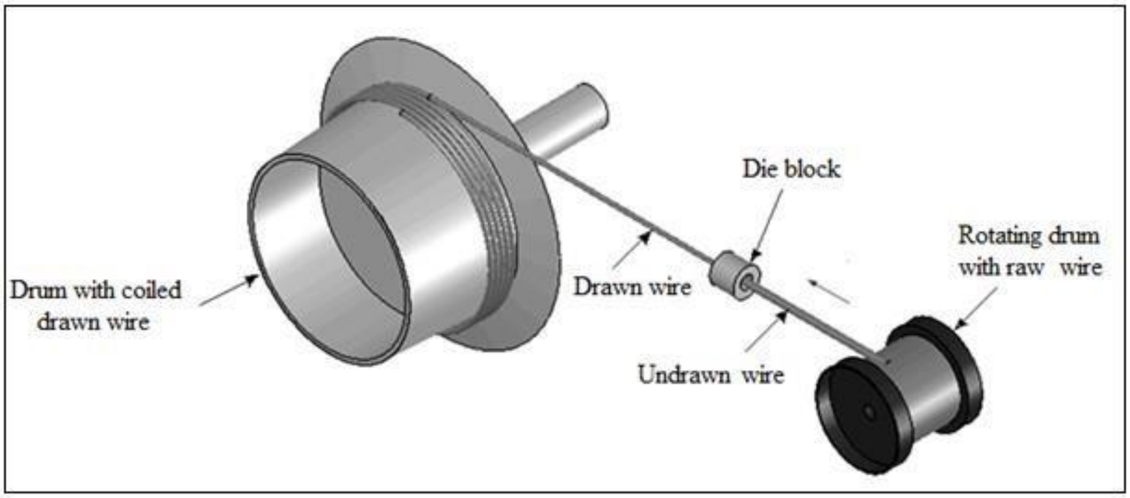

Figure 2.1: Scheme of Wire Drawing Process. (Source: Kabayama, *et al*., 2009)

In conventional wire drawing, the raw wire material is first cleaned of scale and dust by mechanical or chemical treatment and coated with a suitable lubricant. The material is then swaged at the end in order to allow for entry into the die, clamped and then pulled. The machinery type used in wire drawing practice depends on the diameter of the drawn wire. A single block unit called a *draw bench* (Figure 2.2) is used for rods and tubes which cannot be coiled.

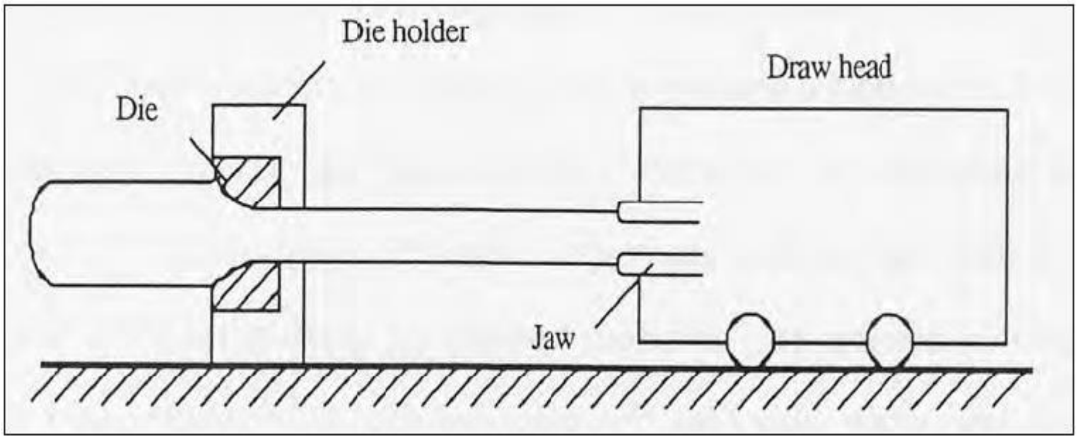

Figure 2.2: Schematic of a Draw Bench. (Source: Dieter, 1988)

The draw head is moved either by a chain drive or a hydraulic mechanism, with draw speeds varying from 0.15 m/s to 1.5 m/s. Coarser wire with a final diameter greater than 6 mm is drawn with a single block called a *bull block* (Dieter, 1988).

Due to limitations in reduction ratios by the use of one die, a series of combined draw benches and bull-blocks are used in practice to carry out wire drawing of large deformations. Figure 2.3 shows the arrangement of a multistage wire drawing machine typically used for making copper wire for electrical wiring. The arrangement consists of capstans (drums) which pull the wire at different speeds after the wire has undergone a required section reduction through the die. The arrangement has a drum-speed control lever that sets different speeds in order to effectively provide the necessary tension in the wire.

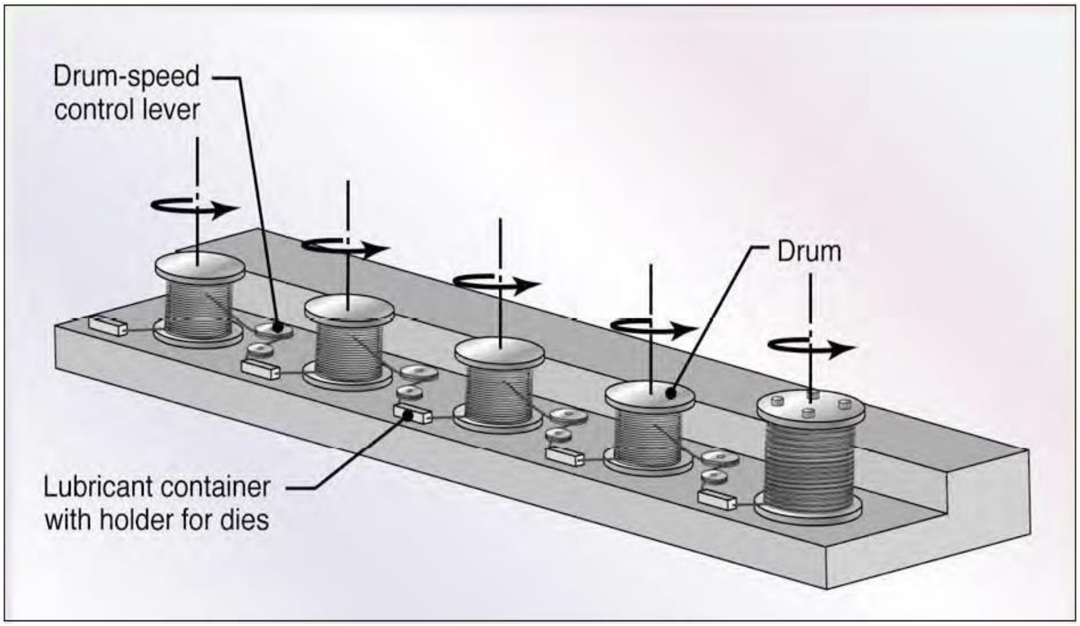

Figure 2.3: Multistage Wire Drawing Machine. (Source: Kalpakjian and Schmid, 2006)

2.2.2 Copper Wire Material Properties

Pure copper refers to copper of purity equal to or exceeding those of electrolytic copper (99.90 Cu % min) up to 99.999 + % Cu, with a total impurity content of less than 10 ppm (Davis, 2001). Such a copper has a standard electrical conductivity fixed by the International Electrotechnical Commission (IEC) as being that of an annealed copper wire 1 m long, weighing 1 g with a density of 8.89 g/cm^3 and exhibiting a resistance of 0.15328 Ω. This value is assigned a volume conductivity of 100% of the International Annealed Copper Standard, written 100% IACS. The highest measured room temperature (20^{o}C) volume conductivity for very pure copper is about 103.6% IACS.

Practical attainable conductivity values for electrolytic tough pitch (ETP) and de-oxidised low residual phosphorous coppers stand at about 101% IACS. Oxygen-free (OF) copper is certified under ASTM B 170 to meet this as a minimum value (Ibid).

The mechanical properties of interest for pure copper are shown in **Appendix 1**. The purity of copper is influenced by processing methods, hence the copper material to be used in this write-up refers to wrought copper and copper alloys as given in **Appendix 2**.

Copper alloys are identified by the Unified Numbering System (UNS) which categorizes families of alloys based upon their elemental make-up. Wrought products range from UNS C10000 through UNS C79999; cast products are assigned numbers between UNS C80000 and UNS C99999 (Copper Development Association, www.copper,org).

2.2.3 Die Materials, Design and Manufacturing

(a) Die Materials

Table 2.1 shows the recommended materials for various wire drawing dies (ASM International, 1988). The wire drawing die is a precision tool which produces round or shaped wire to very tight tolerances. Deformation and elongation of wire material takes place within the profile of the drawing die. A set of dies is required during profile drawing, which involves various stages of deformation to produce the final profile.

As it can be seen from Table 2.1, wire drawing die materials typically are tool steels and carbides. Tungsten Carbide dies are used for drawing hard wires, while diamond dies are the choice for fine wires. For hot drawing, cast-steel dies are used because of their high resistance to wear at elevated temperatures (Ibid).

(b) Elements of Die Design

Proper die design and the proper selection of reduction sequence per pass are necessary for ensuring proper material flow in the die, reducing internal or external defects, and improving surface quality (Conoptica, 2007). The most important elements of die design are shown in Figure 2.4 and include the Bell or Die Entry Geometry, Blending and Entering Angle, Approach or Reduction Angle, Bearing Length or Land and Back Relief.

Table 2.1: Recommended Materials for Wire Drawing Dies.

Drawn Metal	**Wire Size** (mm)	**Recommended Die Material**	
		Round Wire	Special Shapes
Carbon and Alloy steels	< .57	Diamond, natural or synthetic	CPM 10V*, M2**, or cemented tungsten carbide
	> .57	Cemented tungsten carbide	
Stainless steel, titanium,tungsten, molybdenum and nickel alloys	< .57	Diamond, natural or synthetic	CPM 10V, M2, or cemented tungsten carbide
	>1.57	Cemented tungsten carbide	
Copper	< .06	Diamond, natural or synthetic	CPM 10V, D2***, or cemented tungsten carbide
	> .06	Cemented tungsten carbide	
Copper alloys and aluminium alloys	< 2.5	Diamond, natural or synthetic	CPM 10V, D2***, or cemented tungsten carbide
	> 2.5	Cemented tungsten carbide	
Magnesium alloys	< .06	Diamond, natural or synthetic	. . . .
	> .06	Cemented tungsten carbide	

*Proprietary tool steel; **Tool steel; ***Tool steel (Source: ASM International, 1988)

(i) Bell

The Bell causes hydrostatic pressure to increase (Udomphol, 2007) and should be sufficiently open to allow lubricant enter the die and flush out any particles that are generated (Esteves Group, 2008). Wright (2011) indicates that a rapidly sloping, highly flared bell minimizes wire abrasion at the die entry in the event of die misalignment. A lengthy, slowly tapering bell leads to a lubricant pressure build-up and foster hydrodynamic lubrication, similar to the effect of small approach angles.

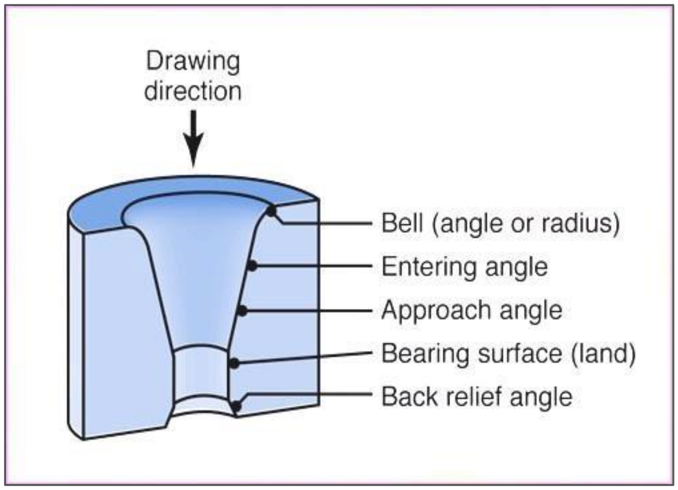

Figure 2.4: Profile of a Drawing Die. (Source: Kalpakjian and Schmid, 2010)

(ii) Blending and Entering Angle

According to Wright (2011) the creation of an appropriate blend or radius at the transition from the approach angle to the bearing length is a critical feature of die design. The entrance should be sufficiently open to allow wire drawing lubricant enter the die and flush out any particles that are generated. It should also be well blended to the top of the reduction angle so that there is no sharp edge at the transition. The standard entrance angle for a drawing die is 60 degrees (Esteves Group, 2008).

(iii) Approach (Reduction) Angle

This is where the actual reduction in wire diameter occurs, and is given as the half die angle, α (Udomphol, 2007).The Approach section is designed such that it allows for a smooth and controlled deformation of the wire. Harder materials are drawn with narrower reduction angles, while softer materials are drawn with wider reduction angles (Esteves Group, 2008).

(iv) Bearing Length or Land

This produces a frictional drag on the wire and also removes surface damage due to die wear, without changing dimensions (Udomphol, 2007). Thus, the bearing land determines the quality of wire surface and the wire diameter. The length of the bearing region is a percentage of the nominal wire diameter at about 20 to 50%, though this varies depending on the material, process used and specifications of the wire to be drawn (Esteves Group, 2008). Wright (2011) indicates that the bearing length may vary from zero to as much as 200% of the wire diameter, though the objection to a large bearing length is the addition to frictional work, and consequently drawing stresses.

(v) Back Relief

This allows the metal to expand slightly as the wire leaves the die, allowing for gradual release of elastic energy and also minimising abrasion if the drawing stops or the die is out of alignment (Udomphol, 2007; Wright, 2011). Wright (2011) argues that the back relief should be specified with a radius and not an angle in order for it to perform its functions better, though this complicates die manufacture.

Table 2.2 shows the various wire materials and the different die geometries used for their processing. The data shown are standard specifications for typical wire drawing applications and apply equally to single crystal natural or single crystal synthetic diamond dies (Fort Wayne Wire Die Inc., 1996).

Table 2.2: Typical Die Specifications for Various Wire Materials.

Wire Material	**Degree of Blending**	**Reduction Angle (2α)**	**Bearing Length**
Bare Copper	Well blended	18° ± 2°	40% ± 10%
Tin or Silver Plated Copper	Very well blended	20° ± 2°	20% ± 10%
Aluminium	Well blended	20° ± 2°	25% ± 10%
Stainless Steel	Slightly blended	14° ± 2°	50% ± 10%
Brass or Copper Covered Steel	Slightly Blended	12° ± 2°	35% ± 10%

(Source: Fort Wayne Wire Die Inc., 1996)

In addition to die geometry, the die life depends on its size. Die life is lost by sizing dies above the minimum allowable diameter. Sizing practice is recommended for improving die life (Wright, 2011).

(c) Die Manufacturing

Manufacturing of tool steel and carbide die blanks is done using the powder-metallurgy (P/M) techniques. Using this process, a metal powder is compacted into the desired and often complex shape and sintered (heated without melting) to form a solid piece (Kalpakjian and Schmid, 2010).

The P/M technology started from the early 1920's with the production of tungsten carbides and the mass production of bronze bushes for bearings. P/M is a rapid, economical and high volume production method for making precision components from powders. P/M is the choice when requirements for strength, wear resistance or high operating temperatures exceed the capabilities of die casting alloys and offers greater precision than castings (Upadhyaya, 2002). It avoids casting defects such as blow holes, shrinkage and inclusions. Figure 2.5 shows the general flow sheet of P/M processing (Ibid).

The blanks are drilled using electrolytic drilling machines, lasers, wire EDM machines and electrical discharge machining centers, creating the basic hole size and shape for each die. The holes, as well as the bearing length, ovality and reduction angle are then verified using software and optical measurement devices (Fort Wayne Wire Die Inc., 2009).

After drilling, wire and ultrasonic polishing systems are used to create and fine tune each die's precise bearing length and reduction angle. When manufacturing a matched die set, physical tests are conducted to verify the elongation rate of the exiting wire at each die in the sequence (Ibid).

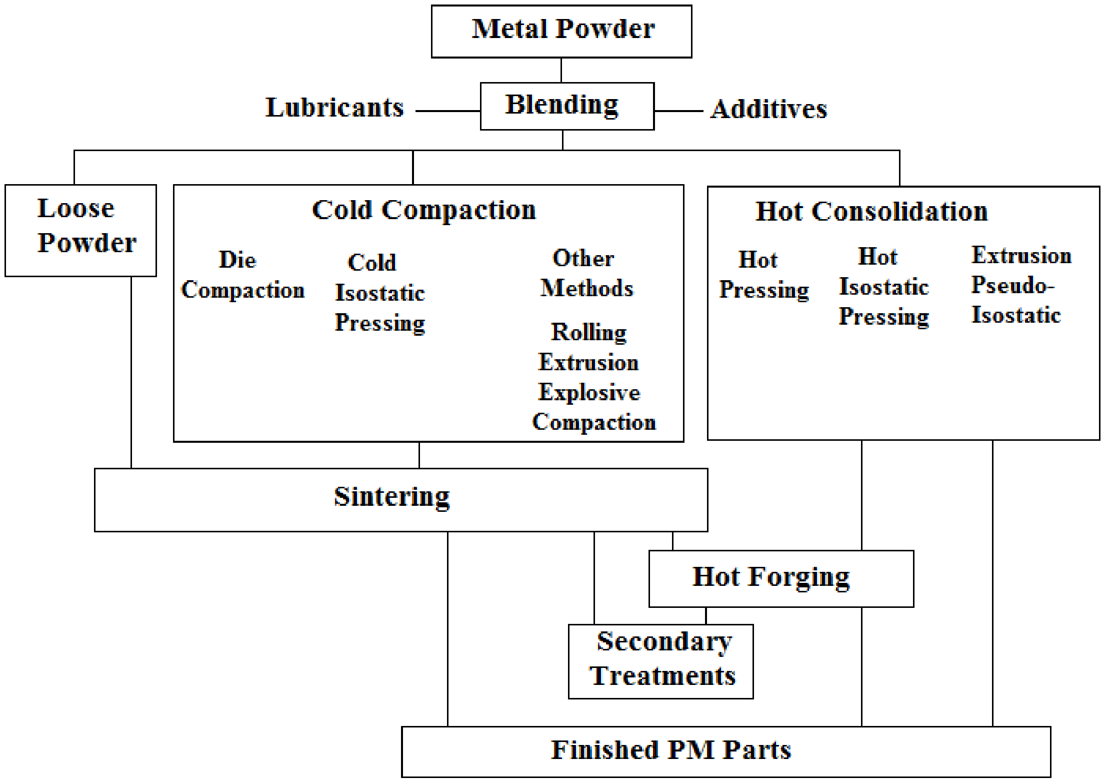

Figure 2.5: Flow Sheet for Powder Metallurgy Processing. (Source: Upadhyaya, 2002)

(d) Selection of Die Materials and Powder Preparation

Material for the tungsten carbide nib was chosen as YG6X grade, conforming to 94WC-6Co which was based on the recommendations of the ASM (1990). The tungsten carbide and cobalt mixture is mixed with jet fuel and rubber mix and kept for more than 24 days for the rubber to melt uniformly. The mixture is then put in an oven for 24 hours under a temperature of 90^{o}C to allow for uniformity of composition and formation of dried granules. The obtained granules are then ground and sieved. The collected powder is then put in a specially designed mould and compacted to a pressure of about 110 kPa in a compacting machine as shown in Figure 2.6. The machine has a capacity of 100 tonnes.

Figure 2.6: Compacting Machine. (Source: Author)

The obtained compact or 'green' material is then sintered in a vacuum furnace as shown in Figure 2.7. The sintering is done in two events: the first day, the compact is sintered at 120 volts and the second day, a voltage of 300 is used. After compaction, a shrinkage allowance of 24% is used.

The obtained carbide nib material has a hardness of 92 HRA and a density of about 15.1 g/cm^3. All sharp edges of the nib need to be filleted in order to avoid stress build-up during wire drawing. This is done by polishing using gauges with boron and diamond particles.


Figure 2.7: Vacuum Furnace. (Source: Author)

(e) Die Assembly

The tungsten carbide nibs obtained from the powder metallurgy process are assembled with the steel shells obtained from cold-rolling. Ensuring that sharp edges have been removed from both the nib and the shell, the shell is sprinkled with borax powder to enhance a 'brazing effect' during assembly. The assembly of the tungsten carbide nib and the steel shell is done using a shrink fit. A shrink fit of dimension H7/s6 as per the recommendations of Shearer (2008) was thus proposed.

2.2.4 Analysis of the Wire Drawing Process

A number of theoretical methods are used to analyse forming processes such as wire drawing. The major concern being the prediction of externally applied loads needed to cause flow of metal and deformation to the desired shape.

1. The Uniform Energy Method

Also called the *ideal work* method, this method considers ideal frictionless homogeneous deformation of the workpiece. It is the simplest and is based on setting up an energy balance, where the energy used in the forming operation is calculated, neglecting effects of friction and inhomogeneous deformation. Considering a rod being reduced from an initial cross section A_i to a wire of final cross section A_f , the deformation energy, W, required to transform this rod into a wire can be computed according to equation (2.1) as follows (Valberg, 2010):

$$\boldsymbol{W = VU = V \int_{\varepsilon_i}^{\varepsilon_f} \bar{\sigma} \; d\bar{\varepsilon} = V\bar{\sigma} \int_{\varepsilon_i}^{\varepsilon_f} d\bar{\varepsilon} = V\bar{\varepsilon}\ (\varepsilon_f - \varepsilon_i)} \qquad \textbf{(2.1)}$$

where *V* is the volume of material

U is the energy dissipation or applied energy per unit volume of material

$\bar{\sigma}$ is the effective stress

$\bar{\varepsilon}$ is the effective strain

The force needed for homogeneous deformation, F_{dh}, can be derived from equation (2.1) and computed as given in equations (2.2) and (2.3) as follows (Ibid):

$$V\bar{\sigma}\left(\varepsilon_f - \varepsilon_i\right) = A_i\, l\bar{\sigma}\bar{\varepsilon} = A_i l\bar{\sigma}\ln\left(\frac{A_i}{A_f}\right) = F_{dh}l \qquad \textbf{(2.2)}$$

Hence,

$$F_{dh} = A_i\bar{\sigma}\ln\left(\frac{A_i}{A_f}\right) \qquad \textbf{(2.3)}$$

2. The Slab Method

This method is based on setting up a force balance for a small slab element inside the deformation zone of the workpiece. The equations thus obtained are developed further, until an expression for the stress distribution inside the workpiece is obtained (Valberg, 2010). The method was developed by George Sachs with the following assumptions:

constant friction, no redundant work and non-work hardening material to obtain expression given in equation (2.4) based on Tresca yield criterion (Huo, 1997):

$$\sigma_d = Y_{avg}\left\{\frac{1+B}{B}\left[1 - \left(\frac{d_f}{d_i}\right)^{2B}\right]\right\} \quad \textbf{(2.4)}$$

where σ_d is the drawing stress

Y_{avg} is the average yield stress of the material

d_f ,d_i are the final and initial wire diameters

$B = \mu cot\alpha B$, where μ is the coefficient of friction and

α is the die semi angle

Sachs theory was modified by Davis and Dokos to take into account strain hardening by making the yield stress a function of the instantaneous area of the drawn wire within the die, leading to equation (2.5) as follows (Huo, 1997):

$$\sigma_d = Y_i\left(\frac{1+B}{B}\right)\left\{\left[1 - \left(\frac{d_f}{d_i}\right)^{2B}\right]\left[\left(1 - \frac{\sigma'}{Y_i B}\right) + \frac{\sigma'}{Y_i}\ln\left(\frac{d_f}{d_i}\right)^2\right]\right\} \quad \textbf{(2.5)}$$

where, Y_i is the initial yield stress of the material

σ' is a constant having the dimensions of stress

In making further assumptions that the total redundant work done per unit volume is equal to $2/3\alpha Y_{avg}$, Siebel considered the equilibrium of total horizontal forces acting on the whole contact area between wire and die and modified equation (2.5) into equation (2.6) as follows (Ibid):

$$\sigma_d = Y_{avg}\left[\left(1 + \frac{\mu}{\alpha}\right)\ln\left(\frac{A_i}{A_f}\right) + \frac{2}{3}\,\alpha\right] \quad \textbf{(2.6)}$$

Yang derived a theoretical expression of drawing stress to include the effect of die land which were neglected by Sachs and Siebel to arrive at equation (2.7) with the following form (Huo, 1997):

$$\boldsymbol{\sigma_d = \left\{Y_i \left(\frac{C}{1-C}\right)\left[\left(\frac{A_i}{A_f}\right)^{1-C} - 1\right] - Y_i\right\} e^{\frac{-4\mu L}{D_f}} + Y_i} \tag{2.7}$$

where L is the length of the land of the die

C is a constant, determined by die geometry and friction, $C = \frac{1+\mu cot\alpha}{1-\mu cot\alpha}$

Valberg (2010) gives the required drawing force by considering an infinitesimal slab element of radius r and integrating the contact pressure over the end face of a cylinder, and arrived at equation (2.8), thus:

$$F_{dr} = \int_0^R p2\pi r\ dr = \int_0^R \left(\bar{\sigma} + \frac{2\tau}{h}(R-r)\right) 2\pi r\ dr$$
$$= 2\pi \left[\frac{1}{2}\bar{\sigma}R^2 + \frac{2\tau}{h}\left(\frac{1}{2}R^2 - \frac{R^3}{3}\right)\right] = \pi\bar{\sigma}R^2\left(1 + \frac{2mR}{3\sqrt{3}\,h}\right) \tag{2.8}$$

where p is the pressure over the end face of the specimen

R is the radius of the cylinder

h is the thickness of the slab element

m is the friction factor from the Tresca friction model, where $0 < m < 1$.

τ is the shear stress

3. The Upper Bound Method

This method is based on the computation of the energy consumption in the process, obtained from the flow field in the actual forming process. When the energy is known, forming parameters like load and die pressure can be determined from it. If different velocity fields are investigated, the best field is the one that provides the lowest energy consumption (Valberg, 2010). Using the upper bound method, estimates of the forming load and the pressure that are either larger or equal to the real load and pressure are obtained. Equation (2.9) is commonly used to calculate the power consumption in metal forming processes (Ibid):

$$\dot{W}_T = Fv_s = \dot{W}_D + \dot{W}_S + \dot{W}_F =$$
$$\int_v \bar{\sigma}\,\dot{\bar{\varepsilon}}\,dV + \int_A k\,|\Delta v|\,dA + \int_A \tau_i\,v_i dA \tag{2.9}$$

where $\dot{W}_D$ is the power required to deform the workpiece homogeneously

$\dot{W}_s$ is the power required to shear-deform the workpiece

$\dot{W}_F$ is the power consumed due to frictional sliding in the die-workpiece interface

k is the shear flow stress of the material

τ_i is the shear stress transferred from workpiece to die surface

v_i is the sliding velocity of the workpiece material against the die

Shear deformation occurs if some or all of the workpiece material flows through a velocity discontinuity during the course of forming (Valberg, 2010). With $\dot{W}_S$ being equal to zero in axisymmetric drawing, equation (2.9) is transformed into equation (2.10) according to Valberg (2010):

$$\boldsymbol{\dot{W}_T = Fv_i = \dot{W}_D + \dot{W}_F = \int_v \bar{\sigma}\,\dot{\bar{\varepsilon}}\,dV + \int_A \tau_i v_i\,dA = \pi R^2 \bar{\sigma} v_i + \frac{2\pi m}{3}\frac{\bar{\sigma}}{\sqrt{3}}\frac{v_i R^3}{h}} \qquad \textbf{(2.10)}$$

The drawing force is, thus, given according to equation (2.11) as follows:

$$F_{dr} = \frac{\dot{W}_T}{v_s} = \pi R^2 \bar{\sigma}\left(1 + \frac{2mR}{3\sqrt{3}h}\right) \qquad \textbf{(2.11)}$$

4. The Slip Line Field Theory

The analysis using the slip line field theory is based upon a deformation field that is geometrically consistent with the shape change, with stresses within the field being statically admissible. The slip lines are the planes of maximum shear stress which are oriented at 45° to the principal planes (Hosford and Cadell, 1983).The method can be used to solve axisymmetric forming processes such as wire drawing. Due to its laboriousness in application and the various assumptions made such as the material being rigid-perfectly plastic, deformation being by plane strain only, nonconsideration of temperature, strain rate and time effects and consideration of either frictionless or sticking friction, the method is not very popular according to Huo (1997).

Hosford and Cadell (1983) however indicate that slip-line fields can be applied to problems with interface conditions intermediate between frictionless and sticking friction conditions as long as the shear stress, τ, at the interface between die and workpiece is a constant fraction, *m*, of the yield stress in shear, *k*, and given according to equation (2.12), thus:

$$\boldsymbol{\tau = mk} \tag{2.12}$$

where m is the friction factor, 0 <*m*< 1.

5. Finite Element Method

Developments due to cheap and efficient computer technology and the implementation of the Finite Element Method (FEM) into user-friendly, window-based programmes, has revolutionised the art of metal forming (Valberg, 2010). The FEM is a numerical method which seeks an approximated solution of the distribution of field variables in the problem domain into several elements. Known physical laws are then applied to each small element with a simple geometry.

In FEM, a continuous function of an unknown field variable is approximated using piecewise linear functions in each sub-domain, called an element formed by nodes (Liu and Quek, 2003). The unknowns are then the discrete values of the field variable at the nodes. With proper principles being followed to establish equations for the elements which are tied to one another, the process leads to a set of linear algebraic simultaneous equations for the entire system that can be solved easily to yield the required field variable. Common physical problems solved using the standard FEM include: mechanics of solids and structures, heat transfer, acoustics, fluid mechanics and others (Ibid).

Analyses of metal forming processes using FEM can be divided into three types according to the basic assumptions about the behaviour of the material under consideration. These types include: *elastic-plastic, rigid-plastic* and *visco-plastic* (Dixit and Dixit, 2008). With reference to Figure 2.8, showing a stress-strain relationship, a material is *elastic-plastic* when it exhibits both an elastic (OY portion) and plastic (YF portion) behaviour. A material which exhibits only plastic behaviour (YF portion) is termed *rigid-plastic*. When a tensile test is conducted at higher rate of loading and it is observed that beyond the initial yielding, the stress required to cause further material flow increases with the strain rate or the rate of deformation, then *viscoplasticity* occurs in such a material. This increase in the stress is due to the *viscous* resistance of the material to further yielding. When the portion YF is straight and parallel to the strain axis, the behaviour of a material is termed as being *ideal* or *perfectly plastic* (Ibid).

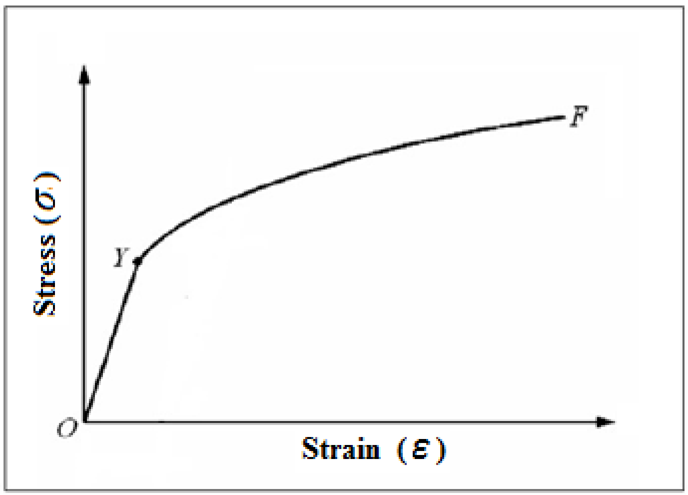

Figure 2.8: Variation of Stress with Strain. (Source: Dixit and Dixit, 2008)

2.2.5 Process Parameters in Wire Drawing

Successful wire drawing requires careful selection of process parameters. Intermediate annealing between passes in multi-pass wire drawing may be necessary to maintain sufficient ductility of the material during cold drawing (Kalpakjian and Schmid, 2010). The wire drawing process is a complex interaction of many parameters which include the following (Kabayama, *et al*., 2009):

- wire properties (yield stress, elastic modulus, strain rate, strain hardening);
- lubricant (friction coefficient, viscosity, surface treatment);

- die geometry (reduction angle, bearing region length, reduction area, and material).

(a) Deformation Zone and the Δ-parameter

The shape of the deformation zone exerts a strong influence upon the redundant work, frictional work, and the total drawing forces (Wright, 2011). It also has important effects on the properties and structure of wire material after drawing; these include homogeneity of hardness, internal porosity, tendency to open cracks during processing, and residual stresses.

The **area reduction, *r***, is a measure of the total deformation in metal forming and is given by the equation (2.13) as follows (Ibid):

$$\boldsymbol{r = \frac{A_i - A_f}{A_i} = 1 - \left(\frac{A_f}{A_i}\right)} \qquad \textbf{(2.13)}$$

The deformation zone geometry can be characterized by the **Δ-parameter**. The **shape of the deformation zone** depends on *r* and the approach angle, *α*, and is fundamental to drawing analysis. Wright (2011) gives an approximate numerical value for the Δ–parameter using equation (2.14):

$$\Delta \approx \left(\frac{\alpha}{r}\right)\left[1 + (1-r)^{\frac{1}{2}}\right]^2 \approx 4\,\frac{tan\alpha}{\ln\left[\frac{1}{(1-r)}\right]} \qquad \textbf{(2.14)}$$

Wright (2011) indicates that analyses of wire drawing makes it clear that the shape of the actual deformation zone is more complicated than a simple trapezoid which is normally used as the basis for process design and practical analysis. It is the aim of this review to delve into the reasons for this complication and show how the participating components within the deformation contributes to crack formation.

Low Δ values (small semi-angle or higher reduction in area) indicate larger friction effects and surface heating due to longer wire contact in the approach zone (Ibid). Higher values of Δ (large semi angle or lower reduction in area) are indicative of increased levels of redundant deformation and surface hardening due to excessive direction change during flow through the die. Large Δ often results in a greater tendency toward void formation and center bursting. Representative values of Δ for a range of die semi-angles and reductions are given in **Appendix 3**. Δ values of 1.50 perform well in many commercial drawing operations while delta factors in excess of 3.0 should be avoided in general (Descargas, nd).

(b) Process Variables during Wire Drawing

The major process variables in wire drawing include the die angle, reduction in cross-sectional area per pass, friction along the die-workpiece interface, thermal effects, drawing speed and drawing force. The die angle influences the drawing force and the quality of the drawn product (Kalpakjian and Schmid, 2010).

Some of the process variables during wire drawing are shown in Figure 2.9. In wire drawing, reductions in the cross-sectional area per pass range up to about 45%. The smaller the initial cross section, the smaller the reduction per pass. Reductions higher than 45% may result in lubricant breakdown, leading to surface finish deterioration (Ibid).

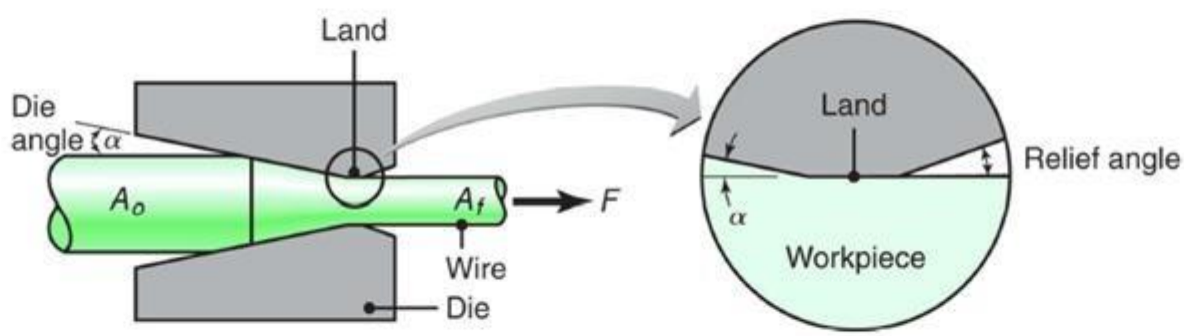

Figure 2.9: Process Variables in Wire Drawing. Source: (Kalpakjian and Schmid, 2010)

(1) Drawing Force

The drawing force can be determined under different analytical approaches using equations (2.3), (2.8) and (2.11). Kalpakjian and Schmid (2010) give generalized equations of the drawing force, F, under ideal and frictionless conditions and under friction and redundant conditions as given by equations (2.15) and (2.16), respectively:

$$F = Y_{avg} A_f \ln\left(\frac{A_o}{A_f}\right) \qquad \textbf{(2.15)}$$

$$F = Y_{avg} A_f \left[\left(1 + \frac{\mu}{\alpha}\right)\ln\left(\frac{A_o}{A_f}\right) + \frac{2}{3}\alpha\right] \qquad \textbf{(2.16)}$$

where Y_{avg} is the average true stress of the material in the die gap

A_o, A_f are the initial and final cross-sectional areas respectively

μ is the coefficient of friction

α is the die semi angle in radians.

(2) Drawing Speed

Drawing speed has an effect on power, strain rate, drawing temperature and lubrication. Drawing speeds depend on the material and on the reduction in cross-sectional area, ranging between 1 to 2.5 m/s for heavy sections to as much as 50 m/s for very fine wires (Kalpakjian and Schmid, 2010).

In the case of bench drawing, the drawing velocity *v* is the same as the pulling speed. For block drawing or multiple die drawing, Wright (2011) expresses *v* according to equation (2.17):

$$v = \pi D w \qquad \textbf{(2.17)}$$

where D is the drawing block diameter

w is the drawing block speed in revolutions per unit time

(3) Friction

The friction coefficient, hence lubrication, affects the drawing speed (Kabayama, *et al*., 2009) which in turn has an effect on wire quality (Byon, *et al*., 2011). Valberg (2010) states that the friction phenomenon is of great importance in metal forming due to the following reasons: forming loads and stresses transferred to the dies depend on friction; the surface quality of the formed workpiece depends on the lubricant used; and wear of the dies can be reduced with appropriate lubrication.

Three notable friction models can be used to describe the friction phenomenon. These include the *Coulomb friction model*, the *Tresca friction model* and the *Wanheim and Bay's friction model* (Valberg, 2010).

(i) Coulomb Friction Model

This model is most appropriate in cases of low contact pressure and describes friction between bodies in sliding contact. The model applies if the mean normal stress component is less than, or approximately equal to, the flow stress of the workpiece material (Valberg, 2010). Such low pressures can exist in rolling, wire drawing and sheet metal forming. The *Coulomb friction coefficient* is given by equation (2.18) and determined as the ratio between the friction force, F, and the normal force on a workpiece, F_N, (Ibid):

$$\mu = \frac{F}{F_N} = \frac{\tau_i A}{pA} = \frac{\tau_i}{p} = \left|\frac{\tau_i}{-\sigma_n}\right| = \frac{\tau_i}{\sigma_n} \qquad \textbf{(2.18)}$$

where τ_i is the friction shear stress, $\tau_i = F/A$

A is the area of contact between the two bodies

p is the mean pressure transferred through the boundary interface

σ_n is the average normal stress component between the workpiece and the surface in contact.

(ii) Tresca Friction Model

This model is applied when the contact pressure is higher than the flow stress of the workpiece material as is experienced in closed die forging and extrusion (Valberg, 2010). The Tresca friction model is derived from equation (2.12) and expressed according to equation (2.19) as follows (Hosford and Caddell, 1983):

$$\boldsymbol{m = \frac{\tau}{k}} \qquad \textbf{(2.19)}$$

(iii) Wanheim and Bay's Friction Model

Wanheim and Bay put forward a general model for expressing friction at the tool-workpiece interface (Valberg, 2010). The model predicts a rounded transition between the Coulomb friction regime and that of Tresca. Lin, *et al*., (2003) states that the aim of the Wanheim and Bay's friction model is to state precisely the friction at the interface when the ratio of the normal stress (σ_n) to material flow stress ($\bar{\sigma}$) is different. The model is given by equation (2.20) and expressed as (Lin, *et al*., 2003):

$$\boldsymbol{\sigma_{fr} = mck\vec{t}} \qquad \textbf{(2.20)}$$

where σ_{fr} is the friction stress
m is the friction factor
c is the ratio of real contact area to the apparent contact area between a smooth tool and a rough workpiece surface
k is the shear intensity of the deformed material
$\vec{t}$ is the velocity vector at the tool-workpiece interface

(4) Thermal Effects

The energy consumed in metal forming operations is mainly transformed into heat, which leads to temperature rise in the die and the workpiece. For aluminium and copper workpieces which are seldom formed at high temperatures, radiation effects are less significant at these low temperatures and can thus be neglected without much error (Valberg, 2010). If radiation effects and cooling to the surrounding air is neglected, equation (2.21) can be used to estimate the temperature, *T*, in a workpiece during metal forming (Ibid):

$$\boldsymbol{T = T_o + \Delta T_D + \Delta T_f - \Delta T_T} \qquad \textbf{(2.21)}$$

where, T_o is the initial temperature of the workpiece

ΔT_D is the temperature increase in the workpiece due to dissipated deformation energy during forming

ΔT_f is the temperature increase due to friction in the interface between die and workpiece

ΔT_T is the temperature decrease in the workpiece because of cooling by colder dies

The **temperature increase in the workpiece due to dissipated deformation energy** during forming is given by equation (2.22) as follows (Valberg, 2010):

$$\boldsymbol{\Delta T_D = \frac{\beta}{c\rho}\bar{\sigma}\,\bar{\varepsilon}} \qquad \textbf{(2.22)}$$

where, β is a factor compensating for energy stored in the workpiece (approximately equal to 0.95)

c is the heat capacity of the workpiece material

ρ is the density of the workpiece material

Wright (2011) modified equation (2.22) to give equation (2.23) as follows:

$$T_W - T_o = \varphi\,\frac{\sigma_a \ln\left[\frac{1}{(1-r)}\right]}{c\rho} \qquad \textbf{(2.23)}$$

where T_W is the temperature due to dissipated total deformation energy

φ is the redundant work factor

σ_a is the average flow stress

r is the reduction ratio, $r = 1 - \frac{A_f}{A_i}$

The **temperature increase due to friction** in the interface between die and workpiece is given by equation (2.24) as follows (Valberg, 2010):

$$\Delta T_f = \frac{m\bar{\sigma}Av\Delta t}{\sqrt{3}cV_a\rho} \qquad \textbf{(2.24)}$$

where m is the friction factor

A is the apparent area of contact

v is the displacement velocity

Δt is the displacement time

V_a is the layer of volume of the interface

Wright (2011) gives a modified version of equation (2.24) to give equation (2.25), thus:

$$\boldsymbol{(T_f - T_o) = \mu\, cot\alpha\, \varphi\, \sigma_a \ln \frac{\left[\frac{1}{(1-r)}\right]}{c\rho}} \qquad \textbf{(2.25)}$$

where, T_f is the temperature due to frictional work

μ is the coefficient of friction

The **temperature decrease in the workpiece because of cooling** by colder dies is given by Wright (2011) as given by equation (2.26):

$$\Delta T_T = (T_o - T)\left(1 + \exp\left[-\frac{\theta t}{c\,\rho}\frac{A}{V_a}\right]\right) \qquad \textbf{(2.26)}$$

where, θ is the coefficient of heat transfer.

2.3 Crack Formation during Wire Drawing

During the forming of materials, the workpiece material undergoes desired and non-desired changes such as material break down or defects. *Workability* refers to the ability of a material to be formed in bulk metal forming processes without breakdown of the material due to formation of cracks of any kind (Valberg, 2010). These breakdowns are a result of partial or full fracture of the material. Partial fracture occurs close to the surface or in the interior of the body subjected to forming, causing surface or internal cracks. When the workability of a material is exceeded, unacceptable defects, or complete fracture, will appear in the formed component (Ibid).

Ductility describes to what extent a material can withstand deformations without risk of breakdown (Wright, 2011). The ductility of a material is strongly influenced by properties of both the matrix and inclusions. The volume fraction, nature, shape and distribution of inclusions are important. Hosford and Cadell (1983) showed that the tensile ductility of copper decreased with increased amounts of artificially added inclusions. Fracture is initiated by the opening of holes or voids around these inclusions. The holes and voids grew by plastic deformation until they linked up to form a macroscopic crack. Ductile fracture may also occur by localized shear. Figure 2.1010 shows a typical internal crack known as a chevron crack.

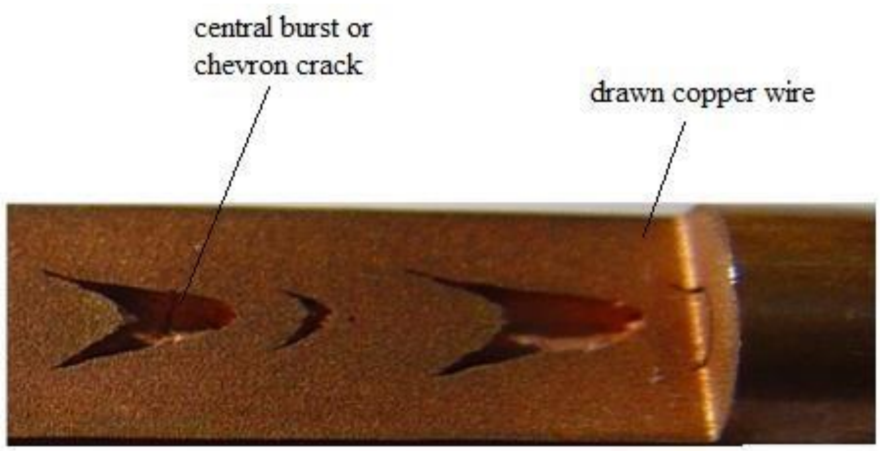

Figure 2.10: Chevron Cracks in Drawn Copper Wire.   (Source: Norasethasopon, 2011)

Fracture strains, ε_f, are strains at which cracks occur as a function of tensile reduction in area. These strains depend upon the level of hydrostastic stress during deformation. High hydrostatic pressure (in compression) suppresses void growth and delays fracture, while hydrostatic tension accelerates void growth and decreases ductility. Hosford and Cadell (1983) further state that fracture strains depend on the process geometry.

Hosford and Cadell (1983) stated that the distinction on whether fracture strains depended on the level of the largest principal stress, σ_1, rather than on the hydrostatic stress, σ_m, was not of importance. This is due to the fact that σ_m and σ_1 usually increase or decrease together as evident from equation (2.27) which shows the flow stress condition:

$$\boldsymbol{\sigma_m + \frac{1}{3}\bar{\sigma} \leq \sigma_1 \leq \sigma_m + \frac{2}{3}\bar{\sigma}} \qquad \textbf{(2.27)}$$

2.3.1 Fracture Criteria

In order to cause plastic deformation, a particular level of stress (the yield strength) must be reached. For most ductile metals such as copper, both the extent of deformation and the change in shape of the original body can continue if the stress to initial yielding is continually increased. Mathematical expressions known as *yield criteria* are used to predict if or when yielding will occur under combined stress states in terms of particular properties of the metal being stressed (Hosford and Caddell, 1983). The two commonly used general yielding criteria are the Tresca and Von Mises criteria.

(a) Tresca Criterion (maximum shear stress criterion)

This criterion postulates that yielding will occur when the largest shear stress reaches a critical value. The criterion predicts yielding according to equations (2.8) under the following conditions (Ibid):

$$\boldsymbol{\sigma_{max} - \sigma_{min} = C} \qquad \textbf{(2.28i)}$$

$$\boldsymbol{\sigma_1 - \sigma_3 = C;\ \ if\ \ \sigma_1 > \sigma_2 > \sigma_3} \qquad \textbf{(2.28ii)}$$

To evaluate constant *C*, a state of uniaxial tension may be used. In uniaxial tension, $\sigma_{max}= \sigma_1$, $\sigma_2 = \sigma_3 = 0$, and yielding occurs when $\sigma_1 = Y$, the yield strength. In that case, equation (2.9) is used, thus:

$$\boldsymbol{\sigma_1 - \sigma_3 = Y = C} \quad \textbf{(2.29)}$$

Yielding occurs when the maximum shear stress reaches the yield strength or the shear yield strength, *k*, in pure shear (when $\sigma_{max} = \sigma_1$, $\sigma_{min} = \sigma_3 = -\sigma_1$, $\sigma_2 = 0$) and given by equations (2.30), thus:

$$\sigma_1 = k \quad \textbf{(2.30i)}$$

$$\sigma_1 - \sigma_3 = 2\sigma_1 = 2k = C \quad \textbf{(2.30ii)}$$

The Tresca Criterion, is thus given by equation (2.31) as follows:

$$\sigma_1 - \sigma_3 = Y = 2k \quad \textbf{(2.31)}$$

σ_1, σ_2 and σ_3 are the principal stresses.

Expressed in general shear situations using τ, equation (2.32) is thus used:

$$\boldsymbol{k = \tau_{max} = \tau_y} \quad \textbf{(2.32)}$$

(b) Von Mises Criterion (distortion energy criterion)

Under this criterion yielding will occur when some value of the root-mean shear stress reaches a constant and given by equation (2.33) as follows (Hosford and Caddell, 1983):

$$\boldsymbol{\sqrt{\left[\frac{(\sigma_1 - \sigma_2)^2 + (\sigma_2 - \sigma_3)^2 + (\sigma_3 - \sigma_1)^2}{3}\right]} = C_1} \quad \textbf{(2.33)}$$

Equivalently,

$$\boldsymbol{(\sigma_1 - \sigma_2)^2 + (\sigma_2 - \sigma_3)^2 + (\sigma_3 - \sigma_1)^2 = C_2} \quad \textbf{(2.34)}$$

At yielding in uniaxial tension, $\sigma_1 = Y$; $\sigma_2 = \sigma_3 = 0$; $C_2 = 2Y^2$

For pure shear, with $\sigma_1 = k = -\sigma_3$ and $\sigma_2 = 0$, $C_2 = 6k^2$.

The Von Mises Criterion is thus expressed according to equation (2.35):

$$(\boldsymbol{\sigma_1} - \boldsymbol{\sigma_2})^2 + (\boldsymbol{\sigma_2} - \boldsymbol{\sigma_3})^2 + (\boldsymbol{\sigma_3} - \boldsymbol{\sigma_1})^2 = 2\boldsymbol{Y}^2 = 6\boldsymbol{k}^2 \qquad \textbf{(2.35)}$$

In a more general form, the criterion can be written according to equation (2.36), thus (Ibid):

$$\left(\boldsymbol{\sigma_x} - \boldsymbol{\sigma_y}\right)^2 + \left(\boldsymbol{\sigma_y} - \boldsymbol{\sigma_z}\right)^2 + (\boldsymbol{\sigma_z} - \boldsymbol{\sigma_x})^2 + 6\left(\boldsymbol{\tau_{xy}^2} + \boldsymbol{\tau_{yz}^2} + \boldsymbol{\tau_{zx}^2}\right) = 2\boldsymbol{Y}^2 = 6\boldsymbol{k}^2 \qquad \textbf{(2.36)}$$

where σ_x, σ_y , σ_z are the normal stresses directed along x, y and z axes, while τ_{xy} is the shear stress directed along the xy-plane.

Udomphol (2007) simplifies the two criteria as:

Tresca Criterion: $\tau_y = \tau_{max} = 0.5\ \sigma_o$

Von Mises Criterion: $\tau_y = \tau_{max} = 0.577\ \sigma_o$

Accordingly, the difference in the maximum shear stress prediction from both criteria lies between 0-15%. Experiments have confirmed that the von Mises criterion is more accurate than the Tresca criterion in describing the actual situations (Udomphol, 2007).

Hosford and Cadell (1983), Ahmadi and Farzin (2008), Xue (2007), Komori (2003) and Bao (2003) presented some more criteria associated with ductile fracture. Bao (2003) states that fracture occurs at a point in a body when the following scalar function reaches a critical value C according to equation (2.37):

$$\int_{\boldsymbol{0}}^{\bar{\varepsilon}_f} \boldsymbol{g}\left(\boldsymbol{\sigma_{ij}}\right)\, \boldsymbol{d\bar{\varepsilon}} = \boldsymbol{C} \qquad \textbf{(2.37)}$$

where g is a weighting function of the stress tensor σ_{ij}

C is a calibration constant or damage indicator

Some of the empirical models based on the relationship in equation (2.37) include the following:

(i) Cockroft and Latham criterion

This states that fracture will occur when the cumulative energy due to the maximum tensile stress exceeds a critical value, C_{CL}, according to equation (2.38) and expressed as follows (Hosford and Cadell, 1983):

$$\int_0^{\bar{\varepsilon}_f} \sigma_1 \, d\bar{\varepsilon} = C_{CL} \quad \textbf{(2.38)}$$

(ii) Rice and Tracy criterion

Under this criterion, the void enlargement is taken as a damage measure, C_{RT}, given by the equation (2.39) as follows (Bao, 2003):

$$\int_0^{\bar{\varepsilon}_f} \exp\left(\frac{3}{2}\frac{\sigma_m}{\bar{\sigma}}\right) d\bar{\varepsilon} = C_{RT} \quad \textbf{(2.39)}$$

(iii) LeRoy, Embury, Edwards and Ashby's criterion

This criterion is based on the value of the difference between the principal and mean stresses able to cause damage measured by the value C_{LEA} and given according to equation (2.40) as follows (Ibid):

$$\int_0^{\bar{\varepsilon}_f} (\sigma_1 - \sigma_m) \, d\bar{\varepsilon} = C_{LEA} \quad \textbf{(2.40)}$$

(iv) Freudenthal's fracture criterion

This states that fracture will occur when the cumulative energy due to the equivalent tensile stress exceeds a certain value, C_F, according to equation (2.41) and expressed as follows (Komori, 2003):

$$\int \bar{\sigma}\bar{\varepsilon} \, dt \geq C_F \quad \textbf{(2.41)}$$

(iv) Brozzo, Deluca and Rendina's fracture criterion

This states that fracture will occur when the cumulative energy due to a relationship between the mean and maximum tensile stresses exceeds a certain value, C_{BDR}, and is given in equation (2.42) as follows (Ibid):

$$\int \frac{2\sigma_{max}}{3(\sigma_{max}-\sigma_m)} \bar{\dot{\varepsilon}}\, dt \geq C_{BDR} \qquad \textbf{(2.42)}$$

(v) Oyane's fracture criterion

This states that fracture will occur when the cumulative energy due to the sum of the ratio between maximum and mean tensile stresses and a material constant, *B*, given in equation (2.43), exceeds a certain value, C_O as shown by the following relationship (Komori, 2003):

$$\int \left(\frac{\sigma_m}{\bar{\sigma}} + B\right) \dot{\bar{\varepsilon}}\, dt \geq C_o \qquad \textbf{(2.43)}$$

(vi) Gurson's fracture criterion

This states that fracture will occur when the change in the void volume fraction of the material, f, under mean stresses exceeds a certain value equal to the critical void volume fraction, C_G, according to the equation (2.44) as follows (Ibid):

$$\int f\, dt \geq C_G \qquad \textbf{(2.44)}$$

Other criteria associated with ductile fracture include the following (Ahmadi and Farzin, 2008 and Komori, 2003):

(vii) Avitzur's criterion

Under this criterion, the condition for central bursting using an upper-bound analysis is predicted by the occurrence of a slight increase in the hole size of an initially hollow billet that causes a reduction in the required drawing stress.

(viii) Hydrostatic Stress criterion

This criterion states that whenever the hydrostatic stress at a point on the centreline in the deformation zone becomes zero and is compressive elsewhere, there is fracture initiation leading to central bursting.

(ix) Critical Void Growth criterion

Along the die axis, if the mean stress component is initially tensile, the voids then begin to grow and coalesce, leading to central bursting.

Although Bao (2003) argues that the preceding metal forming criteria lacks a solid foundation and are based on observation, experience and mathematical simplicity performed using a restricted range of stress state, the versatility of their use has been demonstrated by Reddy, *et al*.,(2000), Tvergaard and Hutchinson (2002), Komori (2003), Xue (2007) and Benesova, *et al*.,(2008) among others.

This current research study makes use of the Von Mises yielding criterion and then uses the Cockroft and Latham fracture criterion to show damage in and on the copper wire. This choice was done because the Abaqus software that was used was able to show the von Mises stresses for yielding. Adding the maximum von Mises stresses and the accumulated strains resulted in the Cockroft and Latham criterion which was thus used to detect failure or fracture at a node.

2.4 Modeling of Wire Drawing Processes

In modeling of metal forming processes, Eulerian formulation is convenient for processes like rolling, drawing and extrusion, whereas the updated Lagrangian formulation is convenient for the processes like forging, deep drawing and sheet bending. In the Eulerian formulation a control volume is chosen as the domain for analysis. A typical control volume for wire drawing is shown in Figure 2., with half the wire being shown due to its symmetry (Dixit and Dixit, 2008).

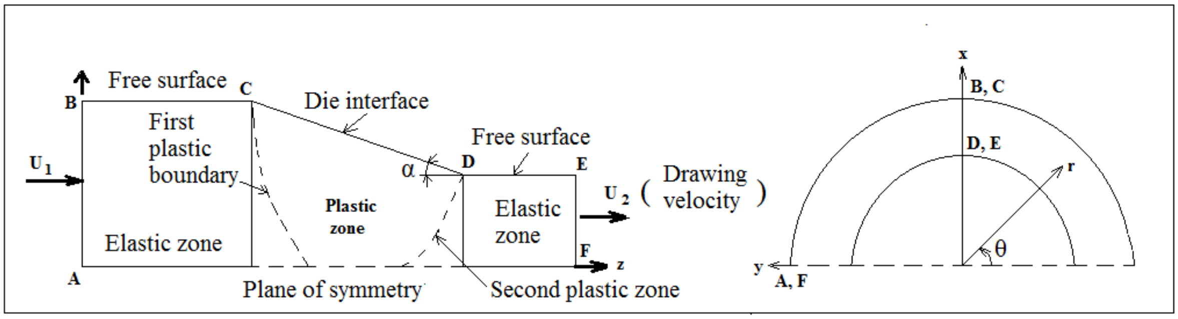

Figure 2.11: Domain for Eulerian Formulation of Wire Drawing.
(Source: Dixit and Dixit, 2008)

Dixit and Dixit (2008) state that in choosing the control volume, boundaries AB and EF need to be placed sufficiently away from the die interface CD so as to simplify the boundary conditions on these boundaries by taking advantage of the uniform velocity fields existing there. Possible plastic boundaries should also be shown, with all boundaries not known *a priori* but need to be determined as part of the solution.

Since heat is dissipated during metal forming due to deformation and mechanical energy, temperature rise in processes like wire drawing is comparatively small, hence the processes being assumed as *isothermal* during modeling. For isothermal processes, the velocity field, v_i, the strain field, $\dot{\varepsilon_{ij}}$, and the stress field, σ_{ij}, in the control volume are governed by equations (2.45), (2.46), (2.47), (2.48) and (2.49) as follows (Ibid):

(1) Strain rate – velocity relations

$$\dot{\varepsilon_{ij}} = \frac{1}{2}\left(v_{ij} + v_{ij}\right) \qquad \textbf{(2.45)}$$

(2) Elastic-plastic stress-strain rate relations

(a) in plastic zone

$$\dot{\varepsilon_{kk}} = \frac{\ddot{\sigma_{kk}}}{3K}, \dot{\varepsilon_{ij}'} = \frac{1}{2\mu}\,\dot{\sigma_{ij}'} + \frac{3\varepsilon_{eq}^{p}}{2\sigma_{eq}}\,\sigma_{ij}' \qquad \textbf{(2.46)}$$

where, $$\boldsymbol{\sigma_{eq} = \sigma_Y + K\left(\varepsilon_{eq}^{p}\right)^{n}} \qquad \textbf{(2.47)}$$

(b) in elastic zone

$$\dot{\varepsilon_{kk}} = \frac{\ddot{\sigma_{kk}}}{3K}, \dot{\varepsilon'_{ij}} = \frac{1}{2\mu} \ddot{\sigma'_{ij}} \tag{2.48}$$

In the relations above, the superscript $\ddot{}$ denotes a Jaumann stress state.

(3) Equations of motion

$$\rho \left(\frac{\partial_{vi}}{\partial t} + v_{i,j}v_j\right) = \rho b_i + \sigma_{ij,j} \tag{2.49}$$

If the density is unknown, then the equations of conservation of mass are needed. For isothermal processes, change in density is very small, hence ρ can be treated as a constant. The equations (2.45), (2.46), (2.47), (2.48) and (2.49) and their subcomponents are differential equations in spatial variables x_j and time t. Boundary and initial conditions are required for solving these equations (Ibid).

2.5 Wire Drawing Focal Research Literature

The focal research literature regarding copper wire drawing was categorised under the following themes: inclusion effects, die geometry and design effects, die wear and failure effects, temperature effects, stress and strain effects, friction and lubrication effects, practice-related effects, process optimisation and fracture criteria. The interdependence of these themes is shown in Figure 2.12.

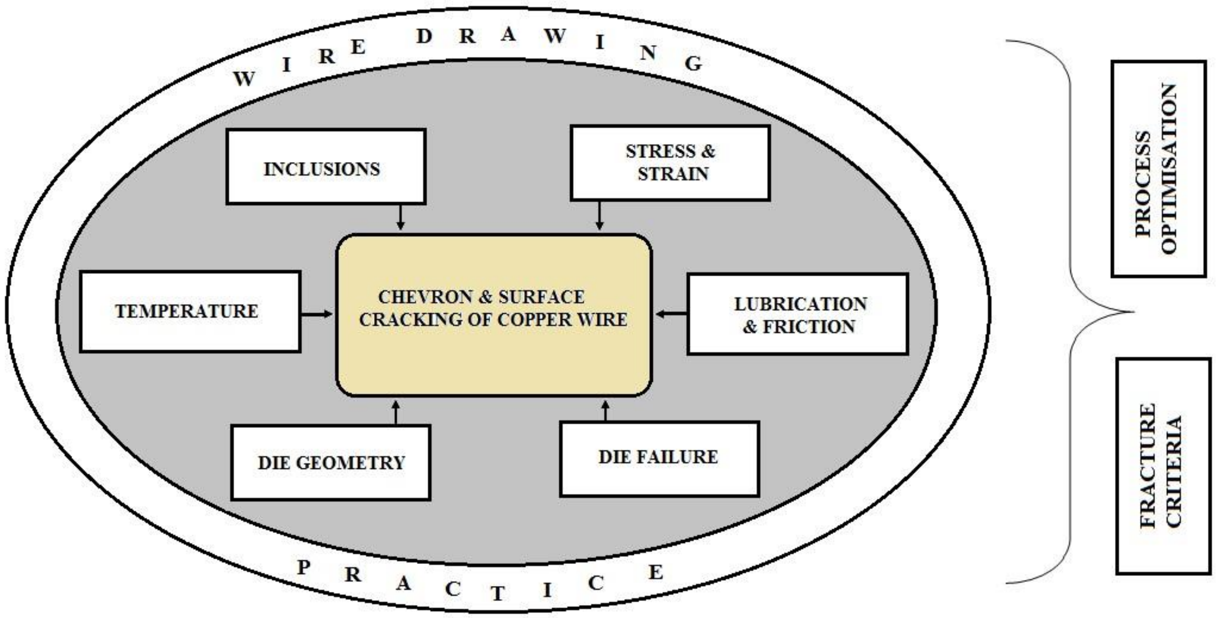

Figure 2.12: Interdependence of Die, Material and Process Parameters in Wire Drawing. (Source: Author)

2.5.1 Research on Effects of Inclusions

The research on the effects of inclusions during wire drawing were done by Norasethasopon and Yoshida (2003), Norasethasopon (2003, 2011) and Xu *et al*. (2009). Norasethasopon and Yoshida (2003) investigated the effects of size and length of an inclusion on multi-pass copper wire drawing with a focus on optimal die semi angle. The results of the investigation showed that the drawing pass numbers, inclusion size and length, inclusion properties and wire properties had an influence on the inclusion deformation, wire deformation and maximum hydrostatic tensile stresses. Necking in the wire occurred due to the presence of the inclusion.

Norasethasopon (2003) investigated the effect of inclusion length on front tensile stress during copper wire drawing. The investigation considered the inclusion as it passed through the die, with necking due to the inclusion occurring on some parts of the copper wire surface in front of and near the leading edge of the inclusion. The results of the investigation showed that necking occurred on copper-shaped wire surface in front of the inclusion near the inclusion boundary and its magnitude increased proportionally with inclusion size and length. A short inclusion length ratio ($1 > L_i/Di > 0.2$) strongly influenced tensile stresses in a wire while, a long inclusion ratio ($L_i/Di > 1.0$) did not affect inclusion front tensile stresses.

Research on possible internal defects which could be formed during wire drawing of a steel rod on the production line of a draw bench and models of the initiation and propagation rule of central flaw were done by Xu, *et al*. (2009). The experimental results from the research showed that as a result of the wire material containing defects, the probability of crack expansion in the final two or one drawing was great in multi-pass drawing, and that a friction coefficient of 0.1 and a pullout angle of approximately 8° were optimal. The fracture toughness of the material (the J-integral) increased with increasing die angle, friction coefficient and the defect dimension. Improving the lubrication conditions in wire drawing reduced the rate of broken wires. Wire breakage did not happen when the diameter of the disc-shaped surface crack in the center of the wire was less than 30μm.

The research by Norasethasopon (2011) was aimed at predicting the initiation of internal or chevron cracks in drawn copper shaped-wire. An inclusion of sintered tungsten carbide (WC) was used and assumed to be introduced in the wire during processing. The results revealed that inclusion deformation occurred when copper wire was repeatedly drawn and that the drawing pass numbers strongly influenced wire deformation, inclusion deformation and the maximum principal stresses. The research also showed that a large number of drawing passes could be performed without chevron crack initiation when the initial inclusion size ratios were below the critical inclusion size ratio of 0.001 (measured as length of inclusion, L_i, over initial wire diameter, D_i, or L_i/D). Chevron cracks, leading to wire breaking, occurred when the inclusion size was larger than the critical inclusion size.

The background to the optimality of the 8^o die semi angle in the experiment by Norasethasopon (2003) needed to be given in order to make a comparative analysis with the other processing parameters. Norasethasopon (2011) stated that crack initiation occurred if the tensile strain-energy density reached a critical value described by a ductile fracture criterion according to Cockroft and Latham. Though the critical value was given, the study did not demonstrate how the obtained inclusion size ratios related to the critical value. The study also gave equations for obtaining the drawing stress (equation 2.4), but did not show a free body equilibrium diagram to explain force analysis at an element in the reduction zone.

The study paper by Xu, *et al*. (2009) indicated that the J-integral value increased with increasing angle of the drawing die, the friction coefficient between drawing die and wire and the initial dimension of the flaw in the input material. However, the study did not show how the J-integral was being applied in this case in order to show the relationship of parameters under study. The optimisation analysis needed to be clearly demonstrated with verification experiments being undertaken to justify the choice of optimum parameters.

2.5.2 Research on Effects of Die Geometry and Design

Research on the effects of die geometry and design were done by McAllen and Phelan (2005), McAllen and Phelan (2007), Campos, *et al*. (2006), Zompì and Levi (2008), Ahmadi and Farzin (2008), Kabayama, *et al*. (2009), León, *et al*. (2010) and Hassan and Hashim (2015).

McAllen and Phelan (2005) demonstrated that irrespective of the die approach angle, α, and at reduction ratios of 9%, 18% and 25%, central burst formation was relatively high, whereas central burst was lower at area reductions ratios of 5% and 39% and also when the effective strain varied periodically along the wire surface. Further research by McAllen and Phelan (2007) indicated that the influence of the die land or die bearing length on the formation of damage in wire drawing had not been fully clarified. For varying friction conditions, the bearing length showed a negligible effect on the effective stress, effective strain and damage distributions in the drawn wire.

Campos, *et al*. (2006) evaluated the effect of the die semi angle on the coefficient of friction during the axisymmetric drawing of copper. Tungsten carbide dies with semi angles of 2^o, 3^o, 4^o, 5^o and 6^o were used with a molybdenum bisulphide industrial grease as the lubricant. The results showed that as the semi angle increased, the friction coefficient initially reduced and then increased, with the optimum die semi angle being reached at 4^o.

Zompì and Levi (2008) researched on the process parameters and evaluated the stress and strain patterns in copper wire drawing. The results of the research showed that the die angle and the reduction ratio were the two major linear effects. Smaller die angles (from 6.5^o to 9^o), larger drawing ratios (from 20% to 25%) and effective prior annealing led to large drawing forces but lower damage of the product, while the effect of friction coefficients was small. Annealing was needed in order to relieve residual strains and restore capability to withstand substantial plastic deformation.

Ahmadi and Farzin (2008) investigated the geometric and friction conditions causing chevron cracking or central bursting in steel wire drawing. The finite element analysis and experimental results showed that chevron cracking occurred under conditions of relatively small area reductions and large die angles (15^o) where the mean stress was mostly tensile, and that low friction conditions ($\mu = 0.05$) increased the tendency of central bursting.

Kabayama, *et al*. (2009) investigated the influence of die geometry on stress distribution on annealed electrolytic copper wire. The results of the experimental investigation showed that the wire drawing force and friction coefficient values decreased with increased drawing speed. A die semi angle of 5^o produced wire drawing forces of up to 23.2% and friction coefficients up to 60.5% lower than those for a die with semi angle of 9^o. The finite element analysis of the draw die reduction zone showed maximum radial stresses on the surface and the intermediate region while the maximum axial stress was on the surface. The residual stress was intense on the reduction zone for a semi angle of 9^o, and was permanent with important influences on fatigue properties after the completion of the wire drawing process. The simulation results showed tensile axial stress on the wire surface and compression stress in the intermediate region.

León, *et al*. (2010) researched on the effect of die angle, percentage of section reduction, friction coefficient and wire cracking due to strain hardening during wire drawing of a 5052 aluminium alloy. The results obtained showed that the manifestation of cracks on and in the wire depended mainly on the semi-cone angle of the die and on the percentage of section reduction. A high value of plastic deformation in the material could lead to excessive cracking inside the wire. The most significant effect on the plastic deformation was the section reduction, followed by the semi-cone angle of the die and the friction coefficient.

The analysis by Hassan and Hashim (2015) when drawing aluminium wire showed that increasing the bearing length effected a proportional increase in the drawing force at higher die semi angles (9 to 15^{o}). This was evident under conditions of constant area reduction (10%). A similar effect was observed at conditions of constant semi angles (10^{o}) but increasing area reductions (10%, 20% and 30%).

Kabayama, *et al*. (2009) studied the effects of the deformation zone and the bearing regions on stress distribution. Whereas it was easier to see the effect of the approach angle on stress distribution, the effect of the two bearing region variations (35% and 50%) on axial and radial stress distributions was not easily seen from the presented graphs. Hassan and Hashim, (2015) observed the effect of bearing length variation on drawing force by varying both the area reduction and approach angle. This is difficult to infer whether the observed effect was due to bearing length change, area reduction change or change in approach angle.

In the analysis of León, *et al*. (2010), the mentioned accumulated damage was difficult to perceive as there were no units given and components of the modified damage equation (equation 2.37) indicated so. Similarly, Ahmadi and Farzin, (2008) needed to further clarify their statement that predictions based on Avitzur, hydrostatic stress and critical void criteria were more conservative than the other mentioned fracture criteria. Table

No.2 on the predictions of central bursting according to different criteria needed to show consistency in using the parameters. Five values of the semi die angle (15^o) were used against only two values of a different semi die angle (6^o), and then the 15^o die angles were repeated as the area reduction was increased.

The restriction of the use of a “unity” delta parameter by Campos, *et al*. (2006) in order to reduce redundant work is an over-elaboration. Wright (2011) states that the principle motivation for maintaining a constant delta parameter is to maintain reasonably consistent drawing mechanics such as die pressure, redundant work and centerline tension. This constancy is dependent on the maintenance of other parameters (such as semi angle and area reduction).

Zompì and Levi (2008) used an empirical third order polynomial with descriptions of components *x*, *y*, *z*, *A*, *B* and *C* missing from the polynomial despite being referred to, while Vega, *et al*. (2009) gave the bearing length as a percentage of the final drawn wire diameter, not as an absolute value. As most practitioners express the bearing length as a fraction of the final wire diameter, more theoretical backing as to why the bearing length is expressed as such is needed, especially knowing that other die design applications do not incorporate a bearing section.

The results given by McAllen and Phelan (2007) indicating an oscillating or up and down nature of the damage values versus wire diameter required clarification as to whether the same set of points were maintained during the analysis.

2.5.3 Research on Effects of Heat

Heat effects during wire drawing were researched by Palkowski, *et al*. (2003), Singh, *et al*. (2007) and Vega, *et al*. (2009). Palkowski *et al.* (2003) researched on the temperature conditions for cold forming of non-ferrous wires in the drawing and continuous annealing process by means of simulation and experimental production. The results of the research showed that approximately 60% of the deformation energy inside the wire was converted into heat. This heat is normally taken up by the lubricant, whose viscosity decreases at higher temperatures.

Singh *et al.* (2007) researched on a comprehensive simulation model for multi-pass wire drawing operation, taking into account deformation and thermal effects in the dies, cooling in between the dies and linking mechanical properties of the final wire to the deformation. Models for wire drawing simulation based on actual plant information which included deformation of wire, heat generation and dissipation in the wire and the dies, cooling of the wire in the atmosphere and on the cooling drum were developed. The experimental results showed that while machine related parameters were independent of the wire and pass schedule, it was observed that the values of friction depended on a number of parameters which could not be directly measured or correlated easily. Thus deformation energy leading to heat had an effect on the value of the friction coefficient, and consequently affecting the 'stick-slip' mechanism during wire drawing, with a likelihood of wire necking and breakage.

An investigation of multi-pass drawing speeds and friction coefficient and their effect on temperature in a copper wire was done by Vega, *et al*. (2009). The investigation was aimed at developing a model with the capability to predict the optimum drawing force and temperature corresponding to different speeds varying between 1 and 7 m/s. The results of the investigation showed that maximum drawing stresses and temperature were obtained at higher speeds (7m/s), while the coefficient of friction increased with temperature rise. The temperature reached a maximum value of 67^{o} C close to the interface, just above the bearing. The results thus showed that increasing the drawing speed led to an increase in die and lubricant temperature, thereby effecting an increase in interface friction. Wire breakage at elevated temperatures was possible.

Singh, *et al*. (2007) should have specified the parameters upon which friction depended and should also have explained the phenomenon of heat to plastic work partition and how the values are arrived at. Palkowski, *et al*. (2003) needed to explain why it was necessary that the transition radii in dies changed when drawing different materials. The temperature conditions in the drawn copper wire needed to be elaborated more in terms of sectional distribution and effectiveness of measurements.

2.5.4 Research on Effects of Stress and Strain

The behaviour of materials during wire drawing was researched by Atkins and Cadell (1968), Gálvez, *et al*. (2002), Cho, *et al*. (2006), Hervias, *et al*. (2009) and Salcedo, *et al*. (2010). Atkins and Cadell (1968) conducted an analytical research in drawing copper, brass, steel and aluminium. They demonstrated analytically how the use of a mean yield stress underestimated the working loads or stresses needed to draw metal in comparison to loads predicted by more exact means which incorporate strain hardening relationships. Further, redundant work was shown to be influenced by the delta parameter. Atkins and Cadell (1968) stated that in computing the drawing stress, a factor to compensate for redundant work needed to be included.

Gálvez, *et al*. (2002) researched on the strain rate effect on the mechanical behaviour of a ferritic steel wire and developed a numerical model of the wire drawing process. The results of the experiments showed that the strain rate during wire drawing had a decisive influence on the material flow and hence should be taken into account when calculating drawing forces, the friction coefficient and the stress and strain fields when making ductile failure predictions.

Cho, *et al*. (2006) investigated the effects of drawing deformation and annealing on the volume fractions and microstructures of the (111) and (100) grain fiber components in copper. Bonding wires of 25 μm size were formed. The performed isothermal annealing experiments were focused on recrystallization and grain fiber growth in the bonding wire. The results of the experiment showed that the (100) grains were located under the surface and the (111) grains occurred mainly in the centre. A combination of drawing and annealing resulted in the elongation of the grain fibers and an intermixing of the (100) and (111) fiber grains. Further drawing was seen to decrease the (100) fiber grains while the (111) fiber grains increased with increased reduction area. Overall, increased drawing deformation reduced the grain size while annealing increased the grain size.

Hervias, *et al*. (2009) carried out investigations to measure the residual stresses in ferritic and pearlitic steel rods. The rods were subjected to a two-pass treatment, with the first pass being a 20 % area reduction while the second one being a 1 % area reduction. The results of the investigation showed that the residual stresses generated by cold drawing were tensile at the surface and compressive at the centre. A 1 % area reduction reduced stresses in the radial direction. Salcedo *et al.* (2010) also studied the effects of residual stresses on a 5052 aluminium alloy during wire drawing. The results of the FEM analysis showed that axial stresses were positive at the surface of the processed material and decreased towards the central region, becoming compressive. The maximum axial stresses increased with an increase in the semi angle and a decrease in the area reduction. The radial stresses were of zero value at the surface and became increasingly negative (compressive) towards the central region of the component, while the angular stresses were positive at the surface and became negative (compressive) towards the centre of the component. Angular stresses increased with the increase in the semi angle and the friction coefficient.

The review by Atkins and Cadell (1968) indicated that the coefficient of friction was equally a factor in determining drawing stresses in redundant work situations. Though of lesser importance than the delta parameter, there was need to demonstrate the actual effect of friction coefficient under such cases. The investigation by Hervias, *et al*., (2009) states the area reduction but does not indicate at what approach angles the drawing was done. This is important in order to relate the residual stress formation with changes in approach angle and area reduction.

The study by Cho, *et al*. (2006) assumed isothermal conditions, a practice normally done when modeling processes (Dixit and Dixit, 2008, pp.189). Temperature effects in the different grain boundary regions needed to be taken into account in order to relate grain growth, temperature and deformation during central bursting of copper wire. The investigation by Salcedo, *et al*. (2010) used a Lagrange formulation in the finite element analysis and wire drawing of aluminium alloy 5052. Though the recommendation by Dixit and Dixit (2008, pp.185) that Lagrangian formulations are better suited to processes like forging, deep drawing and sheet metal forming, and not wire drawing, Salcedo, *et al*. (2010) showed that even wire drawing processes can use Lagrangian formulations. However, the authors needed to state how the coefficient of friction was determined.

2.5.5 Research on Effects of Friction and Lubrication

Tribological effects due to friction and lubrication in wire drawing were researched by Huo (1997), Radojevič, *et al*. (2000) and Dubois, *et al*. (2002).

A research on the mechanics of deformation, friction and lubrication efficiency and die design in wire drawing was done by Huo (1997). The major focus of the research was on lubrication evaluation during wire drawing of low carbon and medium carbon steel wire. The results from the research showed that the drawing stress varied with the variation of the lubricant type, pressure nozzle semi angle and drawing speed. Two different lubricants were used, namely Traxit and Condat Vicafil with melting points of 210^{o}C and 165^{o}C respectively. The drawing stress increased with the increase in percentage area reduction.

Radojevič, *et al*. (2000) investigated the behaviour of two lubricants during copper wire drawing. The tested lubricants were two different emulsifying oils whose concentrations were varied and the wear patterns on the steel die were observed. The results of the investigations showed that the lubricant concentration had an effect on the wear and lubrication behaviour during wire drawing. Dubois, *et al*. (2002) investigated the phosphating time, ageing of surface treatments and contact temperature versus friction coefficient during wire drawing of steel components. The results of the investigation showed that the coefficient of friction decreased with the increase in both temperature and the ageing of the lubricant (soap powder). With an extended ageing (beyond fifteen days), the friction coefficient increased even with additional lubricant.

The friction models given by Huo (1997) do not take into account the lubricant concentration as shown by Radojevič, *et al*. (2000). There is need to analyse the effects of variability of friction coefficient due to concentration changes, with the consequent wear effects. A factor could then be added to the empirical equations given by the mentioned authors. The dies used in the research by Huo (1997) were stated to have an angle of 7.5^{o}, however the figures in the results and discussions show die angles of 6^{o}, 8^{o} and 10^{o}. There was need to clarify this selection of different die angles.

The investigation by Radojevič, *et al*. (2000) only focused on the concentrations of the lubricants under survey. This should have been complemented by studying the consequent changes in the friction coefficient so as to relate the wear patterns with concentration and friction coefficient changes. Die geometry parameters should also have been given in order to make a good comparison for the different die geometries or reduction areas.

The revelation by Dubois, *et al*. (2002) that additional lubricant did not decrease the friction coefficient due to temperature increase and wearing out of the initial lubricant suggests non-mixing of old and new lubricants. The results further suggest that a particular lubricant could only be useful for a number of days of wire drawing practice, hence the need to continuously carry out analytical tests on such lubricants during the course of wire drawing.

2.5.6 Research on Effects Related to Wire Drawing Practice

Practice related effects in wire drawing were reviewed by Chia and Patel (1996) and Canter (2009). Chia and Patel (1996) characterised defects in copper wire arising from the wire drawing operation and revealed that improper wire drawing practices could lead to defects in the wire even if the rod contains minimal or no defects (grade A copper rod). The review showed that surface cracks or checked wire are caused mostly by die misalignment or incorrect entrance of the wire. Central bursting or cuppy wire was produced by incorrect die geometry and improper reduction per pass. Surface markings were caused by worn dies, insufficient lubrication at the die entrance, accumulation of metallic fines at the die entrance, breakdown of lubricant and wire touching the metallic component of the wire drawing machine.

Copper fines are generated in the wire drawing machine due to abrasion of the wire surfaces in the die and concluded that a great synergism should exist between the quality level of the rod and the processing parameters during wire drawing (including the lubricating systems) which would result in a "world class" wire quality material. Canter (2009) reviewed that the performance issues facing wire-drawing lubricant manufacturers involved formulating products that exhibited needed lubricity without excessively generating foam while maintaining a sufficiently bright or clean wire. Water dilutable fluids are mainly used for most copper wire-drawing applications, and these are mostly semisynthetic or synthetic fluids. Neat oils needed are employed in wire-drawing operations of alloys.

Chia and Patel (1996) stated that central bursting was caused by improper drawing practices relating to die geometry and misalignment. This should have been qualified to mean incorrect die semi angles due to the various factors associated with die geometry.

2.5.7 Research on Fracture Criteria

Komori (2003) and Benesova, *et al*. (2008) researched on fracture and the different criteria used to determine fracture in wire drawing. Komori (2003) conducted a study on the mechanics of ductile fracture in bulk metal forming processes by finite-element analysis and experiments, with special attention being focused on the effect of various kinds of ductile fracture criteria on chevron crack formation and evolution during drawing of tough pitch copper. The mechanism of periodic appearance of a central burst was simulated. The results of the experiments showed that under all the four different criteria (Gurson, Freudenthal, Cockroft, Brozzo and Oyane) fracture occurred after the sixth drawing pass at a die angle of $2\alpha = 45^{o}$ and 25% area reduction. At the die angle of 30^{o} and 15% area reduction, fracture occurred after the tenth drawing pass with distances between cracks being larger than those obtained at 45^{o} and 25% die angle and area reduction parameters.

Freudenthal’s fracture criterion was not appropriate for analyzing ductile fracture due to the fact that material fractured on the surface and not at the centre where the analysis was required.

Benesova, *et al*. (2008) investigated the fracture of carbon steel wires in wire drawing and the maximum value of hydrostatic stresses in the wire axis. Critical values of fracture strains using the Cockroft-Latham criterion (which relates principal and equivalent stresses and strains) were determined when the wire was drawn through three dies, with different die semi angles (8°, 10° and 12°), using the FEM with the softwares Deform 2D, ABAQUS and Forge 2. The results from the investigation showed that central bursting occurred due to a corresponding increase in the area reduction, material flow stress, effective strain and number of passes, and that the maximum values of fracture were reached in the cross-section of the wire, where the deformation zone proceeded to the bearing zone or at its initial part. In these areas, the lowest values of the hydrostatic stress were in the wire axis. Effective strain versus fracture curves were parallel and above those where no fracture occurred, with the slope corresponding to the factor of stress concentration.

Using the Cockroft-Latham criterion for different semi-angles when drawing high carbon steel wires, Benesova, *et al*. (2008) demonstrated that central bursting occurred due to a corresponding increase in the area reduction, material flow stress, effective strain and number of passes when using the software Deform 2D. The research elaborated more when the software Deform 2D was used for the FEM, while the use of the ABAQUS and Forge 2 softwares was only limited to hydrostatic stress distributions in the approach and bearing regions. The applicability of all the softwares used was not therefore comprehensive.

The study by Komori (2003) using different fracture criteria on chevron crack formation could be augmented by the observation that Cockroft and Latham's and Brozzo *et al*.'s criteria only agree well with experiments for internal or chevron crack studies, while Freudenthal's criterion would be more appropriate to surface crack studies. The results given by McAllen and Phelan (2007) indicating an oscillating or up and down nature of the damage values versus wire diameter required clarification as to whether the same set of points were maintained during the analysis.

In the categorization of workability, Wright (2011), Hosford and Caddell (1983) and Valberg (2010) referred to the Cockroft and Latham criterion as a commonly applied criterion. Bao (2003) clarified this by stating that the applicability should be based on the range of a stress state.

Wright (2011) gave good practical applications of temperature measurements, but failed short of adding the temperature component due to cooling in equation (2.26) as given by Valberg (2010) in equation (2.22). This could be a source of errors in practical determination of the overall heat effects during wire drawing.

2.6 Research Gap Analysis and Contribution

2.6.1 Research Gap Analysis

This research aims to provide contributions to the field of wire drawing and extend it in terms of both content and processes. The extended literature provides wire drawing practice in relatively broad aspects. Firstly, this research attempts to provide more specific and comprehensive means of wire drawing by focusing on die geometry and the effects of the Δ-parameter during medium size copper wire drawing. Secondly, the factors underlying defect-free wire drawing practice will be developed through integrated qualitative and quantitative research means.

The research on inclusion effects (Norasethasopon, 2003; Norasethasopon, 2011; Norasethasopon and Yoshida, 2003) has gaps concerning the relative effect of metallic and nonmetallic inclusions, sizes and stress build-up relative to wire breakage. Inclusion effects equally need to be analysed when other parameters (die half angle, reduction per pass, strain, coefficient of friction) vary during wire processing.

Some of the gaps concerning die geometry effects include the variation of the Δ-parameter (die angle and deformation zone changes) and the other die geometries (bell, bearing land, exit angle) with other processing parameters (friction and strain) on crack initiation during wire drawing. The effect of die geometry on stress distribution was shown by Kabayama, *et al*. (2009), but effect of this stress on crack formation still needs to be analysed. Ahmadi and Farzin (2008) tested the different fracture criteria for varying die semi angle, area reduction and friction coefficient. Whereas Hassan and Hashim (2015) demonstrated the effect of bearing length on drawing force, there is need to test a fracture criterion during draw die bearing length variation whilst keeping the other die parameters constant.

Investigation of temperature during wire drawing was done by Palkowski, *et al*. (2003), Singh, *et al*. (2007) and Vega, *et al*. (2009) through the effect of drawing speed on temperature and stress due to deformation, heat and friction conditions. The possible research gap in this involves the investigation of heat distribution due to redundant work along the wire centre line, where chevron cracking manifests.

On stress and strain effects during wire drawing, investigations have been done on plastic deformation and modification of material mechanical properties during wire drawing, including the maximum values of damage reached in the cross section of the wire, where the deformation zone proceeds to the bearing zone or at its initial part. Gaps in this research category include the need to investigate the effect of material property variation on crack formation and understanding the profile and length of the deformation zone during wire drawing.

Concerning friction and lubrication effects, different lubricants on drawing speeds and stresses have been investigated. The possible research gap here is to investigate the relative transport mechanism of surface and inner wire material layers, the concentration of lubricants and their effects on the heat distribution and consequent chevron and surface cracking.

2.6.2 Research Contribution

Whereas most of the literature concerning wire drawing deals with temperature, friction, lubrication and die geometry whose focus is normally the semi angle and percentage reduction, this research extends the focus on die geometry by further analyzing the effect of the bearing length on both surface and internal crack formation during copper wire drawing. Secondly, the integrated approach of looking at all the factors involved during wire drawing provides operational decision making tools necessary for the optimisation of the process and consequent reduction or elimination of both internal and surface cracks during wire drawing of copper. This research, thus, extends the investigations by Kabayama, *et al*., (2009) and Hassan and Hashim (2015) by focusing more on bearing length change when other factors are maintained constant, incorporating the Δ-parameter and including die manufacturing mechanisms in the investigations.

A proposed system and subsystem level of analysis is shown in Figure 2.13 as a guide to the machine-die system level investigation of the wire drawing process. The figure indicates that a comprehensive understanding and analysis of the wire drawing process needs to be undertaken at three levels, namely:

(i) Material Level

Under this level, all the physical properties and characteristics regarding the die, wire and lubricant materials need to be taken into consideration. Of great importance is the chemical composition (including metallic and non-metallic inclusions) of the wire to be drawn.

(ii) Process Level

Under this level, the modifying conditions during wire drawing need to be understood. Temperature of both the lubricant and the dies, the stress and strain components obtainable in the wire being drawn, and the friction and lubricating conditions all have an effect on the overall performance of the wire drawing process.

(iii) Die Level

Once the material and process conditions have been taken into account, the third level of analysis is the die level. Under this level, all aspects of the die including the internal geometry and its consequent wear and failure, need to be understood. The condition of the die has an effect on the wire drawing process.

(iv) Integration and Optimisation Level

Under this level, the control of parameters at material, process and die levels is important in order to produce a defect-free wire product. Control of parameters is done so that better-performing or optimal parameters are obtained in order to avert or substantially reduce the defects leading to product failure. Different fracture criteria may be used to assess the parameters.

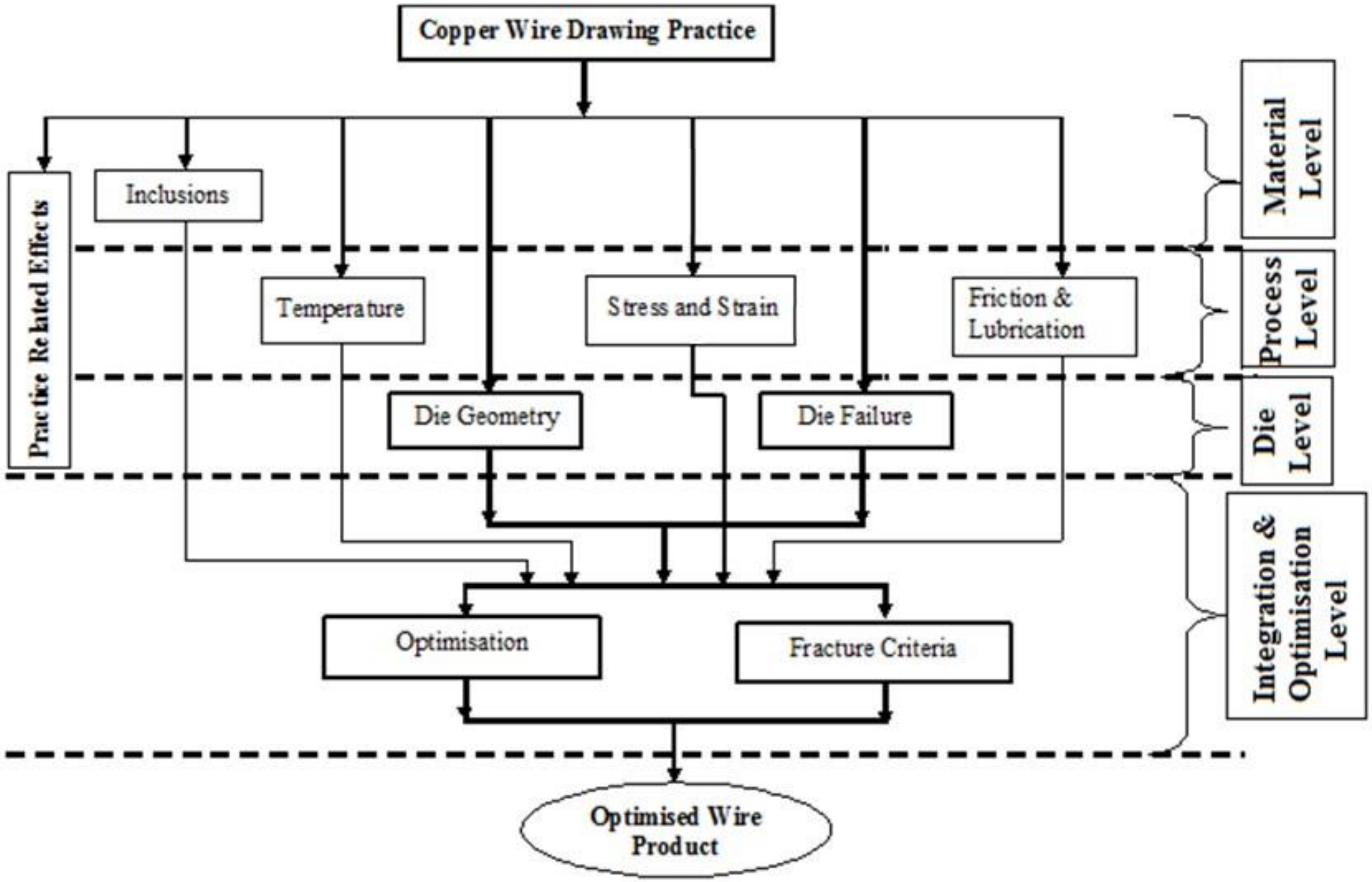

Figure 2.13: Machine-Die System Level Investigation of Wire Drawing Process. (Source: Author)

CHAPTER THREE: CONCEPTUAL FRAMEWORK

3.1 Introduction

This chapter is divided into two major sections. The first section presents a theoretical framework of the research and gives an outline of the various parameters and research focus which are critical to the analysis of wire drawing. The second section presents the conceptual framework of the current study. This section gives insight into the variables used in the research in order to achieve the objectives of the study.

3.2 Theoretical Framework

Copper wire drawing is a manufacturing process that converts inputs (copper raw materials) into usable outputs (copper wire products). In order to efficiently perform the transformation process, conditions favouring smooth interactions among the material being drawn, the die, die-wire interface conditions (temperature and lubrication) and process conditions need to be attained.

3.2.1 Die-Wire Interactions during Copper Wire Drawing

Figure 3.1 shows the die-wire interaction and the various participating parameters. A pulling force, F, and a pressure force from the die, P, combine to cause the wire to extend and reduce in diameter from d_i to d_f. The die parameters participating in the process are α (approach angle), β (entrance angle), γ (exit angle) and L_b (bearing length). Zompì and Levi (2008) showed that smaller approach angles, larger drawing ratios and effective prior annealing led to large drawing forces but lower damage of the product, while the effect of friction coefficients was insignificant.

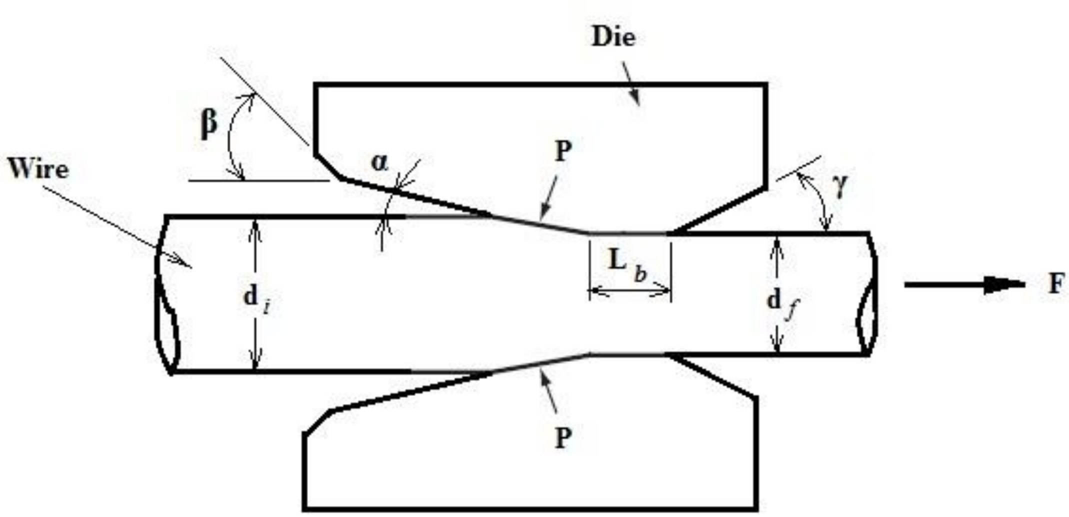

Figure 3.1: Die-Wire Interaction and Process Parameters. (Source: Author)

3.2.2 Material Conditions during Copper Wire Drawing

During the wire drawing process, the copper wire interacts with the die (commonly tungsten carbide or synthetic diamond) at the wire-die interface where the lubricant participates. The applied drawing force causes deformation by overcoming friction forces and internal distortions. Within the material being drawn, internal shearing occurs, hence distortion of internal plane sections resulting in the metal experiencing higher strain and the end product becoming harder, stronger, and less ductile (Hosford and Caddell, 1983).

Norasethasopon and Yoshida (2003) showed that the inclusion properties, size and length and wire properties had an influence on the inclusion deformation, wire deformation and maximum hydrostatic tensile stresses.

Figure 3.2 shows the interacting materials in the copper wire drawing process and their respective parameters. The figure shows that during works on the rod, the types and percentages of inclusions, the hardness and the surface roughness of the rod will determine the mechanical properties of the exiting wire. The hardness and surface roughness of the die have an impact on the wear and life of the die during its interaction with the rod and wire material properties. The concentration and viscosity of the lubricant are important parameters in that as they greatly change, the cooling and friction reduction properties are affected, resulting in an overall effect on wire drawing conditions.

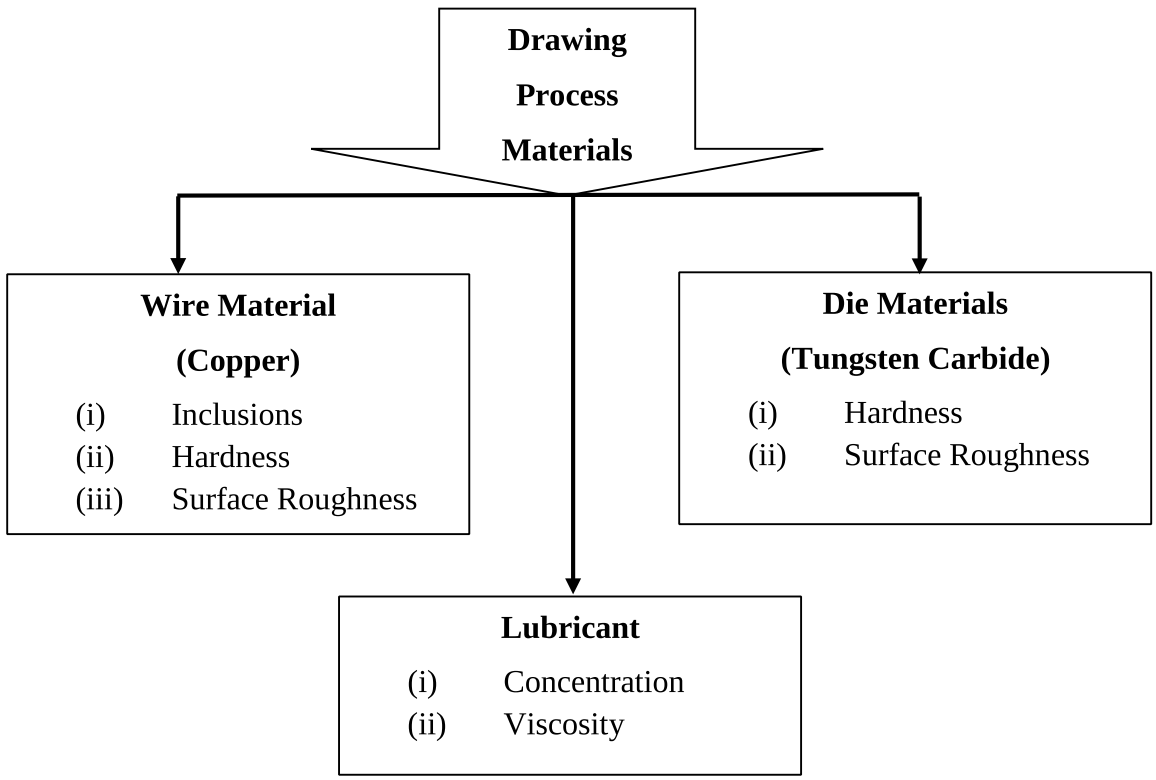

Figure 3.2: Material Parameters in Copper Wire Drawing. (Source: Author)

3.2.3 Ductile Damage and Development of Surface and Chevron Cracks during Copper Wire Drawing

Surface and internal (chevron) cracks occur in a formed component when the workability of a material is exceeded (Valberg, 2010) and the ductility is reduced (Hosford and Caddell, 1983). Both workability and ductility are an indication of drawability or the degree to which a rod or wire can be reduced in cross section in successive dies (Wright, 2011).

Chevron cracking occurs under conditions of tensile stresses under small area reductions and large die angles and low friction conditions (Ahmadi and Farzin, 2008). The probability of crack expansion in the final two or one drawing was great in an eight-pass drawing (Xu, *et al*., 2009).

According to Chia and Patel (1996) surface cracks are caused by die wear, insufficient lubrication, accumulation of metallic fines at the die entrance, breakdown of lubricant and wire touching the metallic component of the wire drawing machine.

The formation of cracks during wire drawing is predicted using the following four parameters:

(i) Die Geometry Parameters

The approach angle (α), the bearing length (L_b), the entrance angle (β) and the exit angle (γ) are the die geometry parameters under study and predicted to affect the formation of chevron and surface cracks (Ahmadi and Farzin, 2008; Kabayama *et al*.. Zompì and Levi, 2008; Kabayama, *et al*. 2009; Hassan and Hashim, 2015; Wright, 2011).

(ii) Wire Drawing Process Parameters

The interaction of the wire and the die presents a contact surface. Due to this interaction, the wire velocity (v_{dr}), the coefficient of friction (μ) and the interface temperature (T_{int}) have an effect on the formation of cracks both on the surface and at the wire centreline (Huo, 1997; Ahmadi and Farzin, 2008; Xu, *et al*. 2009).

(iii) Ductility Parameters

The percent elongation (E_l) and the percent area reduction (A_r) for each given pass are critical parameters for ductility which is the extent to which a material can withstand deformations without risk of breakdown, or formation of cracks. The initial and final wire diameters, $\boldsymbol{d_i}$ and $\boldsymbol{d_f}$ are the input parameters used in ductility measurement (Wright, 2011).

(v) Workability Index

The workability index, C, for ductile fracture is determined using the Cockroft and Latham ductile fracture criterion. The input parameters are (Hosford and Caddell, 1983; Valberg, 2010; Wright, 2011):

- Fracture strain, ε_f
- Maximum tensile stress, σ_{max}
- Effective strain, ε_{eff}

Whereas the workability index *C* can change its value at each rod or wire drawing pass, the ductility parameters (*El* and A_r) are maintained constant for a given drawing pass. Hence, both the ductility and workability conditions need to be fulfilled at each pass (Wright, 2011).

An increase in the ductility parameter A_r signals the presence of necking, leading to the wire section unable to carry the drawing load and consequently breaking. Decrease in A_r is an indication of lack of plastic flow in the material, and *annealing* is used to maintain the flow of material (Ibid).

Figure 3.3 shows the conditions necessitating the application of the workability index, specifically the Cockroft and Latham criterion, during copper wire drawing. The figure shows that for fracture to occur in a ductile material, the criterion for ductile damage (DUCTCRT) and the critical value of the Cockroft and Latham criterion should have been met. These conditions arise due to the presence of a maximum stress and a cumulative strain.

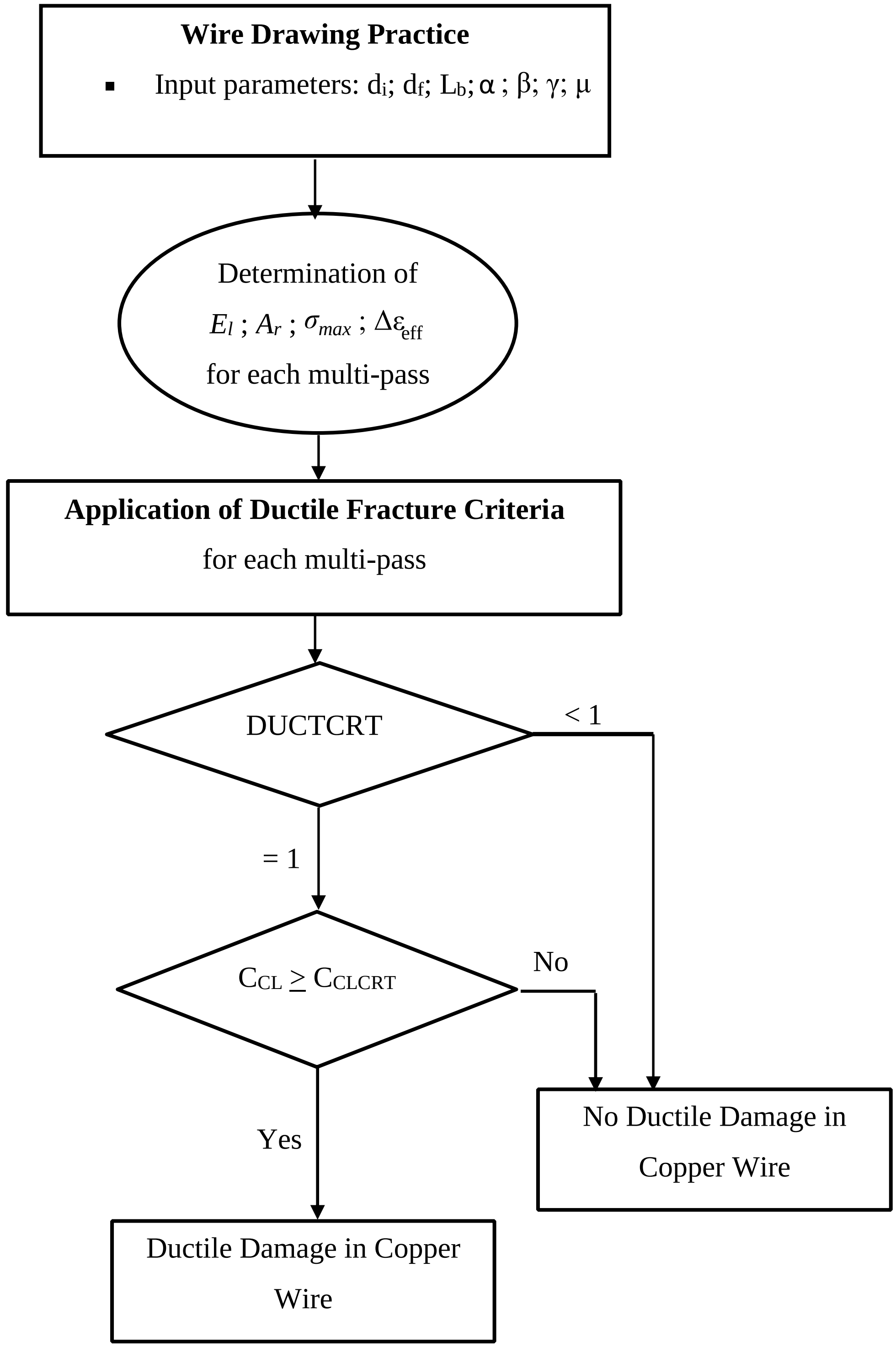

Figure 3.3: Conditions for Ductile Damage during Copper Wire Drawing.
(Source: Author)

3.2.4 Die Wear during Copper Wire Drawing

Wear is the major reason for die replacement and affects the tolerance of the formed part, metal flow, die life and economics of the drawing process Lee, *et al*. (2012). Research by Yang, *et al*. (2007) showed that wear and tear behaviours were different in different die zones, with the approach and bearing zones registering the most severe wear. Hollinger, *et al*. (2003) showed that die wear rate reached a maximum value at the entrance to the approach zone.

According to the ASM Handbook (ASM International, 1988), two types of die materials are recommended for use when drawing copper material. Natural and synthetic diamond die materials are recommended for drawing copper wires of diameters less than 2.06 mm, whereas for diameters greater than 2.06 mm cemented carbide die materials are used.

Die geometry influences the process parameters, including heat generation, during wire drawing (Campos *et al*., 2006; Zompì and Levi, 2008; Ahmadi and Farzin, 2008; Kabayama *et al*., 2009; León *et al*., 2010; Vega *et al*., 2009). Tribological effects due to friction and lubrication during wire drawing were investigated by Huo (1997), Radojevič *et al*. (2000) and Dubois *et al*. (2002).

Since die wear has an influence on the tolerance, and hence the quality of the formed parts and the general economics of the forming process (Lee *et al*., 2012), the presence of surface cracks is influenced by wear. This was demonstrated by Panjan, *et al*., (2005) who showed that die wear occurs when burrs appear on the copper profile surface.

Figure 3.4 shows the interacting influence of die materials, die and process parameters and modifying conditions on die wear and crack formation. The figure shows that depending on the die materials in use, a good selection of die geometry and process parameters, with monitored modifying conditions, will reduce die wear, increase die life and thus guarantee a good quality of wire.

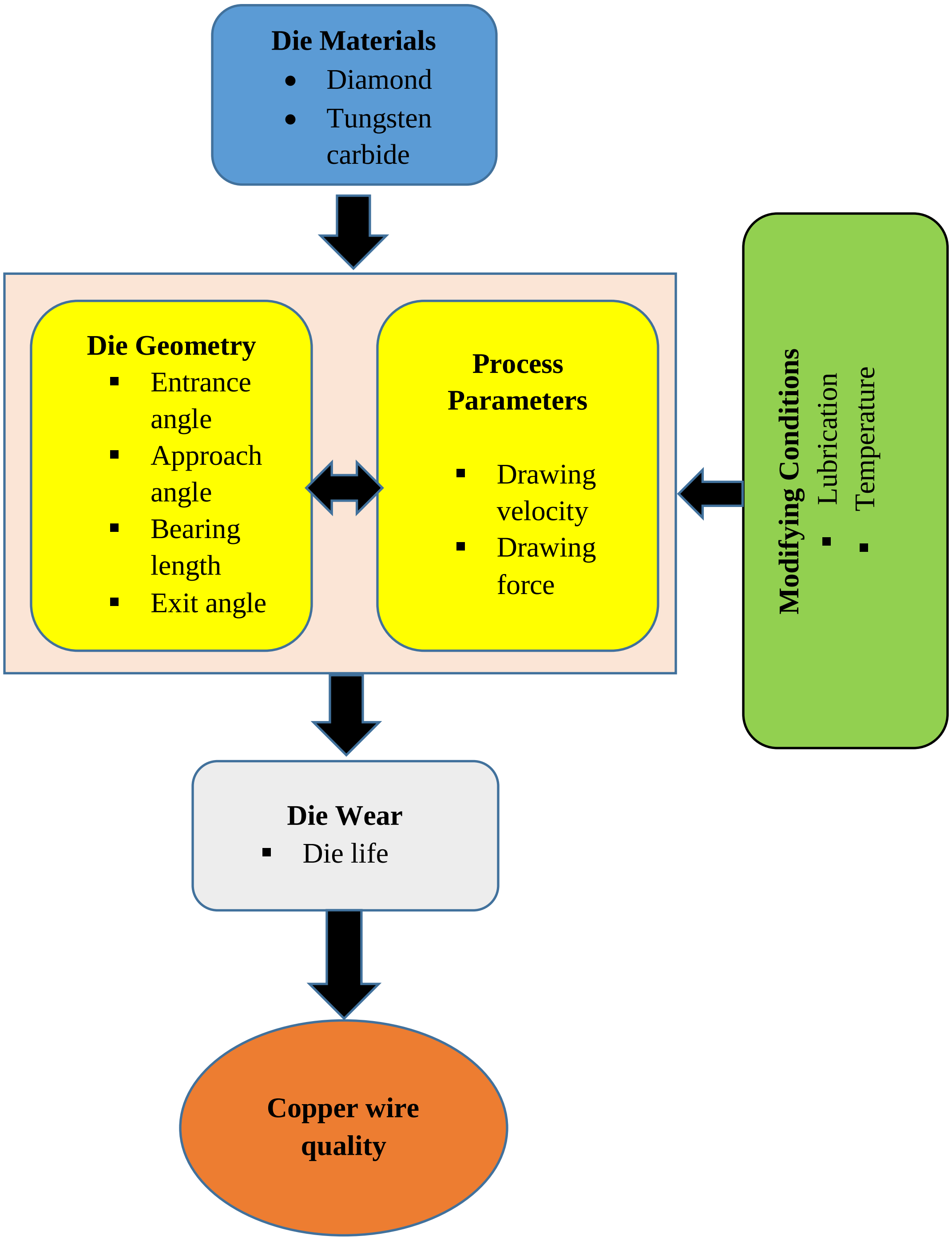

Figure 3.4: Influence of Wire Drawing Parameters on Wire Quality. (Source: Author)

3.3 Conceptual Framework

Different levels of interactions among the properties of the copper wire material, die material and geometry, and the process conditions lead to the formation of wire drawing conditions promoting the presence of, or lack of, surface and internal defects in the copper wire.

3.3.1 Research Variables in Copper Wire Drawing Process

The research variables needed to fully analyse copper wire drawing arise from the parameters indicated in Figures 3.1, 3.2, 3.3 and 3.4. The parameters can be classified as being independent and dependent variables.

(a) Independent Variables

Independent variables are the parameters to be varied or manipulated by the researcher. They are antecedents or the presumed cause. During both simulation and experiments, the independent variable is the parameter to be controlled and manipulated. In the non-experimental case, such as in the die design and manufacturing process where there is no experimental manipulation, the independent variable is the variable that 'logically' has some effect on a dependent variable (Kerlinger, 1986).

The independent variables which participated in the study were:

- area reduction
- approach angle
- entrance angle
- bearing length
- die exit angle
- drawing velocity
- coefficient of friction

(b) Dependent Variables

The dependent variable refers to the status of the 'effect' (or outcome) in which the researcher is interested (Rosenthal and Rosnow, 1991). The dependent variables used in this research were:

- drawing force
- die temperature
- drawing stress
- strain rate
- damage value

3.3.2 Independent Variables

The major independent variable associated with the die geometrical parameters, ***bearing length***, was varied while keeping the other die geometrical parameters (Δ-parameter, entrance angle, exit angle) and process conditions (drawing velocity, coefficient of friction and wire material properties) constant during the study.

The choice of *optimum independent* parameters was based on iterative modelling from which a parameter with less effect on damage value was chosen. Figure 3.5 shows the categorisation of the different independent variables based on die geometry, process conditions and wire material properties. The figure shows that the underlying parameters within each variable have an influence on the progression of wire drawing.

(1) Material State Based Independent Variables

The following are the independent variables pertaining to material properties used in copper wire drawing study:

(i) Inclusions, N_{inc}

These are both non-metallic and metallic additions to a material’s composition. They affect the quality of the input wire and stress distribution in the wire (Norasethasopon, 2003). The inclusions were assumed and kept constant during the study.

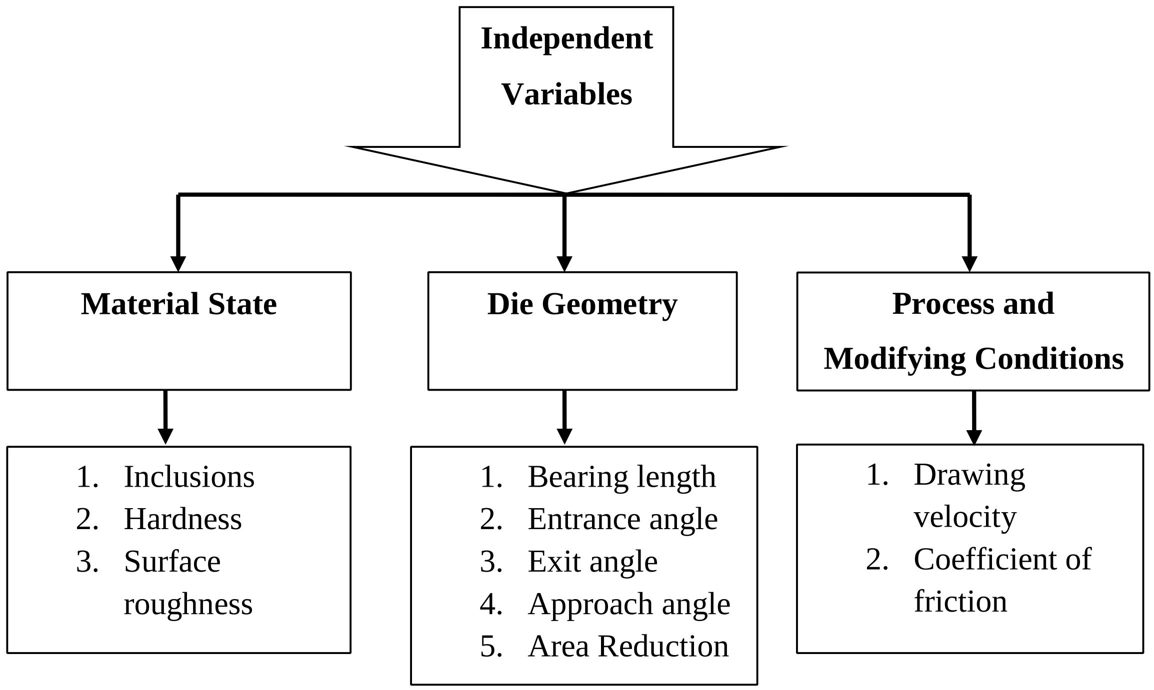

Figure 3.5 Independent Variables in Copper Wire Drawing. (Source: Author)

(ii) Hardness, H

Hardness is the material's resistance to penetration and affects both the wire and die wear and die life. Material hardness of the die was kept constant during the study.

(iii) Surface roughness, R_a

Surface roughness is a measure of the material's surface asperities, hence the quality of finish of the material. The quality of any finished surface influences the function and wear of the component (Simmons and Maguire, 1974). The surface roughness of the tungsten carbide drawing was maintained constant.

(2) Die Geometry Based Independent Variables

The following are the independent variables pertaining to the die geometry:

(i) Approach angle, α

The Approach Angle is designed such that it allows for a smooth and controlled deformation of the wire. Harder materials, larger area reductions and bigger elongations require smaller approach angles of between 6^o to 8^o , whereas softer materials, smaller area reductions and shorter elongations are drawn with bigger approach angles ranging from 8^o to 10^o (Esteves Group, 2008). The approach angle was initially varied then maintained constant. This was based both on models performed and on the findings by Norasethasopon and Yoshida, (2003) and Kabayama, *et al*., (2009) where an approach angle of 9^o was determined as being optimum.

(ii) Area reduction, A_r

The area reduction characterises the extent of deformations imposed on a workpiece, hence influences the redundant work, frictional work and drawing forces (Valberg, 2010; Hosford and Caddell, 1983). In the study, which is a multi-pass wire drawing, the area reduction was initially varied at each pass, ranging from 10% to 20%, and then maintained constant.

Both the area reduction and the approach angle are used to compute the Δ-parameter which characterizes the shape of the deformation zone and is used as a predictor of void formation. Void formation and centre bursting are attributed to higher values of Δ (above 3.0) which are indicative of high levels of redundant deformation and surface hardening (Descargas, nd).

(iii) Die entrance angle, β

The entrance angle facilitates for a smooth transition to the approach zone and conditions of lower die angles, and thus a lower Δ-parameter. This reduces redundant work, die pressure, and centerline tension at the end of the pass (Wright, 2011). The entrance angle, therefore, has an effect on the following: redundant work, die pressure, die wear and central bursting. The entrance angle was initially varied and then maintained constant at 30^o during the study.

(iv) Bearing length, L_b

This produces a frictional drag on the wire and also removes surface damage due to die wear, without changing dimensions (Udomphol, 2007). The bearing land has an effect on the quality of wire surface, frictional work and drawing stress (Esteves Group, 2008; Wright, 2011). The bearing length was varied during the study from 30% to 50% of the final wire diameter.

(v) Die exit angle, γ

This allows the metal to expand slightly as the wire leaves the die and also minimises abrasion if the drawing stops or the die is out of alignment (Udomphol, 2007). The die exit angle has effects on the release of elastic energy and quality of wire surface (Wright, 2011). The exit angle was initially varied and then maintained constant at 40^o during the study.

(3) Process and Modifying Condition Based Independent Variables

The following are the independent variables pertaining to process conditions used in the study of copper wire drawing:

(i) Drawing velocity, v_{dr}

During wire drawing practice, drawing speed has an effect on the drawing power, strain rate, drawing temperature and wire quality (Wright, 2011; Byon *et al*., 2011). The drawing velocity was initially varied then kept constant during the study.

(ii) Coefficient of friction, μ

The friction coefficient, hence lubrication, has an effect on drawing speed (hence drawing force), drawing stress, wire quality and die life (Kabayama *et al*., 2009; Valberg, 2010). The Coulomb coefficient of friction is varied initially then kept constant during the study.

3.3.3 Dependent Variables

The dependent variables arise due to the interaction of the independent variables. Figure 3.6 shows the dependent variables based on material properties, die geometry and process conditions. The figure shows that during processing of copper wire, the levels of stress, strain rate and the damage value have an impact on the final material. The drawing force and die temperature need to be monitored throughout the process.

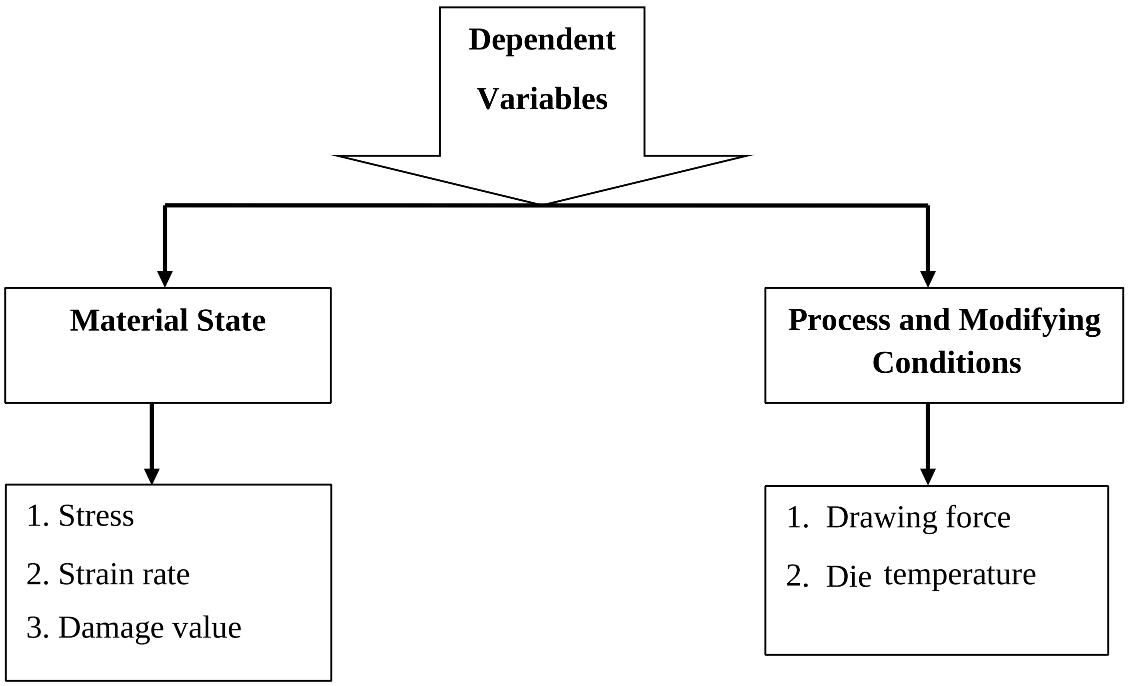

Figure 3.6: Dependent Variables during Copper Wire Drawing. (Source: Author)

(1) Material State Based Dependent Variables

The following are the dependent variables relating to material properties:

(i) Drawing stress, σ_d

Drawing stresses have an effect on the drawability of copper wire and are a result of the interaction of the material yield stress, the Δ-parameter, the friction coefficient and the bearing length.

(ii) Strain rate, $\dot{\varepsilon}$

Strain is the ratio of the change in dimension to the original dimension of the copper wire material, while strain rate is the rate at which this strain occurs. Changes in strain rate have a significant impact on wire flow stress (Wright, 2011).

(2) Die Geometry Based Dependent Variables

The following is the dependent variable used in the study of die geometry during copper wire drawing:

(i) Die wear, δ

Die wear is as a result of contact force between the wire and the die, the temperature and tribological conditions at the wire-die interface

(3) Process and Modifying Condition Based Dependent Variables

Dependent variables used in the study of process conditions during wire drawing include the following:

(i) Drawing force, F_{dr}

The drawing force under friction and redundant conditions is based on the friction coefficient, the value of the Δ-parameter and the flow stress (Kalpakjian and Schmid, 2010).

(ii) Die temperature, T_{int}

Due to heat generated as a result of the frictional and redundant conditions as a result of the interaction between the moving wire and the stationary die, thermal impacts greatly affect wire quality, lubrication effectiveness, surface conditions and die wear (Descargas, nd).

3.3.4 Integrated Model

Having determined the independent and dependent variables for copper wire drawing, the integrated model resulting from the effects of the variables is presented in Figure 3.7. The figure shows that for the production of a good quality wire, all the variables (material state, die geometry, process and modifying conditions) need to interact in order for the attainment of effective workability of the copper rod, and consequently the quality of the copper wire.

3.3.4.1 Selection of Computational Optimum Wire Drawing Conditions

Figure 3.8 shows the algorithm used to select the optimum die and wire drawing operating conditions for the independent variables. The die and process parameters used for the first model were derived from reviewed literature. The consequent parameters were all based on the results of the preceding models based on obtaining the conditions that were unfavourable for both ductile damage initiation and progression. Thus, a copper wire product with good quality and arising from the integrated model in Figure 3.7 was predicted.

The algorithm in Figure 3.8 which is used in modelling a wire drawing process, entails that in a bid to achieve the optimality of the wire drawing process, all the other previously mentioned parameters need to be assessed. Starting with the bearing length, a good performing bearing length size is used and replicated in the assessment of other parameters.

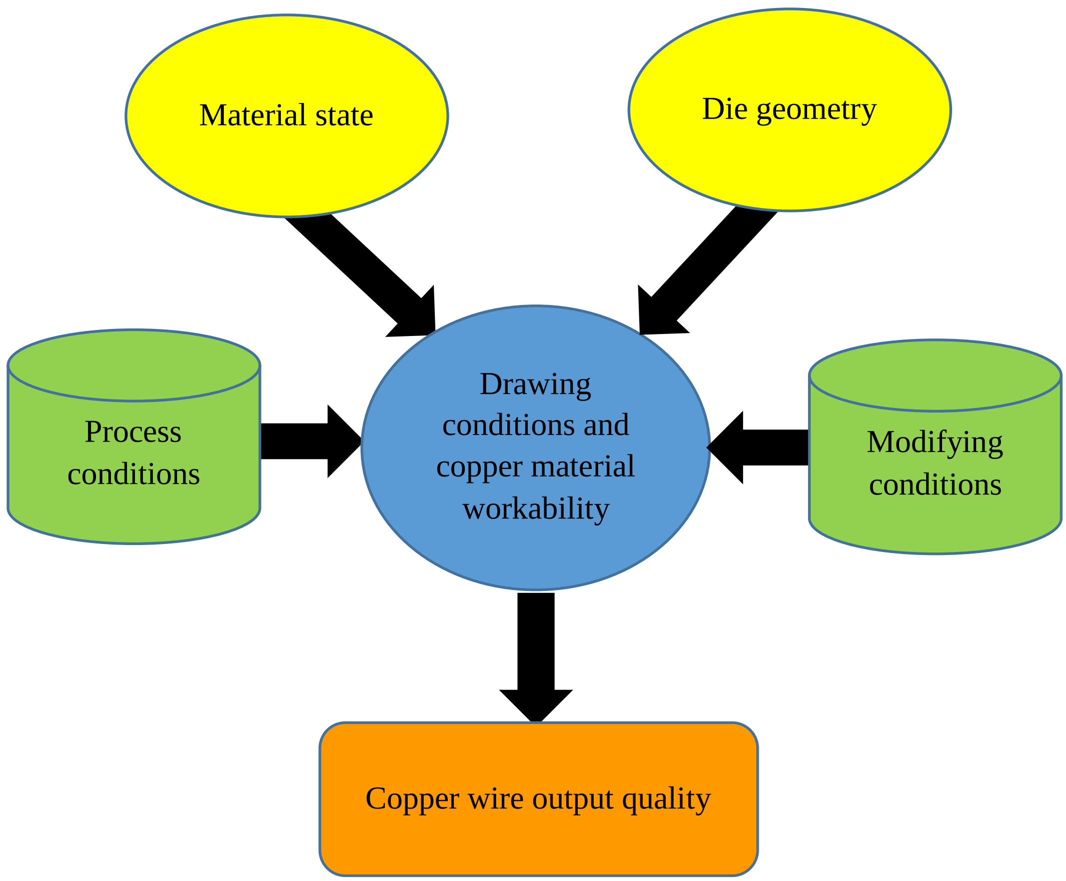

Figure 3.7: Integrated Model for Copper Wire Output Quality. (Source: Author)

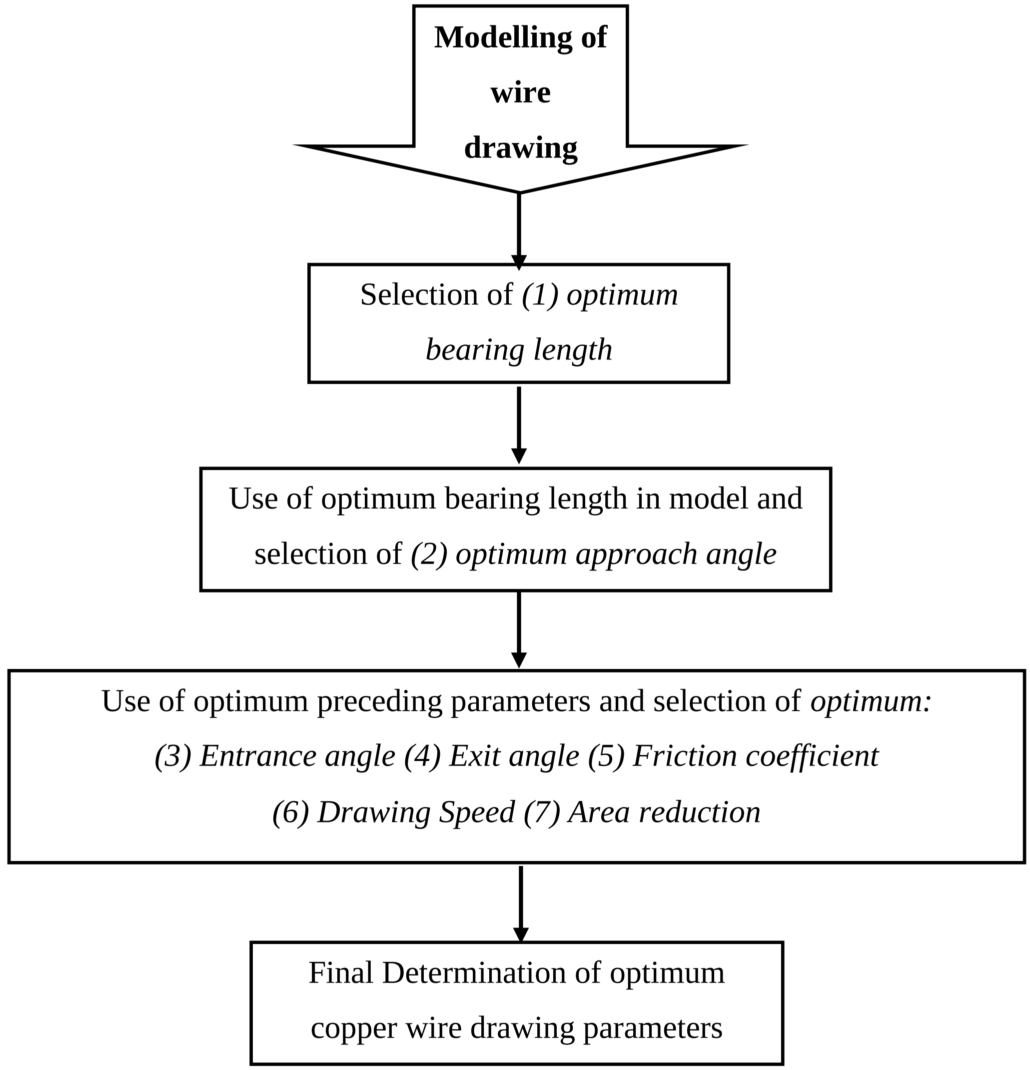

Figure 3.8: Procedure for the Determination of Optimum Variables for Copper Wire Drawing. (Source: Author)

3.4 Die Design and Manufacturing

In order to investigate the die design and manufacturing practices involved in copper wire drawing, a *prototype design and manufacturing* approach is necessary. This involves a model die design and manufacturing phase in order to establish aspects of the die design and manufacturing process that are likely to have an impact during wire drawing practice. Figure 3.9 shows a flow chart for the die design and manufacturing process concept. The figure shows that in trying to achieve a prototype of the die, both the design and manufacturability concerns have to be taken into account. Manufacturing will only take place once the design considerations have been approved, whereas manufacturing proceeds after both the design aspects and process capability aspects have been taken into account.

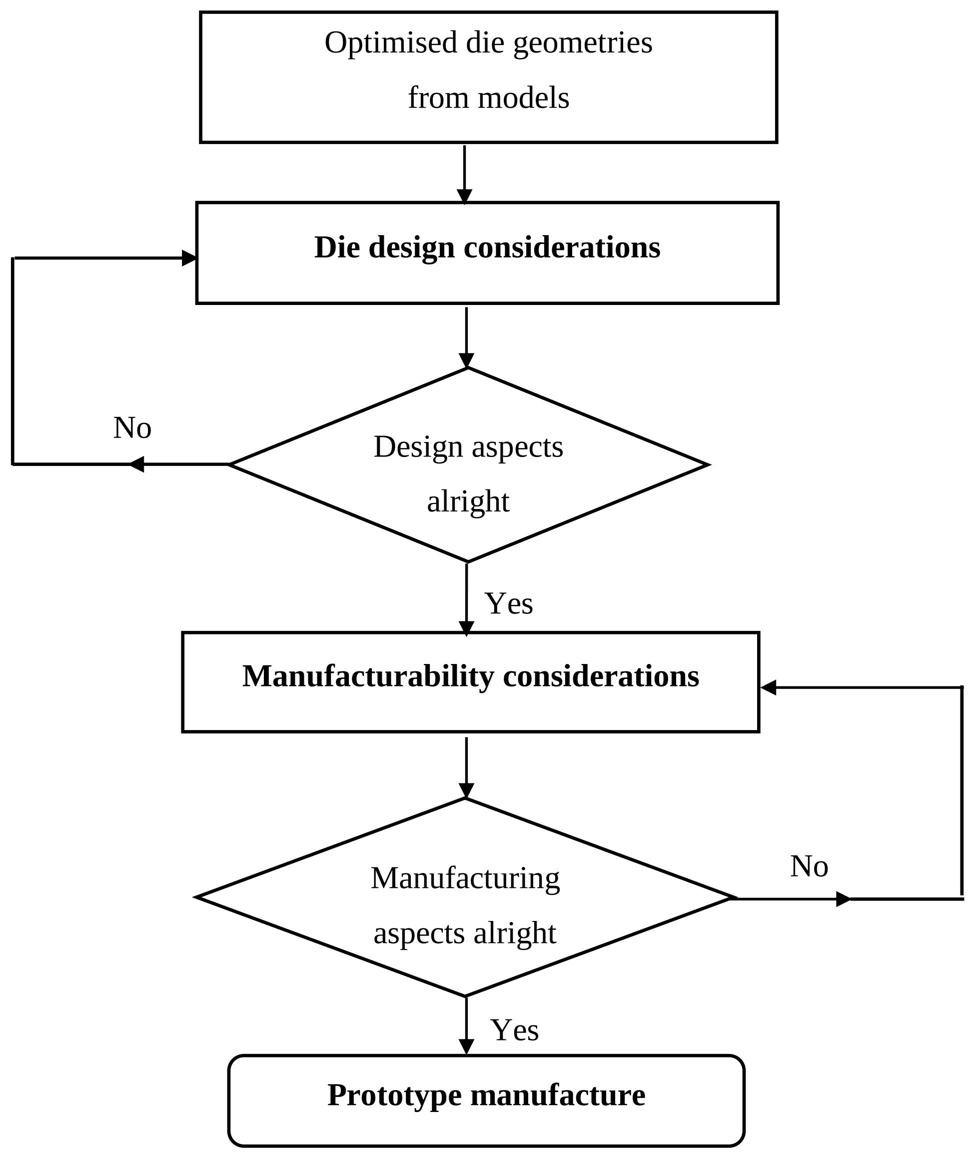

Figure 3.9: Flowchart for Die Design and Prototype Manufacturing. (Source: Author)

3.5 Expected Research Outcomes

Arising from the determination of the dependent variables outlined in Figure 3.7, the expected research outcomes are shown in Figure 3.10. The figure shows that in order to assess the damage value during wire drawing, both the optimized die geometries and the optimized modifying conditions should be have been taken into consideration. These considerations will be influenced by changes in die temperature, drawing force, drawing stress and the strain rate.

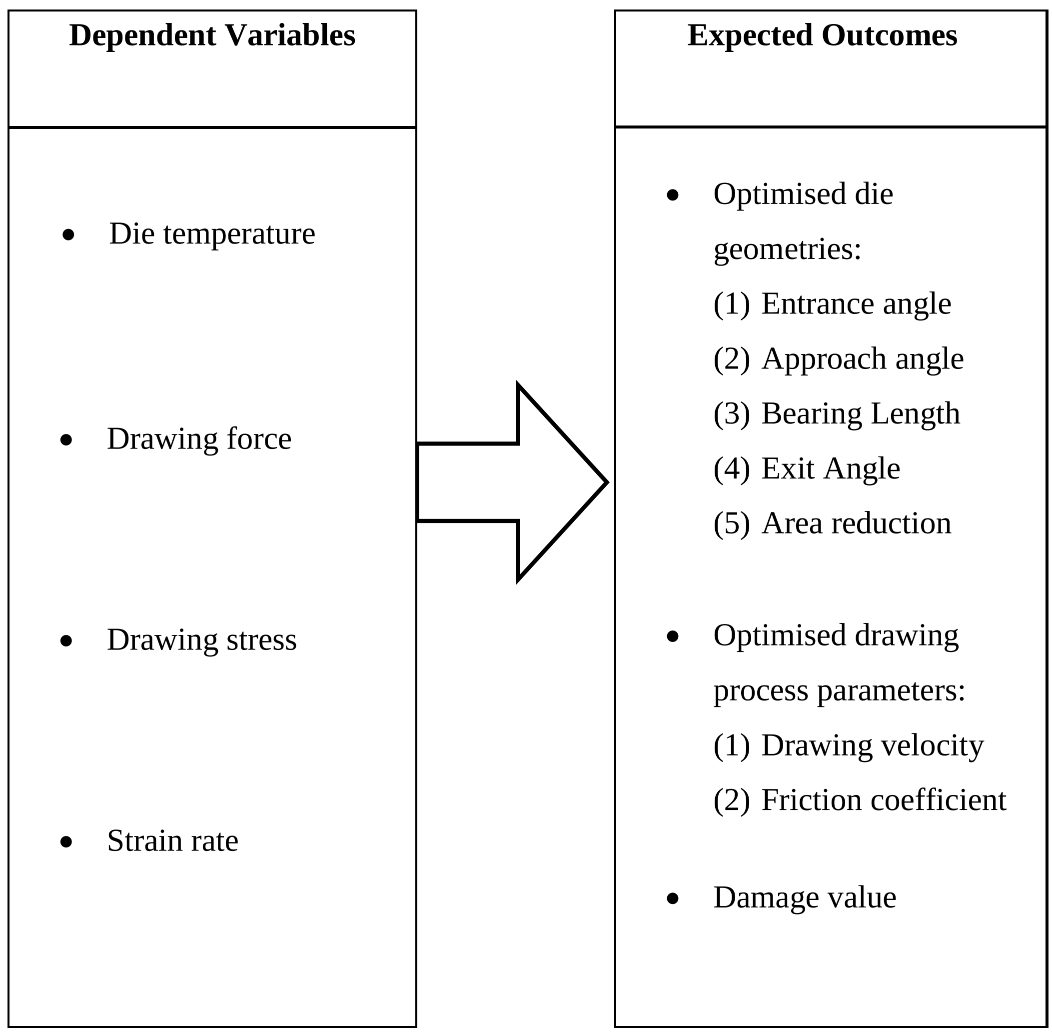

Figure 3.10: Expected Outcomes during Copper Wire Drawing Study. (Source: Author)

CHAPTER FOUR: RESEARCH METHODOLOGY

4.1 Introduction

The research is based on the mechanics and production technology of bulk deformation and copper metallurgy in wire drawing. In order to find solutions to such complex phenomena which involve stress analysis and solid mechanics problems, the FEM approach is used. This numerical or computational approach is widely used to determine the distribution of stress field variables governing processes of metal forming.

The purpose of the research was to investigate the die design, manufacturing practices and copper wire drawing process conditions leading to chevron and surface crack formation. This was done by both developing a copper wire drawing model using the finite element method and experimental investigations of copper wire drawing. In order to achieve the mentioned objectives, the influence of different die geometries and process conditions for copper wire drawing were studied.

The *independent variables* which participated in the study included the area reduction, approach angle, die entrance angle, bearing length, die exit angle, drawing velocity, coefficient of friction, wire material properties, while the *dependent variables* were the drawing stress and strain, die wear, drawing force and die-wire interface temperature. Parametric studies of these factors were carried out in order to establish their effect on chevron and surface crack formation during copper wire drawing.

Each of the die geometrical parameters (area reduction, approach angle, entrance angle, bearing length and die exit angle) were varied while keeping the drawing velocity, coefficient of friction and wire material properties constant against the dependent variables. The *optimum die geometries* and operating conditions during copper wire drawing were thus derived.

Therefore, this chapter discusses how the research was designed and the methods that were used in order to achieve the intended objectives. Also highlighted are limitations and ethical considerations of the research.

4.2 Research Design

4.2.1 General Method

The general method involved modelling and simulation of factors involved in copper wire drawing and carrying out industrial experiments, with an extended literature review of the die design and manufacturing process. The FEM approach was used with ABAQUS 6.14 software to model the problem. This was done for the purpose of studying the effect of die geometries and process conditions on chevron and surface cracking during copper wire drawing.

4.2.2 Specific Procedures

(i) Modelling and Simulation of the Copper Wire Drawing Process

Initially theoretical data pertaining to the major factors involved in copper wire drawing process was used to model and simulate a copper wire drawing process. This data was then analysed and used for comparative analysis with actual experimental data to optimise the wire drawing process. Using the FEM, a computational and geometrical model of copper wire drawing was developed. This incorporated die design, copper wire material properties and dimensions and drawing process conditions. A simulation of the model was then done and analysed. This was followed by an optimisation process which was undertaken in order to identify optimum operating conditions for the process. Table 4.1 gives details of parameters used in the modelling and simulation runs for investigating the effect of bearing length variation, while Table 4.2 provides details of parameters used for investigating other die geometry and process condition effects. The bearing length was fixed at 40% in order to isolate its effects on wire drawing, having been determined as being optimal at 40%.

Table 4.1: Research Design for Modeling Effect of Bearing Length Variation.

Simulation Run	**Multi-Pass Stage**	***Constants:*** $2\alpha = 20^o$; $2\beta = 40^o$; $2\gamma = 60^o$; $\mu = 0.04$; $v_{dr} = 0.08\ ms^{-1}$	
		Bearing Length (%)	**Area Reduction (%)**
1	1-2	30; 35; 40; 45; 50	17.226
2	2-3	30; 35; 40; 45; 50	17.284
3	3-4	30; 35; 40; 45; 50	17.199
4	4-5	30; 35; 40; 45; 50	14.052

(Source: Author)

Table 4.2: Research Design for Modeling Effect of other Independent Variables.

Independent Variable	***Constant:*** Bearing Length = 40%				
	1	**2**	**3**	**4**	**5**
Entrance Angle, β (^{o})	20	25	30	35	40
Approach Angle, α (^{o})	8	9	10	11	12
Exit Angle, γ (^{o})	10	20	30	40	50
Coulomb Friction Coefficient, μ	0.01	0.03	0.05	0.07	0.09
Drawing Velocity, v_{dr} (m/s)	0.04	0.06	0.08	0.10	0.12
Area Reduction (%)	10	12	14	16	18

(Source: Author)

The FEM was chosen due to its strength in easily identifying the key variables involved in wire drawing and creating a 2D representation of the process. Due to its being iterative in nature, the FEM can be easily repeated in order to achieve an optimal performance of the process, thus reducing the cost of undertaking real practical processes. Some of the weaknesses of the FEM include the requirement of large computational times, need for long practice and mastering of the software and the possibilities of introducing errors during the construction of the model (Liu and Quek, 2003).

(ii) Experimental Procedures

Both laboratory and industrial experiments were carried out in the research. They were done in order to test the theories. The laboratory experiments were meant for the analysis of the copper material, the drawing lubricants and the draw dies. Industrial experiments were also undertaken to manufacture sample or prototype draw dies based on the optimised die geometries from the models in order to investigate the interaction and behaviour of wire drawing process parameters.

Tables 4.3, 4.4 and 4.5 give details of variables used in the laboratory experimental design for use in the wire drawing process.

Table 4.3: Details of Laboratory Experimental Research Design: Copper Material Properties.

	Material Properties	
	Composition	*Engineering Properties*
Sample Type	Wrought Copper Rod	Wrought Copper Rod

(Source: Author)

Table 4.4: Details of Laboratory Experimental Research Design: Lubricant Properties.

	Lubricant Material Parameters	
	Specific gravity	*Kinematic viscosity*
Sample Type	Lubricant	Lubricant

(Source: Author)

Table 4.5: Details of Industrial Experimental Wire Drawing Research Design.

Experiment No	**Multi-Pass Stage**	***Die Geometry Constants:*** $2\alpha = 20^o$; $2\beta = 40^o$; $2\gamma = 60^o$;	
		Bearing Length (%)	**Area Reduction (%)**
1	1-2	30; 40; 50	17.226
2	2-3	30; 40; 50	17.284
3	3-4	30; 40; 50	17.199
4	4-5	30; 40; 50	14.052

(Source: Author)

Though industrial experiments have lower level of control, they offer the best alternative due to the high cost of setting up a wire drawing laboratory. The weaknesses associated with the experimental procedures in general include the difficulty of identifying and controlling outside variables that may influence the results, possibility of errors in the accuracy of measurements and the high costs associated with equipment and tooling (Ghosh, 1992).

4.3 Die Design and Manufacturing

The prototype die design and manufacturing approach used involved design of die geometry parameters and their manufacturability, impacting on the wire drawing process. Both die and manufacturing considerations were established.

4.3.1 Die Design Considerations

2D and 3D design drawings of a tungsten carbide draw die were made using ABAQUS and Solidworks softwares. The designs were based on optimised parameters from the FEM models and simulations, and process experimental procedure. The model designs were then subjected to a die design consideration process which focused on the following aspects (Society of Manufacturing Engineers , 1962; Shearer, 2008):

(i) Die Geometry

The design of the draw die conformed to the exact shape of the die, hence the exact shape and size of the wire product.

(ii) Tensile strength

The designed draw die had to withstand the applied loads without fracture.

(iii) Hardness

The designed draw die had to have appropriate hardness levels to withstand wear or abrasion under normal operating conditions.

(iv) Corrosion

The designed draw die had to withstand a corrosive environment or medium during wire drawing practice.

(v) Impact resistance

The draw die had to have the necessary toughness and ability to resist breaking.

(vi) Friction conditions

The draw die needed to be able to maintain a lubricant in the die-wire interface, and thus reduce friction between the die and wire.

(vii) Fatigue

The designed draw die had to withstand breakage under conditions of repeated cyclic loads.

(viii) Thermal properties

The draw die needed to be able to maintain its strength at elevated temperatures.

(ix) Stress risers

All stress risers or stress concentrations in the designed draw die were eliminated.

4.3.2 Die Manufacturability Considerations

Having determined the die design aspects, a prototype draw die was manufactured based on a consideration of the following manufacturability aspects (Upadhyaya, 2002; Suchy, 2006; Shearer, 2008).

(i) Nature of die raw material

Tungsten carbide grain properties and characteristics based on the specific method of producing the raw powder.

(ii) Outline of part and its size

Sharp and feather edges were avoided in the prototype draw die.

(iii) Applicable tolerance ranges

Dimensional and geometrical tolerance ranges were not too tight or out of ordinary.

(iv) Surface finish

A functional smoothness of the die surface was maintained.

(v) Attachment and assembly methods

Due to the brittle nature of tungsten carbide, the die nib was joined to a tougher steel material.

Tables 4.6 and 4.7 show details of the research instruments used and the expected outputs.

Table 4.6: Principle Research Areas and Instruments.

No.	Principle Area	Underlying Theory	Procedure	Research Instrument
1.	Material Properties	• Plasticity and strength of materials • Fracture criteria of metals	• Stress-strain curve • Data collection	• Tensile test • Microscopy
2.	Die Design	• Die design features and characteristics.	• Draw die design • Data collection	• ABAQUS • SolidWorks • Industrial experiment
3.	Draw Die Manufacturing	• Die manufacturing technology	• Material selection • Die manufacturing process selection	• Industrial experiment • Laboratory testing
4.	Copper Wire Drawing	• Conventional wire drawing process • Lubrication	• Computer modeling and simulation • Data collection	• ABAQUS • Industrial experiment • Surface chracteristics

(Source: Author)

Table 4.7: Expected Research Outputs.

No.	Research Objective	Requirements	Required Input Data	Expected Outputs
1.	To develop an integrated model for die geometry and process parameters for multi-pass copper wire drawing	• Die design aspects • Modifying conditions aspects • Multi-pass wire drawing modelling	• Die profile Parameters • Modifying conditions parameters • Multi-pass wire drawing models	• Profiled rigid die model • Copper wire model • Integrated multi-pass wire drawing model
2.	To determine the Δ-parameter values, die geometrical parameters and process conditions leading to the manifestation of surface and chevron cracks during wire drawing	• Copper material • Pass schedules • Die geometry • Friction conditions • Ductile damage multi-pass wire drawing modelling	Copper wire material properties Area reductions Approach angle Coulomb friction coefficient Wire drawing process model with ductile damage	• Stress-strain curve • Flow curve • Drawing stress • Δ-parameter values • Strain rate • Wire damage value

Table 4.7: Expected Research Outputs (Continued)

No.	Research Questions	Requirements	Required Input Data	Expected Outputs
3.	To establish die design and manufacturing aspects influencing accuracy of die geometry	Experimental data on draw die design and manufacturing aspects. Investigation of die manufacturing process	• Die material composition • Die profile design techniques • Die production techniques	• Die materials constituents. • Die profile parameters • Prototype manufacture of draw die
4.	To validate the developed models using industry-based copper wire drawing process setup	Modelling and simulations of the wire drawing process Industrial experimental investigation of wire drawing process	• Copper wire material properties • Die material and design geometry • Wire drawing lubricant properties • Wire drawing process operating conditions	• Optimised die geometries • Optimised wire drawing process parameters

(Source: Author)

4.4 Application of the Methods

(i) The FEM Approach

The FEM approach is based on three stages which involve procedural modelling, simulation and visualisation of the process. The first stage or computational modelling involves four steps which include: modelling the geometry, meshing or discretisation of the geometry, specification of material properties and specification of boundary, initial and loading conditions.

The geometry of the model is meshed or discretised by using a number of elements which are made up of grids and nodes (Liu and Quek, 2003). In this stage, which is a *pre-processing* stage, the raw wire and die materials are specified, designed and analysed. This stage is important due to the need for change or variation of the die profile parameters and processing conditions (indepenedent variables) which are necessary for the current research.

The second stage of the FEM approach involves simulation of the model and this is based mainly on energy principles. In this stage, the created computational model is fed to the solver to solve the discretised system and simultaneous equations for the variables at the nodes of the mesh. This is a *processing* stage and is necessary for obtaining the dependent variables of the wire drawing process.

The third and last stage of the FEM approach is a *post-processing* stage. In this stage the results from the processing stage are visualised. This is necessary because the information generated after processing is a large amount of digital data which needs to be interpolated, analysed and presented. Thus 2D objects and field variables can be displayed. This stage is important for analysis and decision-making concerning the simulated wire drawing process.

(ii) Experimental Procedures

Industrial experiments were done to get data in form of images, movements and behaviour of mechanical systems during die manufacturing and wire drawing. The die manufacturing process was studied in order to fully understand the design, materials and manufacturing technology of the draw die. Design drawings were then made with full material and die geometry specifications in order to manufacture prototype dies.

Laboratory experiments were undertaken in order to obtain both copper wire material properties and behaviour, and the draw die material properties. Wire drawing experiments were conducted based on the current industrial setup of the local firms involved in copper wire drawing. The experiments conducted involved the medium size (1.78 mm diameter) copper wires. This was done in order to validate the data obtained from the FEM approach, and thus optimise the actual process with the aim of reducing defects during the drawing process.

4.5 Major Research Instruments

In order to carry out this research, information and data on die design, manufacturing and copper wire drawing process and practices was collected using the major research instruments given in Tables 4.6 and 4.7. Tables 4.8, 4.9 and 4.10 show details of the various research instruments used and their principle application areas.

(i) Microscopes

An electron microscope, Olympus make and model CH2, was used to determine the microstructure of the 8 mm raw copper rods. A scanning electron microscope (SEM), model Quanta FEG 450, was used to detect the level and size of defects in the copper rod microstructure. The SEM was appropriate in that both macro (surface based) and micro (internal) defect analysis could be done with high resolution. This is because the SEM is able to give magnifications of up to 5000X in order to expose both the micro- and macro-defects.

(ii) Tensile Tester

A universal tensile testing machine, model TUE C-600, with a load cell capacity of 12 to 600 kN capacity and a load accuracy of 1% of indicated load, was used for obtaining the wire material mechanical properties. The test was appropriate for obtaining the stress-strain data under tensile force conditions.

(iii) Wire Drawing Machine

An industrial intermediate copper wire drawing machine, model HT-450 13D, was used in the determination of the wire drawing process parameters. The wire drawing machine was the source of work and power, hence important in the analysis of process efficiency.

Table 4.8: Research Instruments used for Copper Material Investigation.

Principle Area	Task Description	Input Parameter/ Application	Methodology	Equipment	
				Name	Type/Model
Material Investigation	Experimental investigation of copper rod and wire material	Chemical Composition	Experiment	Spectrometer	Atomic Absorption Spectrophotometry
		Microstructure	Experiment	Microscope	Olympus Microscope, model CH2; Scanning Electron Microscope, model Quanta FEG 450
		Engineering properties	Experiment	Tensile Test	Tensile Testing Machine, model TUE C-600
		Physical properties	Experiment	Micrometer/ Vernier Caliper	Bestir micrometer, model 01651 HD Vernier caliper

(Source: Author)

Table 4.9: Research Instruments used for Die Design and Manufacturing Investigation.

Principle Area	Task Description	Input Parameter/ Application	Methodology	Equipment/Software	
				Name	**Type/Model**
Die Design	Die Design	Design Methods	Design and Draughting	ABAQUS CAE Solidworks 2012	2D and 3D Drawings
Die Manufacturing	Die Manufacturing	Manufacturing Methods and Practices	Industrial Experiment	Digital Camera Powder Metallurgy Equipment	Samsung WB 1100F Compacting machine Sintering machine

(Source: Author)

Table 4.10: Research Instruments and Application Areas for Wire Drawing Process Investigation.

Principle Area	**Task Description**	**Input / Output Parameter or Application**	**Methodology**	**Equipment/Software**	
				Name	**Type/ Model**
Multi-pass Copper Wire Drawing Process (Modelling and Analysis)	Finite Element Modelling of the Wire Drawing Process and Coupling with Excel spreadsheets	2D ABAQUS wire and die drawings Material specification Processing conditions	2D draughting Material CAE input Boundary and processing conditions input	2D ABAQUS CAE ABAQUS modelling Spreadsheet Analysis	ABAQUS 6.14 software Microsoft Excel
Multi-pass Copper Wire Drawing Process (Experimental Procedure)	Experimental Analysis of the Wire Drawing Process	Die Temperature	Experiment	Contact Thermocouple	TWOK Digital Thermometer
		Drawing Velocity	Experiment	Velocity tester	Bushnell velocity gun
		Wire surface and internal cracks	Experiment	Microscopy	Scanning Electron Microscope

(Source: Author)

4.6 Data Collection

Wire drawing practice in Zambia is mainly concentrated along the main line of rail in the Central, Copperbelt and Lusaka provinces of Zambia due to the availability of the copper raw material. Apart from the raw materials, the wire drawing industries are also critically dependent on draw die and drawing lubricant supply. Due to the high technical skills needed for draw die design and manufacturing, only one draw die local manufacturing entity located in Central Province currently exists. Lubricant supply is readily available and offered by a number of local oil marketing companies whose offices are found along the main line of rail.

The copper wire drawing firms obtain their raw copper materials from the same local sources which are the mining companies, hence the consistency in the raw copper materials being analysed. The population of copper wire drawing firms is currently four companies in Zambia.

Out of the population of four, two companies were used for investigation. The 8 mm raw wrought copper rod material was collected from one company. The raw rods were then subjected to both rod breakdown and intermediate wire drawing at a second location due to the use of prototype design dies. For each die, about 50 metres of drawn wire were obtained and investigated.

During the modelling and simulation of the wire drawing process, five sets of varying bearing length (30%, 35%, 40%, 45% and 50%) were used and the following data for each multi-pass stage and for two nodes (one surface and one internal) was collected:

- Mises equivalent and hydrostatic stresses
- Equivalent plastic strains and strain rates
- Stress triaxiality values
- Drawing forces
- Damage values
- Cockroft and Latham fracture criterion values

During both the laboratory and industrial experiments, data was collected on the following parameters:

- Engineering properties of copper
- Microstructure of undrawn copper
- Drawing speeds
- Die temperatures
- Lubricant temperatures and properties
- Microstructure of drawn copper (with defect investigation)

Data on the engineering properties and microstructure of the raw wrought copper rods was collected using the universal tensile testing machine and the microscopes. Data on drawing speeds, die and lubricant temperatures was collected in-situ during the wire drawing process, using a velocity gun and a digital thermometer respectively. Data on the properties of the lubricant was collected by collecting a sample of the raw lubricant which was then subjected to a laboratory kinematic viscosity test.

Data on the investigation of defects arising from the wire drawing process was collected by obtaining sections of the drawn wire from each multi-pass stage using three different die bearing sections sets (30%, 40% and 50%) and subjecting the wire sections to both surface and internal microstructure investigation.

The raw materials and copper wires used in the study were fully representative of the current local wire drawing population. The use of an industrial wire drawing machine for purposes of this study was arrived at due to lack of laboratory equipment at local learning institutions.

The data collected was reliable in that it was from the actual industrial practice. The industrial experiments taken at different shifts and for over a month was sufficient for a good analysis of the process.

4.7 Data Analysis

The data collected from simulations for each node and each pass was analysed qualitatively using the stress pattern contours and quantitatively by querying the value of each parameter during the modelling process. The quantitative data was collected by noting the querried values and inserting them into Microsoft excel sheets, from which graphs were then plotted for analysis.

The data collected from industrial experiments for each varying bearing set was analysed quantitatively by noting the value of each parameter during the wire drawing process. Data on microstructure tests was analysed qualitatively by using scanning electron micrographs for each multi-pass stage.

In both cases, the data obtained was subjected to removal of measurement errors and averaged for a standard value of the measured parameter. The major factors involved in copper wire drawing were varied to obtain predictive optimum values from the simulation. The optimum values of the parameters acted as comparative yardsticks to the experimental procedures. From the experimental procedures, standard operational parameters were established. A comparison of the two sets of data (simulated and experimentally obtained) was then done.

4.8 Limitations

Industrial experimental procedures have the limitation of company production targets which hinder the careful and repetitive nature of the required experiments. Unlike with ordinary laboratory experiments, administration of necessary instruments during a production run thus becomes difficult. Often, permission has to be sought through management hierarchy. Despite the limitations mentioned above, all necessary steps were taken to ensure that the required sample size and quality of data was worthwhile.

4.9 Ethical considerations

Potential ethical problems in this research included the possibility of being involved in an industrial dispute due to subjection to company employee rules and the need to safeguard company records and secrets. Thus, line supervisors and managers were consulted and permission sought before any procedure was undertaken. Equally, all data obtained from the companies was treated with the strictest confidence.

CHAPTER FIVE: MODELLING AND SIMULATION

5.1 Introduction

This chapter is divided into four major sections. The first section presents a theoretical background to the Finite Element Method (FEM) and the software ABAQUS 6.14 and its application to the current study. The second section presents the computational conditions used in modelling and simulation of the copper wire drawing process. This section gives insight into the different copper wire material properties, die geometry and wire drawing variables used in the research in order to achieve the objectives of the study. The third section presents results of the simulation using damage for ductile metals procedure for selected surface and centerline nodes.

5.2 Finite Element Method

The Finite Element Method (FEM) is used in engineering practice to model and solve physical problems involving solids, structures, fluids and heat transfer (Bathe, 1996). The physical problem as applied in this case is the drawing of copper wire by metal forming. The copper wire is subjected to loading as it passes through a drawing die. This physical problem is idealised by a mathematical model which is governed by differential equations. The mathematical model is solved by the finite element analysis based on the behaviour of the material under consideration, namely *elastic-plastic*, *rigid-plastic* and *visco-plastic*. For the current study, the elastic-plastic behaviour of material is used in the FEM.

Figure 5.1 gives a summary of the FEM. The figure shows that the FEM is a numerical procedure, hence it is necessary to assess the accuracy of the solution. The solution is normally repeated with refined solution parameters (such as finer meshes) until a sufficient accuracy is reached (Ibid).

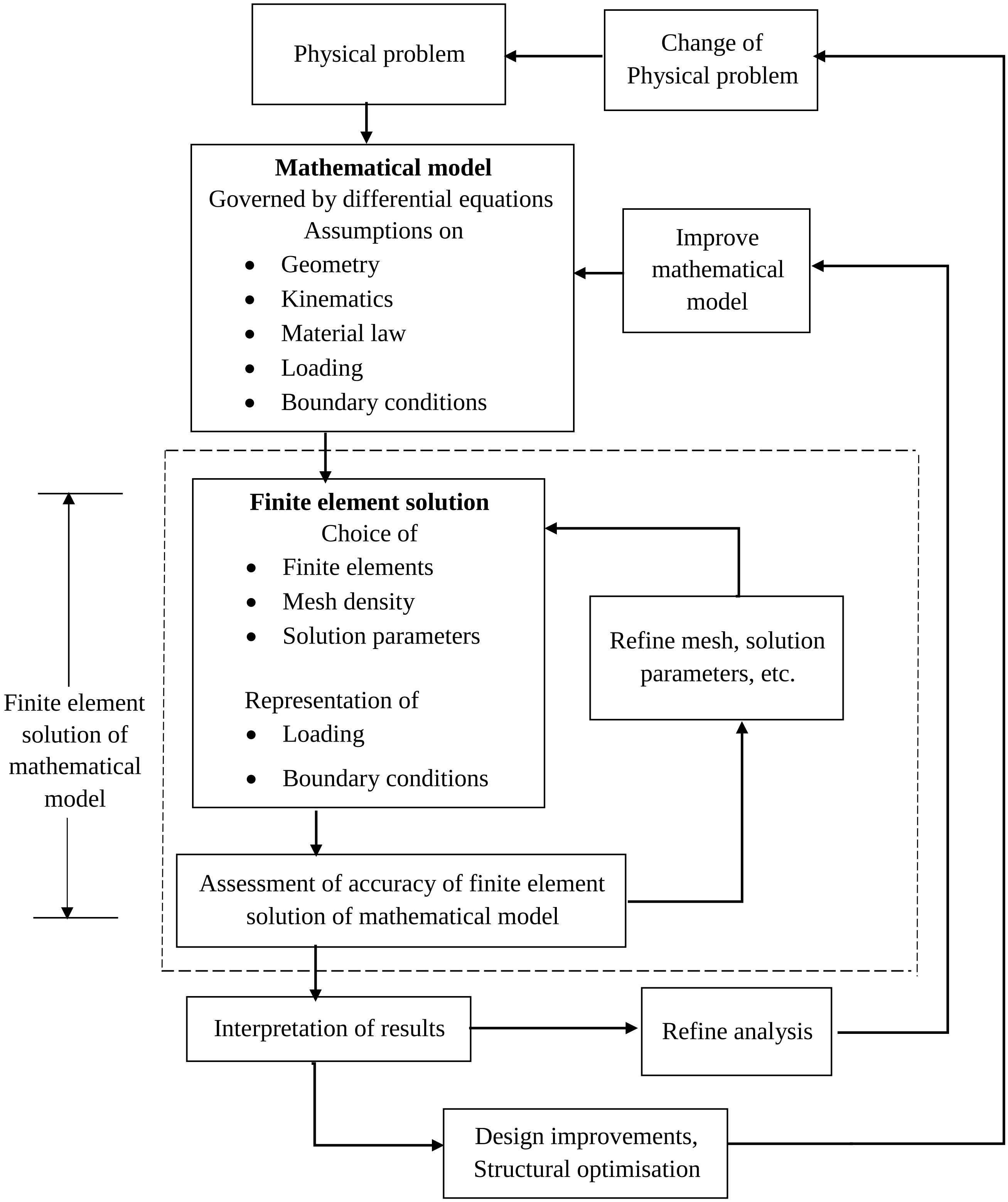

Figure 5.1: The Process of Finite Element Analysis. (Source: Bathe, 1996)

5.3 Finite Element Software: ABAQUS

ABAQUS 6.14 is a suite of engineering simulation programmes based on the finite element method that can solve problems involving linear and non-linear analyses. It contains an extensive library of elements that can model virtually any geometry. ABAQUS contains an extensive list of material models that can simulate the behaviour of many engineering materials which include metals, polymers, composites, rubber, reinforced concrete, crushable and resilient foams, soils and rocks. A complete ABAQUS analysis consists of the following three distinct stages (Dassault Systèmes, 2014a):

(a) Preprocessing

In this stage, the model of the physical problem is defined graphically or with a text editor, and an ABAQUS input file is created.

(b) Simulation

In this stage, a Standard or Explicit ABAQUS packager solves the numerical problem defined in the model.

(c) Postprocessing

This stage evaluates the results once the simulation has been completed. This is done interactively using the Visualisation module of ABAQUS. The Visualisation module reads the output database file and has a variety of options for displaying the results, including contour plots, animations, deformed shape plots and X-Y plots. Figure 5.2 shows how the three stages are linked together by files in ABAQUS.

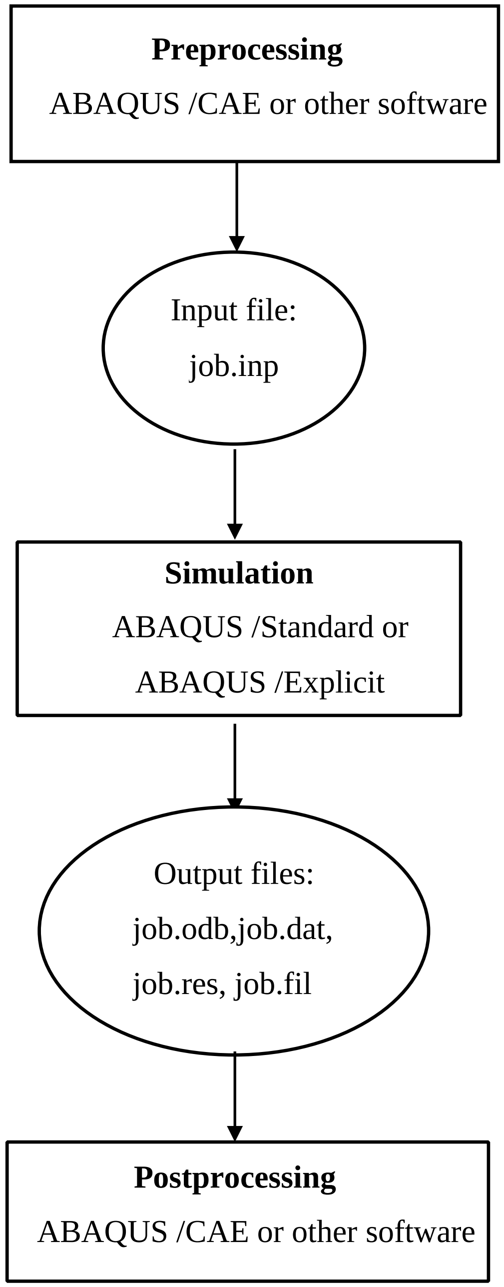

Figure 5.2: Stages in an ABAQUS Analysis. (Source: Dassault Systèmes, 2014a)

5.4 Domain Discretisation

The deformable copper wire as a feature was discretised into 4-node quadrilaterial bilinear shell elements and partitioned in five parts to ease the meshing. The partitioning was done at areas where the wire cross section changed.

5.5 Constitutive Equations

The governing equations for state variables are invoked by element interconnection requirements corresponding to the equilibrium of nodal force increments, $\Delta \boldsymbol{F}$. For corresponding displacement increments, $\Delta \boldsymbol{U}$, the interconnection requirements are given by equation (5.1) according to Bathe (1996):

$$\Delta F = K \Delta U \tag{5.1}$$

In equation (5.1)**,** *K* is the stiffness matrix which is an assembly of matrices that allow for deformation, material incompressibility, and rigid body rotation in the elastic-plastic finite element method. The solution to equation (5.1) gives unknown values of ΔU, hence allows the deformation of the workpiece to be determined. From the deformations thus obtained, stresses and strains can be determined.

The mathematical models used during modelling of the copper wire drawing process arise from the constitutive models of *metal plasticity* and *isotropic elasto-plasticity*.

5.5.1 Metal Plasticity Constitutive Models

ABAQUS Standard/Explicit can be used to model metal plasticity. Metal plasticity models are either rate-dependent or independent, with a Mises yield surface for isotropic materials. For relatively high strain rate applications as obtainable in metal forming, the rate dependence can be presented using equation (5.2) as follows (Dassault Systèmes, 2014a):

$$\dot{\varepsilon}^{pl} = D \left(\frac{\bar{\sigma}}{\sigma^0} - 1 \right)^n, \quad for\ \bar{\sigma} \geq \sigma^0 \tag{5.2}$$

where, $\dot{\varepsilon}^{pl}$ is the equivalent plastic strain

$\bar{\sigma}$ is the yield stress at non-zero plastic strain

σ^0 is the static yield stress which may depend on plastic strain (ε^{pl}), temperature (θ) and other factors (f_i)

D, n are material parameters which can be functions of temperature and other factors

5.5.2 Isotropic Elasto-Plasticity Constitutive Models

Using ABAQUS Standard/Explicit, isotropic elasto-plastic models can be modeled as part of the general metal plasticity models. These models use the assumptions that there is no volumetric plastic strain associated with material flow due to the Mises yield function. The volume change is small due to the fact that the elastic bulk modulus is high. Parameters involving strain under isotropic elasto-plastic models can be computed using equation (5.3) as follows (Ibid):

$$\varepsilon = \varepsilon^{el} + \varepsilon^{pl} \qquad \textbf{(5.3)}$$

where, ε is the total strain

ε^{el} is the strain in the elastic region

ε^{pl} is the strain in the plastic region

The flow rule is, thus given by equations (5.4) and (5.5) as folows (Ibid):

$$\Delta \boldsymbol{e}^{\boldsymbol{pl}} = \Delta \bar{\boldsymbol{e}}^{\boldsymbol{pl}} \boldsymbol{n} \qquad \textbf{(5.4)}$$

$$n = \frac{3}{2} \frac{S}{\sigma_{eq}} \qquad \textbf{(5.5)}$$

where $\Delta\bar{e}^{pl}$ is the incremental equivalent plastic strain

σ_{eq} is the Mises equivalent stress.

S is the deviatoric stress tensor ($S = \sigma + p\mathbf{I}$)

5.5.3 Damage Variable and Material Stiffness

A damage variable can be used to represent the loss of stiffness and integrity attributed to micro-cracks due to ductile failure (Bao, 2003). Ductile material failure involves damage initiation and damage evolution (Dassault Systèmes, 2013).

5.5.3 (a) Damage Initiation

Damage initiation defines the point of initiation of degradation of stiffness and is used for the analysis of the severity of the current deformation state. Using a criterion for ductile damage, or the Cockroft and Latham criterion (C_{CL}), the initiation of damage is noted when the ABAQUS parameter DUCTCRT is specified. Damage initiation occurs when DUCTCRT is equal to one, with damage progression occurring when the criterion C_{CL} = 357.099 MPa for wrought copper.

The initiation of damage is known when the equivalent plastic strain at the onset of damage, $\bar{\varepsilon}_D^{pl}$ is expressed as a function of stress triaxiality ,$\boldsymbol{\eta}$, and strain rate ,$\dot{\boldsymbol{\varepsilon}}^{\,pl}$, according to equation (5.6) as follows (Dassault Systèmes, 2014b):

$$\bar{\varepsilon}_D^{pl}\,(\eta, \dot{\bar{\varepsilon}}^{pl}\,) \tag{5.6}$$

5.5.3 (b) Damage Evolution

This defines the post damage-initiation material behaviour and shows the rate of degradation of stiffness once damage initiation has occurred. Using equation (5.7), the following scalar damage approach is used to determine damage evolution (Dassault Systèmes, 2013):

$$\sigma = \ (1 - D)\bar{\sigma} \tag{5.7}$$

where, σ is the applied stress

$\bar{\sigma}$ is the undamaged response stress

D is a damage variable which captures the combined effect of all active damage mechanisms

Fracture or failure occurs in a material when the variable D is equal to 1. In the elasto-plastic region, damage manifests due to the following (Ibid):

- Softening of the yield stress
- Degradation of elasticity

Figure 5.3 shows a stress-strain curve for an elastic-plastic material with progressive damage.

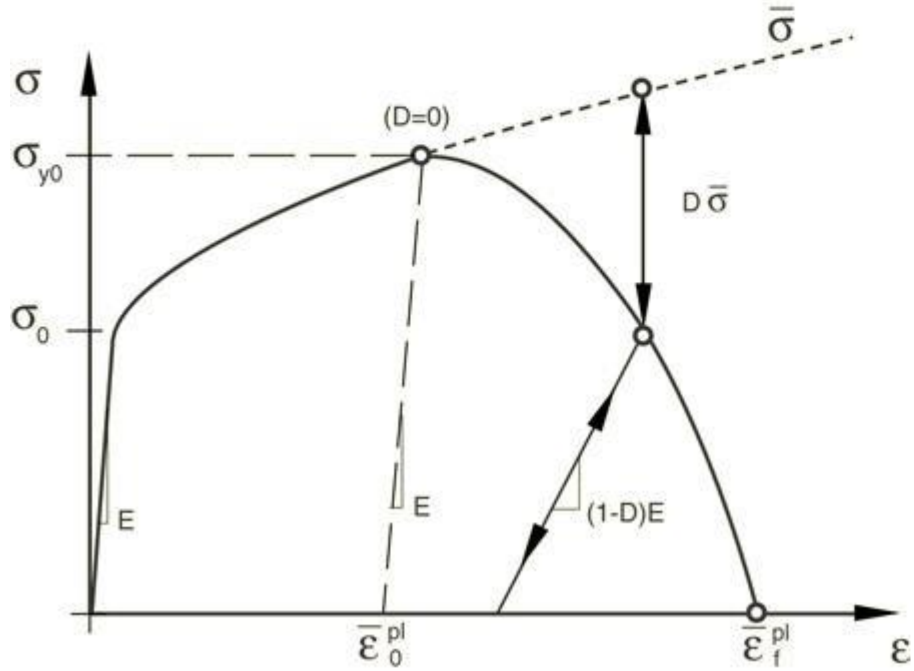

Figure 5.3: Progressive Damage Curve of an Elasto-Plastic Material.
(Source: Dassault Systèmes, 2014a)

5.6 Underlying Assumptions

The underlying assumptions for the current study are:

- The copper raw material has minimal allowable inclusions
- The copper raw material is homogeneous
- The draw die is a rigid mechanical element

5.7 Computational Conditions

The computational conditions were formulated using a copper wire drawing process with initial wire diameter of 2.76 mm and a final diameter of 1.78 mm. The process was modelled using the ABAQUS Explicit environment with a dynamic step, mass scaling and a non-linear geometrical parameter (NLgeom) was specified to accommodate large deformations. The scaling was applied to all regions of the copper wire with a target time increment of 0.00001, a linear bulk viscosity of 0.06 and a quadratic bulk viscosity of 1.2. The modelling process was initially displacement-based and later velocity-based with four sequences of two-passes each. The passes were designed such that results from the preceding pass (last stage) were used as initial information for next pass (first stage).

The copper wire was modelled as deformable and the two dies were designed and modelled as analytically rigid due to the negligible deformation they undergo during the process. **Appendix 4** shows the ABAQUS output file (30%1st2PassesExpl.dat) for the first multi-pass sequence (1-2). Information contained in this output file was repeated for other multi-pass sequences (2-3, 3-4 and 4-5), the only variations being the change in section or area reduction and change in bearing length.

5.7.1 Initial and Boundary Conditions

Figure 5.4 and 5.5 show a 2-dimensional half-assembly view of the copper wire drawing process and the boundary conditions used. The geometry of the model specimen was cylindrical, with tapered sections to reflect the practical configuration. The portion of the model at the outlet face resembles the actual and practical grain size after wire drawing. The model was designed in a half-symmetry of 2-dimensions to reduce the number of elements and ease the computational time. Table 5.1 explains the initial and boundary conditions which applied to the assembly model.

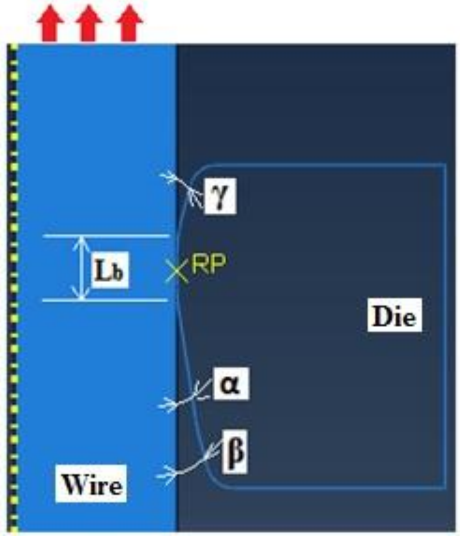

Figure 5.4: Die Parameter and Boundary Conditions Setting. (Source: Author)

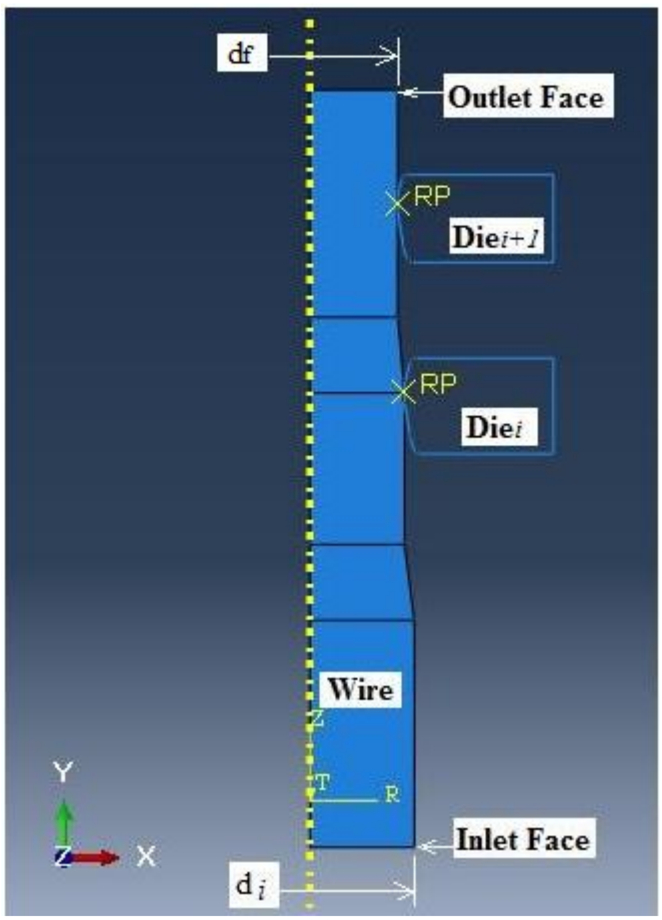

Figure 5.5: Parts Assembly for Multi-Pass Wire Drawing in ABAQUS. (Source: Author)

5.7.2 Finite Element Mesh

The finite element mesh generated for the wire model is shown in Figure 5.6. The elements used were CAX4R which are 4-node 2D axisymmetric quadrilateral elements with reduced integration points and hourglass control. A total of 6000 elements with 6233 nodes were used for each multi-pass sequence model.

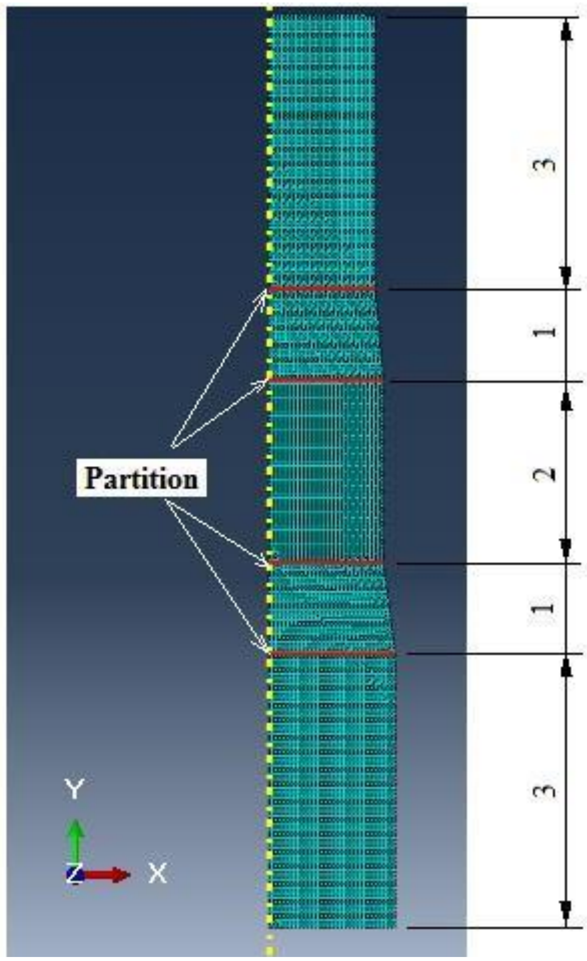

Figure 5.6: Meshing and Partitioning of Copper Wire Material. (Source: Author)

Two sections of the wire model were necked down in order to represent the reality of the wire drawing process in which specimens are swaged to ensure that the material can be pulled easily through the die opening. The wire mesh had an overall fixed length of 10 mm, an initial diameter (d_i) of 2.76 mm and varying final diameters according to pass sequences as shown in Table 5.1. Different area reduction percentages were obtained as a result of the varying final diameters. The wire mesh had a fixed global size of 0.0005 with partitioned edge sizes of 30 each.

Table 5.1: Limit and Boundary Conditions with Variation of Die Bearing Length.

Multipass Sequences	**Feature Geometries**	**Initial Conditions**	**Boundary Conditions**
1 – 2 2 – 3 3 – 4 4 – 5	Copper Wire	d_i = 2.76 mm d_1 = 2.55 mm d_2 = 2.32 mm d_3 = 2.11 mm d_4 = 1.92 mm d_5 = 1.78 mm	(i) 0.08 ms^{-1} velocity of outlet face along y- axis (ii) Centreline symmetry (U_1=0)
	Die_i	$\alpha = 10^o$; $\beta = 40^o$; $\gamma = 30^o$ L_b = (30; 35; 40; 45; 50%)d_f	Encastre boundary condition (U=0;R=0) for die reference point (RP)
	Die-Wire Interaction	μ = 0.04	

(Source: Author)

5.7.3 Contact Conditions and the Rigid Die

Kinematic contact was applied as a mechanical constraint between the wire contact surface and the die external surfaces. Finite sliding was specified at the contact, with a Coulomb friction coefficient of 0.04 maintained in all models except for models involving friction coefficient variation which were varied.

A smooth step was specified for the model, with the rigid dies being designed and modelled with fillets to avoid sharp corners. Figure 5.7 shows the 2D design of the rigid die within the ABAQUS / CAE. The die was modelled using 2D analytic rigid shell elements.

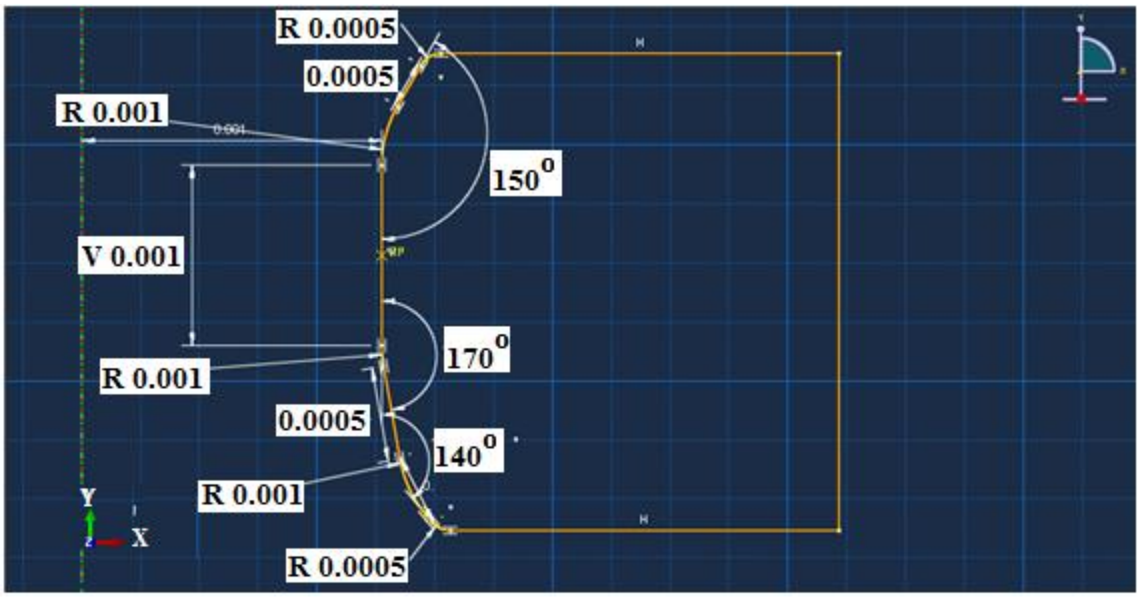

Figure 5.7: Rigid Die Nib with Design Parameters (all unspecified dimensions in mm). (Source: Author)

5.8 Results of the Simulations

Results of the various state variables for the deformed wire are presented and discussed in this section. A centerline node, 306, and a surface node 410, both located near the inlet face and observed from the simulation to be in the regions with a higher concentration of Mises stresses as shown in Figure 5.8, were chosen as the points for assessing the variation of state variables with the independent variables. Using the query function in ABAQUS, values of the different state variables were obtained at nodes 306 and 410.

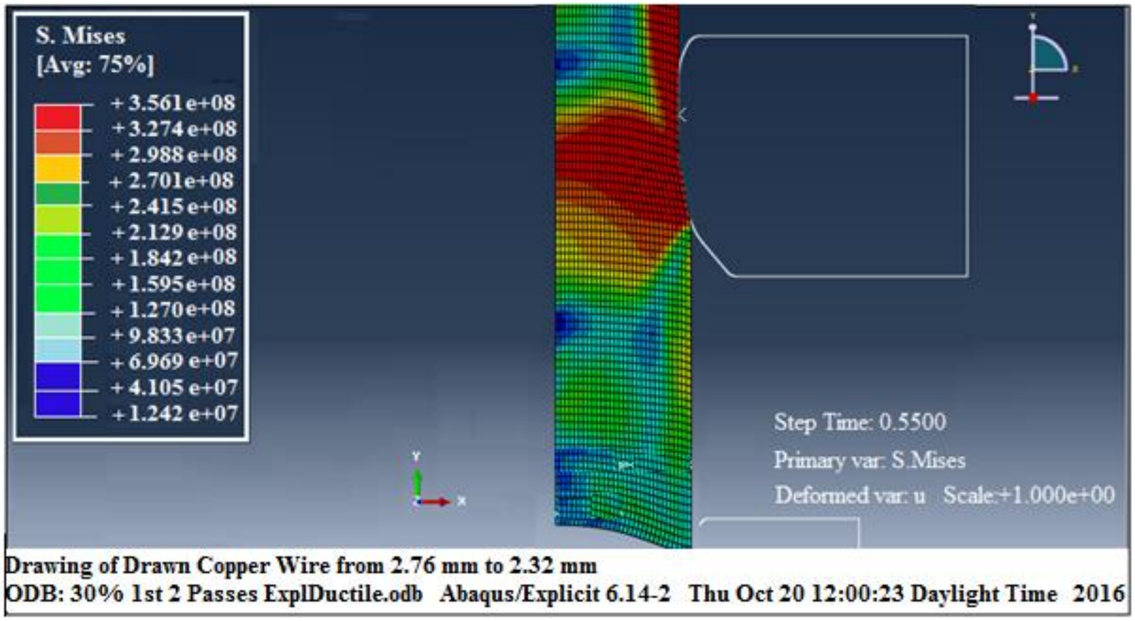

Figure 5.8: Location of Centreline (306) and Surface (410) Nodes. (Source: Author)

Table 5.2 shows material parameters that were used as inputs to the models. The values of E, Y_{avg}, and σ_y were obtained from the stress-strain diagram shown in Figure 6.12. The values of ν and ρ were obtained from standard tables of properties for copper material as obtaining in ASM International (1990). The values of η, ε_{fr} and $\dot{\varepsilon}$ were obtained as calculated parameters.

Table 5.2: Material and Die Parameters used as Inputs to Models.

Parameter			**Parameter**		
Symbol	*Description*	*Value*	*Symbol*	*Description*	*Value*
E	Young's Modulus	118.75 GPa	ν	Poisson's ratio	0.34
Y_{avg}	Average yield stress	210.915 MPa	η	Stress triaxiality	-1.72
σ_y	Yield stress	165.738 MPa	ρ	Density	8960 kgm^{-3}
ε_{fr}	Fracture strain	0.338	$\dot{\varepsilon}$	Strain rate	0.0015s^{-1}

(Source: Author)

5.8.1 Incremental Deformation and Stress Patterns

It was observed from the simulations that the use of more than two dies caused severe mesh disintegration, hence the wire drawing process was modelled using a maximum of two dies per sequence. Models were thus performed with four sequences of two passes each. The sectional mesh deformities observed at intervals were insignificant and the elements and nodes being observed were chosen further away from this region to minimise errors.

Models for 30% , 35%, 40%, 45%, 50% variation of bearing length showed both a reduction of the cross sectional area and a very slight deformity at the outlet face during the third multi-pass sequence (3-4). The Mises stress distribution was observed to be more pronounced during the second pass (die$_{i+1}$), with the stress distribution pattern starting from the die-wire interface and extending towards the wire centerline. Figures 5.9 to 5.13 show the Mises distribution pattern during multi-pass copper wire drawing.

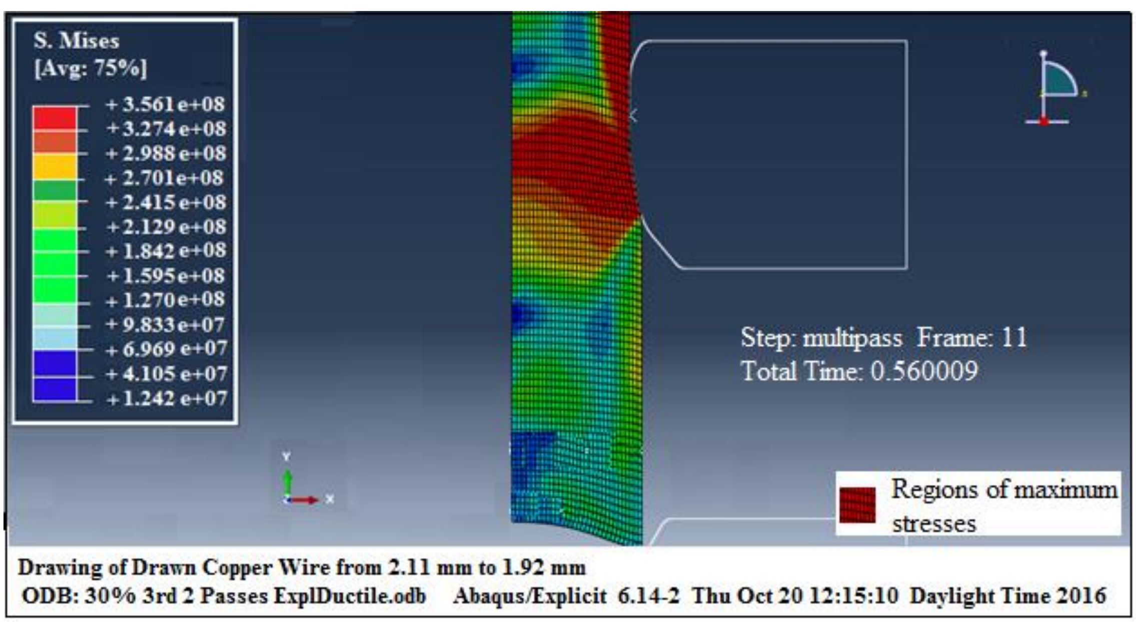

Figure 5.9: Mises Distribution during Third (3-4) Multi-Pass Stage at 30% Bearing Length. (Source: Author)

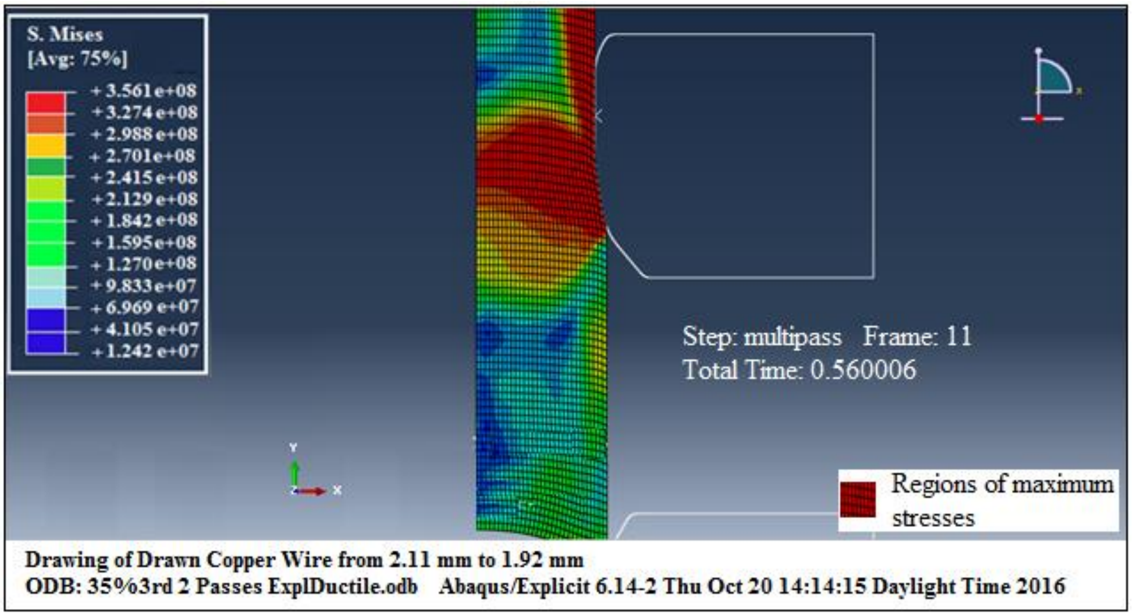

Figure 5.10: Mises Distribution during Third (3-4) Multi-Pass Stage at 35% Bearing Length. (Source: Author)

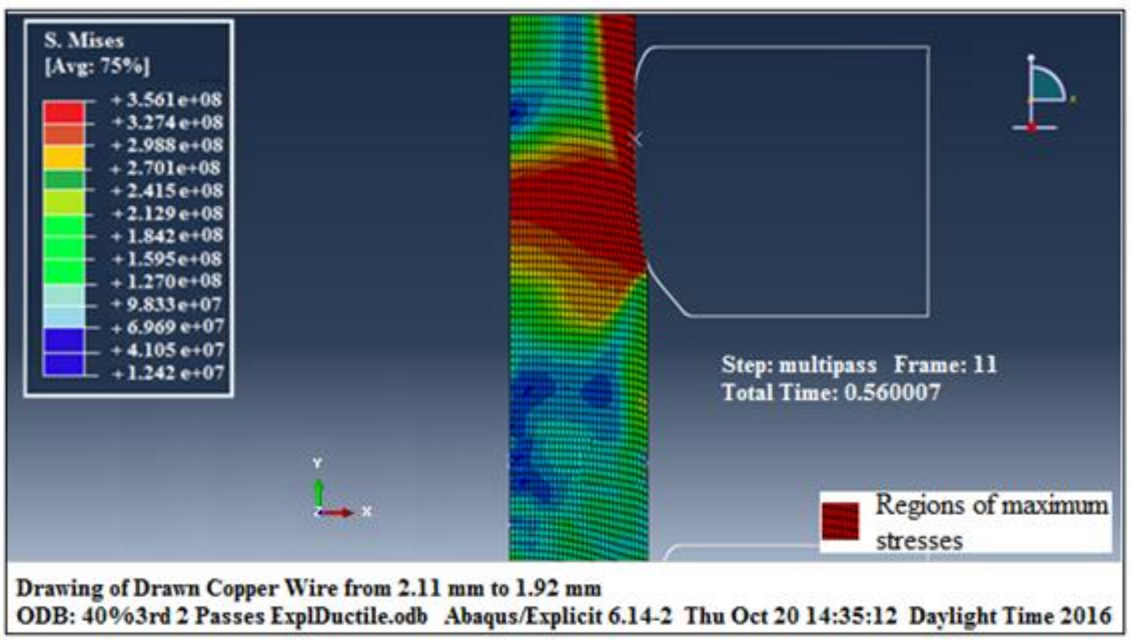

Figure 5.11: Mises Distribution during Third (3-4) Multi-Pass Stage at 40% Bearing Length. (Source: Author)

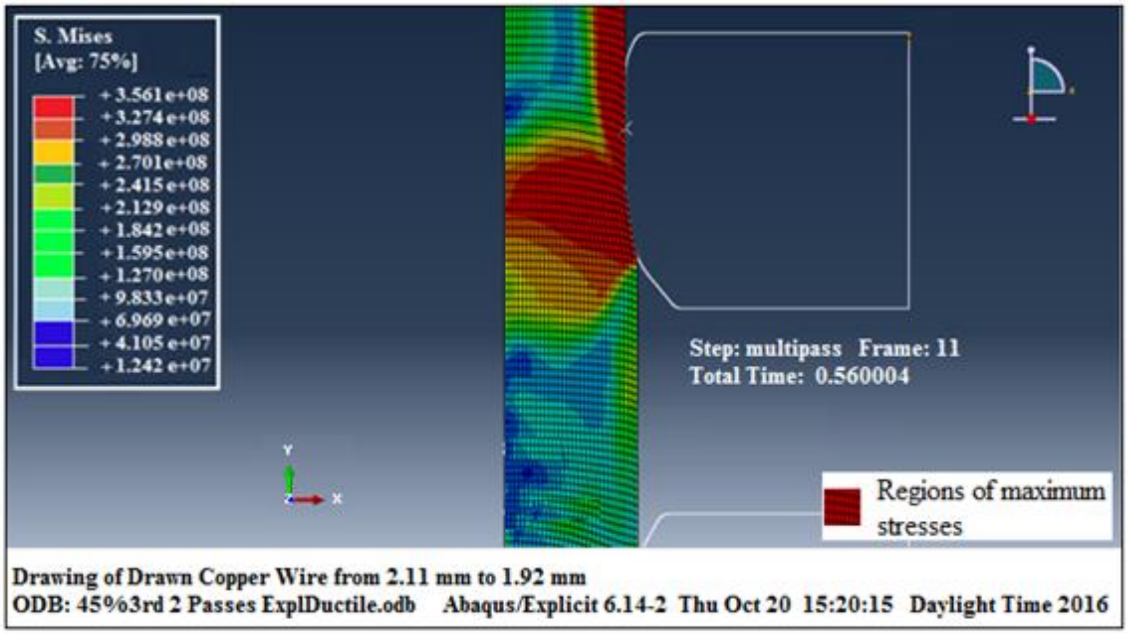

Figure 5.12: Mises Distribution during Third (3-4) Multi-Pass Stage at 45% Bearing Length. (Source: Author)

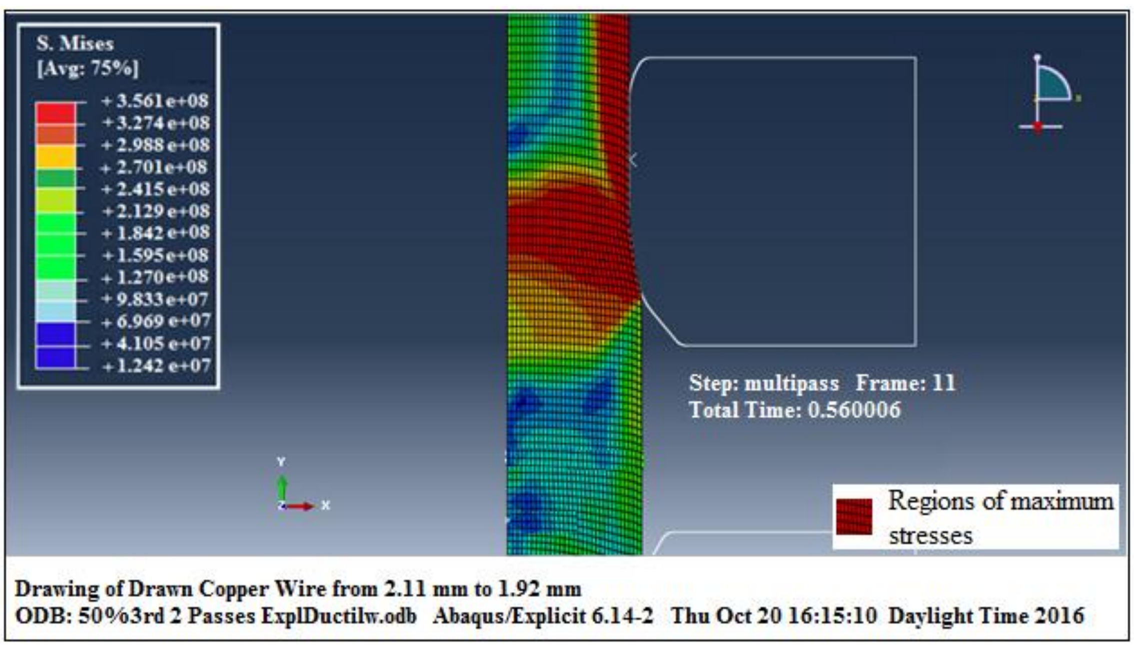

Figure 5.13: Mises Distribution during Third (3-4) Multi-Pass Stage at 50% Bearing Length. (Source: Author)

Models for the entrance angle showed some mesh deformity at the outlet face for entrance angles of 20°, 25°, 30°, 35° and 40° during the third multi-pass sequence.

Modelling with approach angles of less than 8° was not possible due to severe mesh disintegration, especially during the first multi-pass sequence (1-2). The von Mises distribution was more pronounced during all the second multi-pass sequences (3-4) where values of up to 315 MPa were attained when using a 10° approach angle.

Models for friction coefficient showed outlet face mesh deformity at values of 0.07 and above, especially during the second and third multi-pass sequences. Models for exit angle variation showed no changes.

Speeds of values less than 0.03 ms^{-1} were too slow for the models as the passage through the dies could not be completed, whereas speeds of more than 0.12 ms^{-1} showed severe mesh disintegration in the models, especially during the second and third multi-pass sequences.

Area reduction models showed no deformations in the 10% and 12% area reduction models. Small deformities at the outlet face were observed during the last multi-pass sequences at 14% and 16% area reductions, whereas the same was observed during the third and last multi-pass sequences at 18% area reduction. All multi-pass sequences using the 20% area reduction showed increasing levels of mesh disintegration and sectional deformity, with the last multi-pass sequence showing a severe mesh deformation at the outlet face. Models with area reduction above 18% were not used in the analysis.

5.8.2 Distribution of State Variables with Independent Variables

(i) Equivalent Plastic Strain Distribution

The total accumulation of plastic strain during deformation is given by the equivalent plastic strain, defined by Dassault Systèmes (2014b) according to equation (5.8) as follows:

$$\bar{\varepsilon}^{pl} = \frac{2}{3}\int_0^t \dot{\varepsilon}^{pl} : \dot{\varepsilon}^{pl} \quad \textbf{(5.8)}$$

The equivalent plastic strain ε^{pl} is given by the output parameter PEEQ (equivalent plastic strain) in ABAQUS. Figure 5.14, 5.15, 5.16 and 5.17 show the variation of the equivalent plastic strain with die geometry and drawing process modifying conditions for different multi-pass sequences for the centerline node 306 and surface node 410.

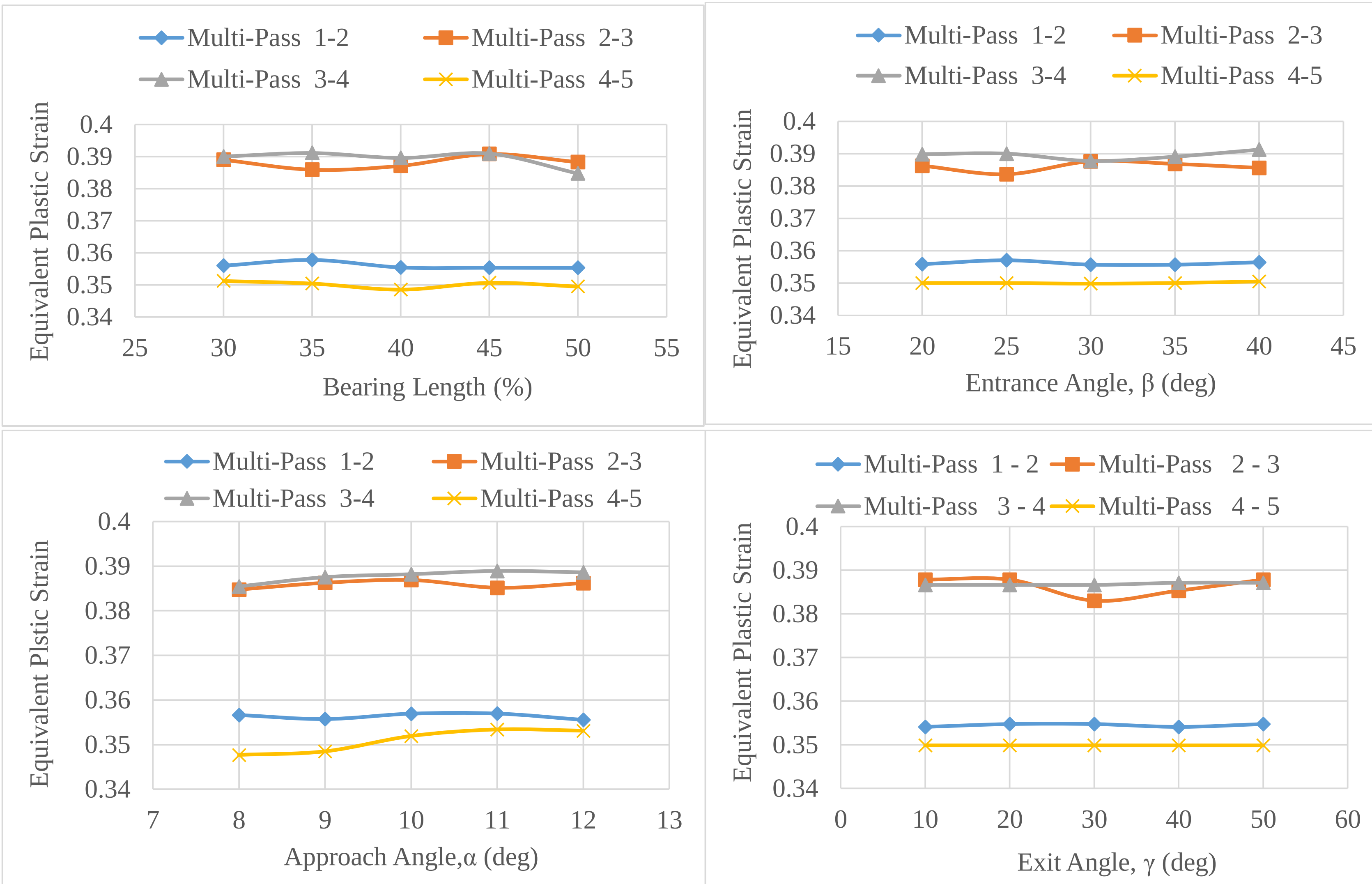

Figure 5.14: Distribution of Equivalent Plastic Strain with Die Geometry for Centreline (306) Nodes. (Source: Author)

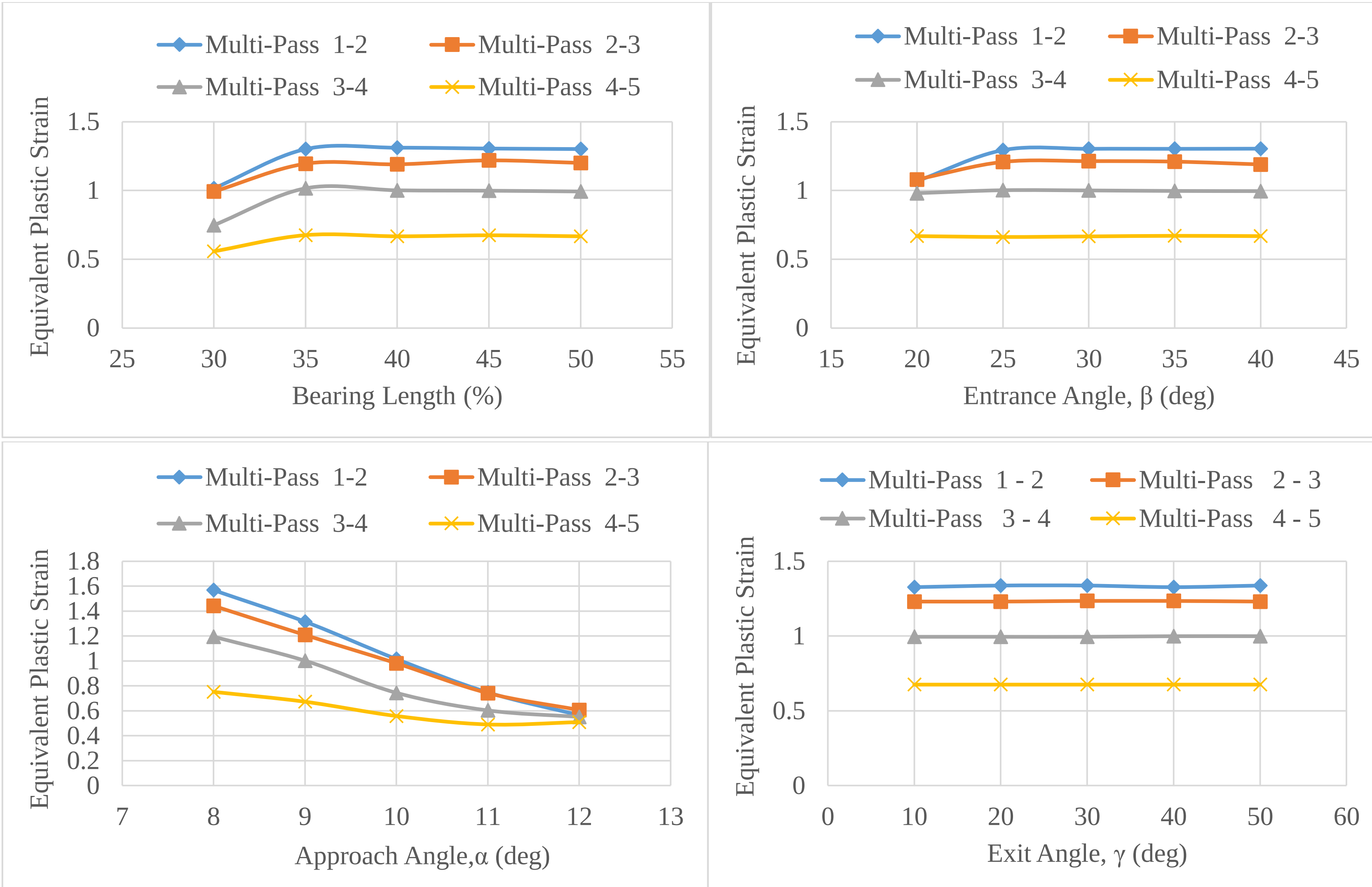

Figure 5.15: Distribution of Equivalent Plastic Strain with Die Geometry for Surface (410) Nodes. (Source: Author)

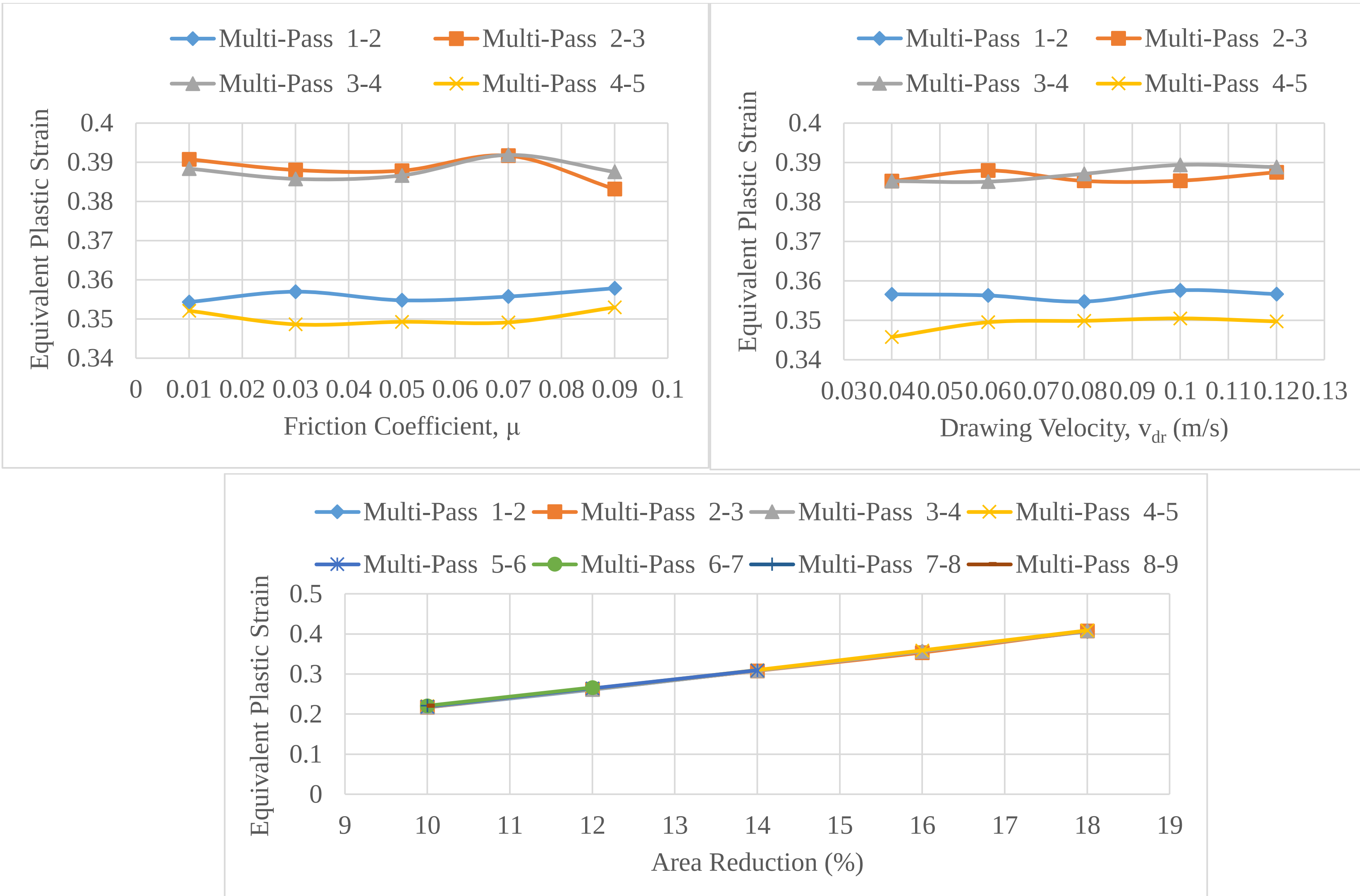

Figure 5.16: Distribution of Equivalent Plastic Strain with Drawing Process Conditions for Centreline (306) Nodes. (Source: Author)

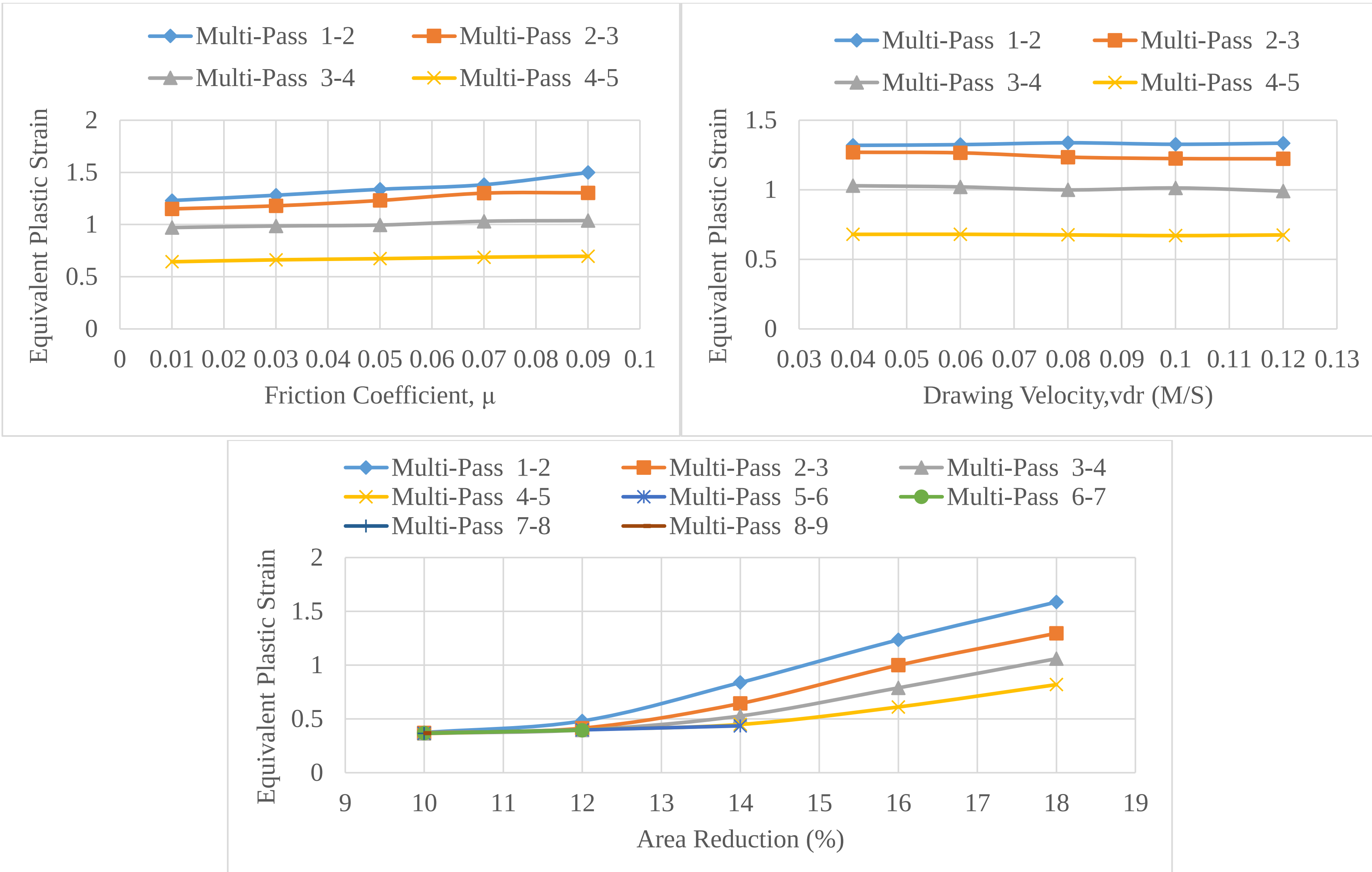

Figure 5.17: Distribution of Equivalent Plastic Strain with Process Conditions for Surface (410) Nodes. (Source: Author)

(ii) Mises Equivalent Stress Distribution

Figures 5.18, 5.19, 5.20 and 5.21 show the distribution of the Mises equivalent stresses with different die geometry and drawing process modifying conditions. Dassault Systèmes (2014b) computes the Mises equivalent in the ABAQUS environment according to equation (5.9) as follows:

$$f(\sigma - \alpha) = \sqrt{\frac{3}{2}}\,(S - \alpha^{dev}) : (S - \alpha^{dev}) \qquad \textbf{(5.9)}$$

where, S is the deviatoric stress tensor ($S = \sigma + p\mathbf{I}$)

p is the pressure

I is the identity matrix

α^{dev} is the deviatoric part of the backstress tensor ($\alpha = \sigma - \sigma^0$)

(iii) Hydrostatic Pressure Distribution

Figure 5.22, 5.23, 5.24 and 5.25 show the distribution of the mean normal stress or hydrostatic pressure with different die design and process parameters. The formula for hydrostatic pressure is given by equation (5.10) as follows (Hosford and Caddell, 1983):

$$\sigma_m = \frac{\sigma_{11} + \sigma_{22} + \sigma_{33}}{3} \qquad \textbf{(5.10)}$$

where σ_{11} is the radial stress (along x-axis)

σ_{22} is the axial stress (along y-axis)

σ_{33} is the circumferential (hoop) stress (along z-axis)

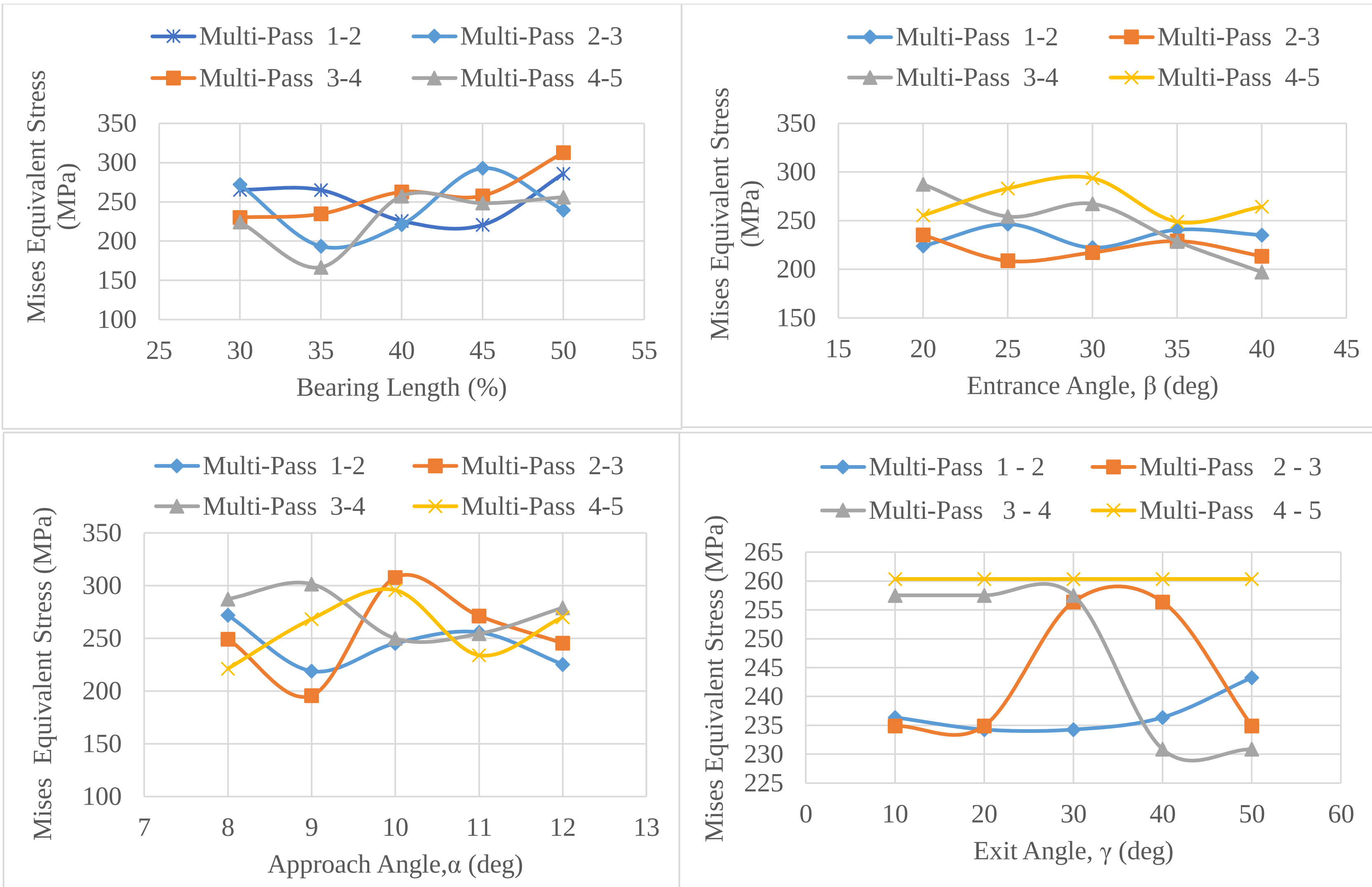

Figure 5.18: Distribution of Mises Equivalent Stress with Die Geometry for Centreline (306) Nodes. (Source: Author)

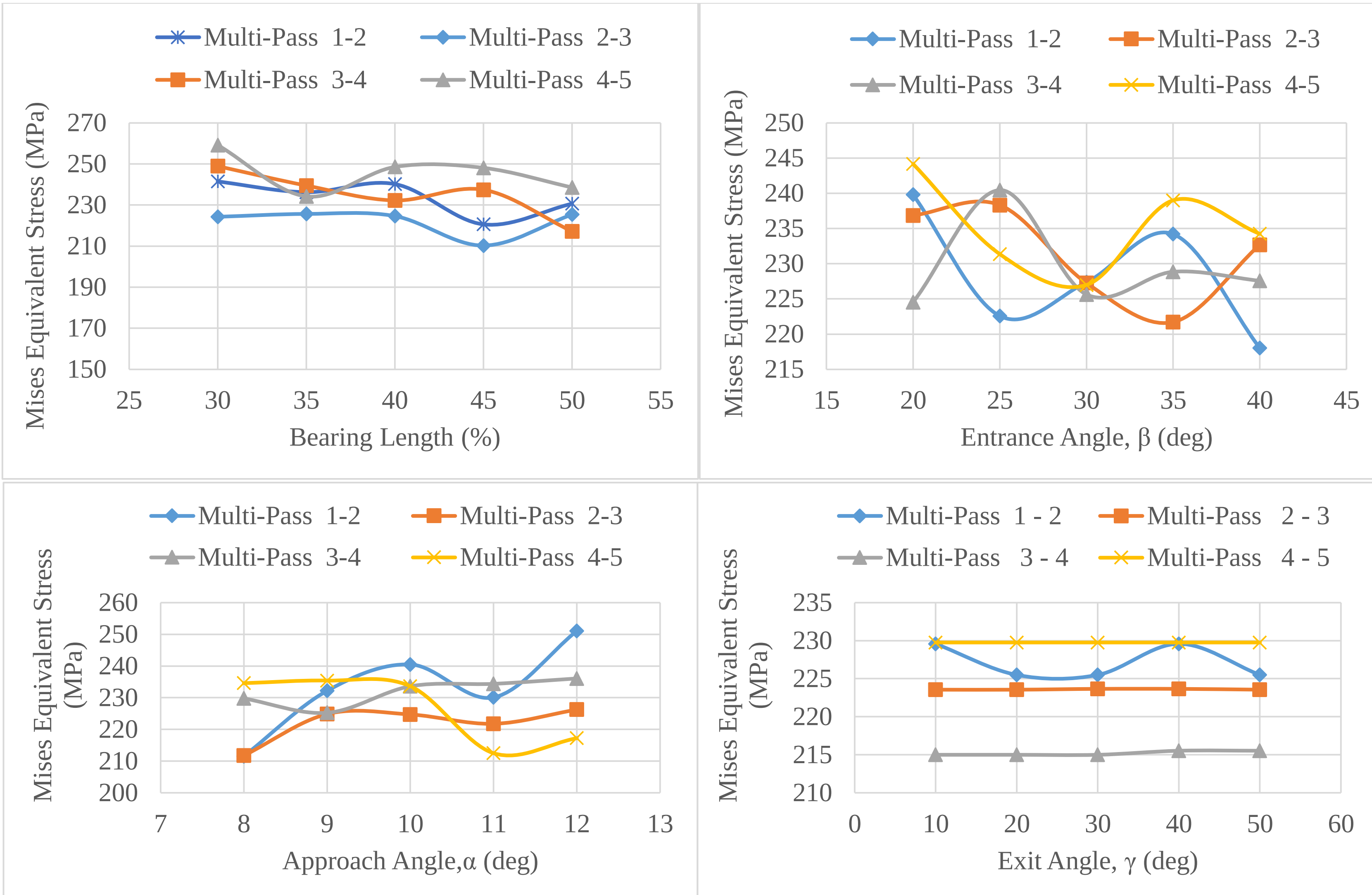

Figure 5.19: Distribution of Mises Equivalent Stress with Die Geometry for Surface (410) Nodes. (Source: Author)

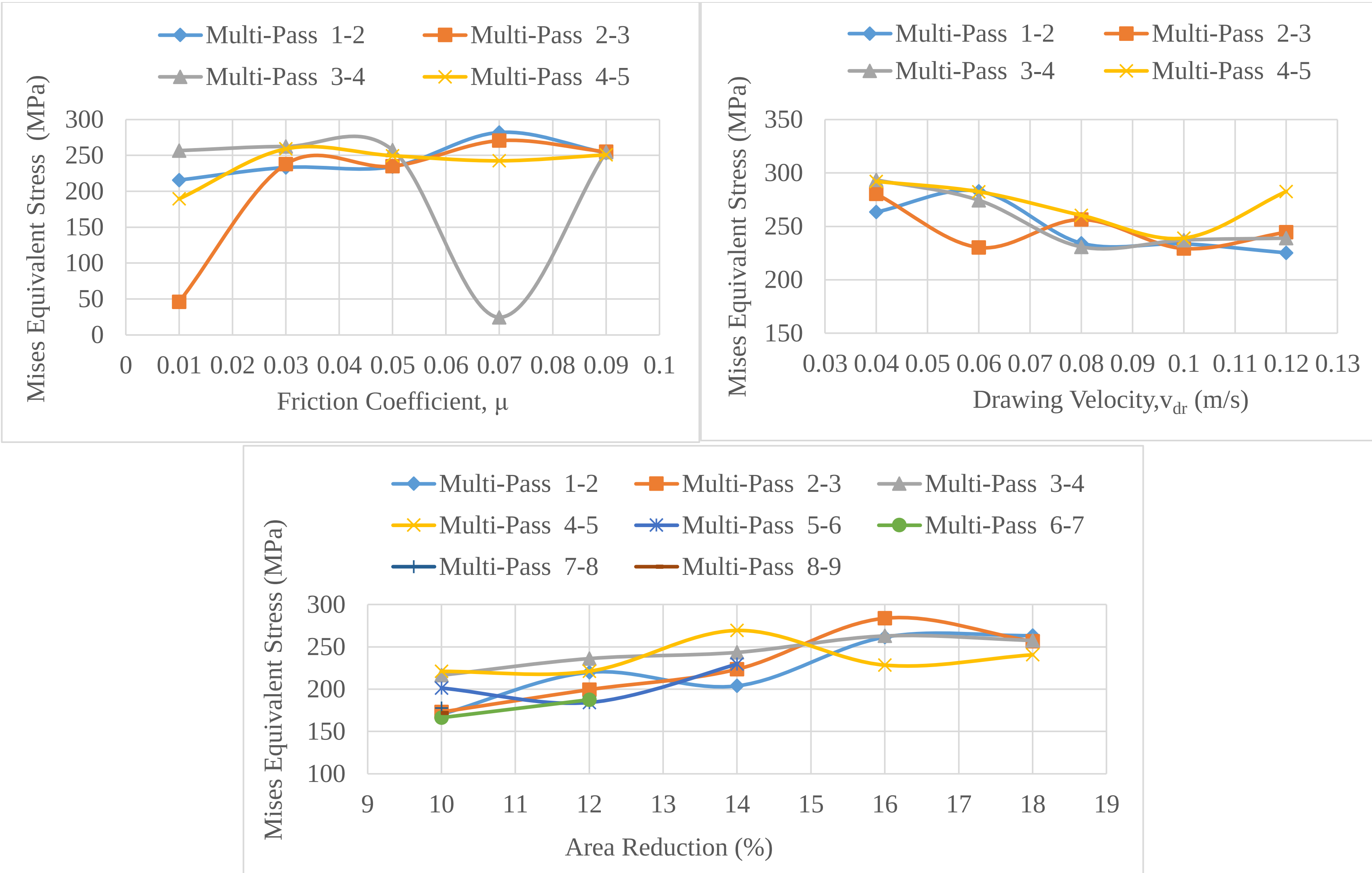

Figure 5.20: Distribution of Mises Equivalent Stress with Process Conditions for Centreline (306) Nodes. (Source: Author)

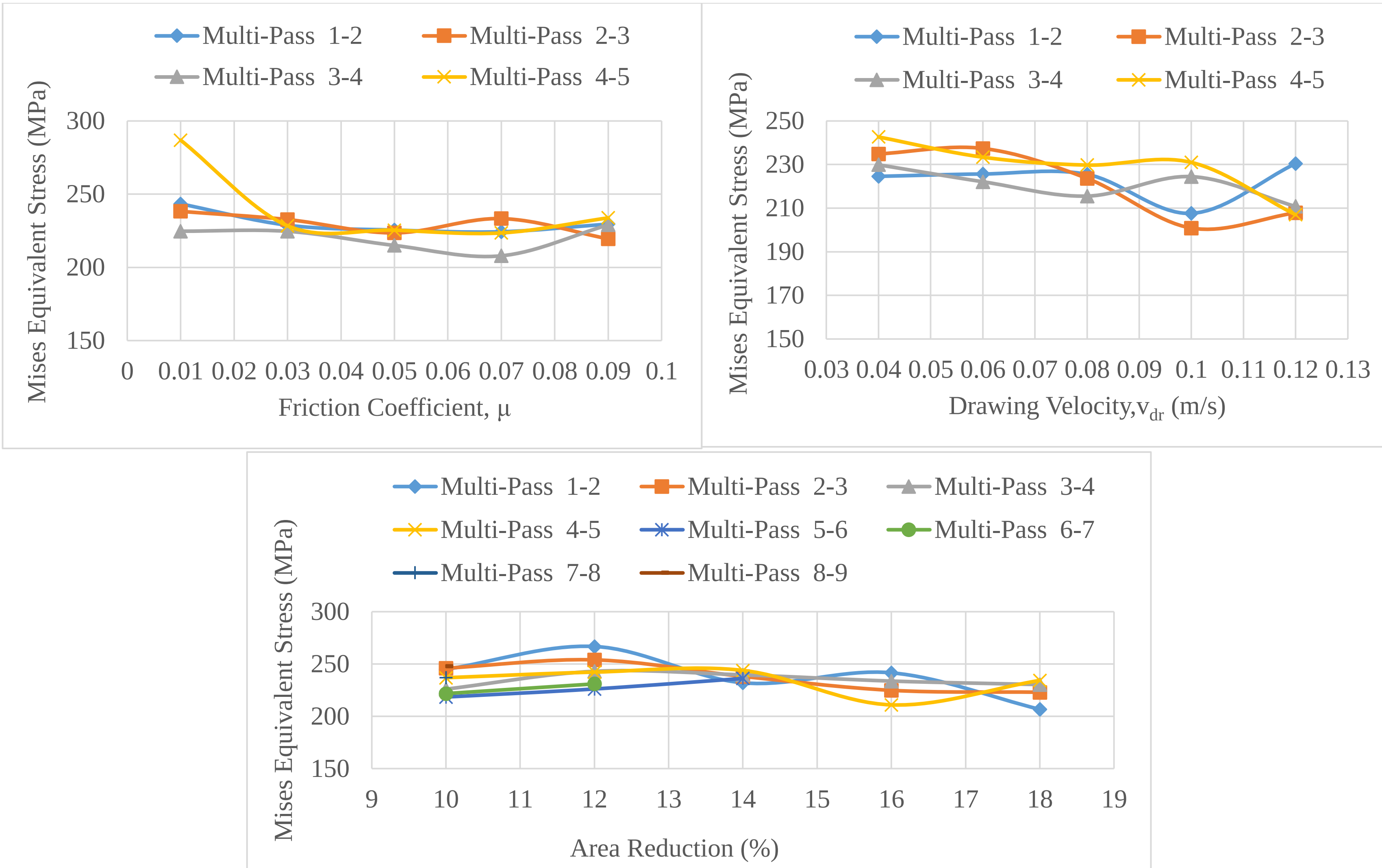

Figure 5.21: Distribution of Mises Equivalent Stress with Process Conditions for Surface (410) Nodes. (Source: Author)

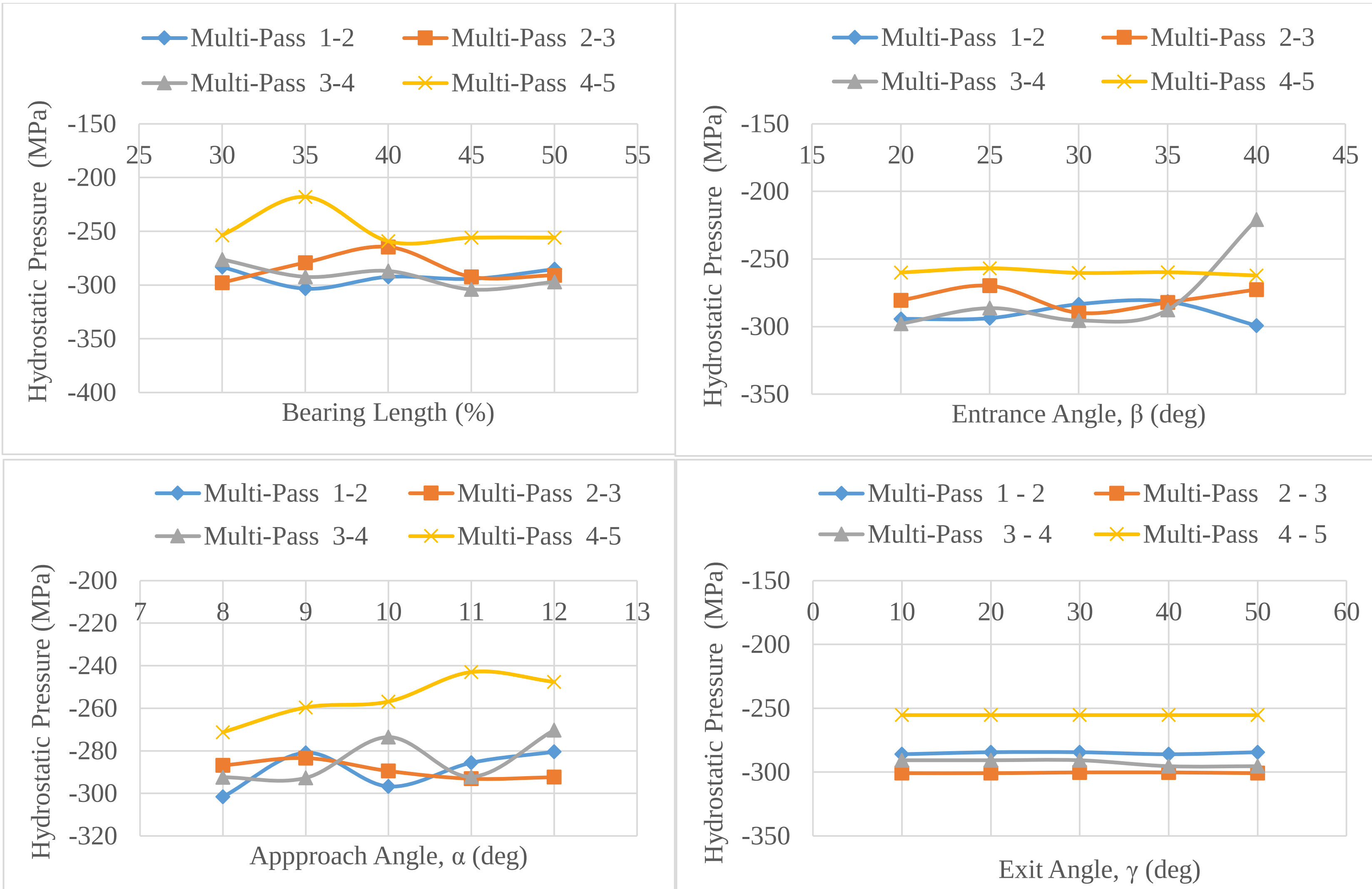

Figure 5.22: Distribution of Hydrostatic Stress with Die Geometry for Centreline (306) Nodes. (Source: Author)

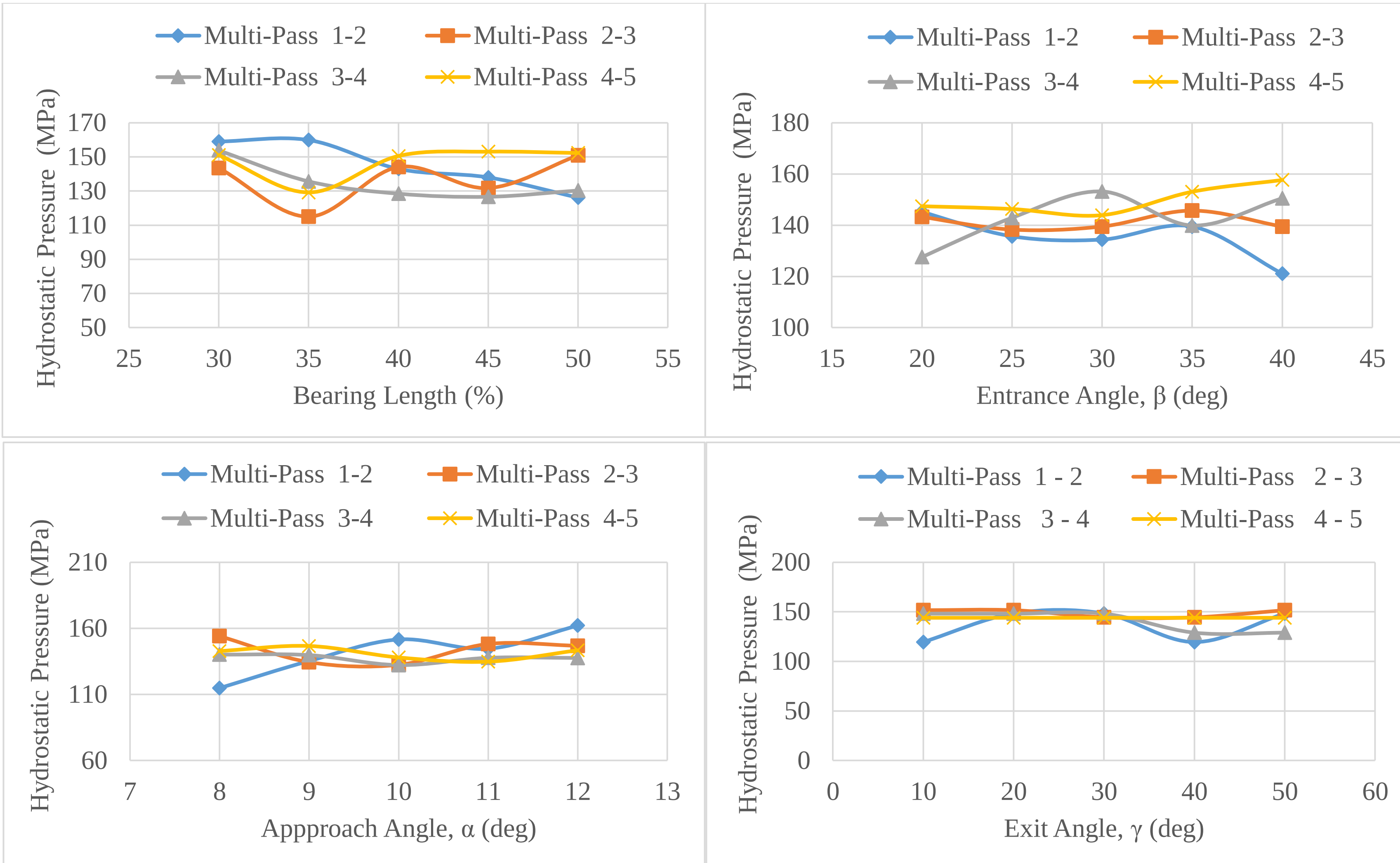

Figure 5.23: Distribution of Hydrostatic Stress with Die Geometry for Surface (410) Nodes. (Source: Author)

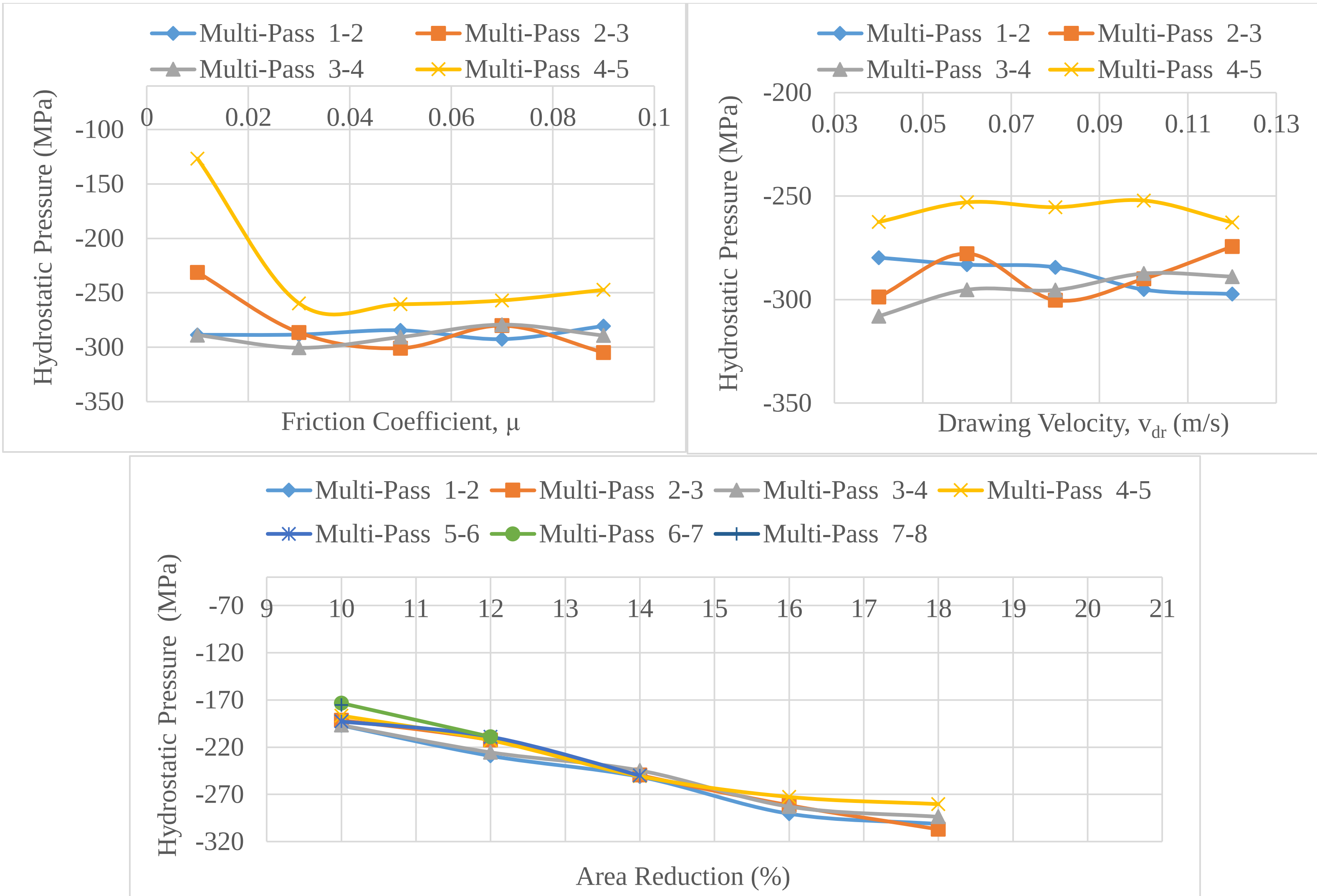

Figure 5.24: Distribution of Hydrostatic Stress with Process Conditions for Centreline (306) Nodes. (Source: Author)

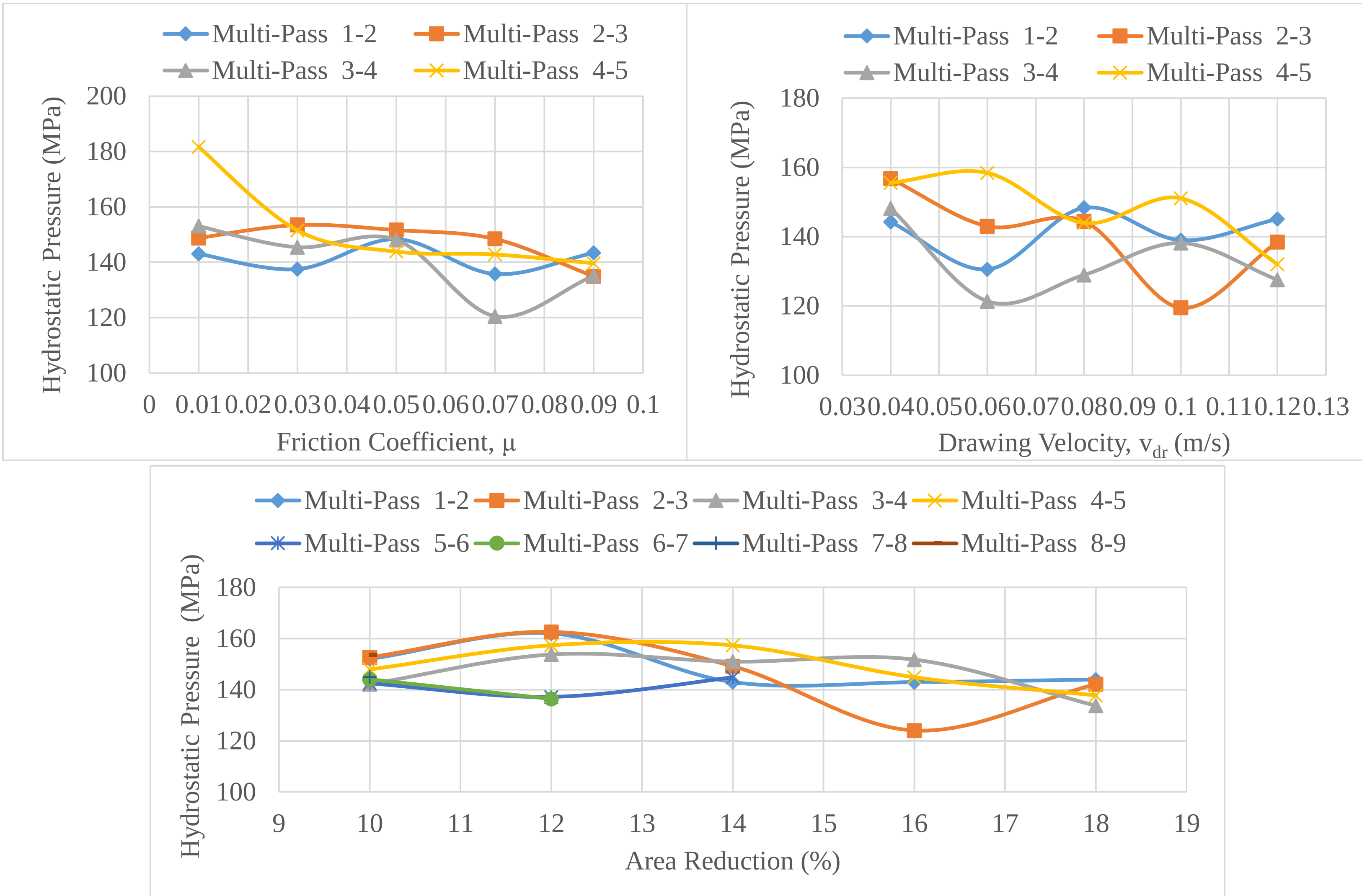

Figure 5.25 Distribution of Hydrostatic Stress with Process Conditions for Surface (410) Nodes. (Source: Author)

(iv) Stress Triaxiality Distribution

Stress triaxiality distributions affect the onset of progressive damage in a material. In ABAQUS, the output parameter TRIAX indicates the stress triaxiality values. Figure 5.26, 5.27, 5.28 and 5.29 show the distribution of stress triaxiality during multi-pass drawing with different die geometry and drawing process conditions. The stress triaxiality, η, is expressed by the equation (5.11) as follows (Dassault Systèmes, 2014):

$$\eta = -\frac{p}{\sigma_{eq}} \qquad \textbf{(5.11)}$$

where, p is the equivalent pressure stress

σ_{eq} is the equivalent Mises stress

(v) Damage Initiation Distribution

Arising from the stress triaxiality distributions and using the ABAQUS output parameter DUCTCRT, initiation of ductile damage in copper wire was assessed. The models showed that the ductile criterion parameter (DUCTCRT) was equal to one for all the multi-pass sequences, except for area reduction models for centerline node (306) where the DUCTCRT parameter was less than one at area reductions below 16%. Ductile damage initiation occurred when the ductile criterion parameter was equal to one.

Figure 5.30, 5.31, 5.32 and 5.33 show the distribution of the ductile criterion (DUCTCRT) parameter with different die design and process parameters.

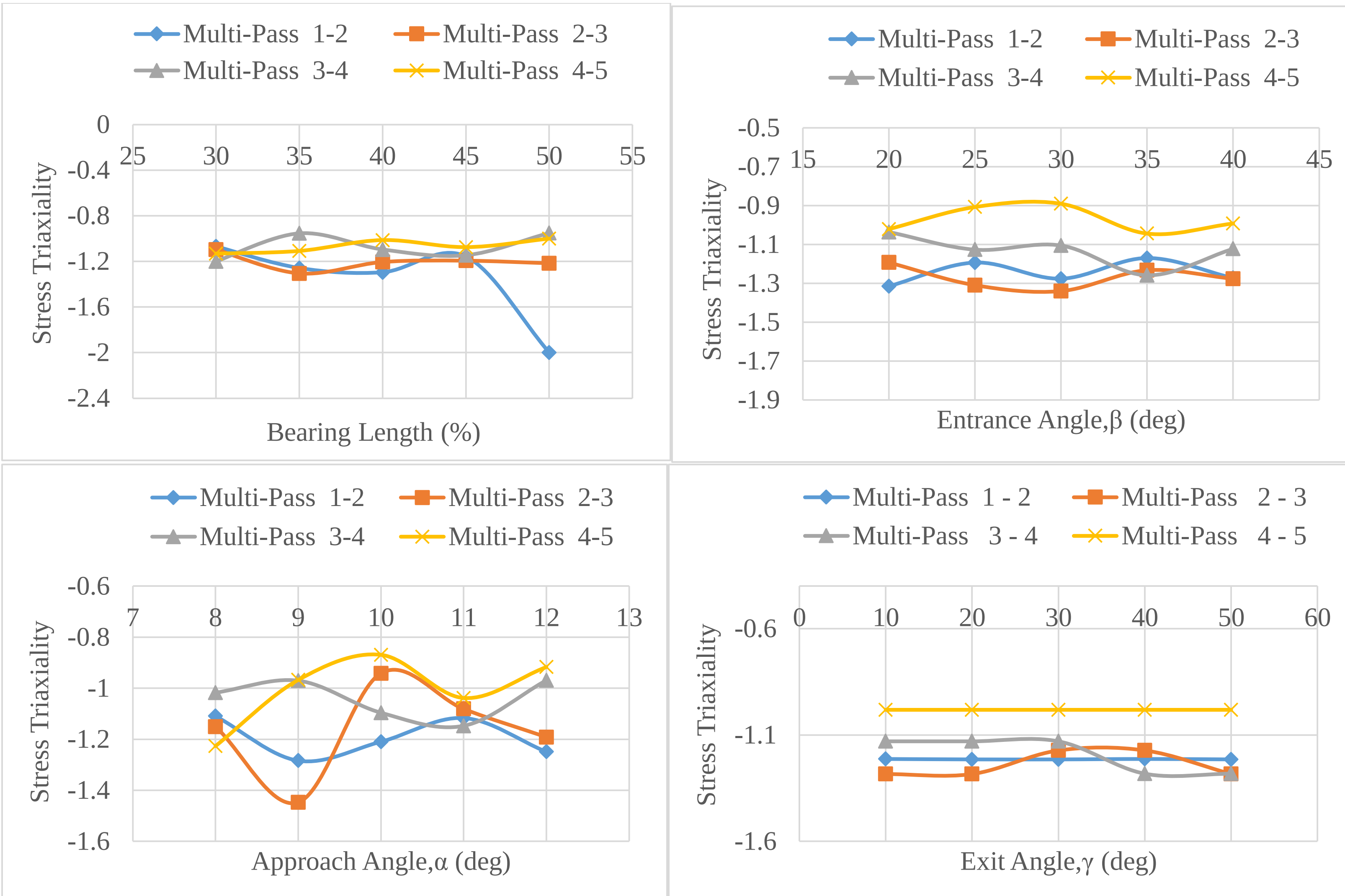

Figure 5.26 Distribution of Stress Triaxiality with Die Geometry for Centreline (306) Nodes

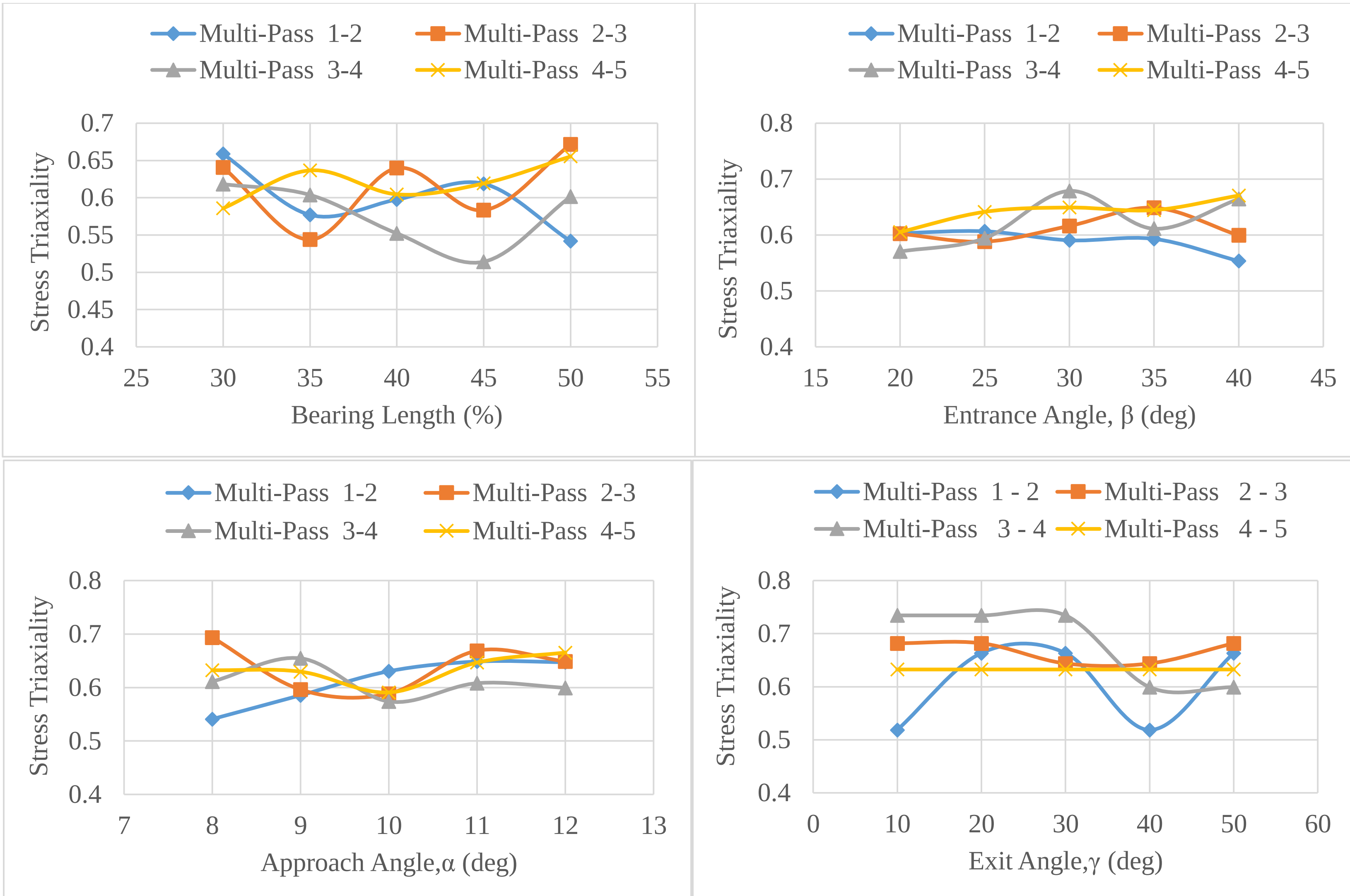

Figure 5.27 Distribution of Stress Triaxiality with Die Geometry for Surface (410) Nodes

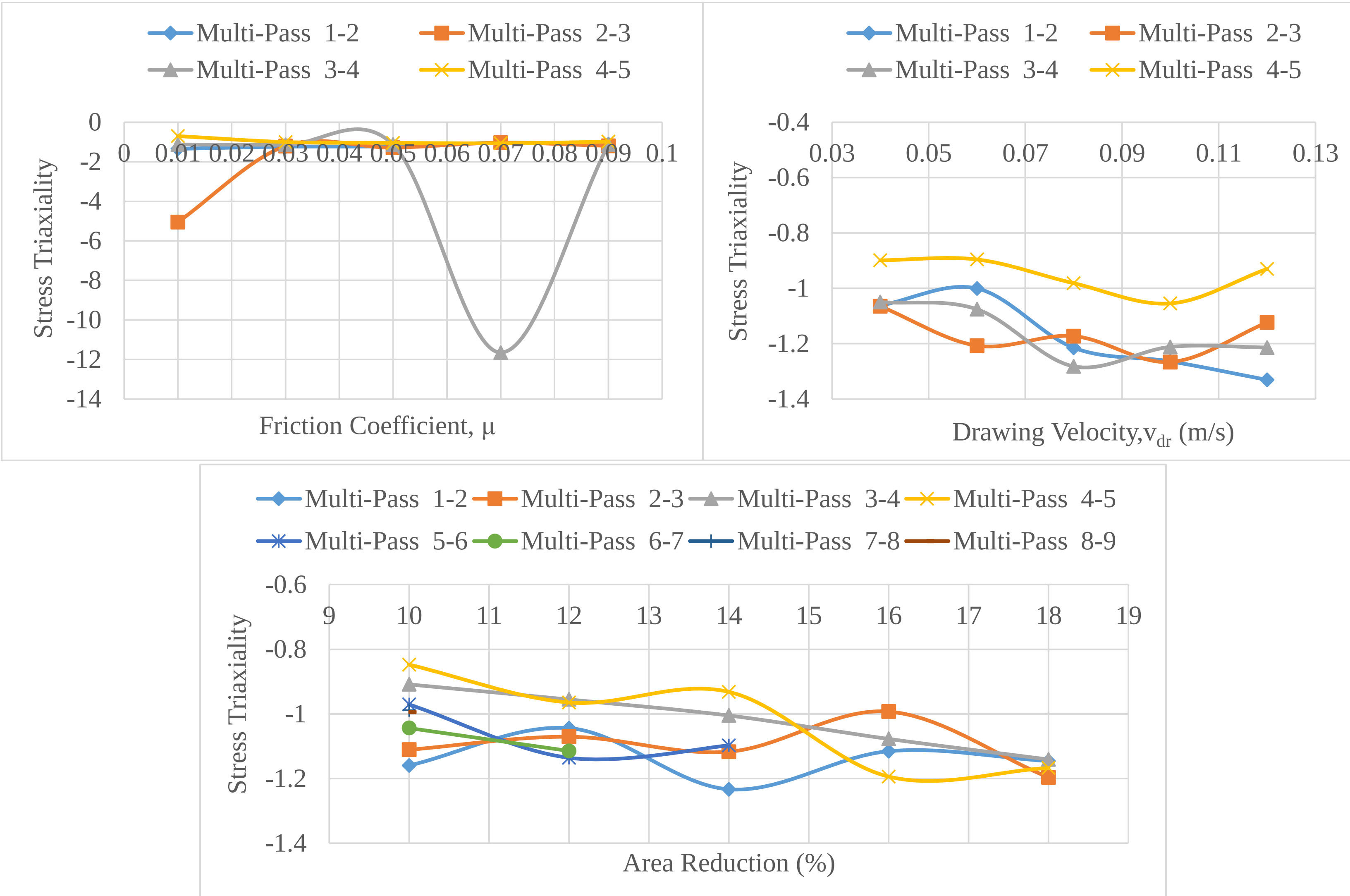

Figure 5.28 Distribution of Stress Triaxiality with Drawing Process Conditions for Centreline (306) Nodes

Figure 5.29 Distribution of Stress Triaxiality with Drawing Process Conditions for Surface (410) Nodes

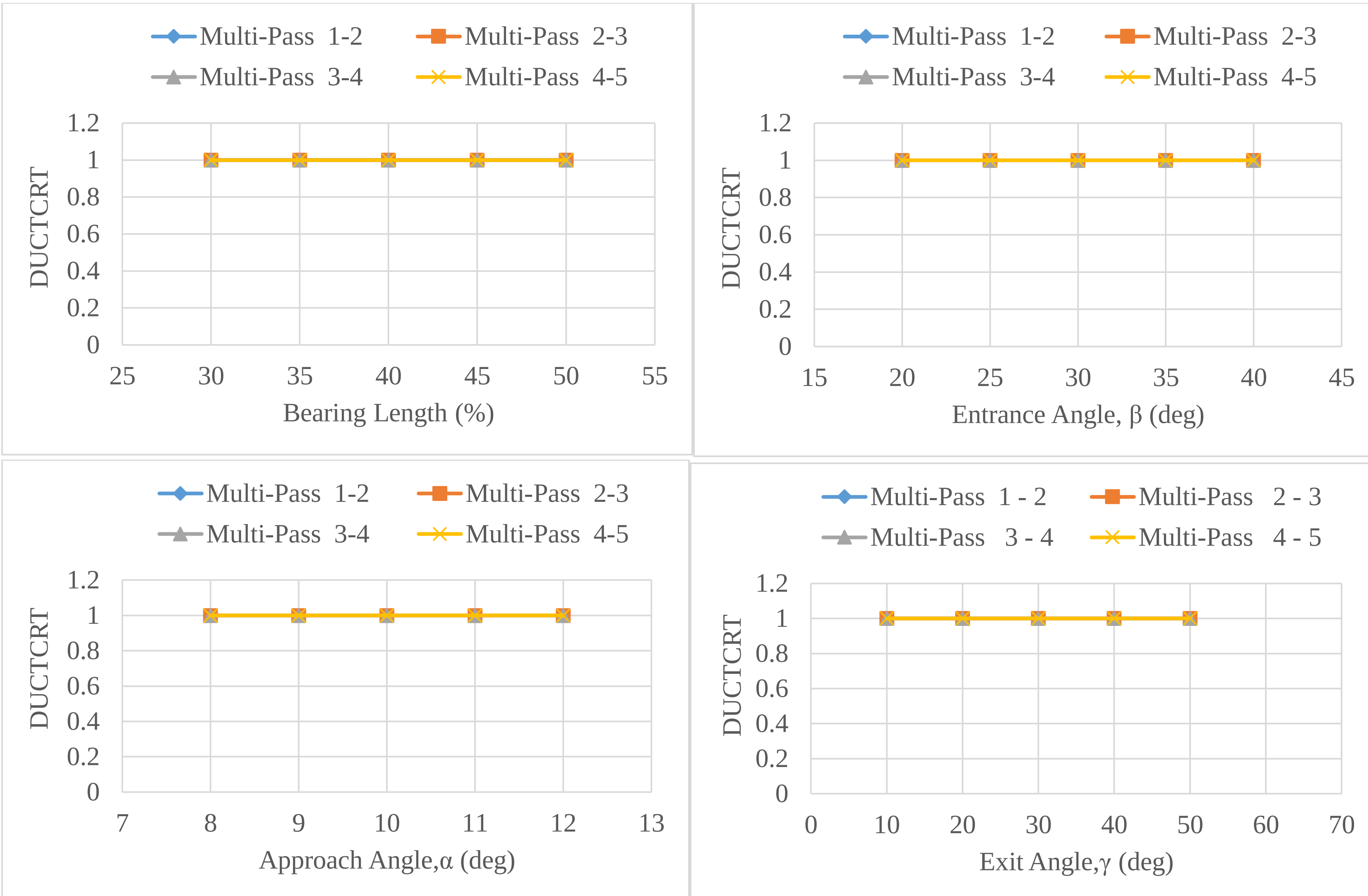

Figure 5.30: Distribution of Ductile Criterion (DUCTCRT) with Die Geometry for Centreline (306) Nodes. (Source: Author)

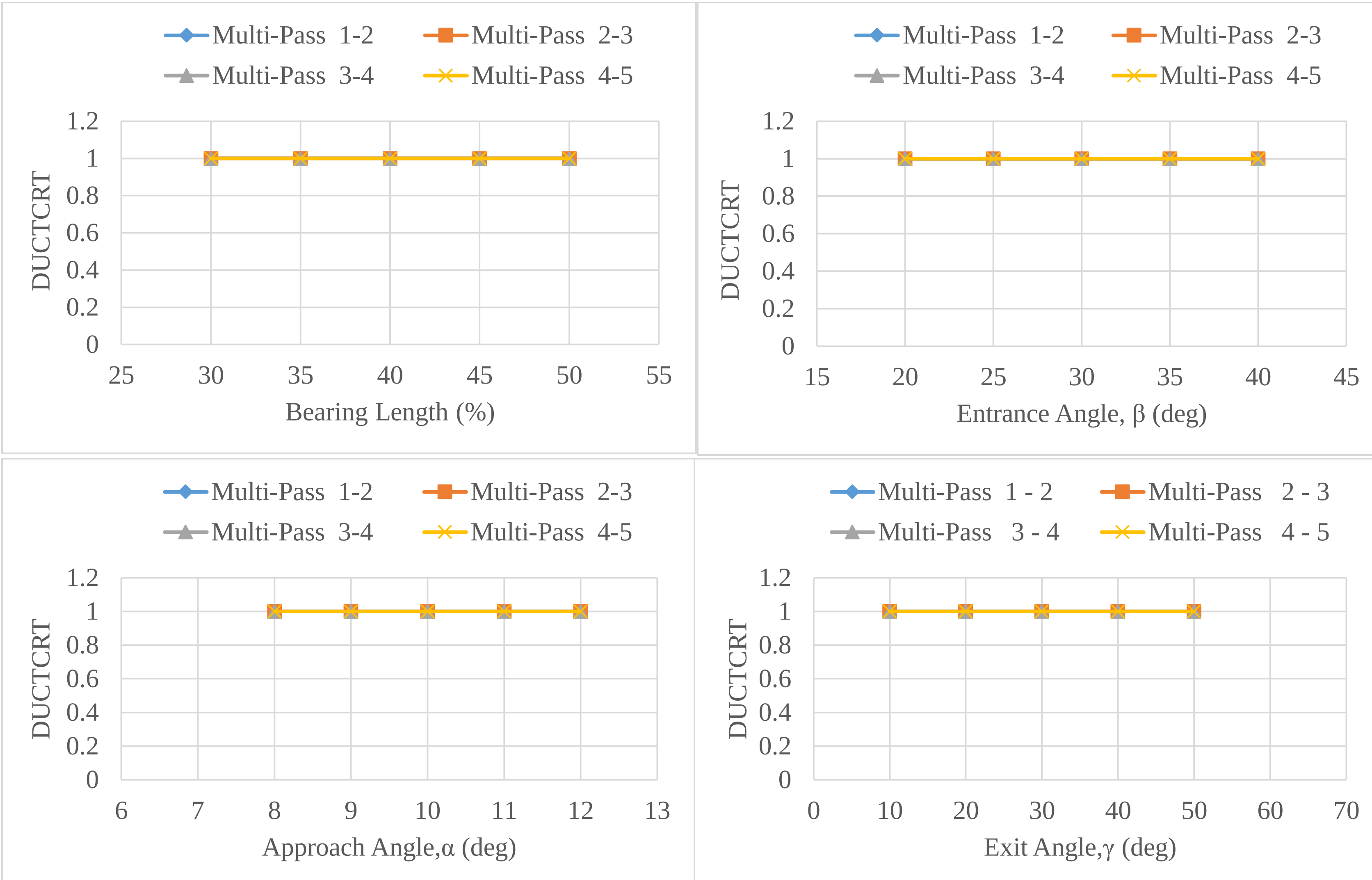

Figure 5.31: Distribution of Ductile Criterion (DUCTCRT) with Die Geometry for Surface (410) Nodes. (Source: Author)

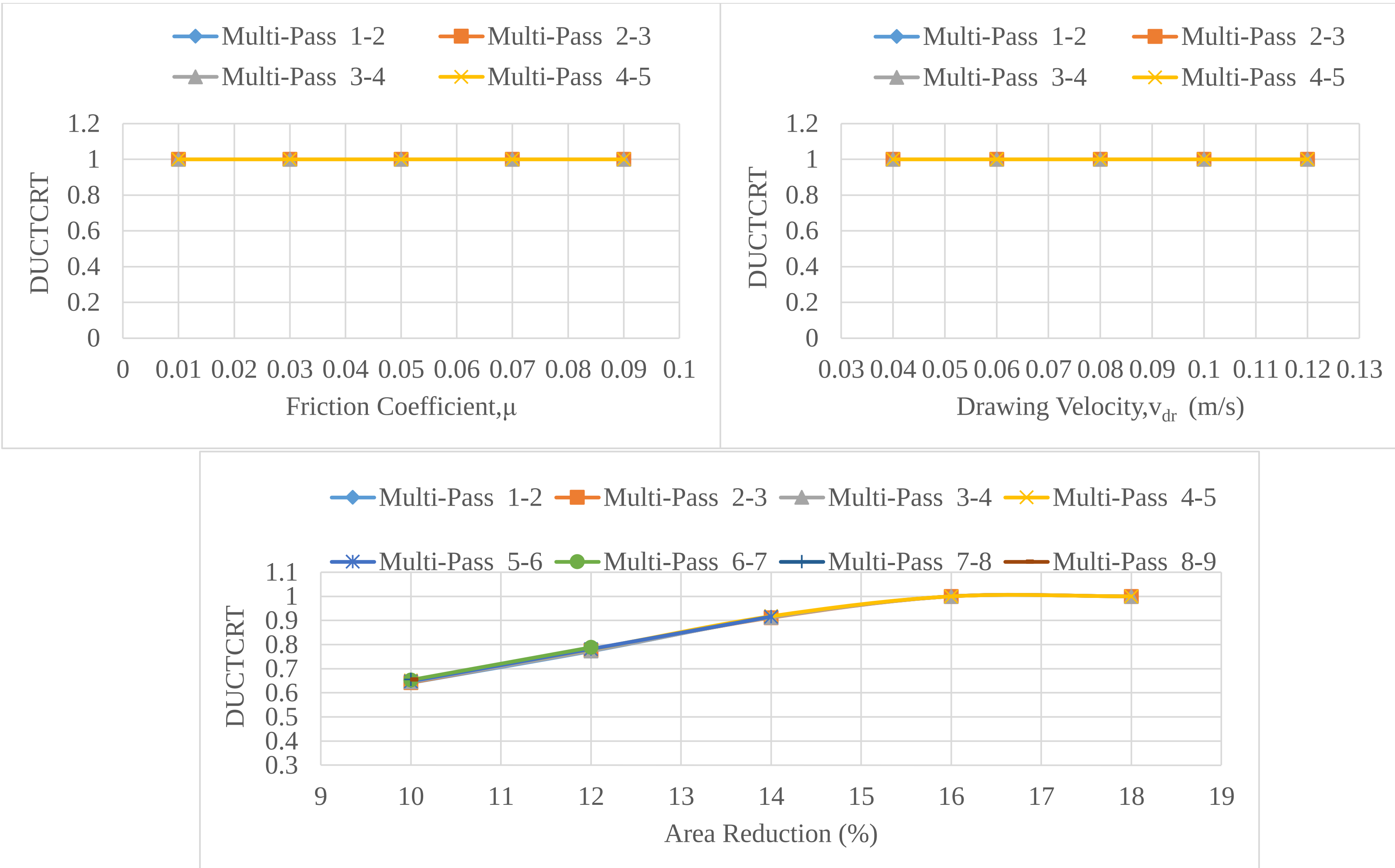

Figure 5.32: Distribution of Ductile Criterion (DUCTCRT) with Process Conditions for Centreline (306) Nodes. (Source: Author)

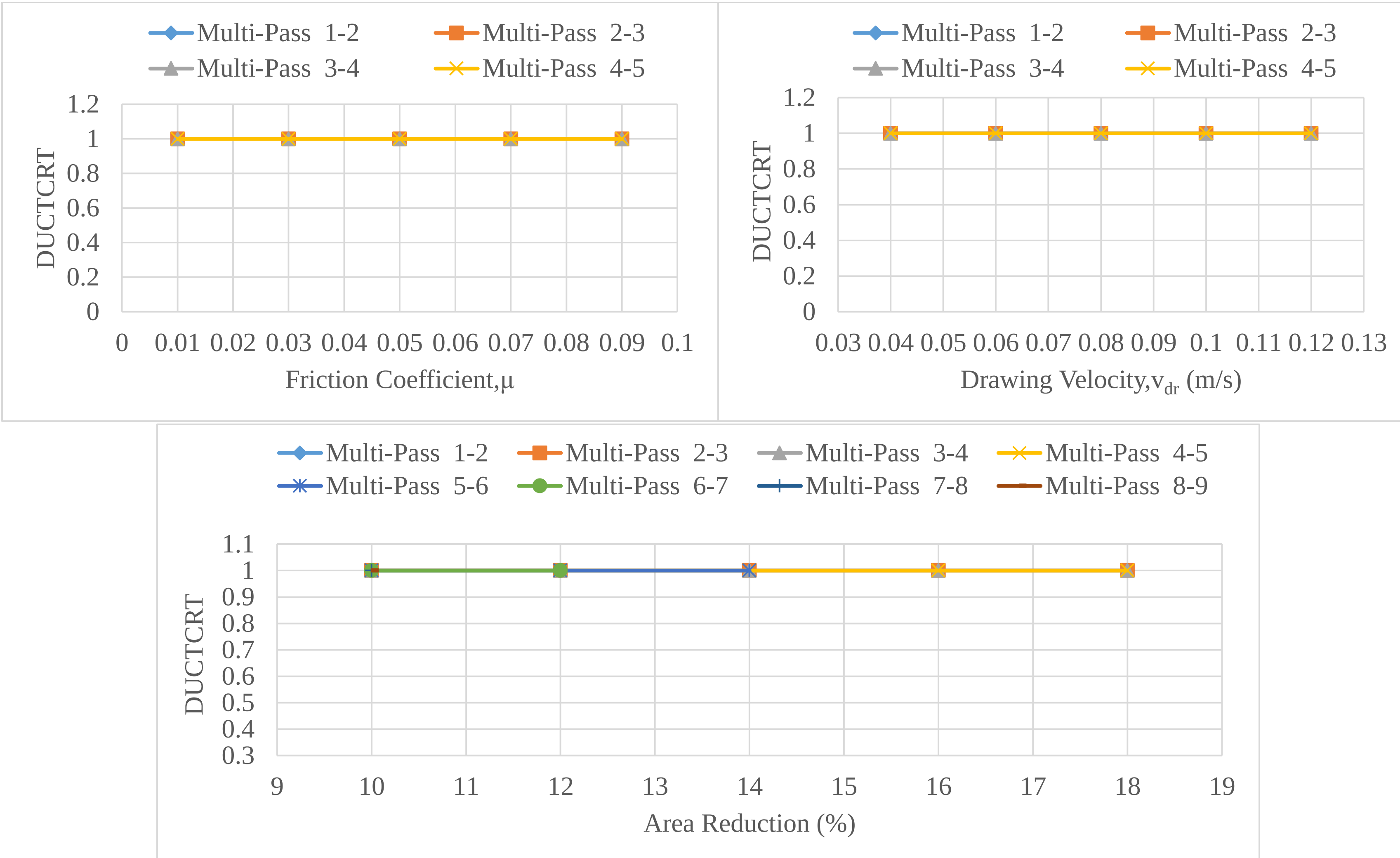

Figure 5.33: Distribution of Ductile Criterion (DUCTCRT) with Process Conditions for Surface (410) Nodes. (Source: Author)

(vi) Cockroft and Latham Criterion Distribution

The Cockroft and Latham criterion is used to show the occurrence of fracture in a material due to cumulative energy as a result of the maximum tensile stress exceeding a critical value (C_{CL} = 357.09 MPa) according to equation (5.12) as follows (Hosford and Caddell, 1983):

$$\int_0^{\bar{\epsilon}_f} \sigma_1 \, d\bar{\epsilon} = C_{CL} \tag{5.12}$$

where σ_1 is the maximum von Mises stress

$\bar{\epsilon}$ is the equivalent plastic strain.

Figure 5.34, 5.35, 5.36 and 5.37 show the distribution of the Cockroft and Latham criterion parameter with different die design and process parameters.

(vii) Damage Evolution (Stiffness Degradation) Distribution

Following the attainment of the ductile damage criterion (DUCTCRT), the inability of a material to carry further load is determined by the damage value or stiffness degradation. The rate of stiffness degradation signifies damage evolution. The scalar damage equation (5.7) is used to show the evolution of damage (Dassault Systèmes, 2014b). The ABAQUS output parameter for damage evolution or stiffness degradation is given by the SDEG parameter. A material is fully degraded (completely fails) when a stiffness degradation (SDEG), or the damage value of one is recorded. Figure 5.38, 5.39, 5.40 and 5.41 show the distribution of the stiffness degradation parameter during multi-pass copper wire drawing.

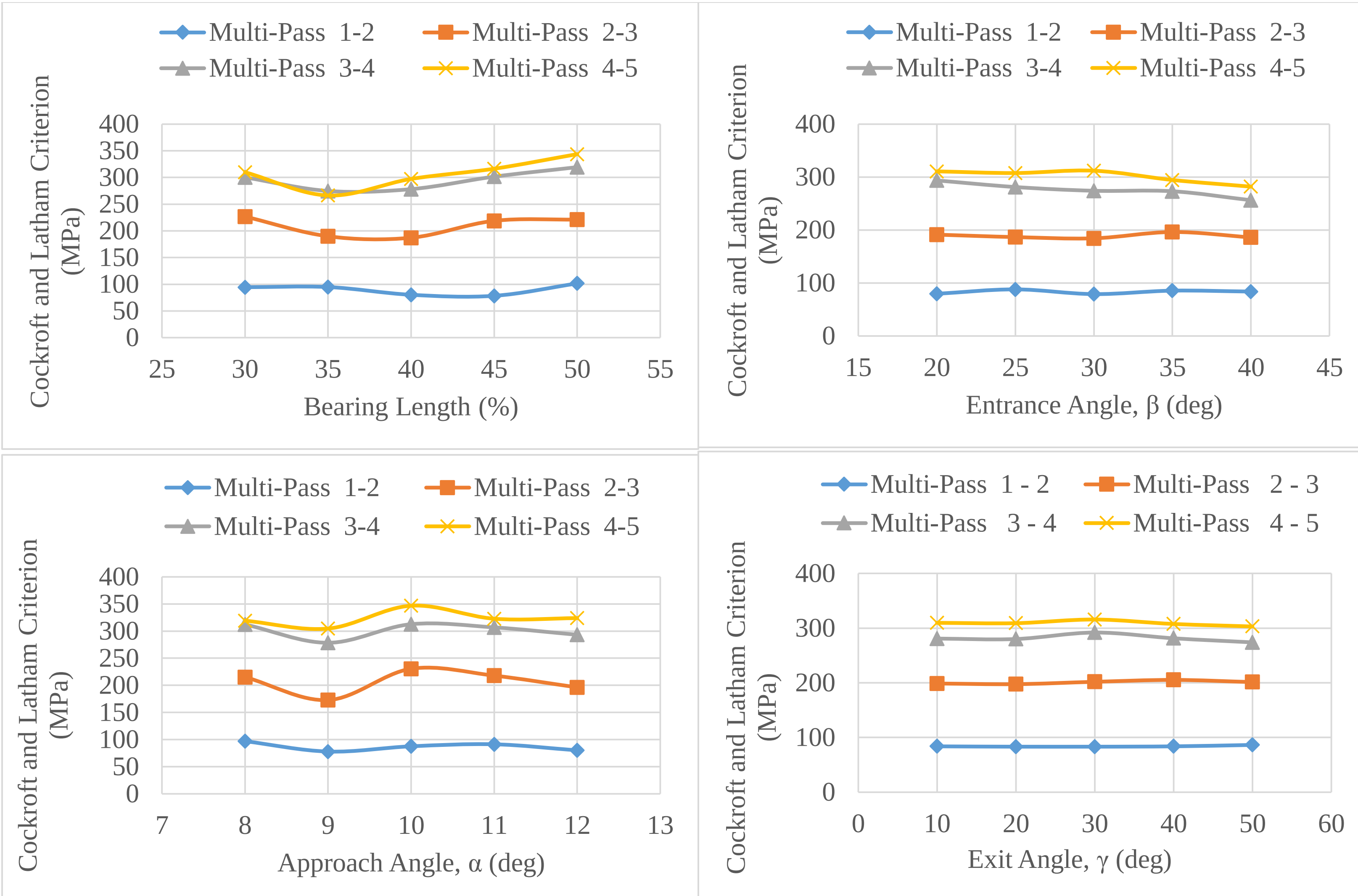

Figure 5.34: Distribution of Cockroft and Latham Criterion with Die Geometry for Centreline (306) Nodes. (Source: Author)

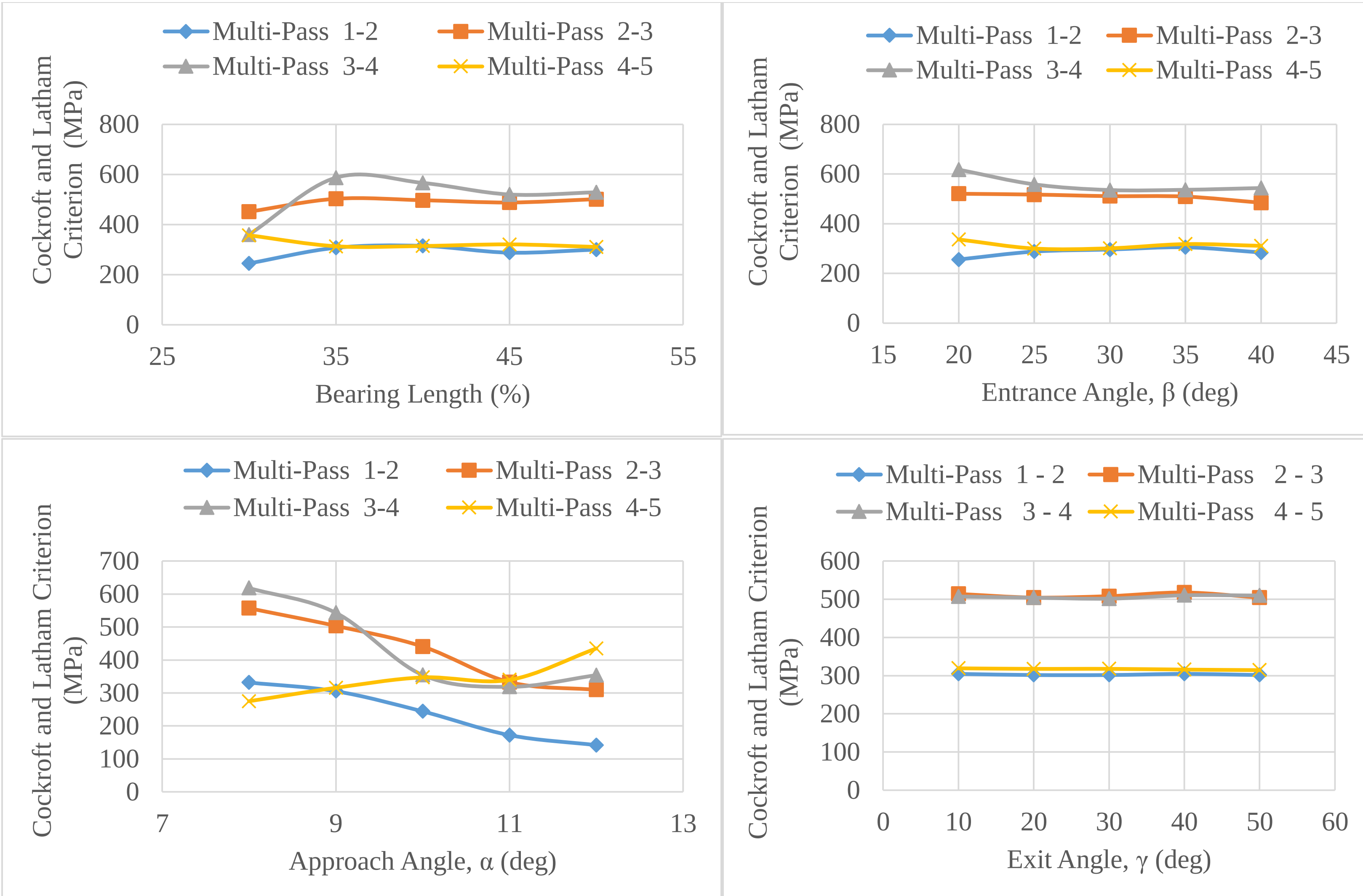

Figure 5.35: Distribution of Cockroft and Latham Criterion with Die Geometry for Surface (410) Nodes. (Source: Author)

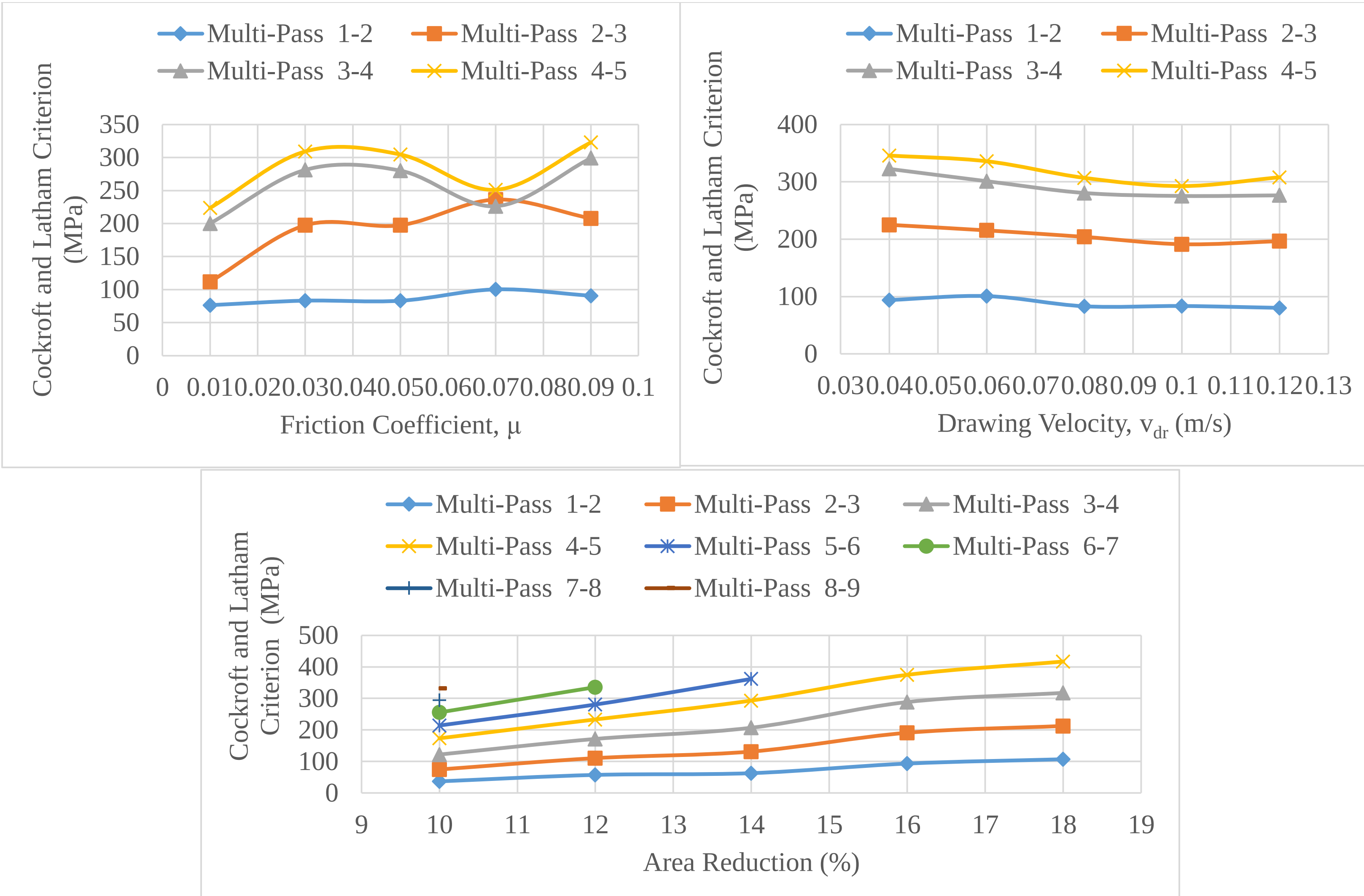

Figure 5.36: Distribution of Cockroft and Latham Criterion with Process Conditions for Centreline (306) Nodes. (Source: Author)

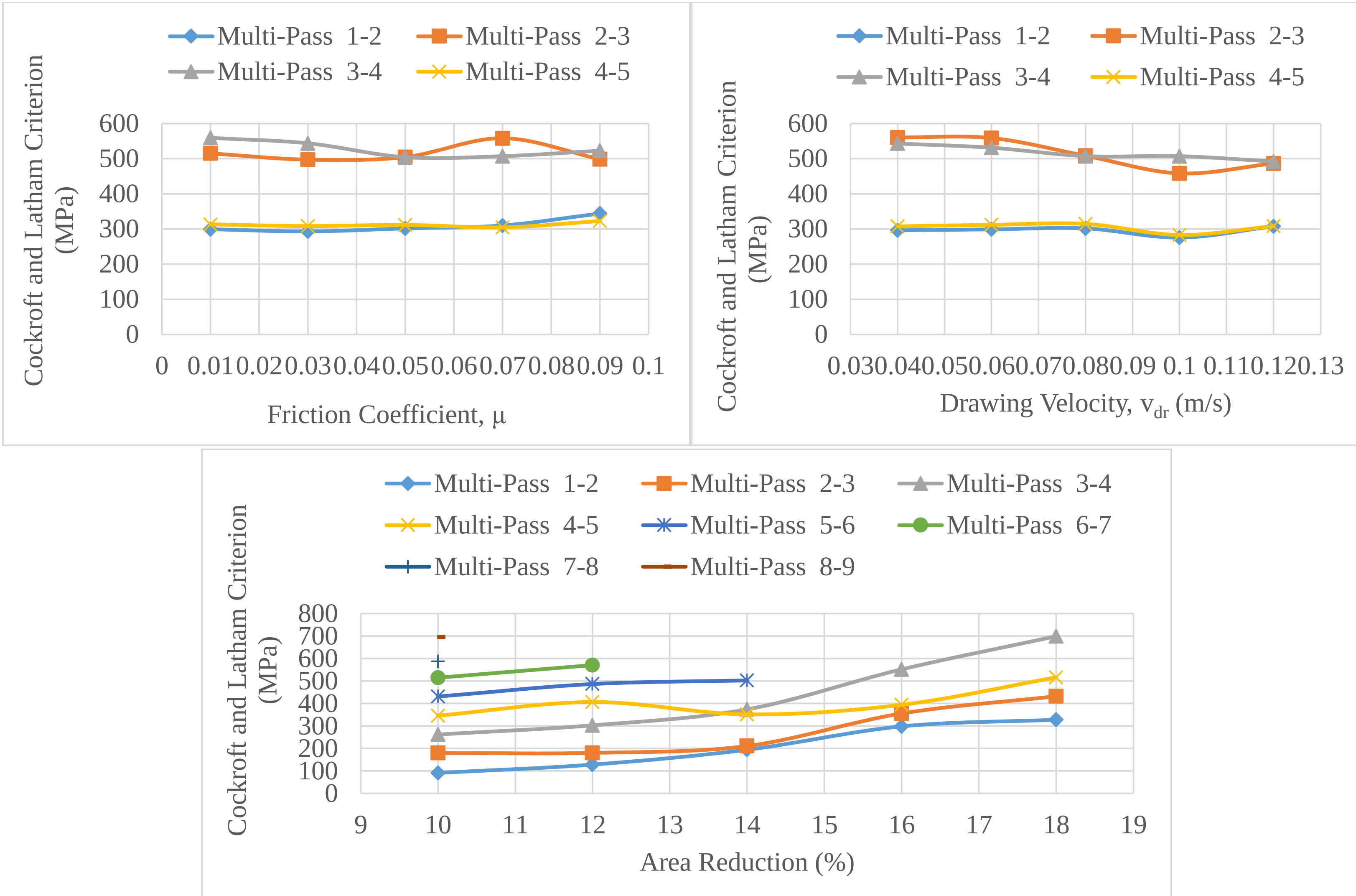

Figure 5.37: Distribution of Cockroft and Latham Criterion with Process Conditions for Surface (410) Nodes. (Source: Author)

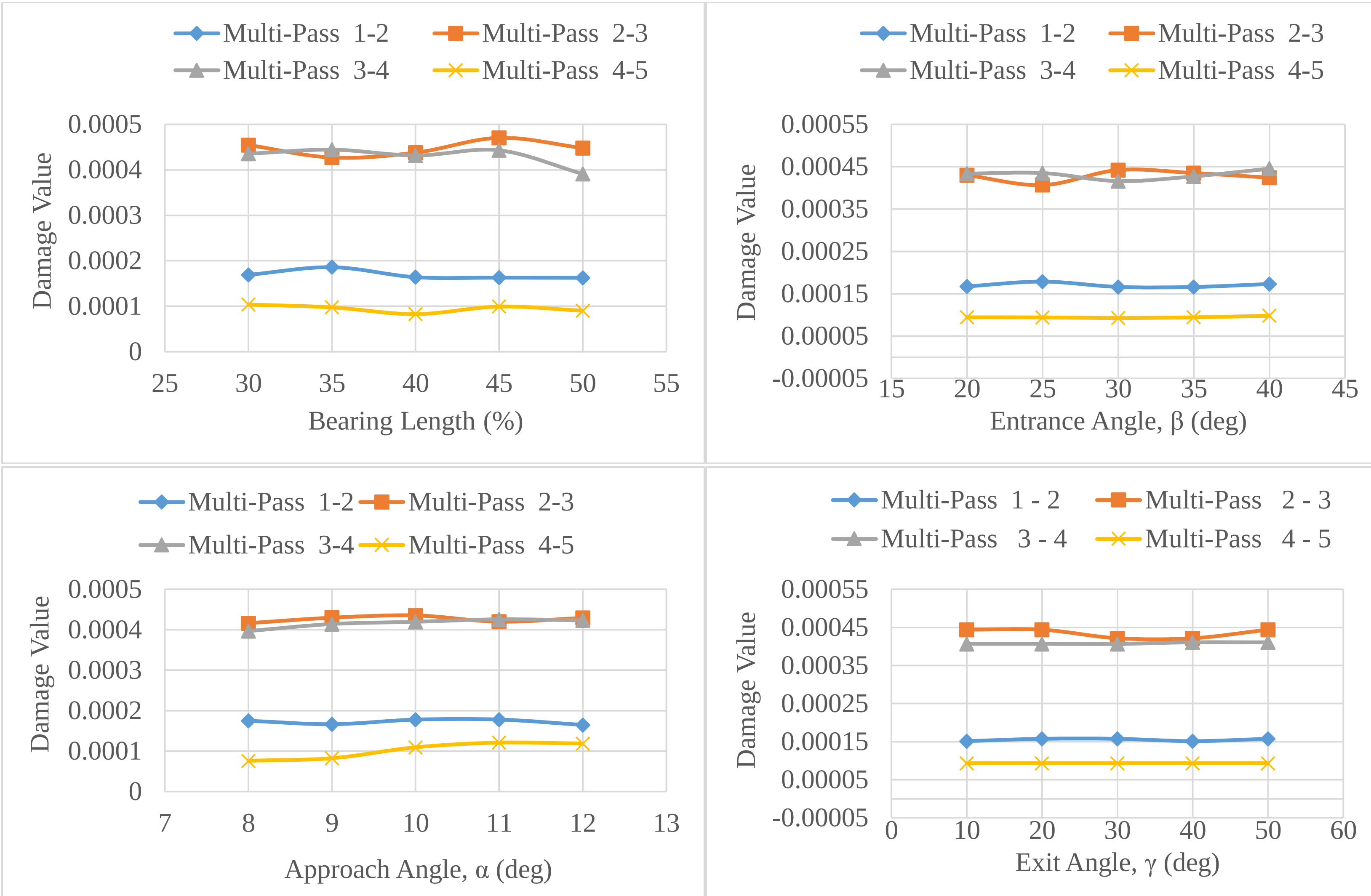

Figure 5.38: Distribution of Damage Value with Die Geometry for Centreline (306) Nodes. (Source: Author)

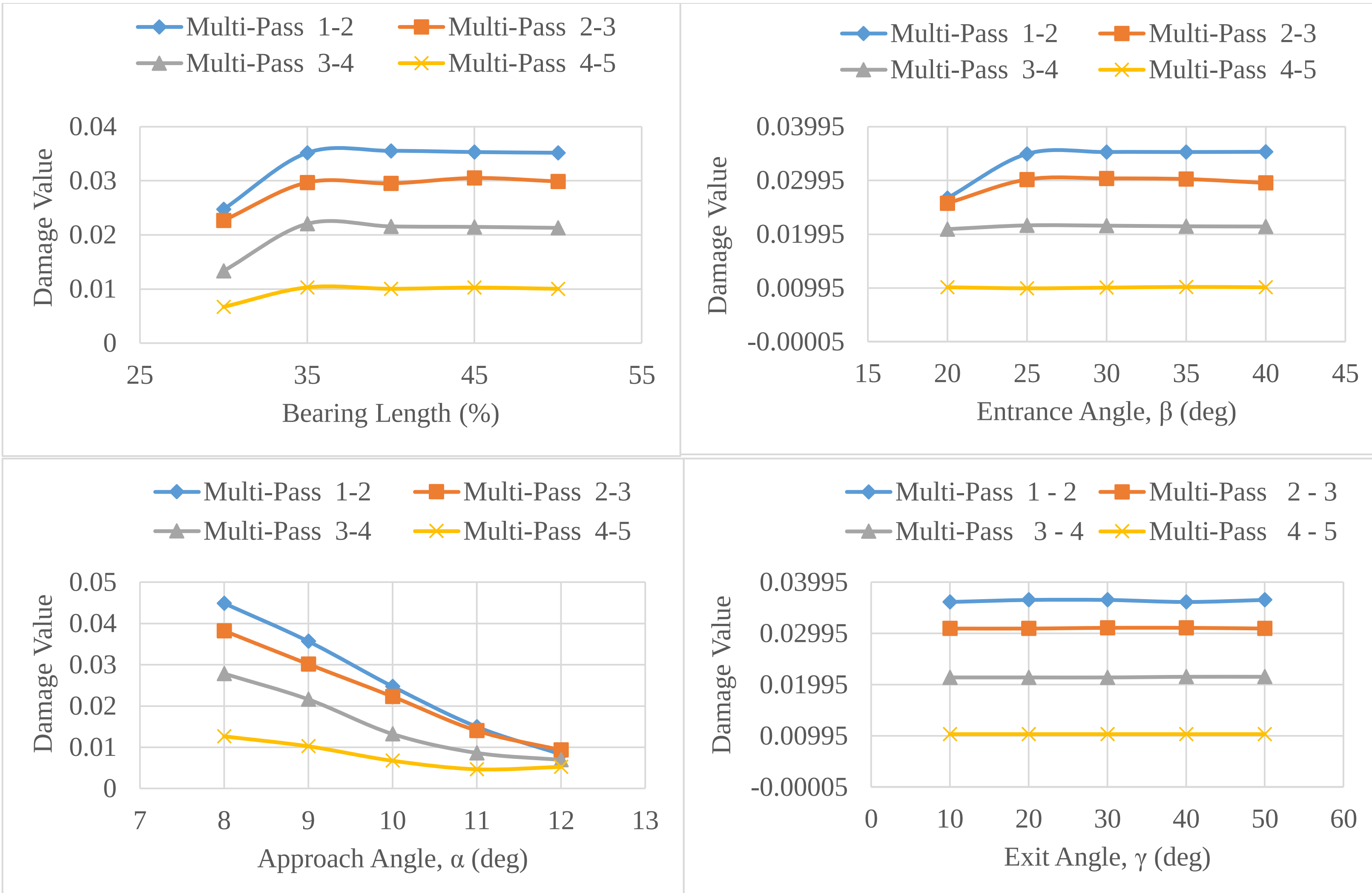

Figure 5.39: Distribution of Damage Value with Die Geometry for Surface (410) Nodes. (Source: Author)

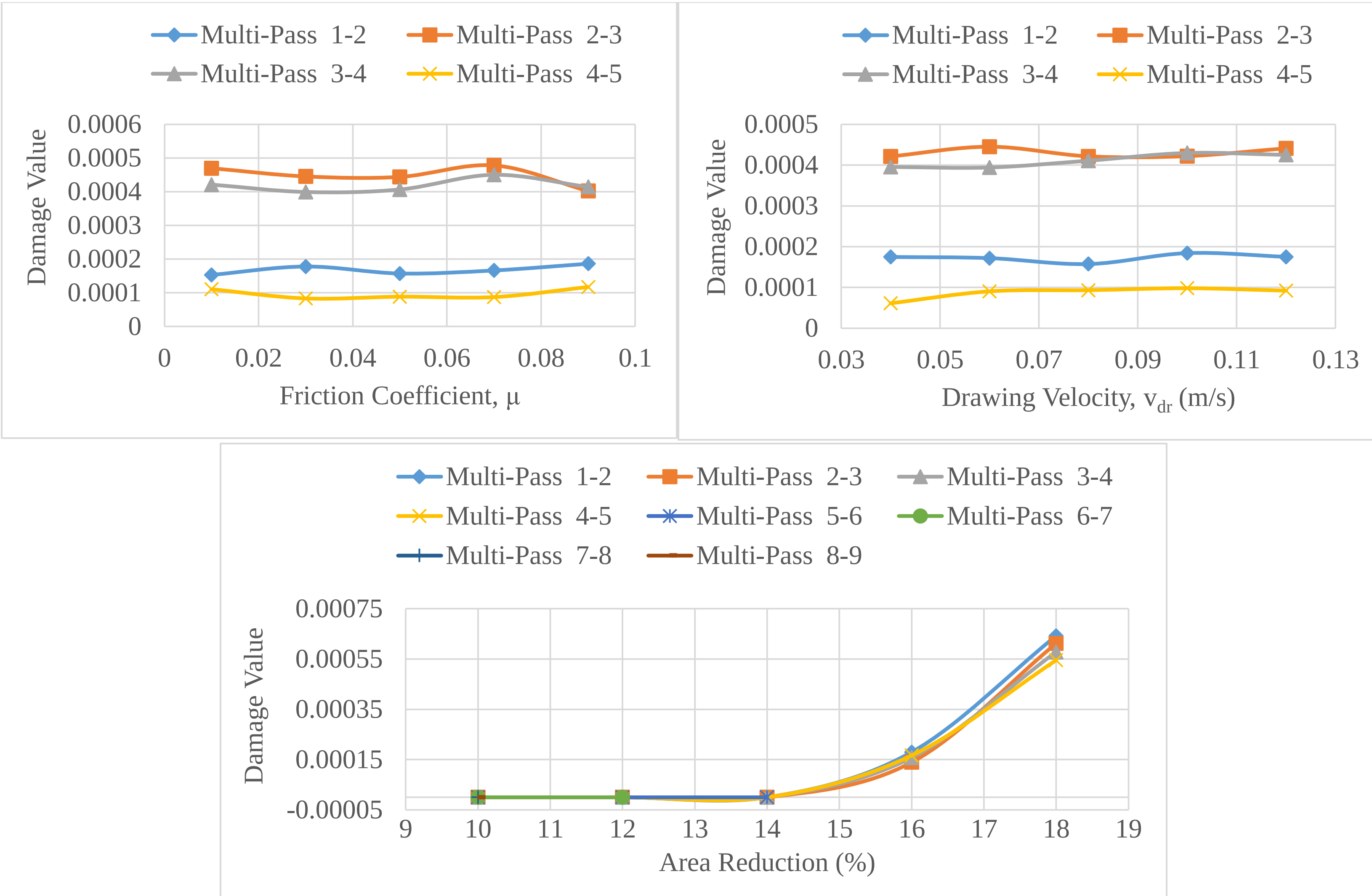

Figure 5.40: Distribution of Damage Value with Process Conditions for Centreline Node (306). (Source: Author)

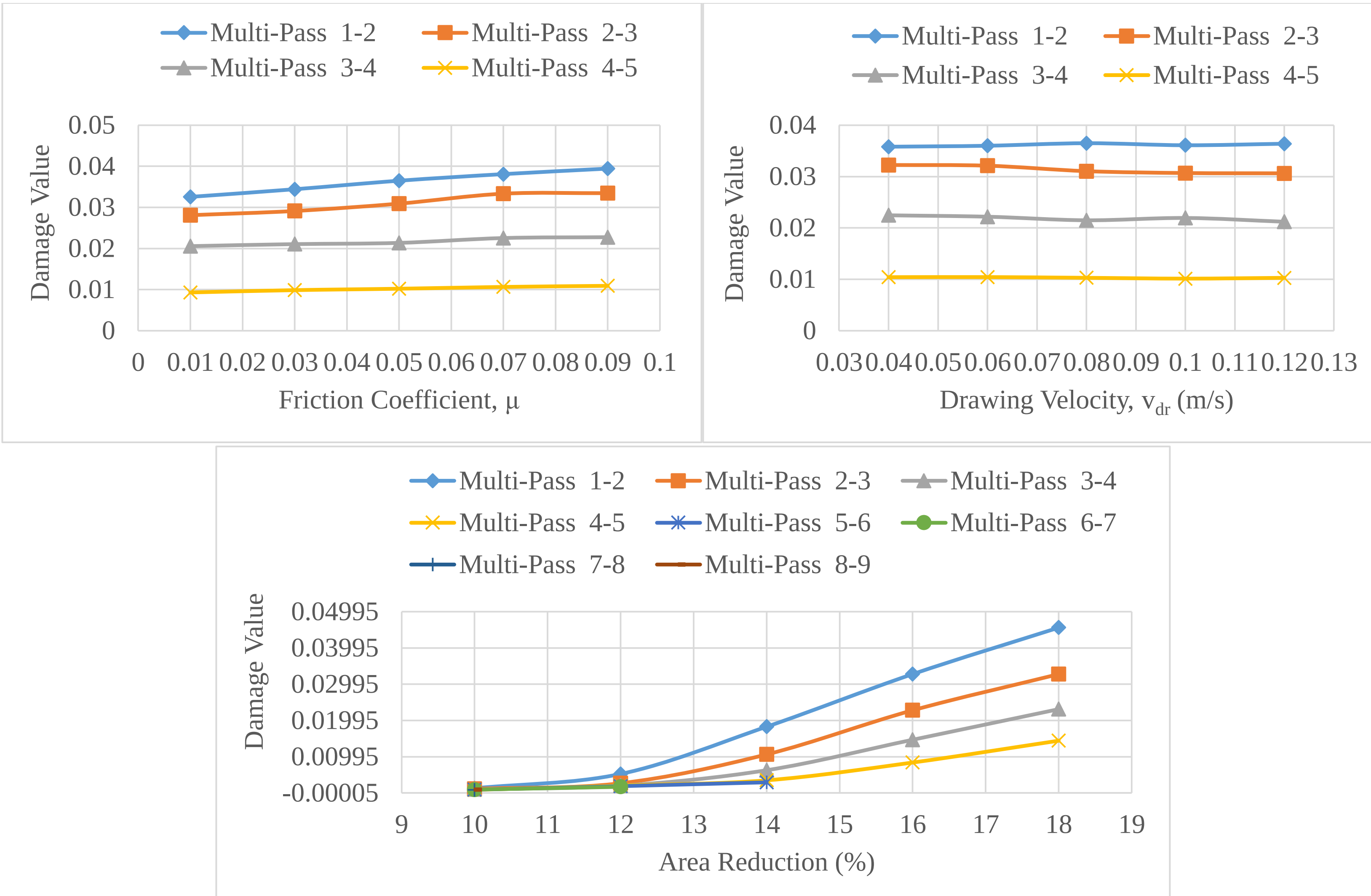

Figure 5.41: Distribution of Damage Value with Process Conditions for Surface (410) Node. (Source: Author)

5.8.3 Selection of Optimum Parameters from Simulation Results

The selection of optimum parameters was based on a combination of minimal mesh distortion and minimum values during distributions for damage value or stiffness degradation, equivalent Mises stresses responsible for yielding and damage formation and the Cockroft and Latham criterion. The results of the simulations show that the following die and process independent variables are predicted to give optimum wire drawing performance with reduced *centerline* material damage when producing a 1.78 mm copper wire with four dies:

- a bearing length of 40%,
- a semi-approach angle of 9^o,
- a semi-entrance angle of 30^o,
- a semi-exit angle of 40^o,
- a friction coefficient of 0.03,
- a drawing speed of 0.1 ms^{-1}
- area reductions of not more than 16% during the last multi-pass stage

The design of the die parameters which were used for the validation of the simulation results was based on the optimum parameters obtained, except for the area reductions. The area reductions were maintained as obtaining in the plant in order to assess the effects of the die geometry.

5.9. General Observations from Simulation Results

Consistency of the simulations was done by maintaining the same meshing and interaction properties. Accuracy of the simulations was achieved by maintaining the same time scaling factor of 1 with a target time increment of 0.00001.

Results of the simulation study indicated the following:

(1) Peaks for *centerline* ductile damage using Cockroft and Latham criterion were observed at the following points:

- bearing lengths of 50% (multi-pass sequences 1-2, 2-3, 3-4 and 4-5);

- approach semi-angles of 8^o (multi-pass sequence 1-2) and 10^o (multi-pass sequences 2-3, 3-4 and 4-5);
- entrance semi-angles of 20^o (multi-pass sequence 3-4), 25^o (multi-pass sequence 1-2), 30^o (multi-pass sequence 4-5) and 35^o (sequence 2-3);
- friction coefficient of 0.07 (multi-pass sequences 2-3, 3-4) and 0.09 (multi-pass sequences 1-2, 4-5);
- drawing velocities of 0.04 ms^{-1} (multi-pass sequences 2-3, 3-4 and 4-5) and 0.06 ms^{-1} (multi-pass sequence 1-2).
- area reductions of 18% (multi-pass sequences 1-2, 2-3, 3-4 and 4-5).

(2) Peaks for *surfaceline* ductile damage using Cockroft and Latham criterion were observed at the following points:

- bearing lengths of 40% to 50% (multi-pass sequences 2-3, 3-4);
- approach semi-angles of 8^o (multi-pass sequences 1-2, 2-3 and 3-4) and 12^o (multi-pass sequence 4-5);
- entrance semi-angles of 20^o (multi-pass sequences 2-3, 3-4 and 4-5) and 35^o (multi-pass sequence 1-2);
- friction coefficient of 0.01 (multi-pass sequence 3-4), 0.07 (multi-pass sequence 2-3) and 0.09 (multi-pass sequences 1-2 and 4-5);
- drawing velocity of 0.04 ms^{-1} (multi-pass sequences 1-2, 2-3, 3-4 and 4-5)
- area reductions of 18% (multi-pass sequences 1-2, 2-3, 3-4 and 4-5)

5.10 Summary of Simulation Results

From the analysis and discussion of results from the modelling and simulation of copper wire drawing, the following conclusions can be made:

(1) All the die geometrical parameters, except the exit angle, have an effect on the development of both wire centerline and surface cracks. The area reduction has a stronger effect on wire damage.

(2) Lubrication, with its related friction coefficient, and drawing velocity influences wire centerline and surface damage. The friction coefficient has a stronger effect.

(3) The drawing force increases gradually with the size of the wire being drawn (die size) and with the increase in area reduction.

(4) At an approach angle of 10^{o}, area reductions above 16% and elongation percentages above 19% have Δ-parameters less than 4.

(5) The strain rate increases uniformly with increased area reduction, with the rate being higher and faster and dependent on multi-pass stage for the surface nodes.

CHAPTER SIX: EXPERIMENTAL DESIGN AND PROCEDURES

6.1 Introduction

This chapter is divided into five major sections. The first section presents the experimental design used in undertaking the experiments. The second section gives an overview of major equipment and instruments used in the laboratory and industrial experiments. Section three explains details of the experimental procedures carried out. The fourth section presents results from the laboratory and industrial experiments.

.

6.2 Experimental Design

The research involved understanding material properties, the copper wire drawing practice and die manufacturing. Laboratory experiments were undertaken for wire and die material property analysis, while industrial experiments were done for wire drawing and validation of models.

The raw material for both laboratory microstructure and other engineering properties determination and further industrial experiments was a 7.9 mm wrought copper rod. This rod was drawn through a rod breakdown machine to a 2.76 mm diameter copper wire for further wire drawing analysis on the intermediate wire drawing machine and for scanning electron microscopy analysis.

Tungsten carbide dies were designed and manufactured according to the simulated optimum die designs and used in obtaining the wire drawing independent and dependent variables in the plant.

6.3 Equipment and Instrumentation

The major equipment used in the laboratory and industrial experiments are explained below.

6.3.1 Laboratory Experiments and Equipment

(i) Microscopy and Spectrophotometry

A light microscope, Olympus B203 with a magnification of up to 100X was used for microstructure analysis of the raw copper. Figure 6.1 shows the Olympus light microscope. The chemical composition of the copper rod was determined using both atomic absorption spectrophotometry (AAS) and scanning electron microscopy analysis.

Figure 6.1: Olympus B203 Light Microscope. (Source: Author)

(ii) Scanning Electron Microscope (SEM)

The Quanta FEG 450 Scanning Electron Microscope was used for both material micro- and macrostructure analysis, and elemental analysis. The Quantax Esprit 1.9 software was used on the SEM to obtain chemical composition of the raw copper materials. Figure 6.2 shows the Quanta FEG SEM.

(iii) Universal Tensile Testing Machine (UTM)

A universal tensile testing machine, TUE C- 600 with an accuracy of +/- 1% and a capacity of 12 to 600 kN was used for carrying out tensile testing. Figure 6.3 shows the universal tensile testing machine.

Figure 6.2: Quanta FEG 450 Scanning Electron Microscope. (Source: Author)

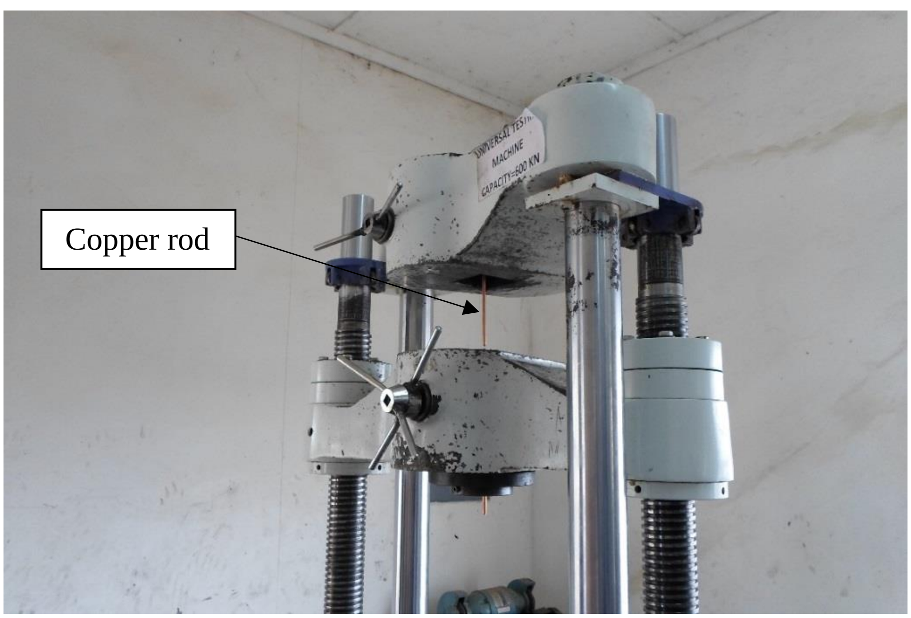

Figure 6.3: Tensile Testing Machine TUE C-600. (Source: Author)

6.3.2 Industrial Experiments and Equipment

(i) Wire Drawing Equipment

An intermediate wire drawing machine, model HT-24DTS was used for conducting wire drawing experiments. The entire machinery shown in Figure 6.4 comprised of the following: a pay-off, a pointing machine, the main drawing machine with a driver motor capacity of 45 kilowatts, an annealer with a current capacity of 543 amps, a tensioner and a spooler of capacity 15 kilowatts.

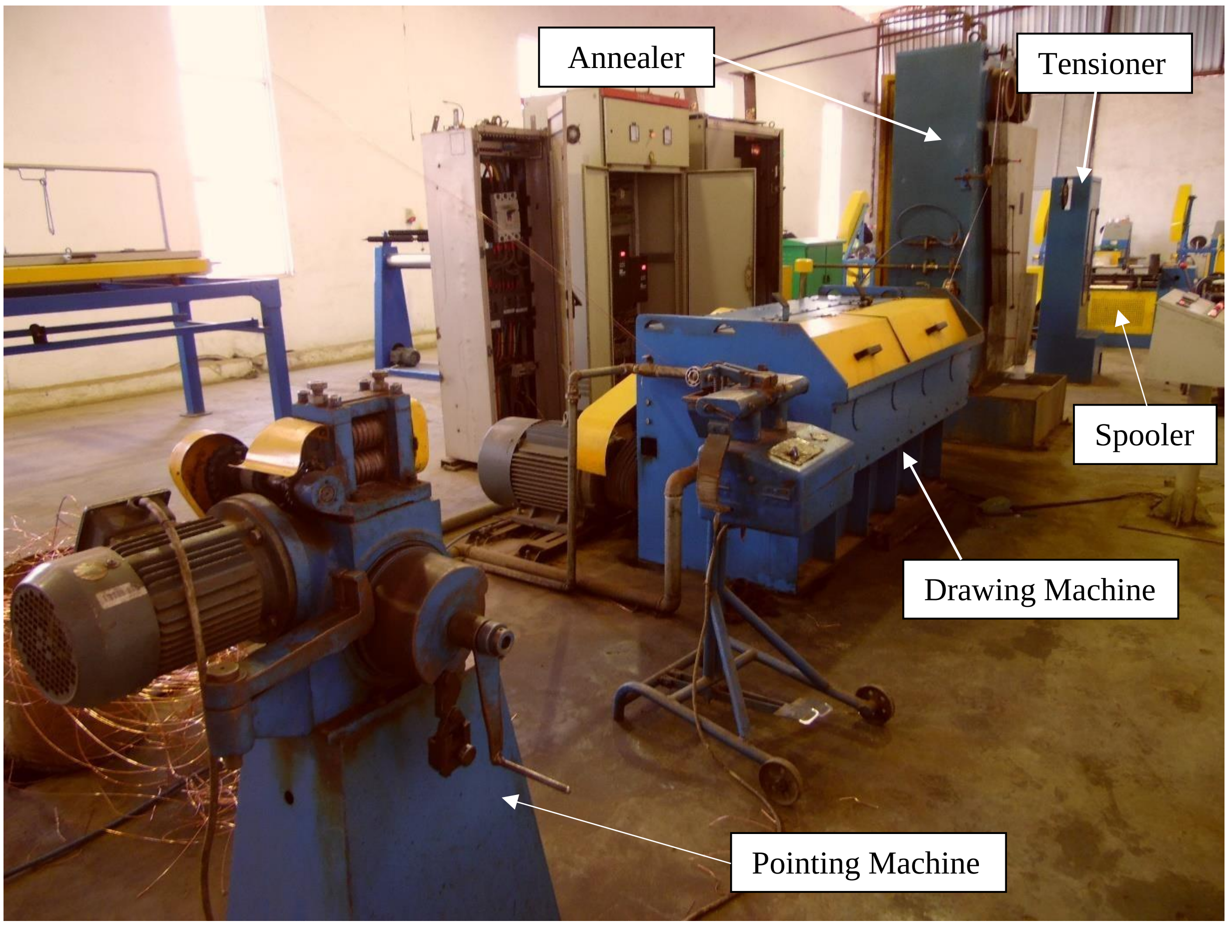

Figure 6.4: Copper Wire Drawing Machine Components. (Source: Author)

6.4 Experimental Procedure

6.4.1 Material Testing

The materials used in the research were 7.9 mm diameter copper rods and medium size (diameter range of 2.76 to 1.78 mm) copper wires. The 7.9 mm diameter copper rods were subjected to tensile testing and microstructure investigation, while the medium size copper wires were subjected to industrial wire drawing and microstructure investigation. Aqueous ferric chloride was used as the etchant for microstructure investigation. Flakes of the copper rods were subjected to atomic absorption spectrophotometry (AAS) for determination of the chemical composition.

6.4.2 Drawing Die Design and Manufacturing

(1) Die Design

The design of the wire drawing die involved design of the tungsten carbide nib, the steel shell and the entire assembly. The dies designed were based on the plant planned die sequence for production of the 1.78 mm copper wire. Figure 6.5 shows the wire-die-shell assembly.

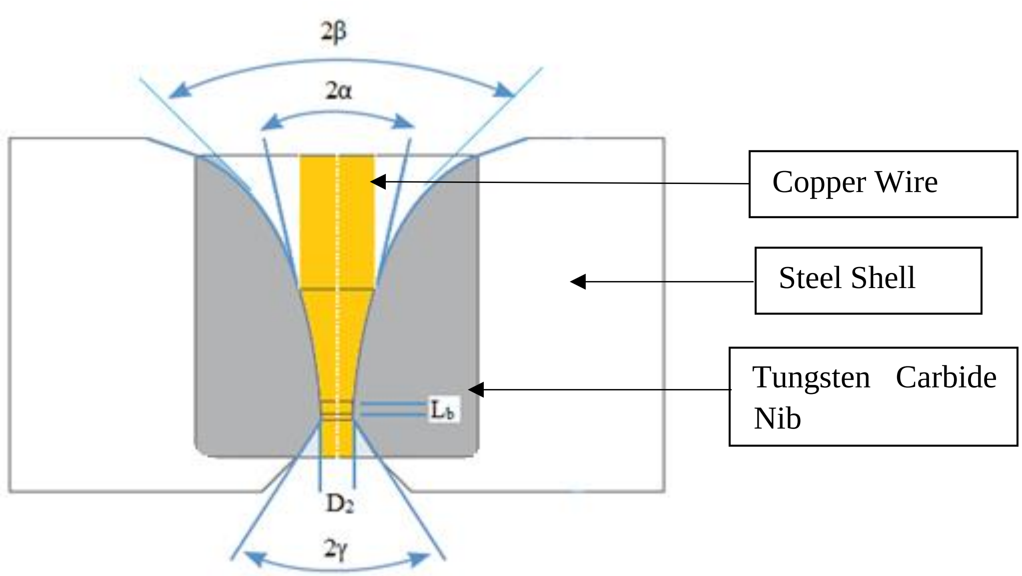

Figure 6.5: Wire-Die Assembly Source: (Esteves Group, 2008)

For the tungsten carbide nib, optimum die geometry values from the models were used, namely the approach angle (2α) was kept at 18°, the entrance angle (2β) was maintained at 60°, while the exit angle (2γ) was maintained at 80°. Table 6.1 shows the different die designations, final wire diameters (D_2), bearing sizes (L_b) and the various shell designs that were used to design the wire drawing dies. **Appendix 7** shows the CAD drawings for the die nib and the steel casing.

(ii) Die Manufacturing

Material for the steel shell was chosen as G10120 (SAE –AISI 1012) which is obtained by cold rolling as recommended by the ASM (1990). The entrance and exit zones of the steel shell were designed such that a smooth transition occurs as the wire approaches the entrance zone and exits from the exit zone of the die nib. Two shell designs with drawing numbers SS03 and SS04 were made to respectively accommodate tungsten carbide nibs of internal bore sizes of 1.78 to 2.32 and 2.55 mm.

Prototype dies were produced according to the design specifications provided by the author in conformity with Table 6.1 to a company in China (Zhuzhou Good Cemented Carbide Company, www.carbide-good.com). The outsourced dies are displayed in Figure 6.6. Figure 6.7 shows the location of the die sets in the wire drawing machine.

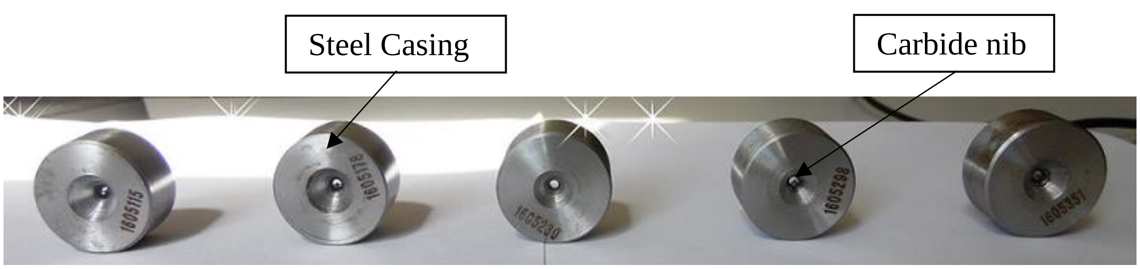

Figure 6.6: Prototype Dies used in Copper Wire Drawing. (Source: Author)

Table 6.1: Drawing Die Specifications

No.	**Designation**	**Carbide Nib Parameters**						**Steel Shell Size**	**Die Assembly**	
		D_2 (mm)	2α (°)	2β (°)	2γ (°)	L_b (mm)	Dwg No.		Fit	Arrangement
1	ϕ 5.0 x 6.3 / ϕ 1.78	1.78	18	60	80	0.71	CN 11	SS 03	ϕ 5.0 H7/s6	DA 02
2	ϕ 5.0 x 6.3 / ϕ 1.92	1.92	18	60	80	0.77	CN 12	SS 03	ϕ 5.0 H7/s6	DA 02
3	ϕ 5.0 x 6.3 / ϕ 2.11	2.11	18	60	80	0.84	CN 13	SS 03	ϕ 5.0 H7/s6	DA 02
4	ϕ 5.0 x 6.3 / ϕ 2.32	2.32	18	60	80	0.93	CN 14	SS 03	ϕ 5.0 H7/s6	DA 02
5	ϕ 5.5 x 7.3 / ϕ 2.55	2.55	18	60	80	1.02	CN 15	SS 04	ϕ 5.5 H7/s6	DA 03

(Source: Author)

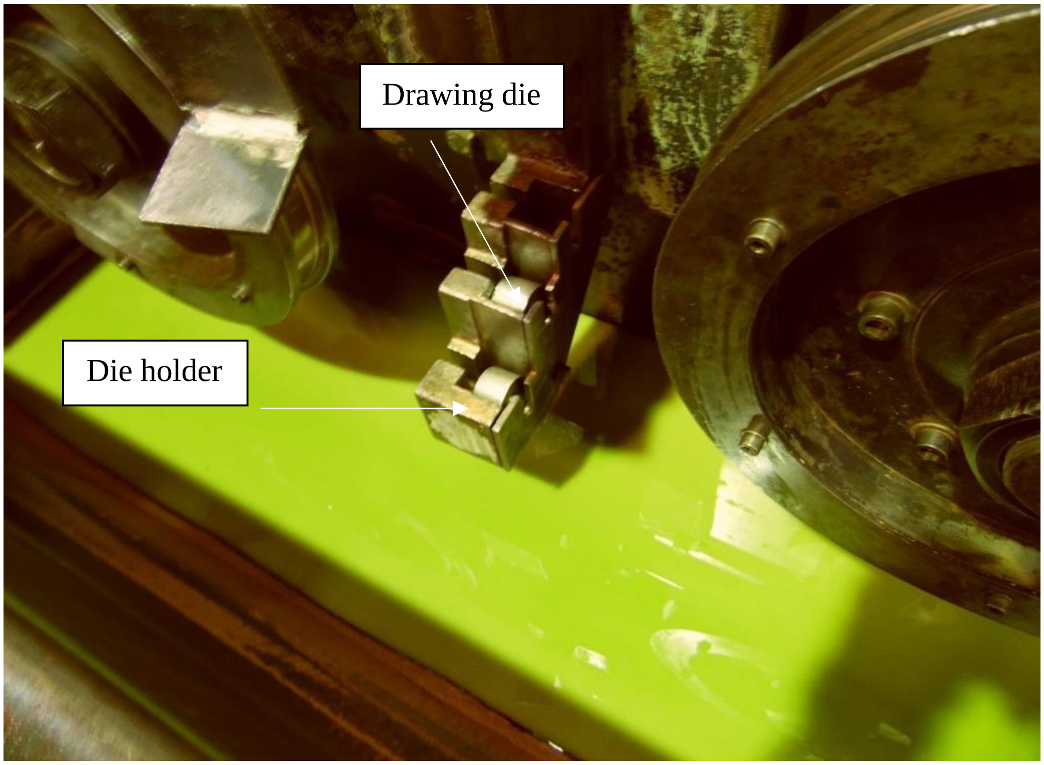

Figure 6.7: Die Location in Wire Drawing Machine. (Source: Author)

6.4.3 Wire Drawing Experiments

Using the 2.76 mm copper rods as the raw material and the equipment shown in Figure 6.4, wire drawing experiments involving prototype tungsten carbide dies were conducted at different intervals in order to observe wire drawing speeds, wire tension, drawing forces, die and lubricant temperatures, annealing parameters and wire breakages. Figure 6.8 shows the intermediate copper wire drawing machine used, with relative positions of the copper wire on capstans and the lubricant.

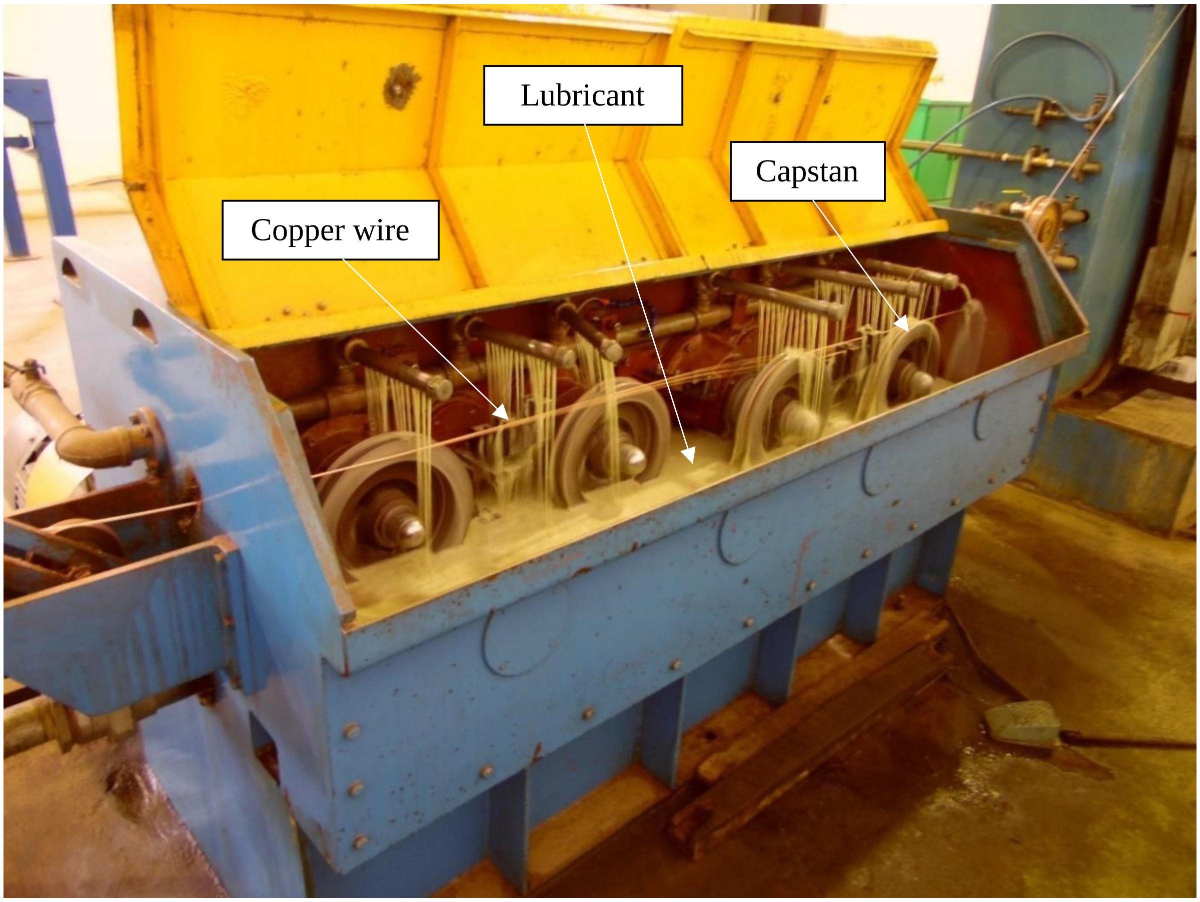

Figure 6.8: Intermediate Copper Wire Drawing Machine. (Source: Author)

6.5 Results from Experimental Procedure

6.5.1 Microstructure and Chemical Composition

Table 6.2 shows the chemical composition of the wrought copper rods according to conforming standard ASTM B49-10. Figure 6.9 shows the microstructure of the wrought copper rod.

Table 6.2: Composition of Wrought Copper.

Constituent Elements (norm. wt %)									
Sb	**As**	**Cd**	**Fe**	**Pb**	**Mn**	**Ni**	**Ag**	**Zn**	**Cu**
<0.04	<0.01	<0.002	0.12	<0.01	0.002	0.003	<0.01	0.04	Bal.

(Source: Author)

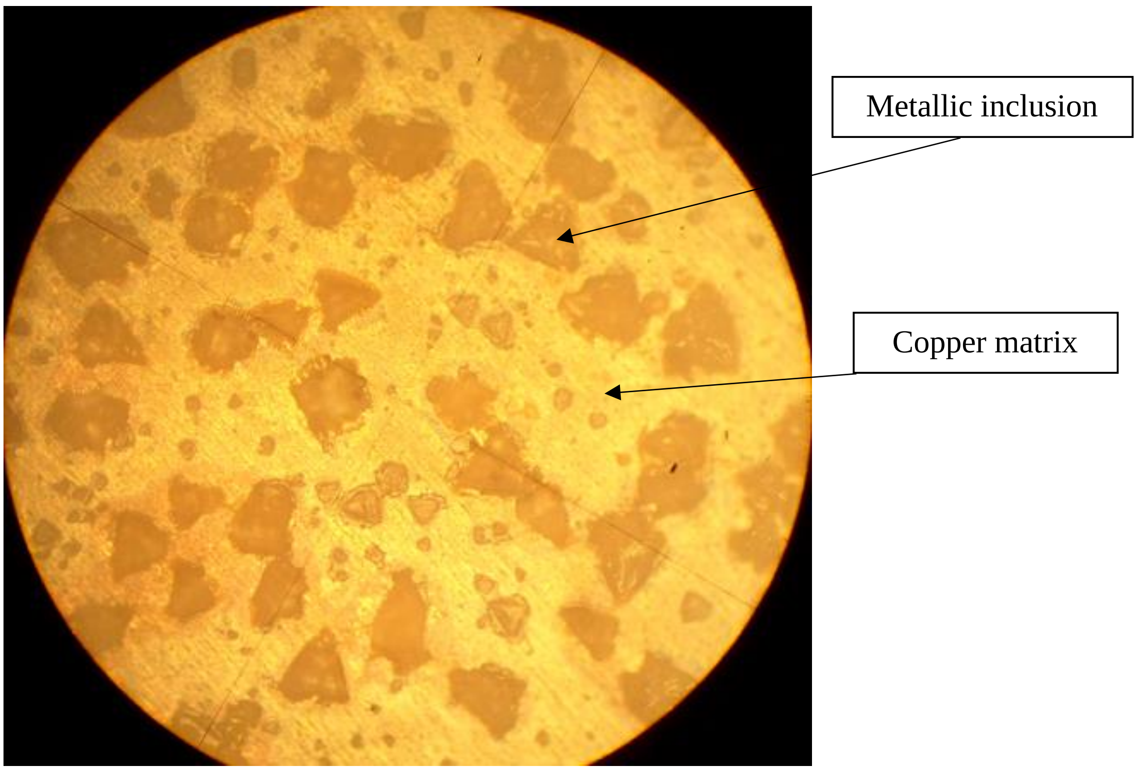

Figure 6.9: Microstructure of Wrought Copper. (Source: Author)

6.5.2 Mechanical Properties of Wrought Copper Rods

A standard density of 8960 kgm^{-3} and a Poisson standard value of 0.34 were used in all formulations as per the recommendations of ASM International (1990). Tables 6.3 and

6.4 show the mechanical properties, while **Appendix 5** shows the values ascertained from the tensile tests for wrought copper rods.

From the tensile test experiment, the flow curve for the wrought copper material used corresponded to the stress-strain graph given in Figure 6.10 and according to equation (6.1) which is a curve-fitting relationship:

$$\boldsymbol{\sigma_0 = k\varepsilon^n = 290\varepsilon^{0.19}} \qquad \textbf{(6.1)}$$

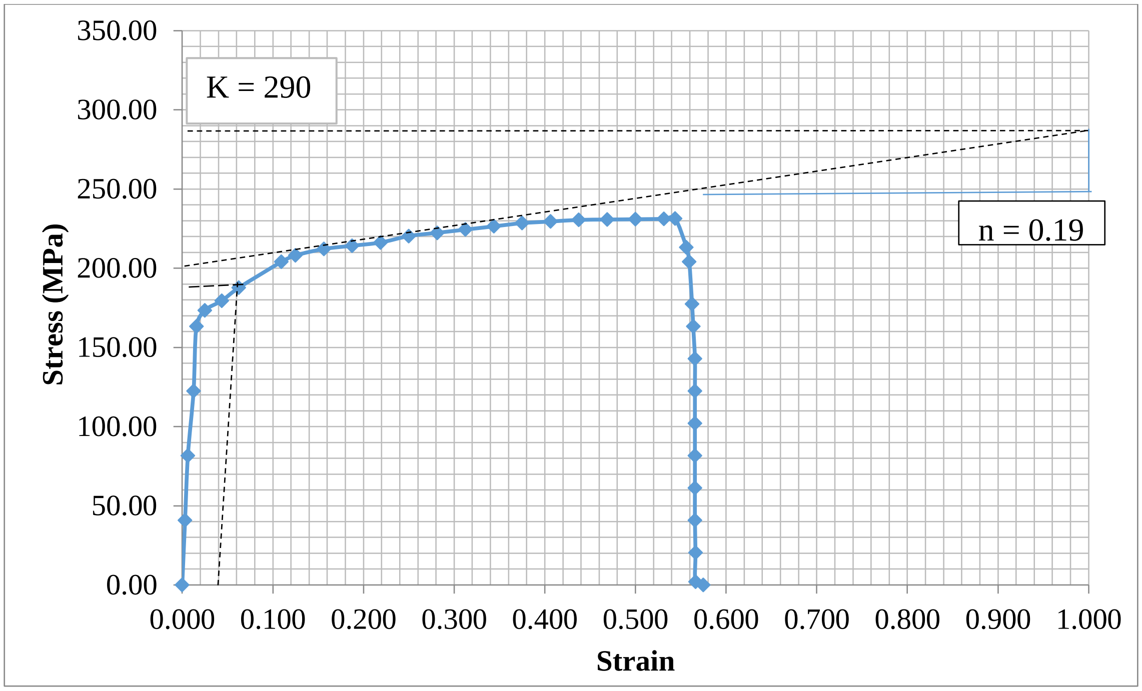

Figure 6.10: Stress-Strain Diagram for Wrought Copper. (Source: Author)

Table 6.3: Mechanical Properties of Wrought Copper.

Young's Modulus (GPa)	Force @Peak (N)	Tensile Strength (MPa)	Yield Stress (MPa)	Strain @Yield	Elongation (%)	Area Reduction (%)
118	11340	237.29	197.11	0.25	52.5	83.6

(Source: Author)

Table 6.4: Material Input Parameters used during Modeling Copper Wire Drawing.

	Parameter				
Description	Youngs Modulus	Average yield stress	Fracture strain	Strain rate	Damage value
Symbol	E (GPa)	Y_{avg} (MPa)	ε_{fr}	$\dot{\varepsilon}$	D (MPa)
Value	118	269.478	0.556	0.0015s^{-1}	357.99

(Source: Author)

6.5.3 Wire Drawing Practice

(i) Copper Electric Cable Production

Figure 6.11 shows the flow chart for electric cable production. The raw material for copper wire production is scrap copper or copper cathodes which are subjected to an upcast furnace in order to produce the 8 mm copper rods. The furnace has a capacity of six tonnes of molten copper at temperatures of 1160^o C. Six sets of 8 mm size graphite nozzles produce the 8 mm rods. The rods are then passed through the rod breakdown machine (first wire drawing machine) in order to produce the 2.76 mm copper wire which becomes the raw material for the second wire drawing machine (intermediate wire drawing machine). Intermediate wire drawing, which is the focus of this research, produces annealed copper wire of sizes ranging from 0.52 to 1.78 mm. This is finished wire which is subjected to polyvinyl chloride insulation and sold as finished electric cables. Fine copper wire of sizes ranging from 0.20 to 0.29 mm is also produced after the intermediate wire drawing process. All wires are subjected to quality assurance testing.

(ii) Pass Schedule Design

The company has internally standardized pass schedule designs according to the size of the wire or conductor being produced. The intermediate wire drawing machine can take up to seventeen dies. Table 6.5 shows the pass schedule design for producing a 1.78 mm wire. Other wire sizes are produced according to tables given in **Appendix 6**. The pass schedules were designed based on varying area reduction.

In this research, the pass schedule designs were not changed due to plant requirements, while the major focus of the research was on the schedule producing the 1.78 mm wire. Recommendations have been made towards ensuring that dies are not selected at random for minimised wire breakages.

Table 6.5: Pass Schedule for Producing 1.78 mm Copper Wire.

	Die Sequence				
Position	1	2	3	4	5
Die Size (mm)	2.55	2.32	2.11	1.92	1.78
Area Reduction (%)	14.6	17.2	17.3	17.2	14.1

(Source: Author)

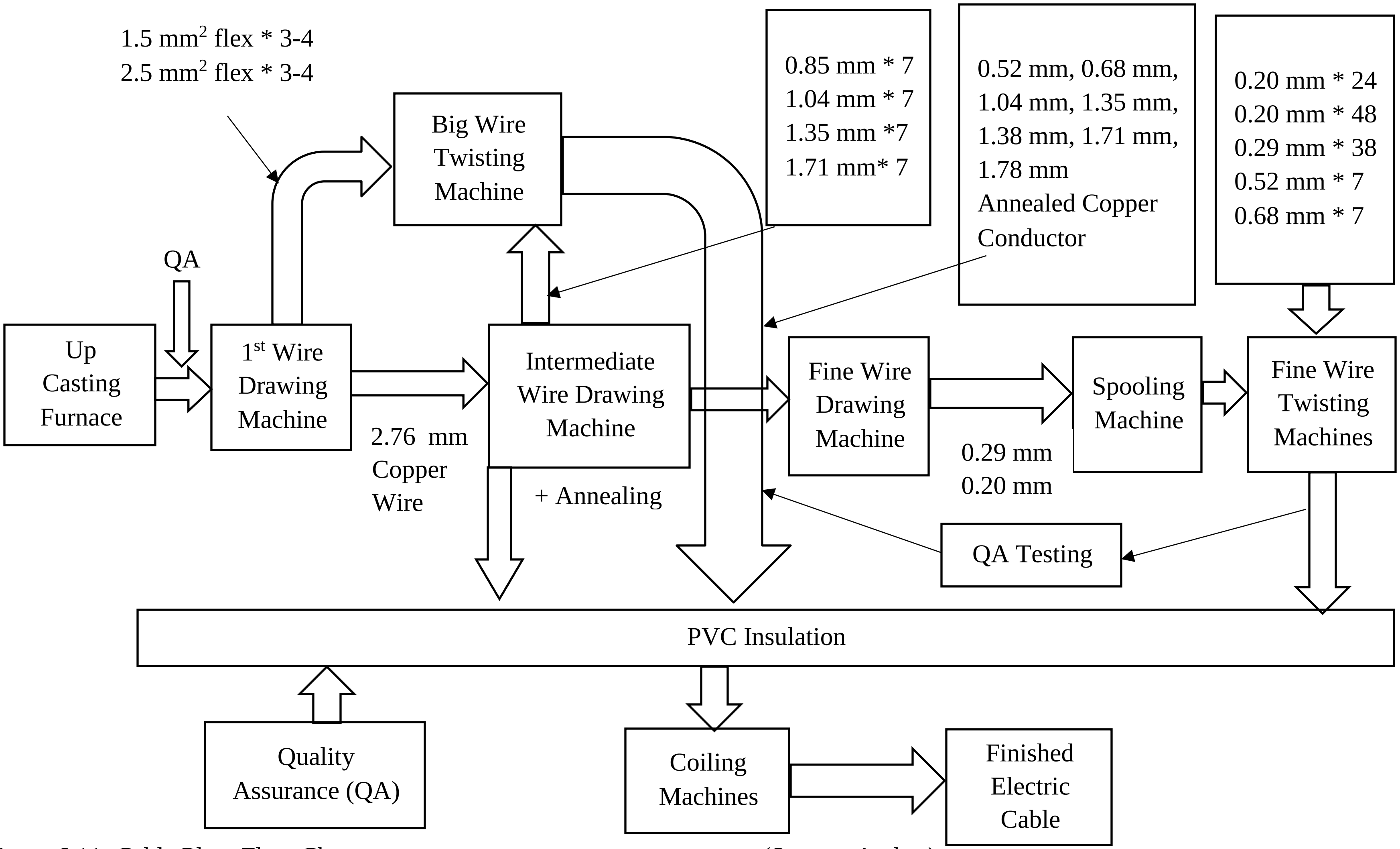

Figure 6.11: Cable Plant Flow Chart (Source: Author)

(iii) Lubrication

The lubricant Mastersol C21 is used both as a lubricant and coolant during copper wire drawing. The lubricant, which is soluble in water, is mixed with water to create an emulsion with a ratio of 1:20.

A 500 ml sample of the lubricant Mastersol C21 was subjected to analytical tests at ZABS. The tests were done according to standards ASTM D 445 and ASTM D 1298 to determine the kinematic viscosity and specific gravity respectively. Table 6.6 shows the results of the analytical tests.

Table 6.6: Viscosity Parameters for Mastersol C21.

Parameter	**Units**	**Test Method**	**Test Results**
Kinematic Viscosity @ 40^{o}C	cSt	ASTM D 445	34.38
Kinematic Viscosity @ 100^{o}C	cSt	ASTM D 445	6.94
Specific gravity	-	ASTM D 1298	0.940

(Source: Author)

(iv) Temperature

Heat is generated during wire drawing. The temperatures of both the lubricant and the die are important in that the die temperature indicates the levels of heat generated during wire drawing, while the outlet temperature of the lubricant indicates the amount of heat being dissipated away from the drawing zone.

Using a digital thermometer, model 6802 II with a test range of -50^{o}C to 1300^{o}C and an accuracy of $\pm 0.1^{o}$C, temperatures of the dies and lubricant were determined at various intervals. An infrared thermometer, model MS 6530 with a range of -20^{o}C to 537^{o}C was used to measure the temperature at the annealing wheels. Figures 6.12, 6.13 and 6.14 show results of the recorded temperatures at the die zones, the inlet and outlet lubricant and at annealing wheels respectively.

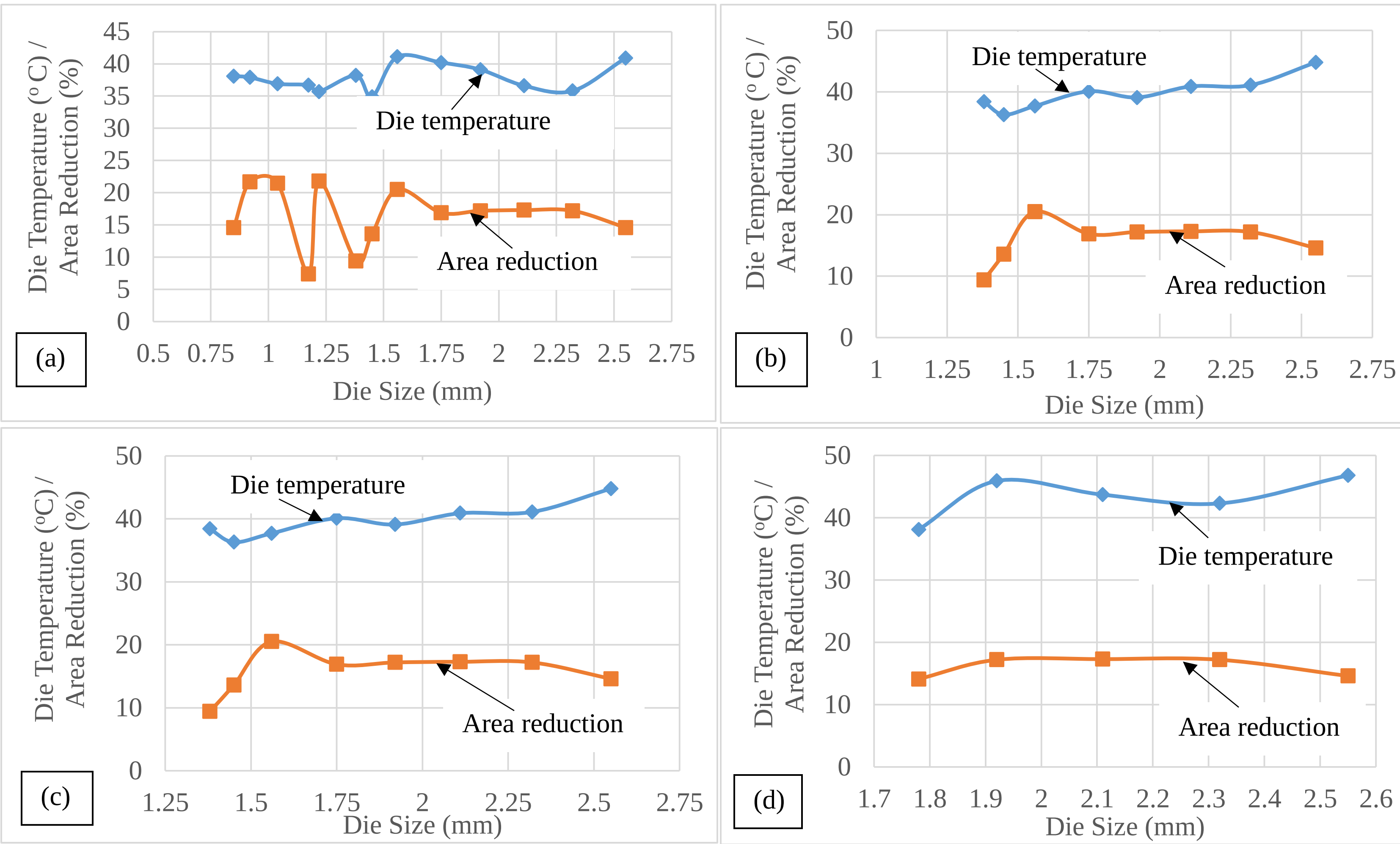

Figure 6.12: Temperatures and Area Reductions for Different Wire Sizes (a) 0.85 (b) 1.38 (c) 1.71 (d) 1.78 mm.

(Source: Author)

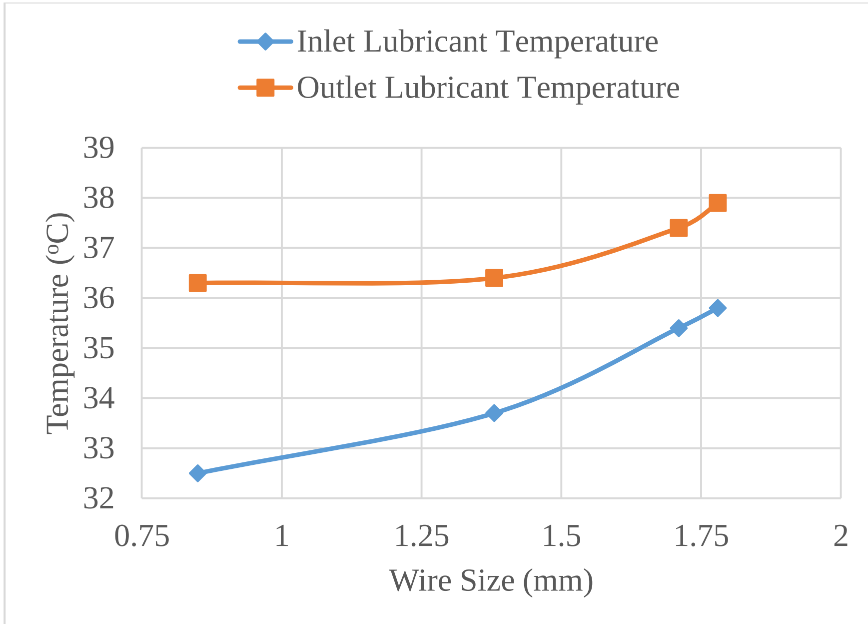

Figure 6.13: Lubricant Temperature Distribution per Wire Size. (Source: Author)

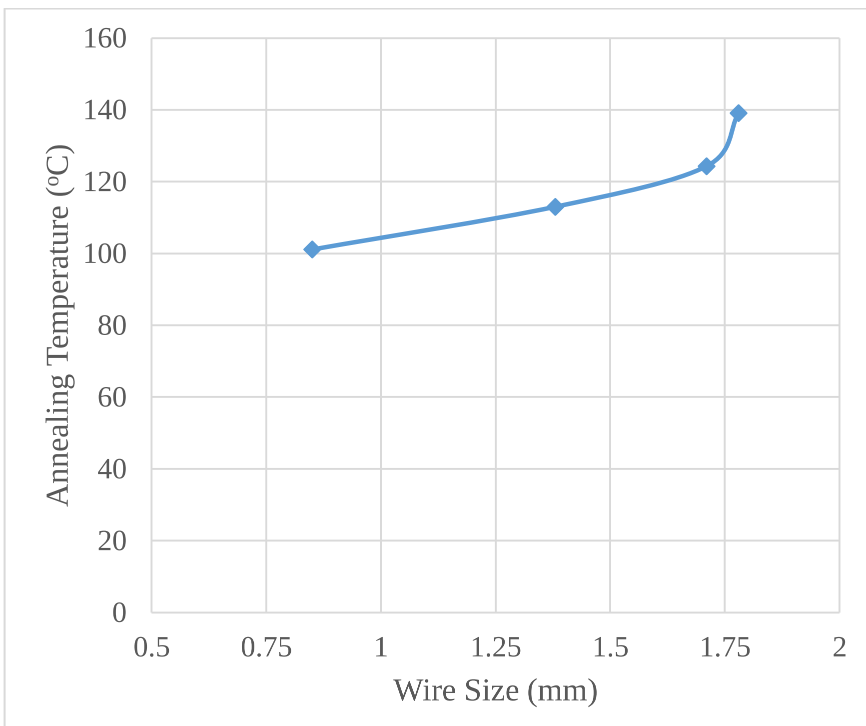

Figure 6.14:1 Distribution of Annealing Temperatures at Different Wire Sizes.

(Source: Author)

(v) Drawing Speed

Simulation runs indicated that the speed of drawing had an effect on wire ductile damage. The speed of the drawn wire was determined using a digital tachometer model DT-2234 C^+ with a test range of 2.5 to 99,999 rpm and an accuracy of ±0.05%. The tachometer measured the average angular speed of the last two pulleys through which the wire passed as shown in Figure 6.15. The angular speed of the pulleys was converted to linear speed of the wire. Figure 6.16 shows results of average wire speeds recorded for different wire size production.

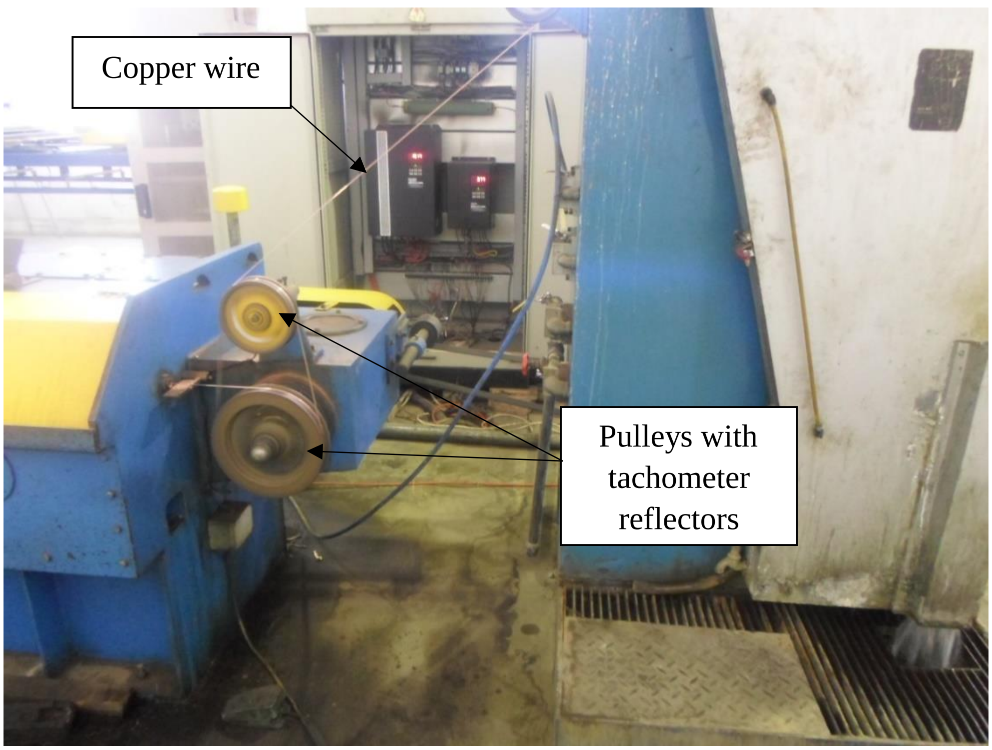

Figure 6.15: Arrangement of Pulleys for Wire Speed Determination.

(Source: Author)

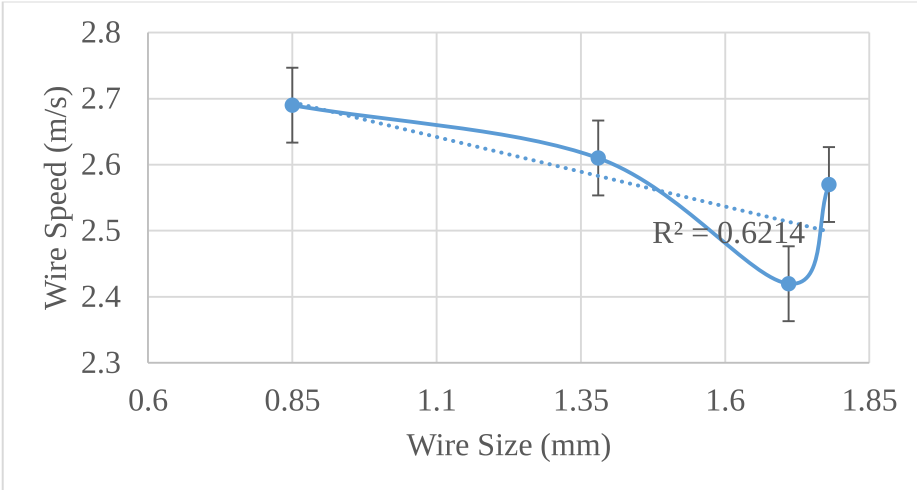

Figure 6.16:2 Distribution of Wire Speeds during Different Wire Size Production. (Source: Author)

From the graph in Figure 6.16, it is seen that the wire speed is lowest when drawing a 1.71 mm wire in comparison to when drawing the other wires. This is attributed to the frequent stoppages experienced during its production, mainly at annealing wheels, hence the need to reduce the speed.

(vi) Drawing Force

Models have shown that the value of the drawing force is influenced by the number of dies used and the area reduction. The drawing force was determined experimentally by measuring both the tension in the wire and by the actual pulling force needed as recorded by a force gauge. A Yisida digital force gauge, model DS2-500N with a capacity of 500N and an accuracy of $\pm 0.2\%$ was used to record both the wire tension and the pulling force through different dies. With trendlines, Figure 6.17 shows the results of wire tensions recorded during production of various wire sizes, while Figure 6.18 shows the results of drawing force recorded using manual pulling of the copper wire through different individual die sizes.

(vii) Wire Defects

Wire defects mainly in form of ‘copper fines’ and wire breaks were observed during industrial experiments. Figure 6.19 and 6.20 show the various defects experienced in the plant, while Figure 6.21 shows the frequency of such breaks during the period under review.

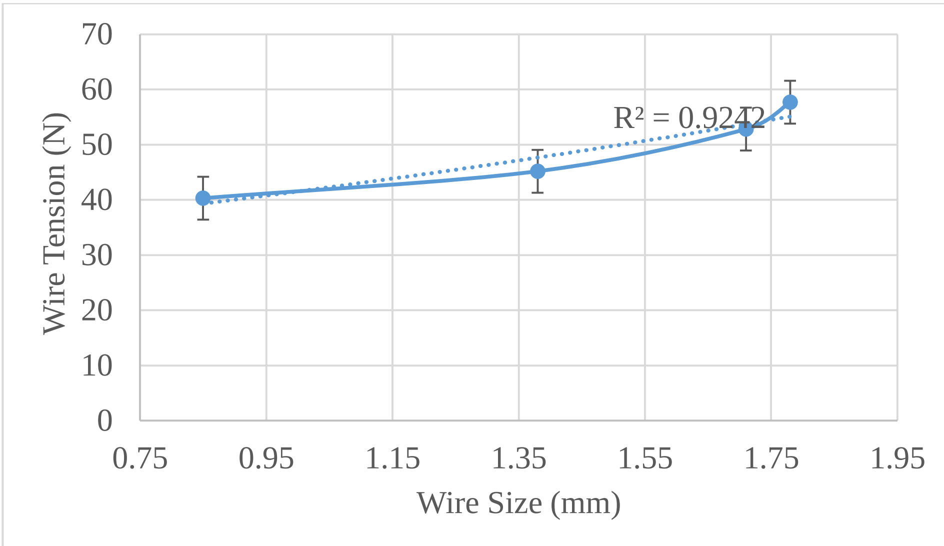

Figure 6.17: Distribution of Wire Tension during Production of Different Wire Sizes.

(Source: Author)

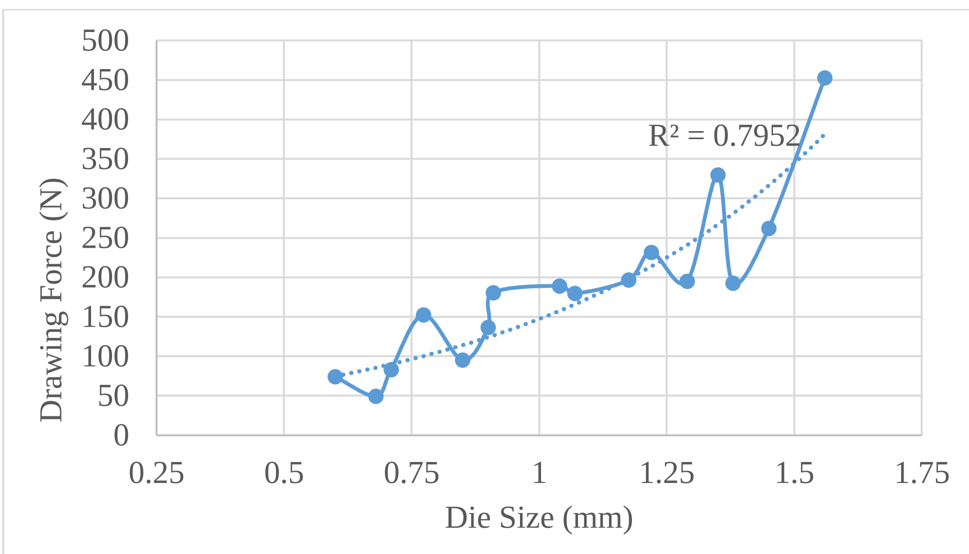

Figure 6.18: Distribution of Drawing Force for Various Die Sizes.

(Source: Author)

Figure 6.19: Copper "Dust" or "Fines" Accumulation with Lubricant.

(Source: Author)

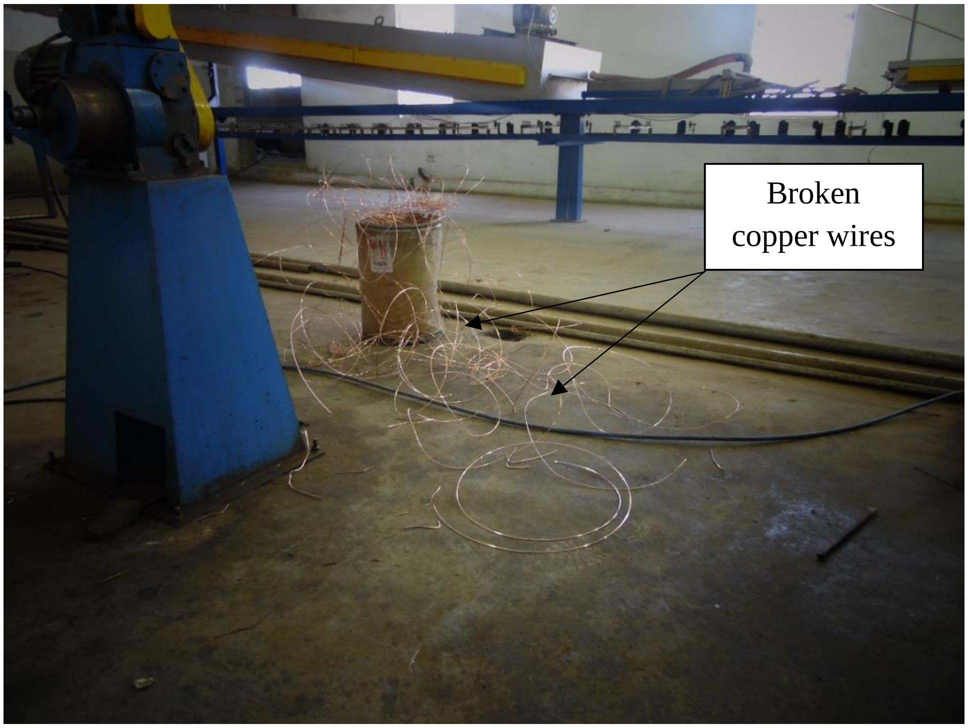

Figure 6.20:3 Wire Breakages. (Source: Author)

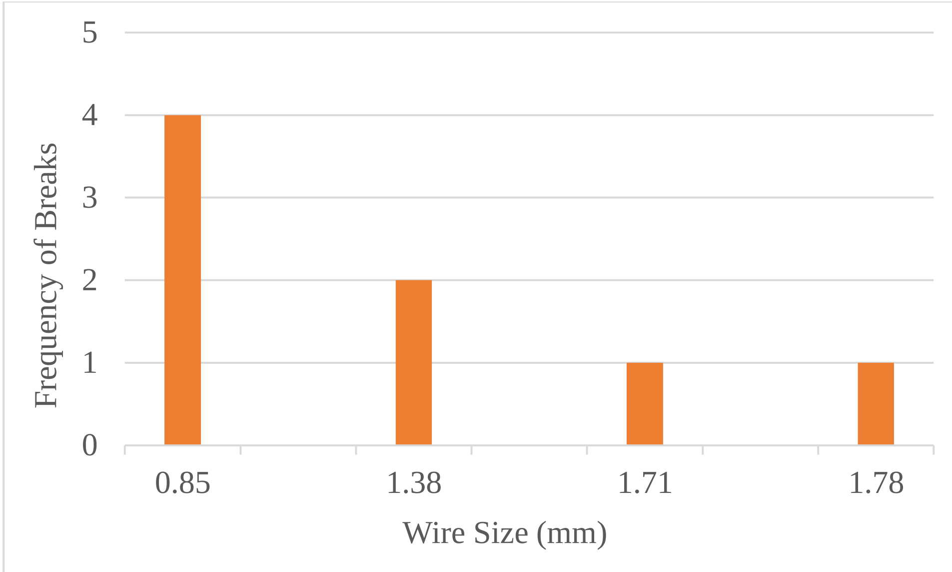

Figure 6.21: Frequency of Wire Breaks versus Wire Size. (Source: Author)

6.5.4 Drawn Wire Micrography

Sections from the industrial experiments during production of the 1.78 mm copper cable under varying bearing length were collected and subjected to both surface and internal micrography investigation using the SEM at 400X and 3000X magnifications. Figures 6.22 to 6.45 show the micrographs obtained for the internal and surface sections.

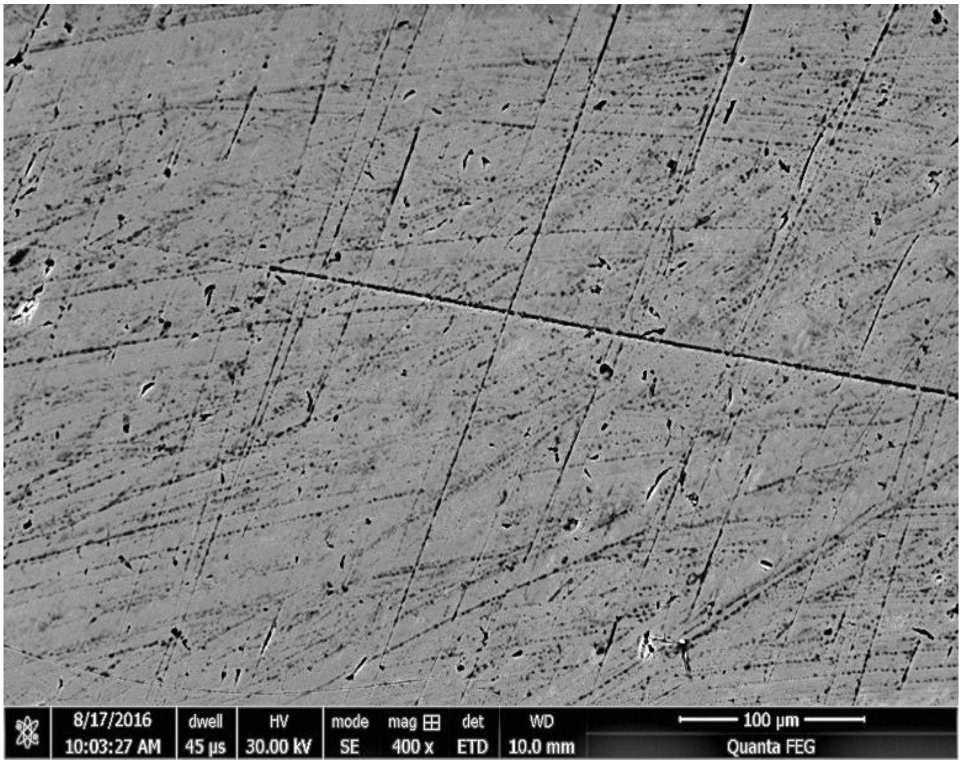

Figure 6.22: Internal Section Micrograph for Multi-Pass 1-2 at 30% Bearing Length.

(Source: Author)

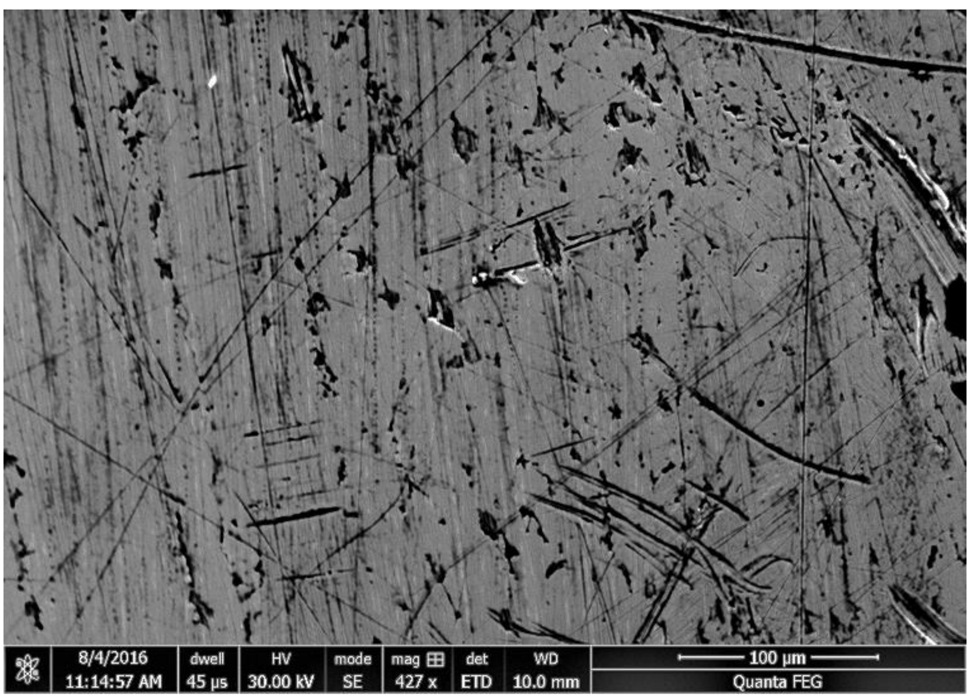

Figure 6.23: Surface Section Micrograph for Multi-Pass 1-2 at 30% Bearing Length.

(Source: Author)

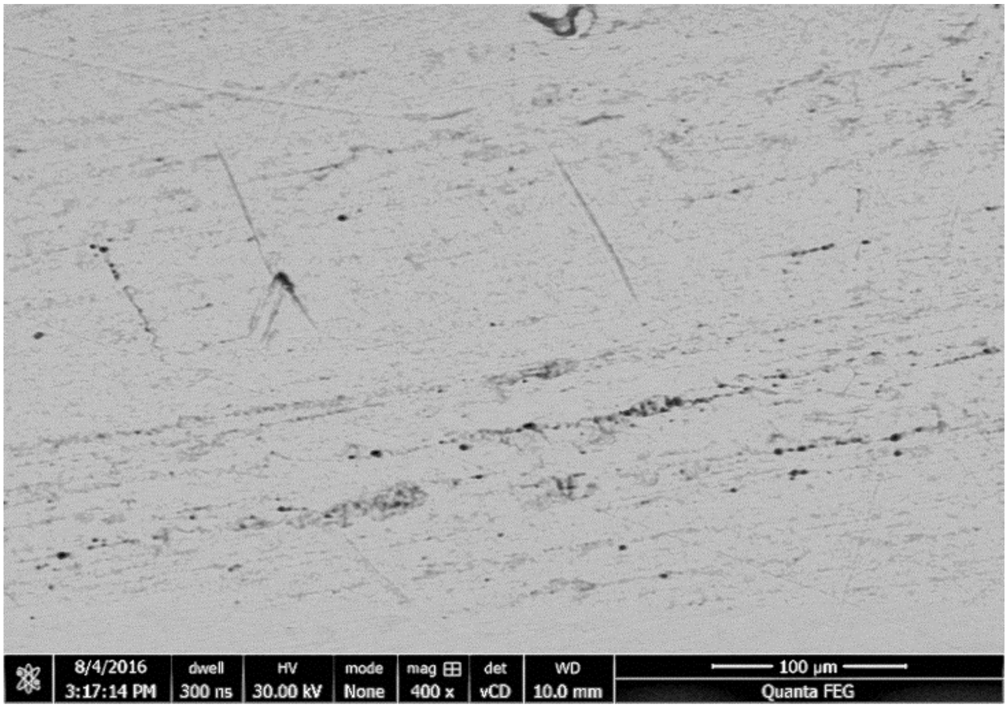

Figure 6.24: Internal Section Micrograph for Multi-Pass 2-3 at 30% Bearing Length.

(Source: Author)

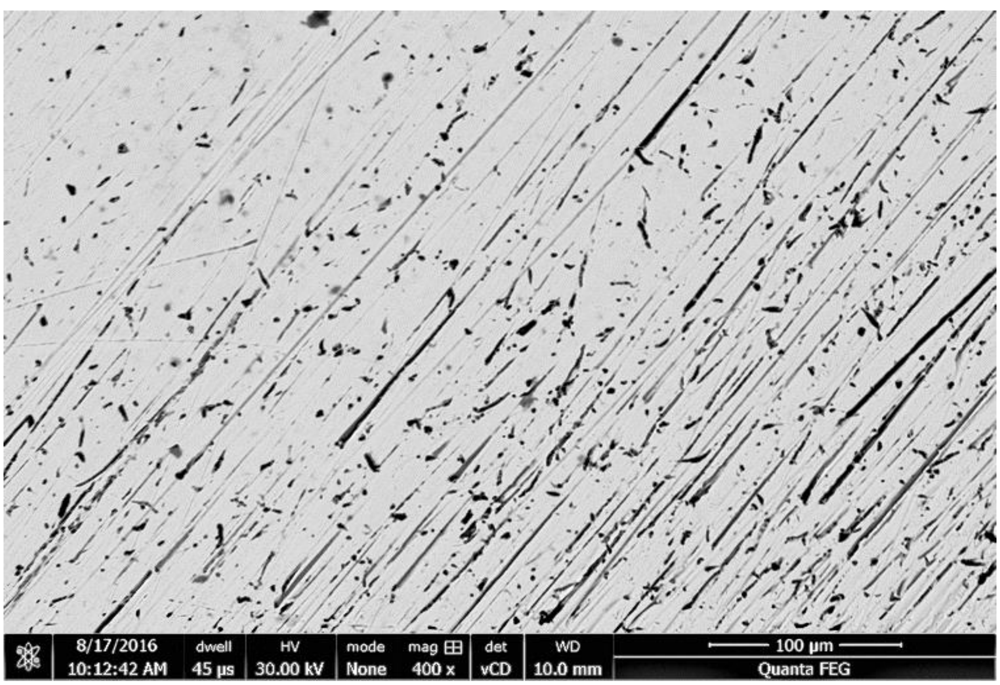

Figure 6.25: Surface Section Micrograph for Multi-Pass 2-3 at 30% Bearing Length.

(Source: Author)

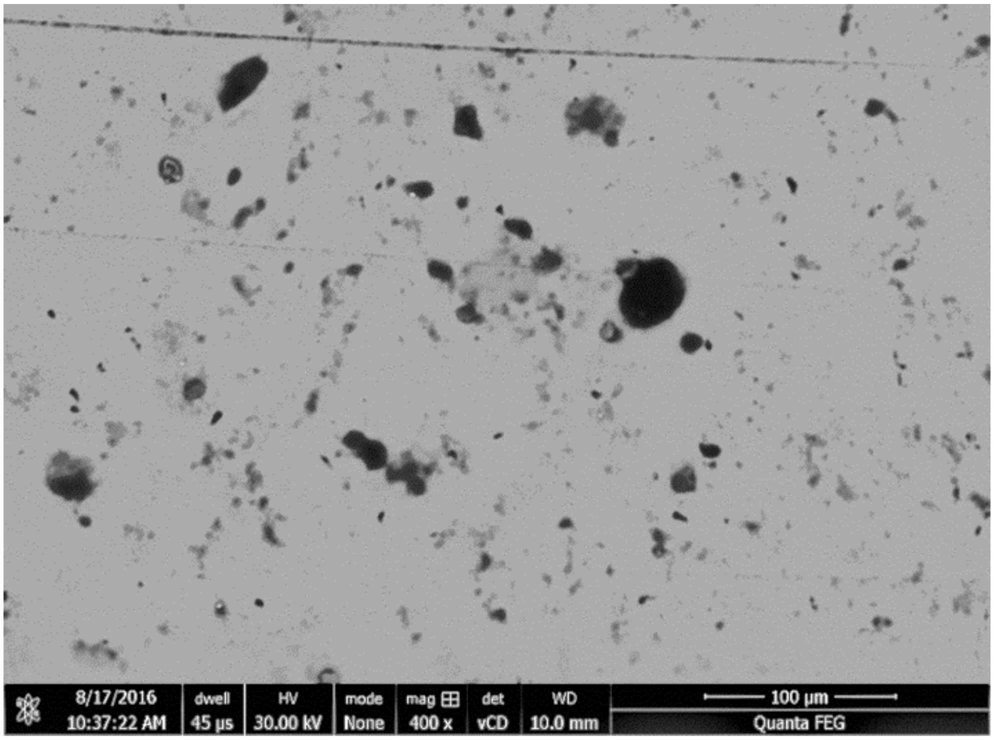

Figure 6.26: Internal Section Micrograph for Multi-Pass 3-4 at 30% Bearing Length.

(Source: Author)

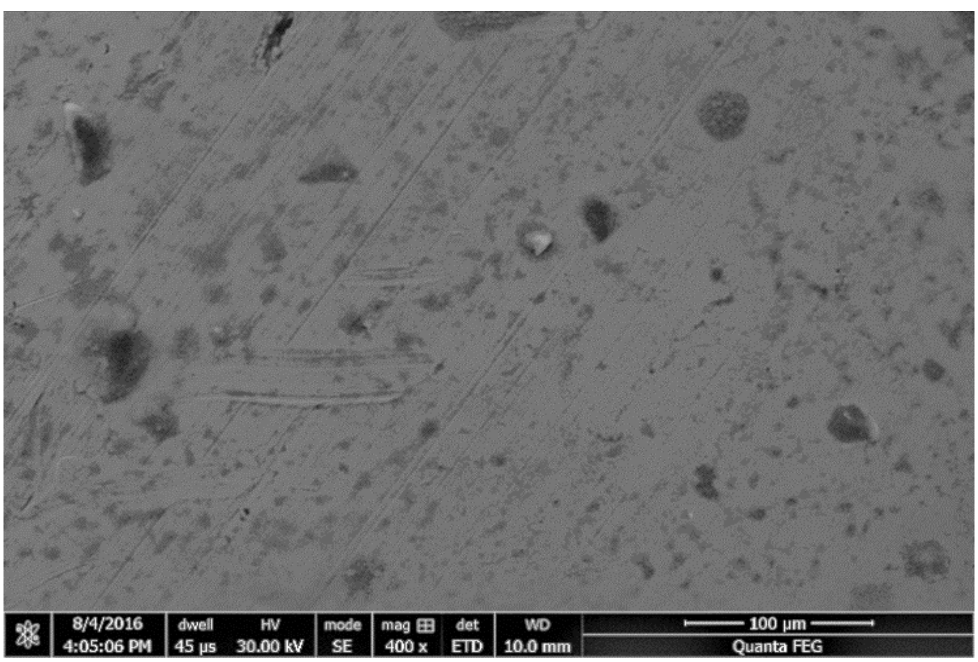

Figure 6.27: Surface Section Micrograph for Multi-Pass 3-4 at 30% Bearing Length.

(Source: Author)

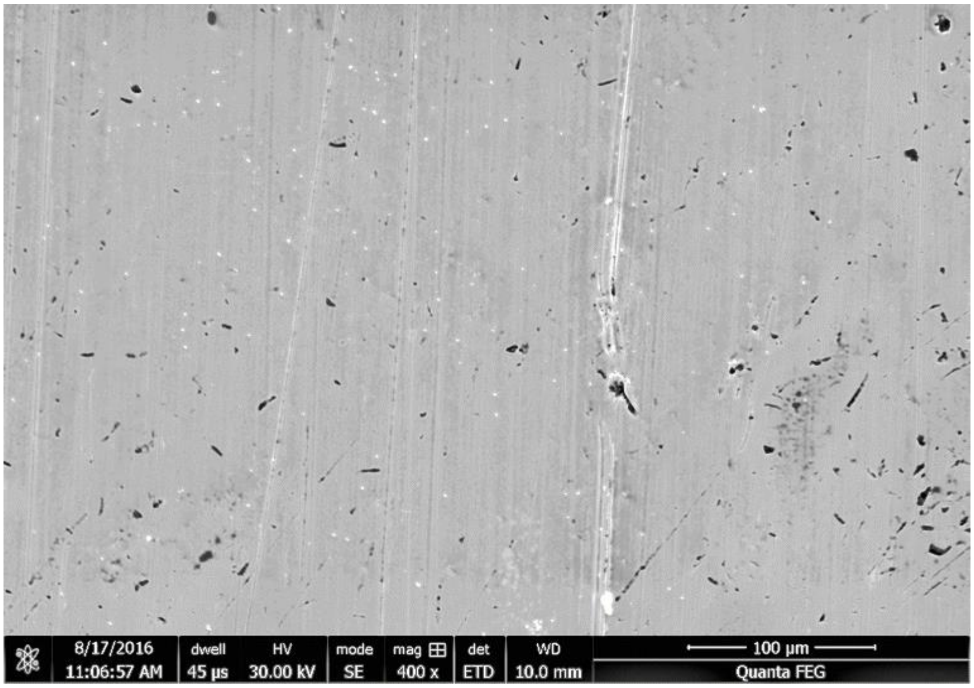

Figure 6.28: Internal Section Micrograph for Multi-Pass 4-5 at 30% Bearing Length.

(Source: Author)

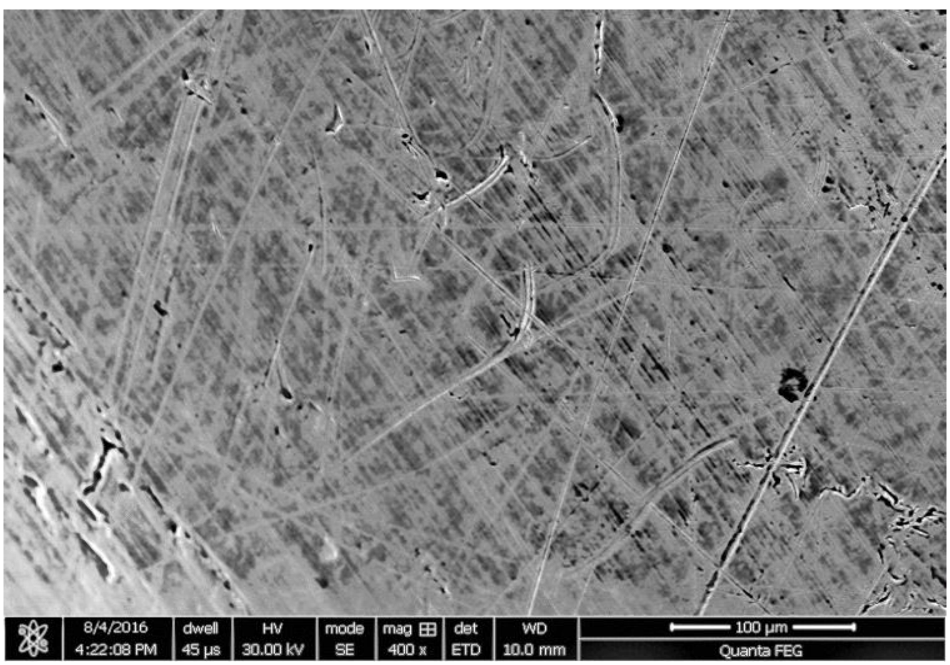

Figure 6.29: Surface Section Micrograph for Multi-Pass 4-5 at 30% Bearing Length.

(Source: Author)

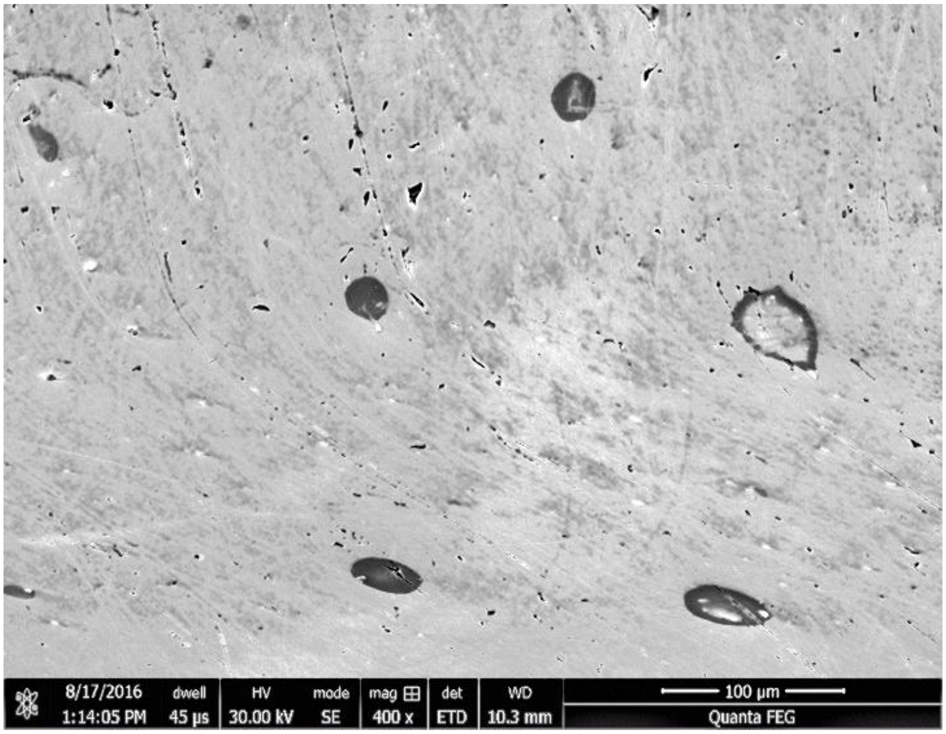

Figure 6.30: Internal Section Micrograph for Multi-Pass 1-2 at 40% Bearing Length.

(Source: Author)

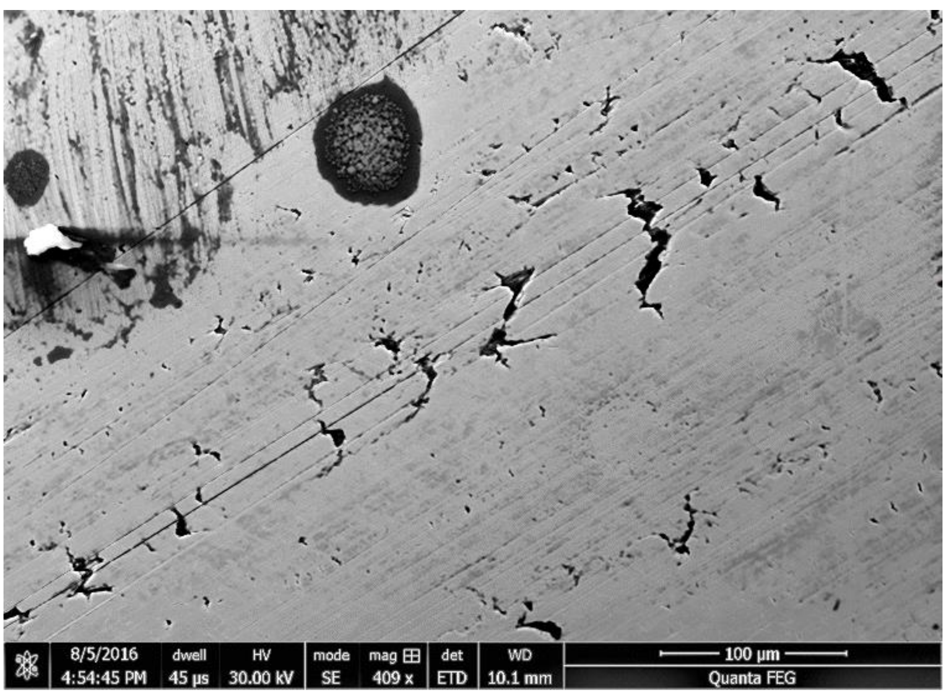

Figure 6.31: Surface Section Micrograph for Multi-Pass 1-2 at 40% Bearing Length.

(Source: Author)

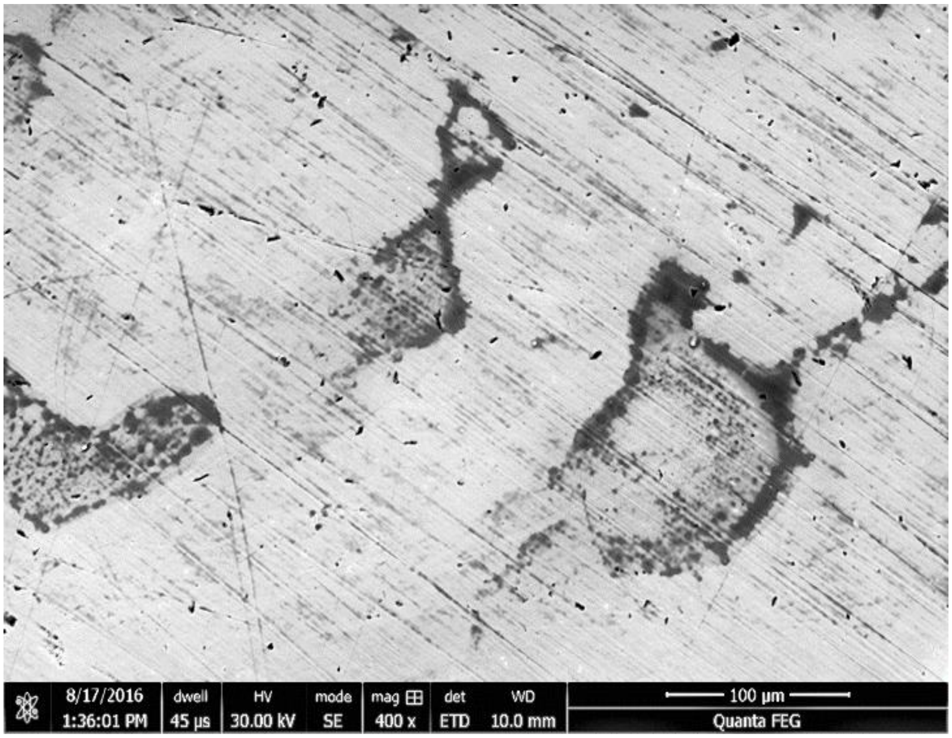

Figure 6.32: Internal Section Micrograph for Multi-Pass 2-3 at 40% Bearing Length.

(Source: Author)

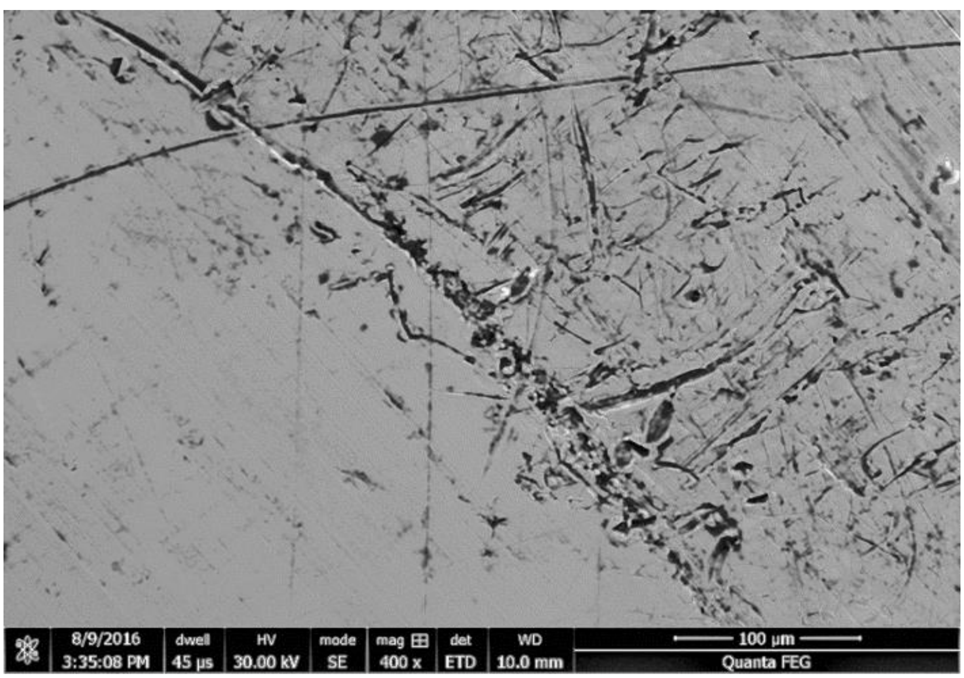

Figure 6.33: Surface Section Micrograph for Multi-Pass 2-3 at 40% Bearing Length.

(Source: Author)

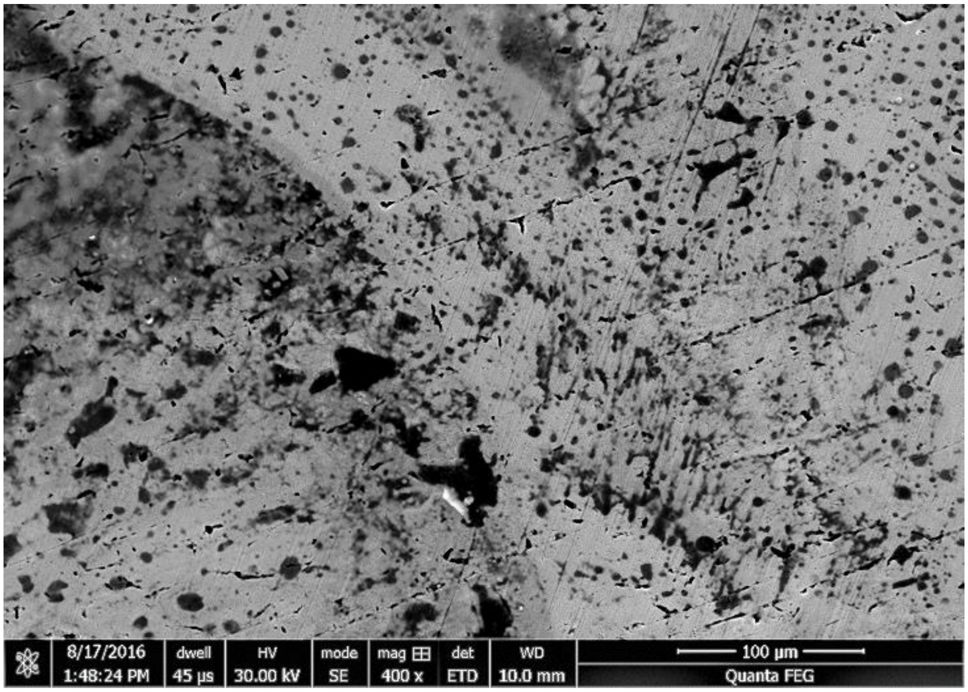

Figure 6.34: Internal Section Micrograph for Multi-Pass 3-4 at 40% Bearing Length.

(Source: Author)

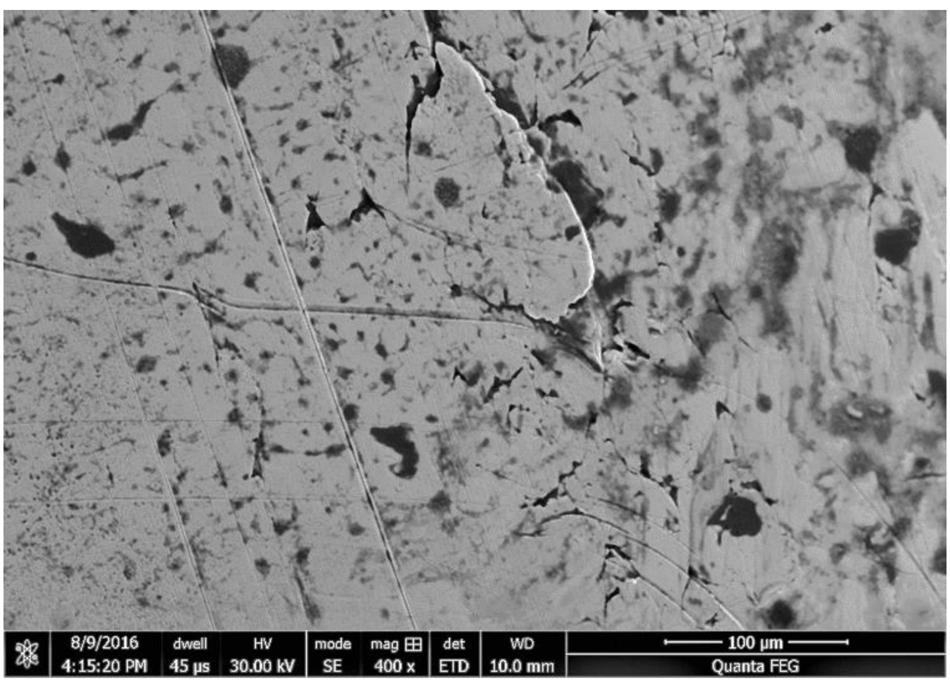

Figure 6.35: Surface Section Micrograph for Multi-Pass 3-4 at 40% Bearing Length.

(Source: Author)

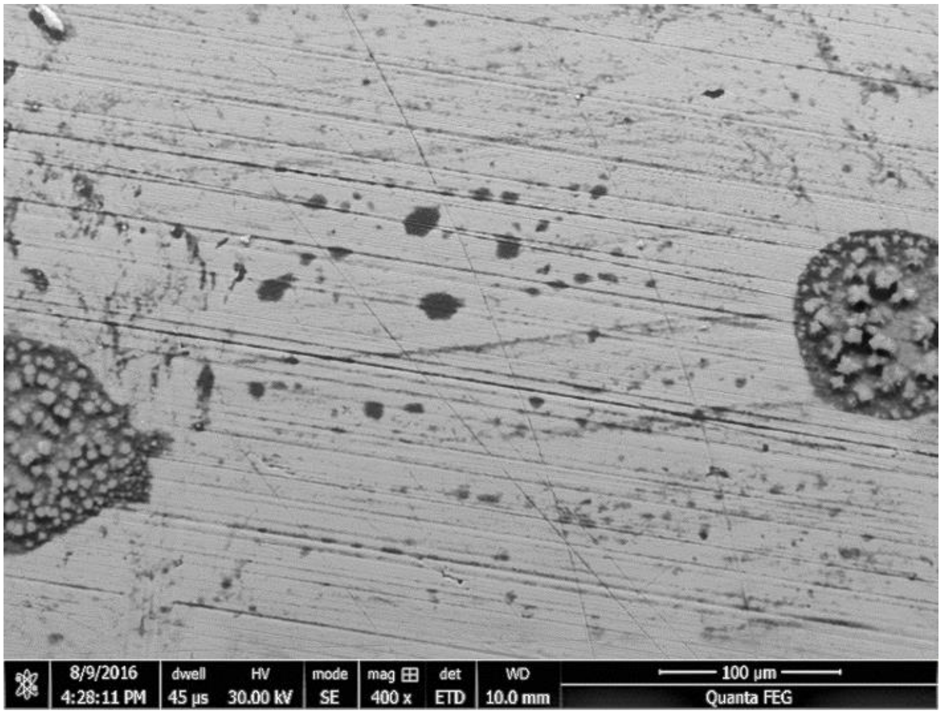

Figure 6.36: Internal Section Micrograph for Multi-Pass 4-5 at 40% Bearing Length.

(Source: Author)

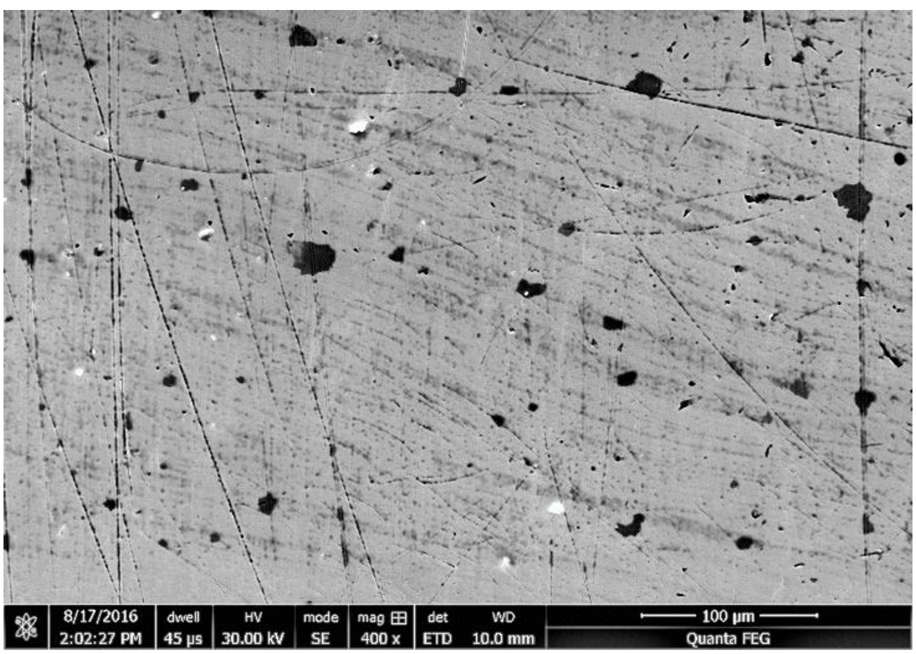

Figure 6.37: Surface Section Micrograph for Multi-Pass 4-5 at 40% Bearing Length.

(Source: Author)

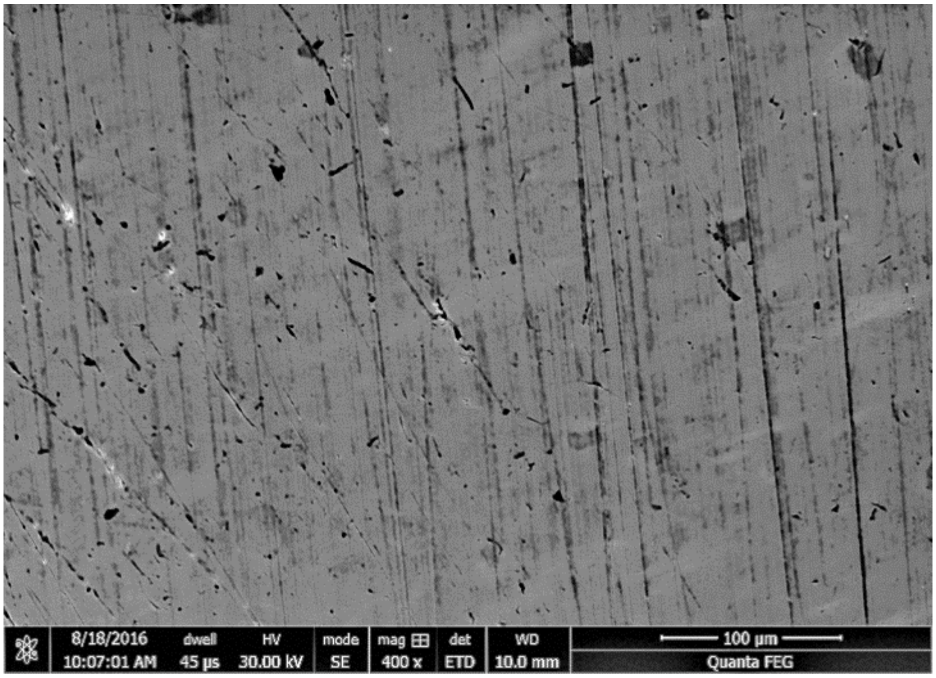

Figure 6.38: Internal Surface Micrograph for Multi-Pass 1-2 at 50% Bearing Length.

(Source: Author)

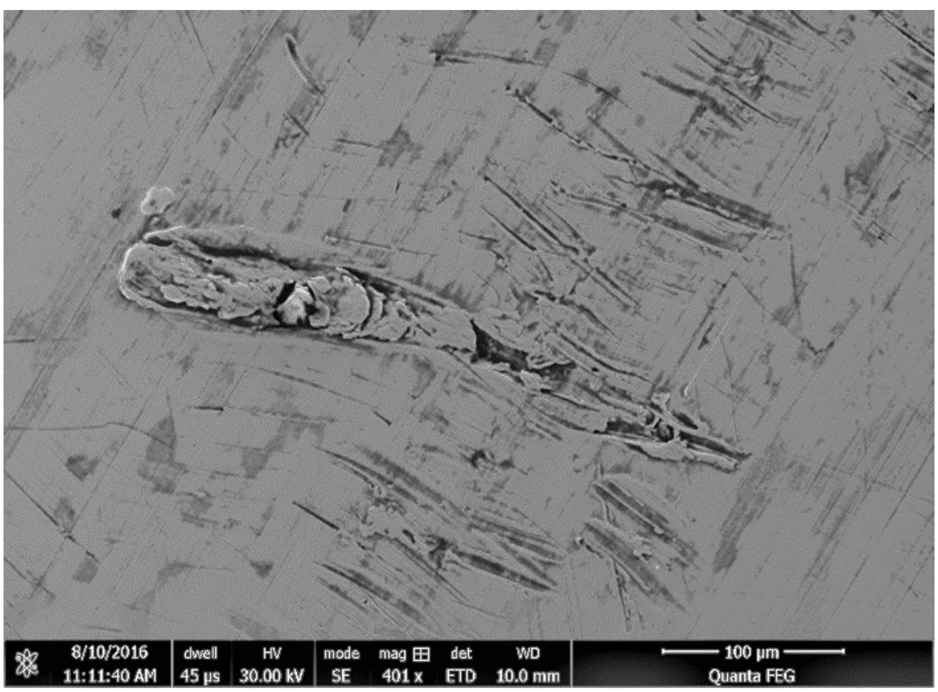

Figure 6.39: Surface Section Micrograph for Multi-Pass 1-2 at 50% Bearing Length.

(Source: Author)

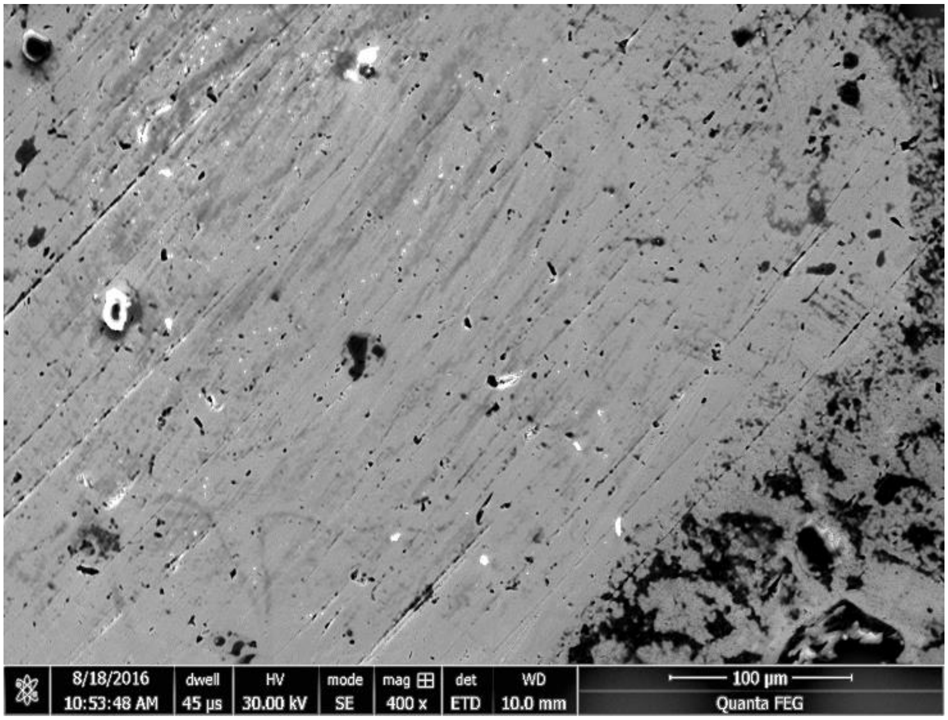

Figure 6.40: Internal Section Micrograph for Multi-Pass 2-3 at 50% Bearing Length.

(Source: Author)

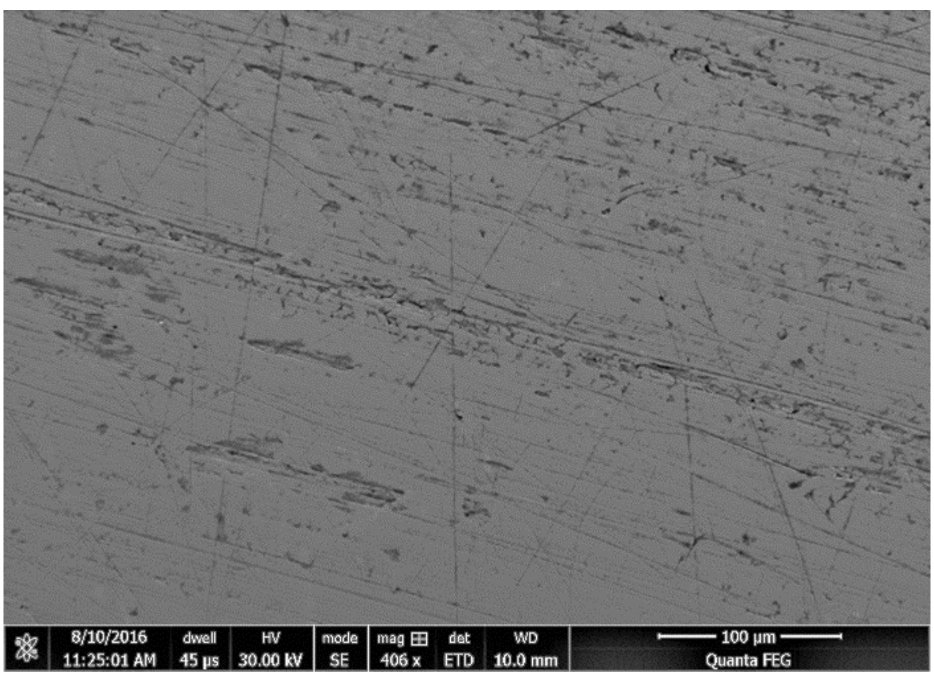

Figure 6.41: Surface Section Micrograph for Multi-Pass 2-3 at 50% Bearing Length.

(Source: Author)

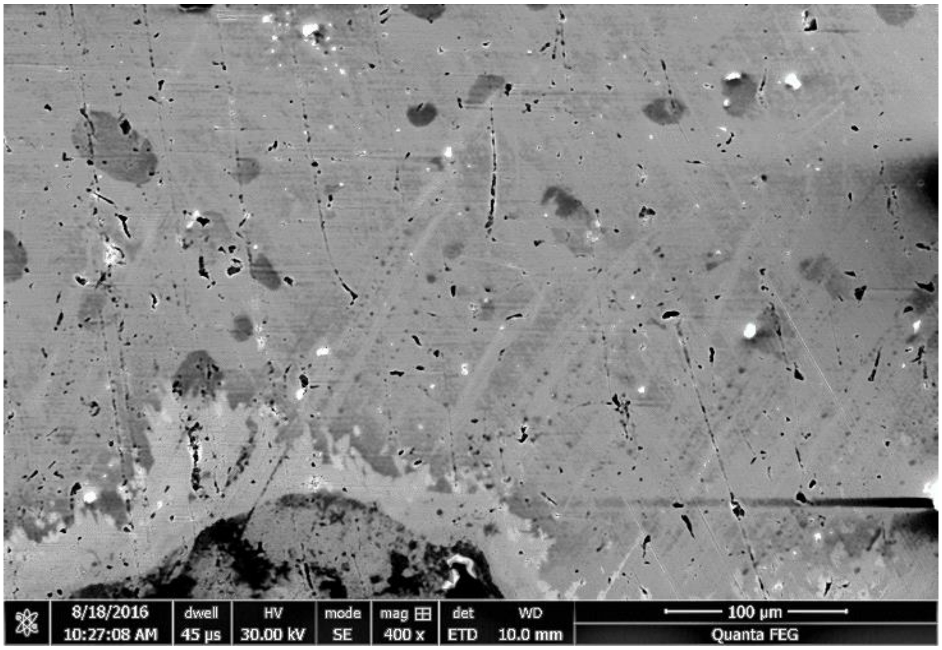

Figure 6.42: Internal Section Micrograph for Multi-Pass 3-4 at 50% Bearing Length.

(Source: Author)

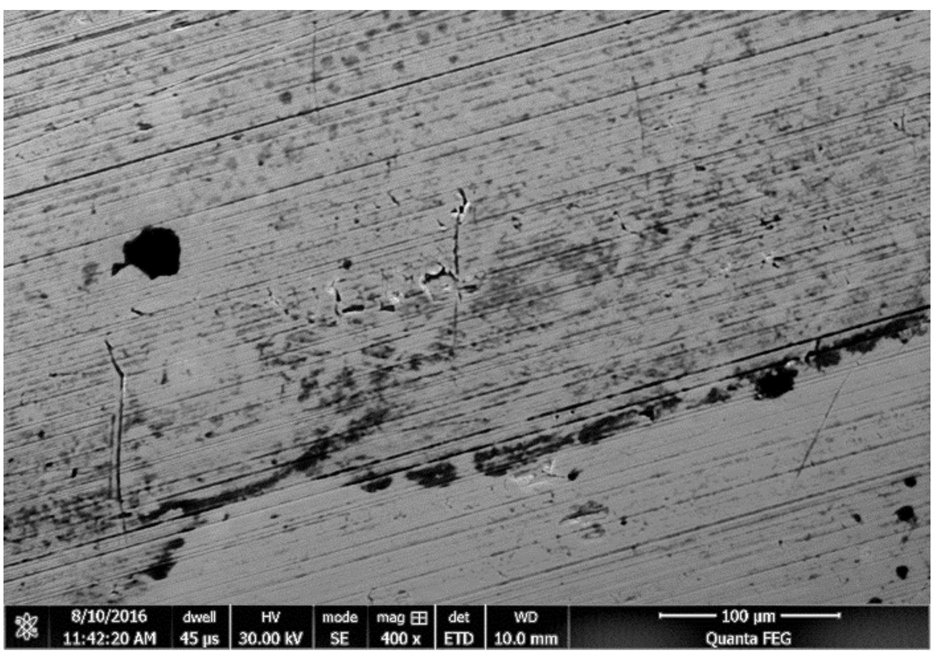

Figure 6.43: Surface Section Micrograph for Multi-Pass 3-4 at 50% Bearing Length.

(Source: Author)

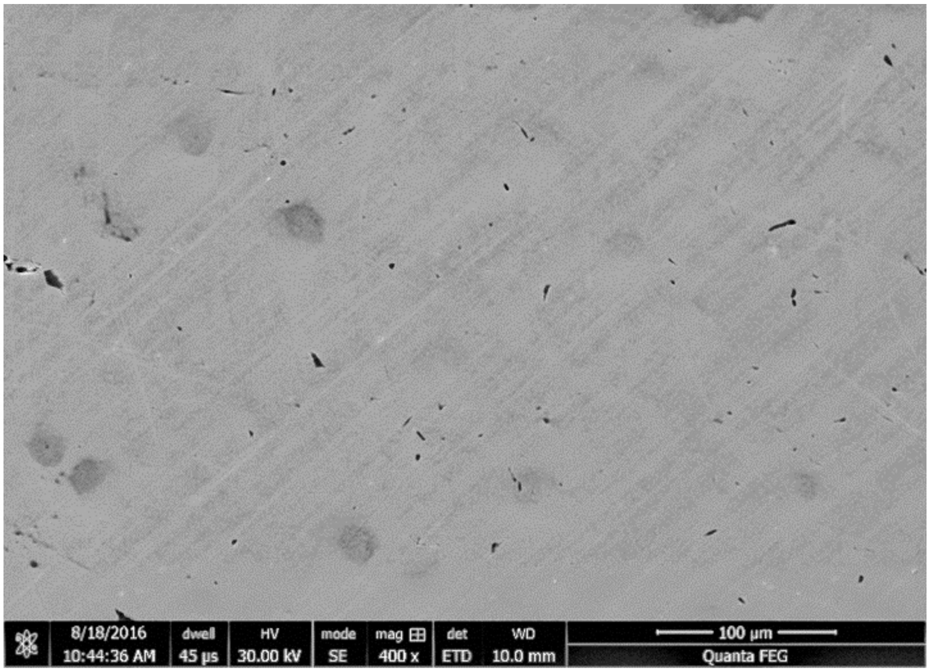

Figure 6.44: Internal Section Micrograph for Multi-Pass 4-5 at 50% Bearing Length.

(Source: Author)

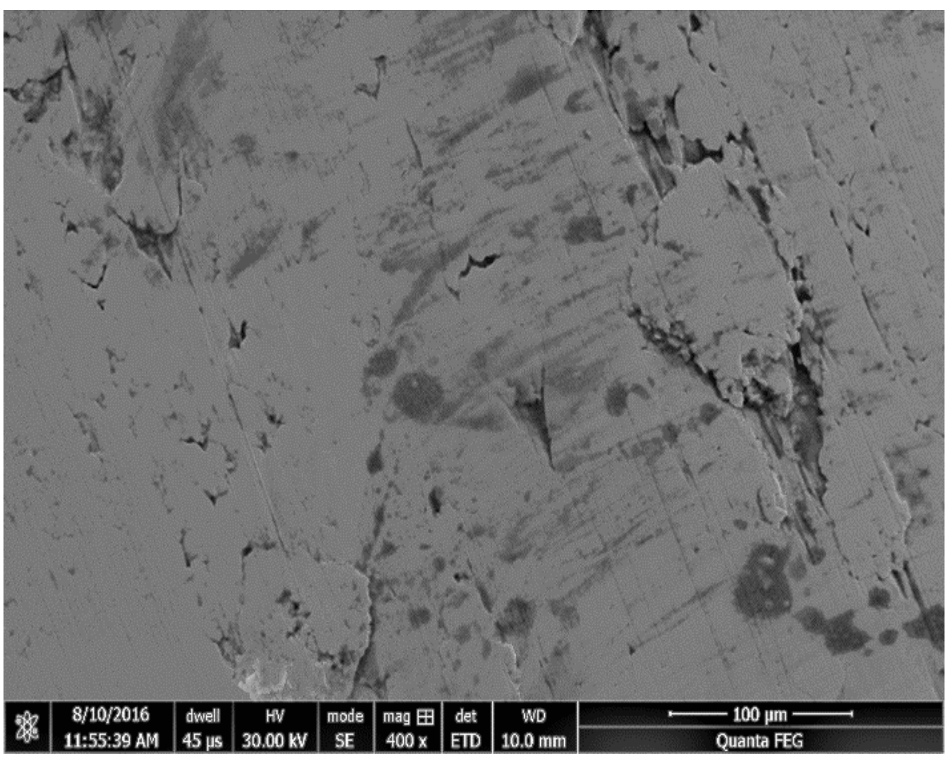

Figure 6.45: Surface Section Micrograph for Multi-Pass 4-5 at 50% Bearing Length.

(Source: Author)

Figure 6.46 shows a micrograph taken at 3000X magnification for showing cross-sectional sizes of internal cracks during the 4-5 multi-pass stage at 50% bearing length variation. Ten sizes (possible maximum from each micrograph) were taken from each micrograph and the average crack length determined. Figures 6.47 and 6.48 show the variation of the average crack lengths measured from the SEM for the internal and surface sections respectively.

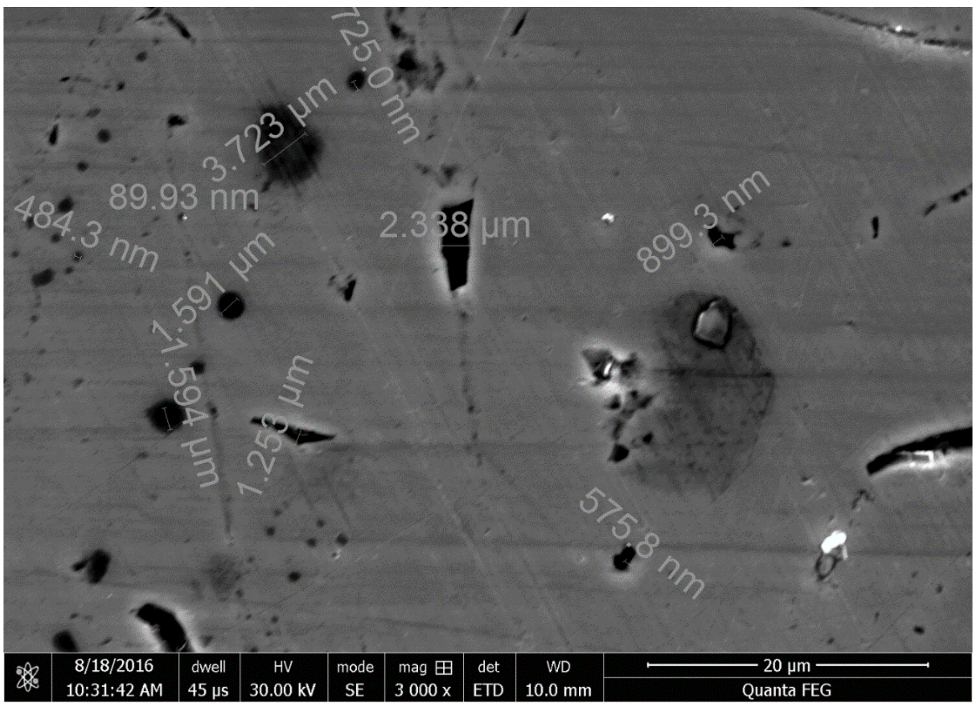

Figure 6.46: Measured Void Sizes on a Micrograph. (Source: Author)

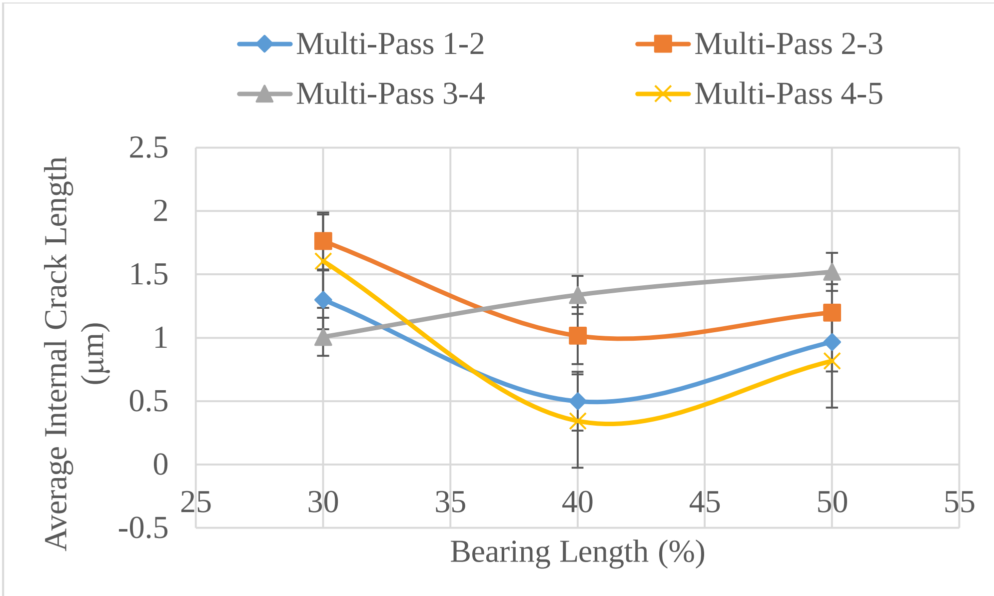

Figure 6.47: Variation of Measured Internal Crack Length with Bearing Length.

(Source: Author)

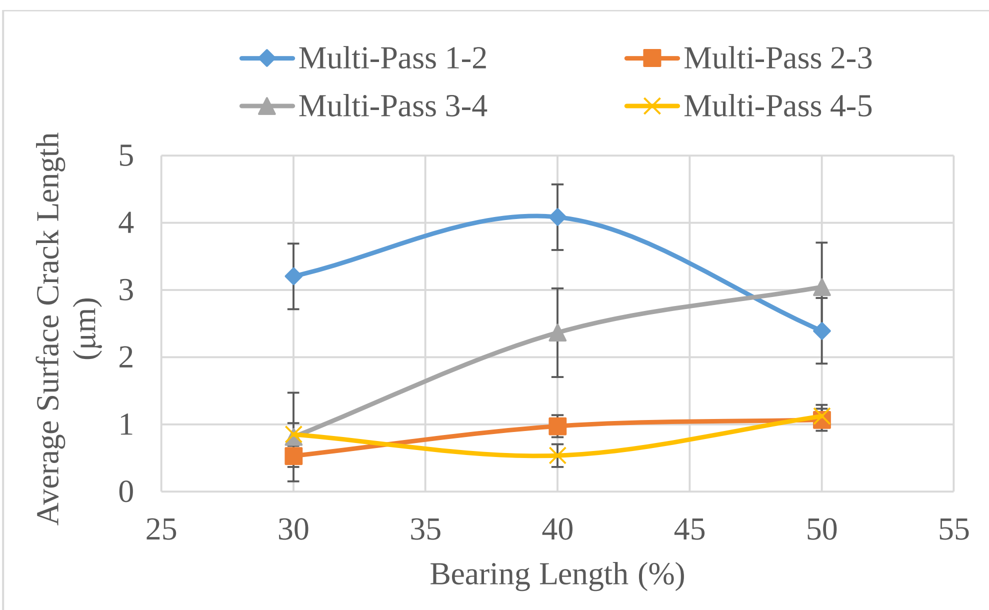

Figure 6.48: Variation of Measured Surface Crack Length with Bearing Length.

(Source: Author)

6.6 General Observations from Industrial Experiments

The industrial wire drawing experiments were conducted with well-functioning machinery, and the experiments were stable and repeatable.

6.7 Summary of Results from Experimental Procedures

Results of the experimental procedures indicated the following:

(1) Presence of second phase particles within the copper material with different grain sizes. Iron has the highest percentage of metallic inclusions in the two copper samples, with the wrought copper taking a higher percentage.

(2) Pass schedule designs showed that the wire drawing practice was concentrated on the use of Δ-parameter values above 3. This was typical for low area reductions and high approach angles under conditions of increased levels of redundant deformation and surface hardening. Annealing the copper wire was, thus, inevitable.

(3) The lubricant did not suffer much loss of its viscosity properties due to the fairly low operating temperatures. Lubrication was thus effective, though the presence of copper ‘fines’ compromised the inherent properties.

(4) Larger size dies, with corresponding higher area reductions, recorded higher temperatures.

(5) Production of larger size wire required higher annealing temperatures.

(6) Drawing speeds were higher when drawing smaller size wire.

(7) Tension in the wire during wire drawing increased with increased wire size being produced. The drawing force showed an accelerated increase with increased die size. High wear and shorter consequent die life were therefore likely for larger dies than smaller dies.

(8) Tendency of a wire break was higher when drawing smaller size wires.

(9) Micrographs showed less internal damage at 40% bearing length while dies with 30% bearing length showed less surface damage.

CHAPTER SEVEN: RESULTS ANALYSIS AND DISCUSSIONS

7.1 Introduction

The overall effects of die geometry parameters, process parameters, manufacturing aspects and wire drawing practice influencing formation of chevron and surface crack in copper during wire drawing as obtained from the simulation and experimental studies were analysed and discussed.

This chapter presents observations and detailed discussions based on the comparative analysis of results from the modelling and simulations and industrial experiments involving bearing length variation.

7.2 General Observations

The current research study on copper wire drawing involved development of a copper wire drawing model and establishment of die design and manufacturing practices and processing conditions leading to chevron and surface crack formation.

Validation of the results from modelling was done by using micrographs from the wire drawing industrial experiments. The micrographs showed that there was more internal wire damage when using bearing lengths of 30% and 50%, whereas more surface damage was seen when using bearing lengths of 50%. This was evident in the simulations which showed the same pattern. Therefore, there was a high degree of confidence that the results presented and discussed were reliable.

7.3 Analysis and Discussion of Results

The results presented were two-fold: results from modelling and simulation as presented in Figures 5.14 to 5.41, and results from laboratory and industrial experiments as presented in Figures 6.12 to 6.48.

7.3.1 Analysis and Discussion of Simulation Results

All the copper wire drawing models were based on a four sequence multi-pass stages, except for the models involving area reduction which used up to eight sequences.

(a) Effects of Die Geometry Independent Variables

Effects of the die geometry and area reduction on equivalent plastic strain were presented in Figures 5.14 5.15, 5.16 and 5.17. Figures 5.34, 5.35, 5.36, 5.37, 5.38, 5.39, 5.40 and 5.41 presented the effects of the die geometry and area reduction on damage value (stiffness degradation) and the Cockroft and Latham criterion leading to ductile damage of the copper wire.

(i) Effects of Entrance Angle

The figures showed that for the *centerline nodes*, both the plastic strain and damage values were high during the second (2-3) and third (3-4) multi-pass stages. The Cockroft and Latham criterion showed that ductile damage was high during the third (3-4) and fourth (4-5) multi-pass stages, with highest values at 20^{o} entrance angle.

For the *surface nodes*, the figures showed that both the equivalent plastic strain and damage values were high during the first (1-2) and second (2-3) multi-pass stages. For the Cockroft and Latham criterion, it was shown that ductile damage was highest during the third (3-4) multi-pass stage, with highest value at 20^{o} entrance angle and the criterion being reached.

The figures showed that the entrance angle had a very minimal effect on ductile damage. From the simulations it was observed that contact between the wire and the entrance zone was more evident at the first die (die$_{i}$) than the second die (die$_{i+1}$). Opening of the entrance zone by way of larger entrance angles removes contact between the copper wire and the entrance zone. This is in accordance with Wright (2011) and Esteves Group (2008) that an open bell minimizes abrasion on the wire and facilitates lubricant entry.

(ii) Effects of Approach Angle

The figures in chapter five showed that for the *centerline nodes*, the Cockroft and Latham criterion showed that ductile damage was high during the third (3-4) and fourth (4-5) multi-pass stages, with peaks at 10^o approach angle for most of the passes. The equivalent plastic strain and damage values were high during the second (2-3) and third (3-4) multi-pass stages.

For the *surface nodes*, the figures showed that both the plastic strain and damage values were high during the first (1-2) and second (2-3) multi-pass stages. The Cockroft and Latham criterion showed that ductile damage was highest during the third (3-4) multi-pass stage, with highest value at 8^o approach angle and the criterion being reached.

The figures showed that the approach angle had a strong effect on ductile damage. In agreement with Zompì and Levi (2008), smaller approach angles presented less damage to the centerline nodes. The simulations also showed that the axial stresses were compressive for centerline node and tensile for surface nodes, which is in accordance with the findings by Kabayama *et al*. (2009).

(iii) Effects of Exit Angle

From the figures, it was shown that for the *centerline nodes*, the equivalent plastic strain and damage values were high during the second (2-3) and third (3-4) multi-pass stages. The Cockroft and Latham criterion showed that ductile damage was high during the third (3-4) and fourth (4-5) multi-pass stages.

The figures also showed that for the *surface nodes*, both the plastic strain and damage values were high during the first (1-2) and second (2-3) multi-pass stages. The Cockroft and Latham criterion showed that ductile damage was high during the second (2-3) and third (3-4) multi-pass stage, with no peaks being recorded.

From the figures, it was shown that the exit angle had no effect on ductile damage. This is supported by Wright (2011) and Esteves Group (2008) that the exit angle or back relief allows the wire to exit freely from the bearing region, thus minimizing scrapping of the exiting wire.

(iv) Effects of Bearing Length

It was shown from the figures that for the *centerline nodes*, the equivalent plastic strain and damage values were high during the second (2-3) and third (3-4) multi-pass stages. The equivalent Mises stresses were tensile and showed an increase with increased bearing length during the second (2-3) and third (3-4) multi-pass stages. The hydrostatic stresses were compressive and high during the first (1-2) and third (3-4) multi-pass stages while the stress triaxiality was high during the first (1-2) and second (2-3) multi-pass stages. Ductile damage using the Cockroft and Latham criterion was shown to be high during the third (3-4) and fourth (4-5) multi-pass stages, with peaks at 30 and 50% bearing lengths. The critical criterion value of 357.09 MPa was however not met.

For the *surface nodes*, it was shown from the figures that the equivalent plastic strain and damage values were high during the first (1-2) and second (2-3) multi-pass stages. The equivalent Mises stresses were also tensile and reduced with increased bearing length during the second (2-3) and fourth (4-5) multi-pass stages. The hydrostatic stresses were tensile and fluctuated during the second (2-3) multi-pass stage, while the stress triaxiality equally fluctuated during most of the multi-pass stages. Ductile damage using the Cockroft and Latham criterion was shown to be high during the second (2-3) and third (3-4) multi-pass stages, with a peak at 30% bearing length and during which the critical criterion value of 357.09 MPa was met.

The figures showed that the bearing length had an effect on wire ductile damage. Contrary to the findings by McAllen and Phelan (2007), the influences of the bearing length on equivalent strain and damage are not negligible. The findings show that in agreement with Benesova *et al*. (2008) the highest damage values based on the Cockroft and Latham criterion are found in the later (fourth) multi-pass stage where the hydrostatic stress is lowest and compressive.

(v) Effects of Area Reduction

In considering the results of figures for the *centerline nodes*, the equivalent plastic strain for all multi-passes increased with increasing area reduction while the damage value was zero up to 14% area reduction after which the increase in damage value had an accelerated form. Ductile damage using the Cockroft and Latham criterion increased with area reduction for all multi-passes and the critical damage value was met during the fourth (4-5) multi-pass stages at area reductions above 16%.

For the *surface nodes*, the equivalent plastic strain and damage values increased with increasing area reduction and were highest and lowest during the first (1-2) and fourth (4-5) multi-pass stages respectively. The Cockroft and Latham criterion showed an increase in ductile damage with increasing area reduction for all multi-passes and was highest during the third (3-4) multi-pass stage. The critical criterion value of 357.09 MPa was met at 16% area reductions during the third (3-4) and fourth (4-5) multi-passes and at 18% area reduction during the second (2-3) multi-pass.

The figures showed that the area reduction had a very strong effect on wire ductile damage. This is an agreement with the theory of Avitzur (1983) and Wright (2011). The results support the findings by McAllen and Phelan (2005), Zompì and Levi (2008), Kabayama *et al.* (2009) and Hassan and Hashim (2015) where increased area reduction led to an increased tendency for wire damage.

(b) Effects of Drawing Process Conditions

The influences of the friction coefficient and drawing speed on equivalent plastic strain were presented in Figures 5.16 and 5.17, while Figures 5.36, 5.37, 5.40 and 5.41 presented the effects on damage value (stiffness degradation) and the Cockroft and Latham criterion leading to ductile damage of the copper wire.

(i) Effects of Coulomb Friction Coefficient

For the *centerline nodes*, both the plastic strain and damage values were high during the second (2-3) and third (3-4) multi-pass stages. The Cockroft and Latham criterion showed that ductile damage was high during the third (3-4) and fourth (4-5) multi-pass stages, with peaks at 0.09 for both multi-passes.

For the *surface nodes*, the figures showed that both the equivalent plastic strain and damage values were high during the first (1-2) and second (2-3) multi-pass stages. The Cockroft and Latham criterion showed that ductile damage was highest during the second (2-3) and third (3-4) multi-pass stages, during which the critical criterion was met. The highest value of 0.07 friction coefficient was attained during the second multi-pass stage.

The figures showed that the friction coefficient had an effect on ductile damage. Wright (2011) indicates that friction has an effect on development of fracture inside and outside the wire surface due to the persistence of sticking and the intermittent release of local surface frictional stress. The findings are supported by Valberg (2010) who stated that the quality of a drawn surface depended on the lubricant used.

(ii) Effects of Drawing Speed

From the figures for both the equivalent plastic strain and damage values for *centerline nodes*, both were high during the second (2-3) and third (3-4) multi-pass stages. Although the criterion was not met, the ductile damage using the Cockroft and Latham criterion showed high values during the third (3-4) and fourth (4-5) multi-pass stages, with damage reducing with increasing drawing speed.

Figures for the *surface nodes* show that both the equivalent plastic strain and the damage values were high during the first (1-2) and second (2-3) multi-pass stages. The Cockroft and Latham criterion showed that ductile damage was highest during the second (2-3) and third (3-4) multi-pass stages, during which the critical criterion was met. Damage reduced with increasing drawing speed for these multi-pass stages.

From the figures, it was seen that the drawing speed had an effect on ductile damage. Wright (2011) indicates that the drawing speed had a direct effect on lubricant film thickness and the related coefficient of friction.

(c) Effects on Dependent Variables

Effects of the die geometry parameter variation on dependent variables and their influence on the Cockroft and Latham criterion leading to ductile damage of the copper wire are presented in the following sections:

(i) Influence on Drawing Force

A generalised equation of the drawing force, $\boldsymbol{F_d}$, under friction and redundant conditions is given by equation (7.1) according to Kalpakjian and Schmid (2010):

$$F_d = Y_{avg} A_f \left[\left(1 + \frac{\mu}{\alpha}\right) \ln\left(\frac{A_i}{A_f}\right) + \frac{2}{3}\,\alpha\right] \qquad \textbf{(7.1)}$$

Figure 7.1 shows the distribution of drawing forces for the area reductions used during the different multi-pass wire drawing stages, while Figure 7.2 shows the distribution of force with die size.

It is seen from Figure 7.1 that the drawing force rises with increased reduction ratios, while Figure 7.2 shows that the drawing force also increases with the die or wire size being drawn.

The findings agree with the works of Zompì and Levi (2008) that large drawing ratios led to large drawing forces.

(ii) Influence on Drawing Stress

Figure 7.1 shows the distribution of the drawing stress with area reductions for multi-pass wire drawing. The drawing stress, $\boldsymbol{\sigma_d}$, is computed based on the slab method, under friction and redundant conditions and is given by the equation (7.2) as follows (Huo, 1997):

$$\sigma_d = Y_{avg}\left[\left(1 + \frac{\mu}{\alpha}\right)\ln\left(\frac{A_i}{A_f}\right) + \frac{2}{3}\,\alpha\right] \quad \textbf{(7.2)}$$

From Figure 7.1 it is seen that the drawing stress increases slowly with increased area reduction and is almost constant during multi-pass wire drawing.

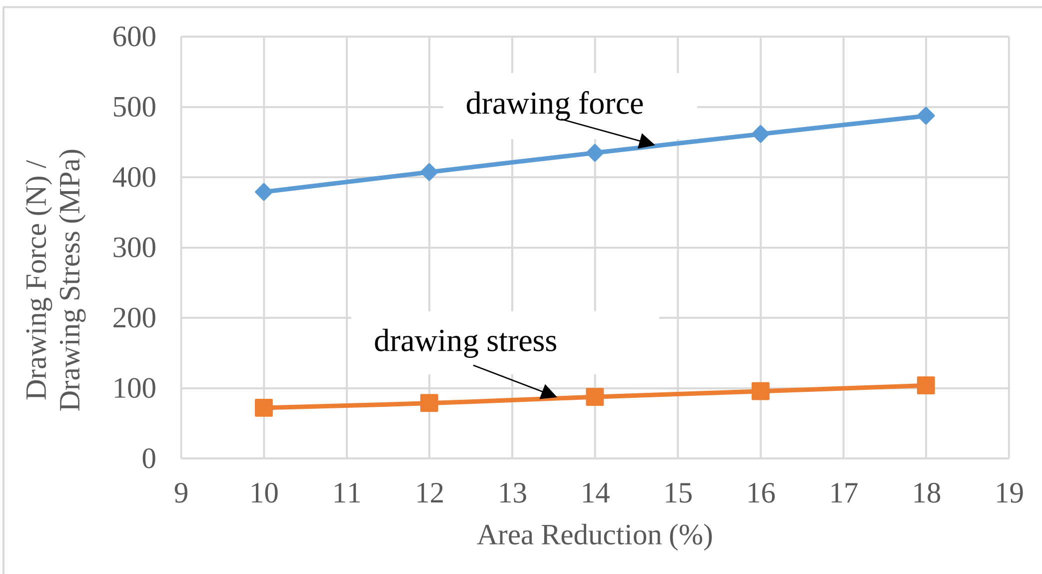

Figure 7.1: Distribution of Drawing Force and Stress during Multi-Pass Wire Drawing. (Source: Author)

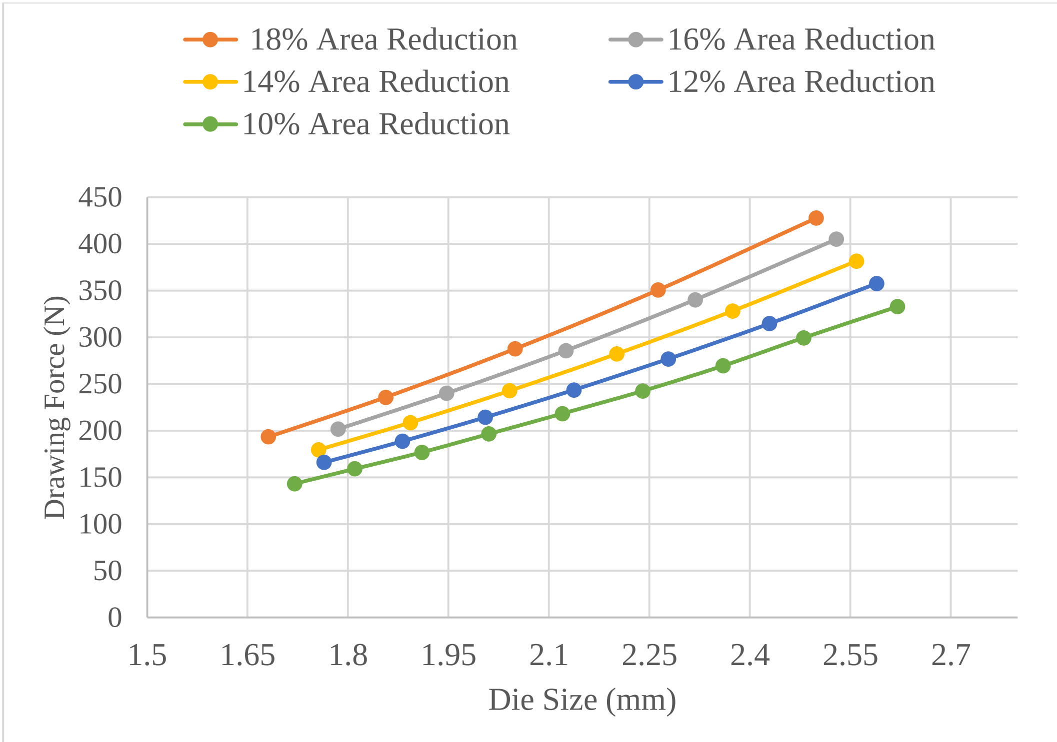

Figure 7.2: Distribution of Drawing Force with Die Size during Multi-Pass Wire Drawing. (Source: Author)

(iii) Influence on Elongation and Δ-Parameter

Figure 7.3 shows the distribution of percent elongation and Δ-parameter at different area reductions during multi-pass wire drawing. According to Esteves Group (2008), the percent elongation (***E%)*** during wire drawing is expressed by equation (7.3):

$$E(\%) = \left[\left(\frac{d_i}{d_f}\right)^2 - 1\right] x\ 100 \qquad \textbf{(7.3)}$$

Wright (2011) expresses the Δ-parameter during wire drawing according to equation (7.4):

$$\Delta = \frac{4\ tan\alpha}{\ln\left[\frac{1}{(1-AR)}\right]} \qquad \textbf{(7.4)}$$

Figure 7.3 shows that the percent elongation increases with area reduction whereas the Δ-parameter decreases with increasing area reduction. This is agreement with Wright

(2011) that low Δ values are associated with large area reductions while high Δ values are associated with small area reductions.

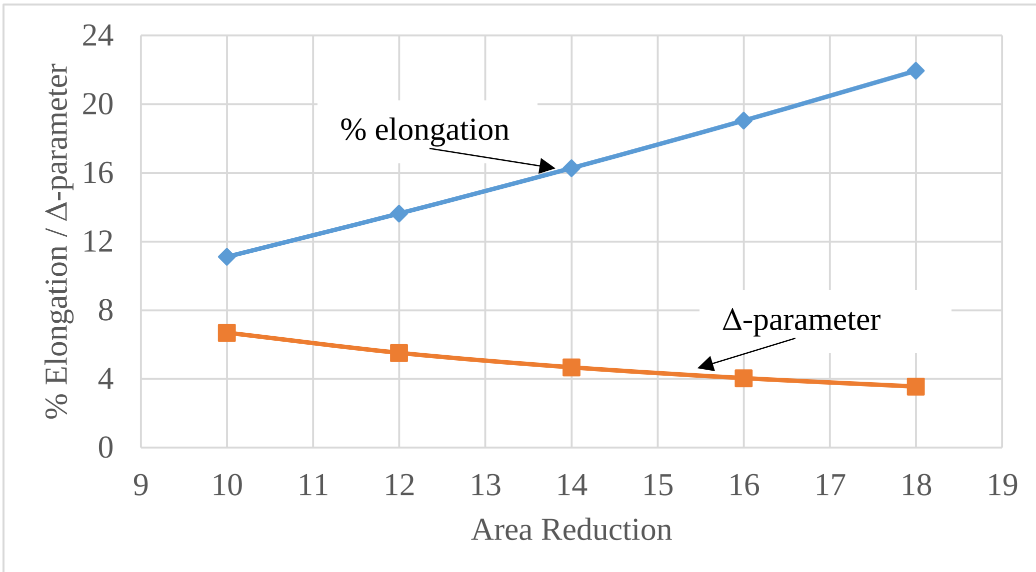

Figure 7.3: Distribution of % Elongation and Δ-Parameter with Area Reduction. (Source: Author)

.

(iv) Strain Rate during Multi-Pass Wire Drawing

The equivalent plastic strain rate, $\dot{\varepsilon}_p$, is calculated according to equation (7.5) as the product of the equivalent plastic strain and the drawing velocity, v_d , divided by the node displacement, L, i.e:

$$\dot{\varepsilon}_p = \frac{\varepsilon_p \, x \, v_d}{L} \qquad \textbf{(7.5)}$$

Figure 7.4 and 7.5 show the distribution of strain rate for the centerline and surface nodes using different area reductions and a drawing velocity of 0.1 m/s. The figures show that the strain rate in both cases increases with area reduction. The strain rate for surface nodes also depends on the multi-pass stages, with the first multi-pass (1-2) having a higher strain rate than the subsequent multi-passes.

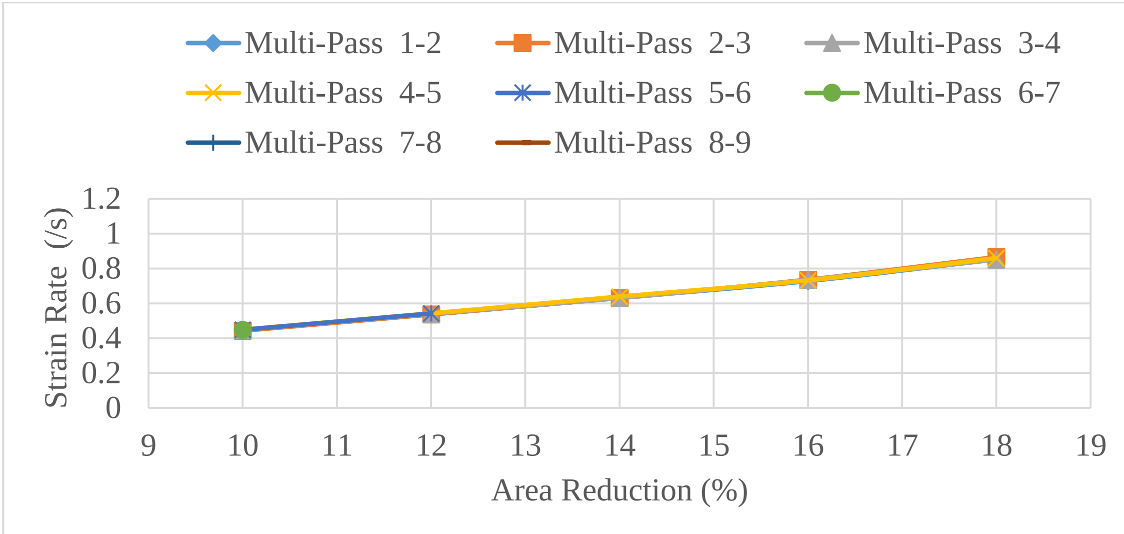

Figure 7.4: Distribution of Strain Rate for Centreline Node (306). (Source: Author)

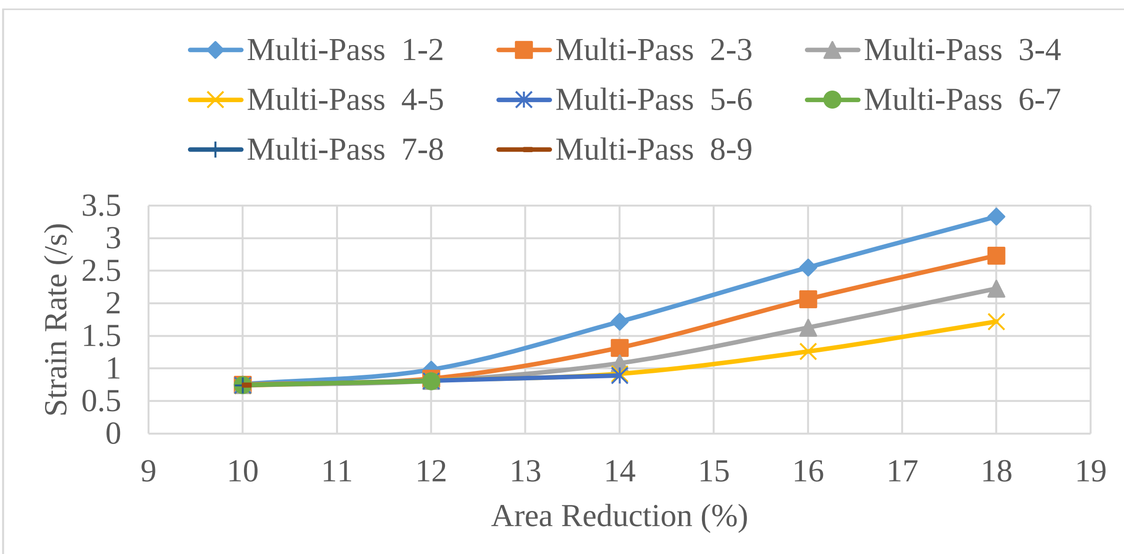

Figure 7.5: Distribution of Strain Rate for Surface Node (410). (Source: Author)

7.3.2 Analysis and Discussion of Experimental Procedures Results

The copper wire drawing experimental procedures were mainly based on the multi-pass sequence involving the 2.55, 2.32, 2.11, 1.92 and 1.78 dies. Other multi-pass sequences used were based on the pass schedules as given in **Appendix 6**.

(a) Effects of copper material state

It was seen from the ascertained chemical composition that the raw wrought copper rods contained metallic elements within the prescribed limits by the standard ASTM B49-10. The microstructure showed the presence of second phase particles with varying grain sizes within the copper material matrix. Iron showed the highest percentage of metallic inclusions. This could be attributed to the nature of the production processes, where during electro refining steel starter sheets are used, or that the molten copper comes into contact with steel boundaries during rod formation.

Of greater importance to wire drawing is the presence of silver. Silver is partially soluble in copper and forms an inclusion or second phase (Wright, 2011) within the copper matrix. The presence of silver particles is a likely source of micro-void initiation and progression, leading to wire failure during wire drawing (Norasethasopon, 2011). The results of the tensile tests for the wrought copper were given in Tables 6.3 and 6.4, and **Appendix 5**.

(b) Effects from die design and manufacturing

During 2D design and simulation of the copper wire drawing process, it was observed that the use of non-filleted die regions were seen to result in larger Mises stresses during wire movement. This was evidence of possible flow problems by the introduction of ‘stress risers’ during simulations. This agreed with the recommendations by Society of Manufacturing Engineers (1962) and Shearer (2008) that all stress raisers needed to be removed.

(c) Effects from copper wire drawing practice

(i) Effects of drawing pass schedules

The drawing pass schedules used by the company varied according to the wire size produced. Figure 7.6 below shows the variation of the Δ-parameter with area reduction for the different wire sizes and number of dies used.

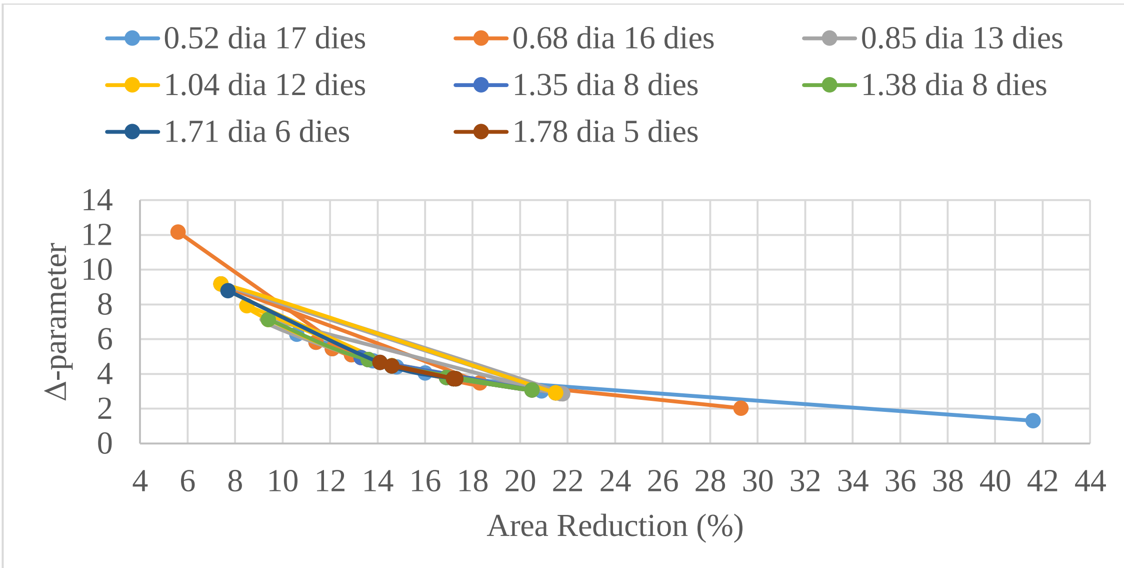

Figure 7.6: Variation of Delta Parameter with Area Reduction for Different Multi-Passes. (Source: Author)

From Figure 7.6, it was shown that a range of pass schedules were used which involved area reductions of between 5% and 42%, and corresponding Δ-parameters ranging from 1.31 to 12.17. The concentration of pass schedules was shown to be in the area reduction range of 8% to 22%. According to Wright (2011), the pass schedules were generally characterised by high Δ-parameters (above 3.0) with low area reductions and high approach angles (12^{o}). The high Δ-parameter values were indicative of increased levels of redundant deformation and surface hardening, with a tendency toward void formation and center bursting (Descargas, nd).

(ii) Effects of lubrication and lubrication temperatures

The lubricant Mastersol C21 which was used both as a lubricant and coolant during copper wire drawing was subjected to analytical tests at ZABS according to standards ASTM D 445 and ASTM D 1298. According to equation (7.6) the kinematic viscosity, v, is related to the dynamic viscosity, μ, and the density, ρ, as follows (Rajput, 2014):

$$v = \frac{\mu}{\rho} \tag{7.6}$$

It was thus seen that at a working temperature of 40^{o}C, the dynamic viscosity was equal to 34.38 cSt, whereas at a temperature of 100^{o}C, the dynamic viscosity dropped about five times to a value of 6.94 cSt. This is in agreement with Rajput (2014) that the viscosity of a lubricant decreases with increase in temperature due to the decrease in the shear stress of the lubricant. As the lubricant temperature was maintained below 45^{o}C throughout the experiments, there were no major changes in viscosity. There was, therefore, no major changes in the viscosity of the lubricant. Lubrication was, thus effective.

(iii) Effects of die temperatures

The temperatures at die faces during wire drawing were seen to increase with increase in die or wire size. This was due to the fact that larger wires or die sizes needed larger drawing forces, hence increased die-wire temperatures.

(iv) Effects of drawing speed

The drawing speeds were generally low for larger wire size production and higher for smaller size wires. The drawing speeds were observed to be on average low as they ranged from 2.4 to 2.7 m/s for the medium size wires (Kalpakjian and Schmid, 2010).

According to Huo (1997) the drawing speed has an effect on drawing force and drawing stress in that a change in drawing speed results in a change in the flow stress of the drawn material and also changed the lubrication and friction characteristics in the wire drawing.

(v) Effects of drawing force

The drawing force increased with increasing wire size, thus necessitating the use of lower speeds for larger size wires. This was done in order to reduce the drawing stress and thus reduce the volume of defects due to wire breakages.

(vi) Effects on wire damage

Generation of 'copper fines' happened throughout the wire drawing process. The fines were evident at wire entry (first die) and at wire exit (last die) due to the deposit of dry fines. For the other dies, the copper fines were collected in the lubricant.

It was observed that wire breakage occurrences were more for smaller size wires (less than 1.04 mm) than larger size wires greater than 1.04 mm. This is attributed to the fact that the smaller size wires were drawn at higher speeds while the larger wires were drawn using lower speeds.

Results from microscopy showed that during all multi-passes both internal micro-voids and surface cracks were unavoidable during wire drawing. Cracks on the surface of the wire were more pronounced than the internal micro-voids as discussed below:

(a) Multi-Pass 1-2

During the first multi-pass, internal micro-voids were more evident at 30% and 50% than at 40% bearing length. Surface cracking was very pronounced at 30% bearing length, while at 40% bearing length signs of surface chevron cracking was evident and the 50% bearing length surface showed signs of sheared surfaces.

(b) Multi-Pass 2-3

The second multi-pass was characterized by more internal micro-void formation during the 40% and 50% than at 30% bearing length. Surface cracking was very pronounced at 30% and 40% bearing length, while at 50% bearing length the extent of surface cracking was reduced. This could be attributed to the facts that for internal micro-voids the relaxation of material during the 40% bearing length happens, hence the pronounced micro-voids. The seemingly reduction of surface cracks at 50% bearing length could be due to the 'forming' effect on the already cracked surfaces, thus closing up the cracks.

(c) Multi-Pass 3-4

From the micrographs, it was seen that the third multi-pass had fewer internal micro-voids in the 30% than the 40% and 50% bearing length. Surface cracking was more evident during the 40% and 50% bearing lengths. As damage is progressive, the behaviour of internal voids could be due to movements in shear layers due to drawing stress, thus the micrographs only being captured for layers with minimal void formation. Surface cracking could be due to the afore-said, whereby forming effects due to wire interaction with the die occasion a smoother surface than the preceding layers.

(d) Multi-Pass 4-5

The last multi-pass stage during wire drawing practice was characterised by more internal micro-voids at 30% and 50% than at 40% bearing length. Surface cracking was equally more pronounced at 30% and 50% bearing lengths, while at 40% bearing length signs of surface micro-voids were evident. This characteristic behaviour in the last multi-pass could be due to the fact that 'impact' damage during wire entry to the die zone effected damage at 30% bearing length, while progression of micro-voids and consequent movement of shear layers effected increased damage during the 50% bearing length.

Measurement of micro-void sizes across the length at 3000X magnification showed that the average internal crack length was highest during the 30% bearing length, and lowest during the 40% bearing length. Surface crack measurements showed that the average crack length was highest at 50% and lowest at 30% bearing length.

7.4 Effects of Bearing Length Variation

(a) Centreline (Internal) Damage

Effects of the bearing length on damage value (stiffness degradation) and the Cockroft and Latham criterion leading to ductile damage of the copper wire in simulations showed higher damage during the second (2-3) and third (3-4) multi-pass stages. Progressive damage using the Cockroft and Latham criterion was high during the third (3-4) and fourth (4-5) multi-pass stages, with peaks at 30 and 50% bearing lengths. The equivalent plastic strain was high during the second (2-3) and third (3-4) multi-pass stages, while the hydrostatic pressure was principally compressive and increased during the second (2-3) and third (3-4) multi-pass stages.

A critical look at the Mises contours in Figures 5.9 to 5.13 showed that the Mises stresses progressed from the surface contours towards the centreline during the movement of the copper wire. The density of highly stressed areas towards the centreline tended to be higher at 50% than at 30% bearing length variations. This is evident from the stick-slip effect postulated by Avitzur (1983).

From the simulation models it was shown that progressive damage using the Cockroft and Latham criterion was high at relatively low drawing speeds and periodic friction coefficient values. This can be due to the longer periods of wire in contact with the die surface, hence the larger being the die-wire contact area and consequently, the drag or frictional effets being prolonged for such surfaces. The copper wire surface layers in contact with the die tend to move slower than the centreline layers, thus effecting velocity difference between the surface layers and the centreline layers.

Scanning image micrographs in Figures 6.32 and 6.40 showed that the second (2-3) multi-pass was characterized by more internal micro-void formation during the 40% and 50% bearing length variation than the 30% bearing length as shown in Figure 6.24. During the third (3-4) multi-pass more internal micro-voids were observed in the 40% and 50% bearing length (Figures 6.34 and 6.42) than in the 30% bearing length variation (Figure 6.26). The fourth (4-5) multi-pass stage was characterised by more internal micro-voids at 30% and 50% (Figures 6.28 and 6.44) than at 40% bearing length (Figure 6.36).

The findings were in agreement with McAllen and Phelan (2005) for area reductions of 17% where the plastic strain and centreline damage were shown to be high during the second and third multi-pass stages. The findings by Komori (2003) and Benesova, *et al.*, (2008) can be supported here that ductile fracture is likely at later multi-pass stages and when hydrostatic stresses are compressive for wire centreline sections. It can be inferred thus, that at higher area reductions and at bearing lengths of 50%, centreline damage is higher. Smaller bearing length values (40% and below) are preferrable for reduced internal damage.

(b) Surface (External) Damage

For the *surface nodes*, it was shown that both equivalent plastic strain and damage values were high during the first (1-2) and second (2-3) multi-pass stages. Ductile damage using the Cockroft and Latham criterion was shown to be high during the second (2-3) and third (3-4) multi-pass stages. Damage was seen to be lower during the 30% bearing length variation than during the 40% to 50% bearing length range.

Scanned micrographs of drawn surfaces during the first (1-2) multi-pass showed evidence of chevron cracking at 40% bearing length (Figure 6.31), with the 50% bearing length surfaces displaying sheared sections (Figure 6.39). The second multi-pass (2-3) showed less surface cracking during the 50% bearing length variation (Figure 6.41) than the 30% and 40% bearing length range (Figures 6.25 and 6.33). The third (3-4) multi-pass showed increased surface cracking during the 40% to 50% bearing length range (Figures 6.35 and 6.43).

In agreement with McAllen and Phelan (2005), it can be inferred that increased plastic strain for area reductions of 17% where the plastic strain and surface damage were shown to be high during the second and third multi-pass stages. The observed generation of copper fines and as attributted to by Chia and Patel (1996) could be as a result of a prolonged wire to die contact surface, exacerbated by a possibility of non-aligned wire movement. It can be inferred thus, that at higher area reductions and at bearing lengths of 40% and above, surface damage is higher. Smaller bearing length values (30%) are preferrable for reduced surface damage.

7.4.1 Summary of the Effects of Bearing Length Variation

From the analysis in section 7.4, it can be summarised that variation of the bearing length has an effect on progressive damage of copper wire during wire drawing.

For both wire centerline or internal surfaces and external surfaces, bearing lengths of not more than 40% are recommended for reduced internal and surface damage.

CHAPTER EIGHT: CONCLUSIONS AND RECOMMENDATIONS

8.1 General Conclusions

From the research carried out in the study, the following conclusions can be made:

(1) With the exception of the *exit angle*, all the die geometrical parameters, lubrication, temperature and drawing speed had an influence on the development of both wire centerline and surface cracks.

(2) Ductile damage was more evident in the second (2-3) and third (3-4) multi-pass stages where area reductions of 17% were attained.

(3) The area reduction had a stronger effect on damage, although drawing at area reductions above 18% using smaller approach angles of 9^o kept the Δ-parameter below the recommended threshold of 3.

(4) Bearing length values between 30% and 40% gave better wire performance in relation to wire centerline damage which is more troublesome than wire surface damage. Bearing lengths of 30% gave wire surface less damage.

(5) Use of lubrication during wire drawing is emphasised, with the need to control the lubricant temperatures arising from die-wire contact. Most wire drawing setups use flood lubrication which is directed at die blocks. This maintains effective lubrication through reduction of die working temperatures which have an effect on lubricant viscosity.

(6) Drawing wires above 1.04 mm demands larger drawing forces. This is compromised by the relative reduction of the drawing speed which lowers the effectiveness of lubrication. The wires thus become prone especially to surface damage. Such wires should therefore be drawn using higher area reductions.

(7) The accelerated strain rate with area reduction renders the wire surface layers more prone to strain hardening and cracking. The use of annealing the wire after each pass

may be a better, though expensive, method than the usually practiced annealing of the final wire.

8.2 Summary of Conclusions

The following conclusions arising from the findings and addressing the research objectives can be made:

(i) Establishment of die design and manufacturing aspects influencing accuracy of die geometry

- Low cost tungsten carbide nibs assembled in carbon steel casings are used at low production volume levels. High wire drawing volume levels and fine wires demands the use of polycrystalline or natural diamond nibs assembled in stainless steel casings.
- Design of die profile geometries is easily done using computer aided software. Smooth fillets along the die nib geometrical surface are emphasized.
- Accurate mould design is essential to producing an accurate die nib
- The type of die nib material used (tungsten carbide or polycrystalline diamond) is likely to affect the life of the die, with the polycrystalline diamond projected to have a longer die life than tungsten carbide.

(ii) Determination of the Δ-parameter values, die geometrical parameters and process conditions leading to the manifestation of surface and chevron cracks during wire drawing

The following die geometrical parameters promote wire damage:

- Smaller entrance angles of 20^o are likely to cause both internal and surface wire damage
- Bearing lengths of 50% inflict centerline damage while 40% to 50% bearing lengths cause surface damage

- Approach angles of 10 or 12^o are likely to cause centerline damage, whereas approach angles of 8^o are likely to cause surface damage
- High friction coefficients of 0.07 and 0.09, signifying low lubrication regimes, are likely to cause both centerline and surface damage
- Low drawing speeds, typical when drawing wires larger than 1.04 mm, promote internal and surface damage
- High temperatures (above 40^{o}C) reduce the viscosity of the lubricant, increase the friction coefficient and promote wire damage
- High area reductions (above 18%) with very small approach angles give small Δ-parameter values and promote crack formation due to increased friction. Low area reductions (below 16%) with large approach angles promote surface hardening and redundant deformation, thus promoting crack formation. A 'balanced-effect' between these two regions is needed.

(iii) Development of an integrated model for die geometry and process parameters for multi-pass copper wire drawing

- Correctly designed die geometrical parameters (entrance angle, approach angle, bearing length, area reduction) and process parameters (temperature, drawing speed, friction coefficient and lubrication) participate in an integrated manner towards the production of a defect-free copper wire.

(iv) Validation of the developed models using industry-based copper wire drawing process setup

Based on the results and analysis of both the models and scanning micrographs, the following are optimum bearing length parameters:

- Centreline damage is minimized when using bearing length values between 30% and 40% while surface damage is minimal when using bearing lengths of 30%.

8.3 Summary of Research Contributions

(1) The study has given contributions concerning the preferred use of 40% bearing lengths during copper wire drawing practice. This region has shown that favourable wire drawing conditions in regard to the internal and surface ductile damage are obtainable when utilized.

(2) The research has delved into new territory regarding analysis of micro-voids inside and on the outside of copper wire surfaces. Using defect micrographs, the quality of internal and external copper wire surfaces can be easily assessed.

(3) The study has also explored new concerns arising from the industrial wire drawing practice that unlike having pass schedules designed based on constant area reduction or constant Δ-parameter, a combination of both concepts is preferred.

8.4 Suggestions for Further Research

(1) Further analysis, modelling and experimental investigation into the effects of the entrance angle on ductile damage during copper wire drawing, especially when large reduction angles are used. Preliminary modelling has shown that the entrance angle has an effect on ductile damage.

(2) The effects of wear and lubrication mechanisms in the die bearing region and their impact on both internal and external wire damage need investigation.

(3) The determination of critical crack or micro-void sizes impacting on wire performance by assessment with elongation and electrical resistivity is necessary.

(4) Need for the development and application of shorter *time-to-market* moulds for die nib manufacture when using conventional powder metallurgy equipment.

8.5 Recommendations for Implementation

(1) Wire drawing practitioners to always have a *Tool Room* which should ensure that dies are procured according to technical specifications by engineers and an inventory of all dies is kept for die maintenance purposes.

(2) Wire die practitioners to stick to the planned die sequences and not use any available similar size die. This practice impacts on the Δ-parameter and therefore the onset of wire damage.

(3) Wire drawing machinery manufacturers to incorporate effective pressure-based sieving systems with easily removable basins for collection of copper 'fines' which compromise the viscosity of the lubricant.

(4) Incorporation of an annealer after rod breakdown to improve flow properties of the 2.76 mm raw wire before being subjected to intermediate wire drawing.

REFERENCES

Ahmadi, F. and Farzin, M., (2008), Investigating Geometric and Friction Conditions Causing Chevron Cracks in Wire Drawing Process using FEM. Steel Research International Journal, Volume 2, pp. 382-388.

ASM International, (1990), Properties and Selection Non Ferrous Alloys and Special-Purpose Materials. In: ASM Handbook Vol 02 . ASM International .

ASM International, (1988), Vol 14: Forming and Forging. ASM Handbook. ASM International.

ASM International, (1990), Properties and Selections of Irons, Steels and High-Performance Alloys. In: Vol 01 ASM Handbook Vol 01. ASM International, p. 1618.

ASTM International, (2010), Standard Specification for Copper Rod Drawing Stock for Electrical Purposes, Designation: B49-10. ASTM International.

Atkins, A. and Caddell, R., (1968), The Incorporation of Work Hardening and Redundant Work in Rod-Drawing Analyses. International Journal of Mechanical Sciences, Pergamon Press, Volume 10, pp. 15-28.

Avitzur, B., (1983), Handbook of Metal-Forming Processes. New York: John Wiley and Sons, Inc. ISBN 0 471 03474 6.

Bao, Y., (2003), Prediction of Ductile Crack Formation in Uncracked Bodies, PhD Thesis. Massachusetts: Massachusetts Institute of Technology.

Bathe, K.-J., (1996), Finite Element Procedures. New Jersey: Prentice Hall. New Jersey: Prentice Hall.

Benesova, S., Krnac, J., Wludzik, R. and Pilarczyk, J., (2008), Application of Cockroft-Latham Criterion in FEM Analysis of Wire Fracture in Conventional Drawing of High Carbon Steel Wires. [Online] Available at: http://home.zcu.cz/~sbenesov/Pittsburgh08. Doc, [Accessed 14-03-2012].

Byon, S. M., Lee, S.J., Lee, D.W., Lee, Y.H. and Lee,Y., (2011), Effect of Coating Material and Lubricant on Forming Force and Surface Defects in Wire Drawing Process. Transactions of the Nonferrous Metal Society of China, pp. 104-110.

Campos, H. B., Reis, R.I., Corrêa, E.C.S., Aguilar, M.T.P. and Cetlin, P.R., (2006), Variation of Friction Coefficient with Die Semi-Angle in the Axisymetric Drawing of Copper, 17º CBECIMAT - Congresso Brasileiro de Engenharia e Ciência dos Materiais, 15 - 19 de Novembro, Foz do Iguaçu, Brasil.

Canter, N., (2009), Challenges in Formulating Metal Forming Fluids. Tribology and Lubrication Technology, pp. 56-63.

Ceratizit, n.d. Drawing Tools for Wire Production. [Online] Available at: http://www.ceratizit.com , [Accessed 08-03-2012].

Chia, E. and Patel, G., (1996), Characterisation of Rod and Wire Defects Produced During The Manufacturing of Copper. Wire Journal International, pp. 50-59.

Cho, J. et al., 2006. Investigation of Recrystallisation and Grain Growth of Copper and Gold Bonding Wires. Metallurgical and Materials Transactions , Volume 37 A, pp. 3085-3097.

Cho, J.H., Rollett, A.D., Cho, J.-S., Park, Y.-J., Moon, J.-T. and Oh, K.H., (2006), Investigation of Recrystallization and Grain Growth of Copper and Gold Bonding Wires. Metallurgical and Materials Transactions, Volume 37A, pp. 3085-3097.

Conoptica, (2007), Drawing Die Profile: Inner Geometry Measurement, Application Note 002. [Online] Available at: http://www.conoptica.com, [Accessed 08 03 2012].

Copper Development Association, n.d. The Copper Advantage: A Guide to Working with Copper and Copper Alloys. [Online] Available at:http://www.copper.org/publications/pub_list/pdf/a1360.pdf, [Accessed 06-03-2013].

Dassault Systèmes, (2013), Modelling Fracture and Failure with Abaqus. Dassault Systèmes.

Dassault Systèmes, (2014a), ABAQUS 6.14: Theory Guide. Dassault Systèmes.

Dassault Systèmes, (2014b), ABAQUS Analysis Users Guide. Dassault Systèmes.

Davis, J.,(ed), (2001), Copper and Copper Alloys. ASM Specialty Handbook. ASM International.

Descargas, (nd), Theory of Wire Drawing, [Online] Available from: http://www.antaac.org.mx/descargas/TheoryOfWire drawing.pdf, Retrieved:[24-03-2012].

Diamond Innovations, (2004), Compax Diamond Die Blanks. [Online]
Available at: http://www.diamondinnovations.com, [Accessed 22-08-2012].

Dieter, G., (1988), Mechanical Metallurgy. McGraw Hill.

Dixit, P. and Dixit, U., (2008), Modelling of Metal Forming and Machining Processes by Finite Element and Soft Computing Methods. Springer. e-ISBN 978-1-84800-189-3.

Dubois, A., Lazzarotto, L., Dubar, L. and Oudin, J., (2002), A Multi-Step Lubricant Evaluation Strategy for Wire Drawing–Extrusion–Cold Heading Sequence. Wear Journal, Volume 249, pp. 951-961.

Esteves Group, (2008), The e-Wizard: Your Wire Die Handbook. [Online] Available at: http://www.estevesgroup.com/ewizard/esteves_ewizard_en/ [Accessed 25 01 2013].

Fort Wayne Wire Die Inc., (1996), Single Crystal Diamond Dies: Specifications.
[Online] Available at: http://www.fwwd.com/images/Pdfs/FWWD-SCD_specs.pdf
[Accessed 25 01 2013].

Fort Wayne Wire Die Inc., (2009), Wire Die Manufacturing. [Online]
Available at: http://www.fwwd.com, [Accessed 22 08 2012].

Gálvez, F., Atienza, J., Ruiz, J. and Elices, M., (2002), The Effect of Strain Rate on Steel Wires Failure During Cold Drawing. [Online] Available at: http://www.mater.upm.es/fgalvez/PDF/MSMSE%2010%20(2002)%20167-276.pdf
[Accessed 08-03-2012].

Ghosh, B., (1992), Scientific Method and Social Research. New Delhi: Sterling.

Hassan, A. and Hashim, A., (2015), Three Dimensional Finite Element Analysis of Wire Drawing Process. Universal Journal of Mechanical Engineering, 3(3), pp. 71-82.

Hervias, J.R., Hofmann, M., Kornmeier, J.R., Luzin, V. and Elices. M., (2009), Residual Stresses in Cold-Drawn Rods: Effect of a Novel Post-Drawing Treatment. JCPDS-International Centre for Diffraction Data, ISSN 1097-0002, pp. 747-754.

Higgins, R., (1994), The Properties of Engineering Materials. Arnold.

Hofstee, E., (2006), Constructing a Good Dissertation: A Practical Guide to Finishing a Master's, MBA or PhD on Schedule. Sandton: EPE.

Hollinger, S., Depraetere, E. and Giroux, O., (2003), Wear Mechanism of Tungsten Carbide Dies during Wet Drawing of Steel Tyre Cords. Wear Journal , Volume 255, pp. 1291-1299.

Hosford, W. and Caddell, R., (1983), Metal Forming: Mechanics and Metallurgy. Englewood Cliffs: Prentice-Hall International, Inc. ISBN 0-13-577214-1.

Huo, B., (1997), Lubrication Efficiency and Die Design in Wire Dawing: PhD Thesis, Birmingham: University of Aston.

International Copper Study Group, (2016), World Copper Fact Book 2016, Lisbon: International Copper Study Group.

John, V., (1992), Introduction to Engineering Materials. 3rd ed. Macmillan.

Kabayama, L., Taguchi, S. and Martínez, G., (2009), The Influence of Die Geometry on Stress Distribution by Experimental and FEM Simulation on Electrolytic Copper Wire Drawing. Materials Research, 12(3), pp. 281-285.

Kalpakjian, S. and Schmid, S., (2006), Manufacturing Engineering and Technology. 5th ed. Pearson. ISBN 0-13-148965-8.

Kalpakjian, S. and Schmid, S., (2010), Manufacturing Engineering and Technology. 6th ed. Pearson.

Kerlinger, F., (1986), Foundations of Behavioural Research. Holt Rinehart and Winston Inc.

Komori, K., (2003), Effect of Ductile Fracture Criteria on Chevron Crack Formation and Evolution in Drawing. International Journal of Mechanical Sciences, Volume 45, pp. 141-160.

Lee, K., Lee, S. and Kim, B., (2012), Advanced Simulation of Die Wear Caused by Wire Vibrations during Wire Drawing Process. Transactions of Nonferrous Metals Society of China, Volume 22, pp. 1723-1731.

León, J., Luis, C.J., Salcedo, Luri, D.R., Puertas, I. and Pérez, I., (2010), Effect of the Die Geometry on the Imparted Damage in Wire Drawing. 14th International Research/Expert Conference, pp. 73-76.

Lin, X., Xiao, H. and Zhang, Z., (2003), Research on the Selection of Friction Models in the Finite Element Simulation of Warm Extrusion. ACTA Metallurgica Sinica, XVI(2), pp. 90-96.

Liu, G. and Quek, S., (2003), The Finite Element Method: A Practical Course. Oxford: Butterworth Heinemann.

McAllen, P. and Phelan, P., (2005), A Method for the Prediction of Ductile Fracture by Central Bursts in Axisymmetric Extrusion. Proceedings of the Institution of Mechanical Engineers, Part C: Journal of Mechanical Engineering Science, pp. 237-250.

McAllen, P. and Phelan, P., (2007), Numerical Analysis of Axisymmetric Wire Drawing by Means of a Coupled Damage Model. Journal of Materials Processing Technology, Volume 183, pp. 210-218.

Norasethasopon, S., (2003), Effects of Inclusion on Inclusion Front Tensile Stress During Copper-Shaped Wire drawing by 2D FEA. Naresuan University Journal, Vol.11, No.2, pp. 11-18.

Norasethasopon, S., (2011), Chevron Crack Initiation in Multi-Pass Drawing of Inclusion Copper-Shaped Wire. Materials and Minerals, Vol.21, No.1, pp. 1-8.

Norasethasopon, S. and Yoshida, K., (2003), Influence of an Inclusion on Multi-Pass Copper-Shaped Wire Drawing by 2D Finite Element Analysis. IJE Transactions B: Applications, Vol.16, No.3, pp. 279-292.

Palkowski, H., Kleiber, M. and Groth, C., (2003), 21st CAD-FEM Users Meeting. Potsdam.

Panjan, P., Bončina, I., Bevk, J. and Čekada, M., (2005), PVD Hard Coatings Applied for the Wear Protection of Drawing Dies. Surface and Coatings Technology , Volume 200, pp. 133-136.

Panteghini, A. and Genna, F., (2010), An Engineering Analytical Approach to the Design of Cold Wire Drawing Processes for Strain-hardening Materials, International Journal of Material Forming, Vol.3, pp.279-289.

Pops, H., (1997), The Metallurgy of Copper Wire. [Online], Available at: http://www.copper.org/publications/newsletters/innovations/1997/12/wiremetallurgy.html, [Accessed 23-03-2012].

Radojevič, M., Radojičič, M., Nakič, M. and Babič, M., (2000), Lubricant as a Parameter of Processing Tribomechanical System in the Process of Wire Drawing. Tribology in Industry, Vol.22, Nos. 1 & 2, pp. 23-27.

Rajput, R., (2014), Fluid Mechanics and Hydraulic Machines. S.Chand.

Reddy, N., Dixit, P. and Lal, G., (2000), Ductile Fracture Criteria and its Prediction in Axisymmetric Drawing. International Journal of Machine Tools and Manufacture, Volume 40, pp. 95-111.

Rosenthal, R. and Rosnow, R., (1991), Essentials of Behavioural Research: Methods and Data Analysis. McGraw-Hill Inc.

Salcedo, D., Luis, C.J., León, J., Luri, R., Puertas, I. and Pérez, I., (2010), Analysis of Residual Stresses in Wire Drawing Processes, 14th International Research/Expert Conference "Trends In The Development of Machinery and Associated Technology", TMT 2010, Mediterranean Cruise, 11-18 September, pp.69 -72.

Shearer, T., (2008), The Designer's Guide to Tungsten Carbide. General Carbide.

Simmons, C. and Maguire, D., (1974), A Manual of Engineering Drawing Practice. Edward Arnold.

Singh, S.K., Gautham, B.P., Goyal, S., Joshi, A. and Gudadhe, D., (2007), Development of a Virtual Wire Drawing Tool for Process Analysis and Optimization. Wire Journal International, pp. 72-78.

Society of Manufacturing Engineers , (1962), Fundamentals of Tool Design. Prentice-Hall Inc.

Solomon, N., Chika, M., Famous, A., Chioma, O. and Ebele, E., (2010). Development of New Copper Wire drawing Lubricant. Journal of Applied Sciences Research, Vol.6, No.11, pp. 1669-1673.

Suchy, I., (2006), Handbook of Die Design. McGraw Hill.

Tvergaard, V. and Hutchinson, J., (2002), Two Mechanisms of Ductile Fracture: Void by Void Growth versus Multiple Void Interaction. International Journal of Solids and Structures, Volume 39, pp. 3581-3597.

Udomphol, T., (2007), Drawing of Rods, Wires and Tubes. Suranaree University of Technology [Online] Available at: http://www.sut.ac.th/engineering/Metal/pdf/ MetForm/05_Drawing%20of%20rod-wire%20and%20tubes.pdf, [Accessed 08 03 2012].

Upadhyaya, G., (2002), Powder Metallurgy Technology. Cambridge International Science Publishing. ISBN 1- 898326 40-1.

Valberg, H. S., (2010), Applied Metal Forming, Including FEM Analysis. Cambridge: Cambridge University Press. ISBN 9780-521-51823-9.

Vega, G., Haddi, A. and Imad, A., (2009), Temperature Effects on Wire-Drawing Process: Experimental Investigation. [Online] Available at: http://web.univ-ubs.fr/ limatb/EG2M/Disc_Seminaire/ESAFORM_09/data/pdf/paper195psohm.pdf [Accessed 06-03-2012].

Wright, R., (2011), Wire Technology: Process Engineering and Metallurgy. Butterworth-Heinemann. ISBN 978-0-12-382092-1.

Xue, L., (2007), Ductile Fracture Modelling - Theory, Experimental Investigation and Numerical Verification: PhD Thesis, Massachusetts: Massachusetts Institute of Technology.

Xu, G., Fang, F. and Li, Z., (2009), Optimisation of the Technology of Wire Drawing Based on Finite Element Modeling. Modern Applied Science, 3(5), pp. 193-198.

Yang, X., Deng, J., Wang, H. and Ze, X., (2007), Wear Behaviors and Lubrication Medium of TiC/Al2O3 Ceramic Wire Drawing Dies. Transactions of Non-Ferrous Metal Society of China, Volume 17, pp. s663-s666.

Zhuzhou Good Cemented Carbide Co. Ltd, n.d. [Online] Available at: http:// www.carbide-good.com, [Accessed 06-09-2016]

Zompì, A. and Levi, R., (2008), Advances in Wire Drawing Process by Theoretical and Numerical Analysis. [Online] Available at: http://www.utfscience.de [Accessed 06-03-2012].

APPENDICES

Appendix 1: Properties of Pure Copper

Condition	**Tensile Strength**	**Yield Strength at 0.5 % extension under load**	**Poissons ratio**	**Elastic modulus (GPa)**		**Strain hardening Exponent**	**Elongation**	**Reduction in Area**	**Hardness (HRB)**
				Tension	Shear				
Annealed	209	33	0.343	125	46.4	0.54	60	92	
Cold Drawn	344	333.4	0.364	112			14	88	37

(Source: Davis, 2001)

Appendix 2: Properties of Wrought Copper (@2mm wire section)

UNS Number	Chemical Composition (%)	Condition	Physical Properties				Mechanical properties		
			ρ g/cm^3	**EC** MegaSiemens/cm @ 20^{o}C	**TC** W/m ^{o}K @ 20^{o}C	**E (MPa)**	**σ (MPa)**	**τ (MPa)**	**PE***
C10100 (Oxygen Free Electrolytic Copper - ETP)	99.99 Cu; 0.0004 Sb; 0.0005 As; 0.0005 O; 0.0003 P; 0.0002 Te	Annealed (OS050)	8.94	0.591	391.1	117000	241	165	35
		Cold Worked (H04)	8.94	0.591	391.1	117000	379	200	1
C10200 (Oxygen Free - OF)	99.95 Cu; 0.001 O		8.94	0.591	391.1	117000			

(Source: Copper Development Association)

Appendix 2: Properties of Wrought Copper (@ 2 mm wire section) (continued)

C10700 (Oxygen Free Copper with Silver – OFS)	99.95 Cu; 0.001 O; 0.085 Ag	Annealed (OS050)	8.94	0.585	387.7	117000	241	165	35
		Cold Worked (H04)				117000	379	200	1
C11000 (Electrolytic Tough Pitch)	99.9 Cu;	Annealed (OS050)	8.94	0.591	391.1	117000	241	165	35
		Cold Worked (H04)	8.94	0.591	391.1	117000	379	200	1
C12500 (Fire Refined Tough Pitch)	99.88 Cu; 0.003Sb; 0.012 As; 0.003 Bi; 0.004 Pb; 0.050 Ni; 0.025 Te	Annealed (OS050)	8.94	0.535	349.9	120000	241	165	35
		Cold Worked (H04)	8.94	0.535	349.9	120000	379	200	1

(Source: Copper Development Association)

Appendix 3: **Δ-**Values for Various Approach Semi Angles and Reductions in Wire Drawing

	Percent Reduction in Area							
	5	10	15	20	25	30	35	40
Semi-Angle (degrees)								
2	2.72	1.33	0.86	0.63	0.49	0.39	0.33	0.27
4	5.44	2.65	1.72	1.25	0.97	0.78	0.65	0.55
6	8.17	3.98	2.58	1.88	1.46	1.18	0.98	0.82
8	10.89	5.30	3.44	2.51	1.94	1.57	1.30	1.10
10	13.61	6.63	4.30	3.13	2.43	1.96	1.63	1.37
12	16.33	7.95	5.16	3.76	2.92	2.35	1.95	1.65
14	19.06	9.28	6.02	4.38	3.40	2.75	2.28	1.92
16	21.78	10.60	6.88	5.01	3.89	3.14	2.60	2.20
18	24.50	11.93	7.74	5.64	4.38	3.53	2.93	2.47
20	27.22	13.26	8.60	6.26	4.86	3.92	3.25	2.75

(Sources: Descargas, nd)

Appendix 4: ABAQUS Simulation Output File (30%1st2PasesExplDuctile.dat)

ABAQUS 6.14-2 Date 20-Oct-2015 Time 12:00:29

```
 * * * * * * * * * * * * * * * * * * * * * * * * * * * * * *
*               ****************               *
*               * N O T I C E *               *
*               ****************               *
*                ABAQUS 6.14-2                *
*                                             *
*  Please make sure you are using release 6.14 manuals    *
*  plus the notes accompanying this release.              *
 * * * * * * * * * * * * * * * * * * * * * * * * * * * * * *
```

PROCESSING PART, INSTANCE, AND ASSEMBLY INFORMATION

****

END PROCESSING PART, INSTANCE, AND ASSEMBLY INFORMATION

****

OPTIONS BEING PROCESSED

****

*Heading

Drawing of Drawn Copper Wire from 2.76 to 2.32 mm

*Node

*Nset, nset=ASSEMBLY_DIE1-1_DIE1-1-REFPT_

*Nset, nset=ASSEMBLY_DIE1-1_REFPT

*Node

*Nset, nset=ASSEMBLY_DIE2-1_DIE2-1-REFPT_

*Nset, nset=ASSEMBLY_DIE2-1_REFPT

*Node

*Element, type=CAX4R

*Nset, nset=ASSEMBLY_WIRE-1_ALL

*Nset, nset=ASSEMBLY_WIRE-1_CENTRELINE

*Nset, nset=ASSEMBLY_WIRE-1_INLETSURFACE

```
*Nset, nset=ASSEMBLY_WIRE-1_OUTLETFACE
*Elset, elset=ASSEMBLY_WIRE-1_ALL
*Elset, elset=ASSEMBLY_WIRE-1_CENTRELINE
*Elset, elset=ASSEMBLY_WIRE-1_INLETSURFACE
*Elset, elset=ASSEMBLY_WIRE-1_OUTLETFACE
*Elset, elset=ASSEMBLY_WIRE-1__CENTRELINE_S2
*Elset, elset=ASSEMBLY_WIRE-1__CENTRELINE_S4
*Elset, elset=ASSEMBLY_WIRE-1__CONTACSURFACE_S2
*Elset, elset=ASSEMBLY_WIRE-1__CONTACSURFACE_S4
*Elset, elset=ASSEMBLY_WIRE-1__INLETSURFACE_S3
*Elset, elset=ASSEMBLY_WIRE-1__OUTLETSURFACE_S3
*rigidbody, refnode=ASSEMBLY_DIE1-1_DIE1-1-REFPT_,
analyticalsurface=ASSEMBLY_DIE1-1_DIE1SURF
*rigidbody, refnode=ASSEMBLY_DIE2-1_DIE2-1-REFPT_,
analyticalsurface=ASSEMBLY_DIE2-1_DIE2SURF
*rigidbody, refnode=ASSEMBLY_DIE1-1_DIE1-1-REFPT_,
analyticalsurface=ASSEMBLY_DIE1-1_DIE1SURF
*rigidbody, refnode=ASSEMBLY_DIE2-1_DIE2-1-REFPT_,
analyticalsurface=ASSEMBLY_DIE2-1_DIE2SURF
*rigidbody, refnode=ASSEMBLY_DIE1-1_DIE1-1-REFPT_,
analyticalsurface=ASSEMBLY_DIE1-1_DIE1SURF
*rigidbody, refnode=ASSEMBLY_DIE2-1_DIE2-1-REFPT_,
analyticalsurface=ASSEMBLY_DIE2-1_DIE2SURF
*rigidbody, refnode=ASSEMBLY_DIE1-1_DIE1-1-REFPT_,
analyticalsurface=ASSEMBLY_DIE1-1_DIE1SURF
*rigidbody, refnode=ASSEMBLY_DIE2-1_DIE2-1-REFPT_,
analyticalsurface=ASSEMBLY_DIE2-1_DIE2SURF
*surface, type=SEGMENTS, name=ASSEMBLY_DIE1-1_DIE1SURF
*surface, type=SEGMENTS, name=ASSEMBLY_DIE2-1_DIE2SURF
*surface, type=ELEMENT, name=ASSEMBLY_WIRE-1_INLETSURFACE
*surface, type=ELEMENT, name=ASSEMBLY_WIRE-1_OUTLETSURFACE
```

*surface, type=ELEMENT, name=ASSEMBLY_WIRE-1_CENTRELINE

*surface, type=ELEMENT, name=ASSEMBLY_WIRE-1_CONTACSURFACE

*surface, type=SEGMENTS, name=ASSEMBLY_DIE1-1_DIE1SURF

*surface, type=SEGMENTS, name=ASSEMBLY_DIE2-1_DIE2SURF

*surface, type=ELEMENT, name=ASSEMBLY_WIRE-1_INLETSURFACE

*surface, type=ELEMENT, name=ASSEMBLY_WIRE-1_OUTLETSURFACE

*surface, type=ELEMENT, name=ASSEMBLY_WIRE-1_CENTRELINE

*surface, type=ELEMENT, name=ASSEMBLY_WIRE-1_CONTACSURFACE

*rigidbody, refnode=ASSEMBLY_DIE1-1_DIE1-1-REFPT_, analyticalsurface=ASSEMBLY_DIE1-1_DIE1SURF

*rigidbody, refnode=ASSEMBLY_DIE2-1_DIE2-1-REFPT_, analyticalsurface=ASSEMBLY_DIE2-1_DIE2SURF

*material, name="Drawn Copper"

*damageinitiation, criterion=DUCTILE

*damageevolution, type=DISPLACEMENT

*density

*elastic

*plastic

*surfaceinteraction, name=FRICTION

*friction

*solidsection, elset=ASSEMBLY_WIRE-1_ALL, controls=EC-1, material="Drawn Copper"

*sectioncontrols, name=EC-1, elementdeletion=YES

*rigidbody, refnode=ASSEMBLY_DIE1-1_DIE1-1-REFPT_, analyticalsurface=ASSEMBLY_DIE1-1_DIE1SURF

*rigidbody, refnode=ASSEMBLY_DIE2-1_DIE2-1-REFPT_, analyticalsurface=ASSEMBLY_DIE2-1_DIE2SURF

*rigidbody, refnode=ASSEMBLY_DIE1-1_DIE1-1-REFPT_, analyticalsurface=ASSEMBLY_DIE1-1_DIE1SURF

*rigidbody, refnode=ASSEMBLY_DIE2-1_DIE2-1-REFPT_, analyticalsurface=ASSEMBLY_DIE2-1_DIE2SURF *solidsection, elset=ASSEMBLY_WIRE-1_ALL, controls=EC-1, material="Drawn Copper"

*solidsection, elset=ASSEMBLY_WIRE-1_ALL, controls=EC-1, material="Drawn Copper"

*rigidbody, refnode=ASSEMBLY_DIE1-1_DIE1-1-REFPT_, analyticalsurface=ASSEMBLY_DIE1-1_DIE1SURF

*rigidbody, refnode=ASSEMBLY_DIE2-1_DIE2-1-REFPT_, analyticalsurface=ASSEMBLY_DIE2-1_DIE2SURF

*friction

*elementoutput, directions=YES

*rigidbody, refnode=ASSEMBLY_DIE1-1_DIE1-1-REFPT_, analyticalsurface=ASSEMBLY_DIE1-1_DIE1SURF

*rigidbody, refnode=ASSEMBLY_DIE2-1_DIE2-1-REFPT_, analyticalsurface=ASSEMBLY_DIE2-1_DIE2SURF

*amplitude, name=AMP-1, definition=SMOOTHSTEP

*output, field

*output, history, variable=PRESELECT, frequency=1

*Step, name="multipass drawing", nlgeom=YES

*Step, name="multipass drawing", nlgeom=YES

*dynamic, explicit

*fixedmassscaling, elset=ASSEMBLY_WIRE-1_ALL, dt=1e-05, type=BELOWMIN

*boundary

*boundary, amplitude=AMP-1, type=VELOCITY

*boundary

*boundary

*output, field

*nodeoutput

*elementoutput, directions=YES

*contactoutput

*output, history, variable=PRESELECT, frequency=1

*endstep

***WARNING: THE REQUEST FOR MISES OUTPUT WILL BE REPLACED BY A REQUEST FOR S OUTPUT

***WARNING: OUTPUT REQUEST E IS NOT AVAILABLE IN A NONLINEAR STEP -- LE (LOG STRAIN) WILL BE OUTPUT INSTEAD.

***WARNING: OUTPUT REQUEST EVF IS NOT AVAILABLE FOR ELEMENT TYPE CAX4R

***WARNING: OUTPUT REQUEST PEEQVAVG IS NOT AVAILABLE FOR ELEMENT TYPE CAX4R

***WARNING: OUTPUT REQUEST PEVAVG IS NOT AVAILABLE FOR ELEMENT TYPE CAX4R
*surface, type=SEGMENTS, name=ASSEMBLY_DIE1-1_DIE1SURF
*surface, type=SEGMENTS, name=ASSEMBLY_DIE2-1_DIE2SURF
*surface, type=ELEMENT, name=ASSEMBLY_WIRE-1_INLETSURFACE
*surface, type=ELEMENT, name=ASSEMBLY_WIRE-1_OUTLETSURFACE
*surface, type=ELEMENT, name=ASSEMBLY_WIRE-1_CENTRELINE
*surface, type=ELEMENT, name=ASSEMBLY_WIRE-1_CONTACSURFACE
*surfaceinteraction, name=FRICTION
*friction
*surfacebehavior, pressure-overclosure=HARD
*Step, name="multipass drawing", nlgeom=YES
*dynamic, explicit
*boundary

***WARNING: THE OPTION *BOUNDARY,TYPE=DISPLACEMENT HAS BEEN USED; CHECK STATUS FILE BETWEEN STEPS FOR WARNINGS ON ANY

JUMPS PRESCRIBED ACROSS THE STEPS IN DISPLACEMENT VALUES OF TRANSLATIONAL DOF. FOR ROTATIONAL

DOF MAKE SURE THAT THERE ARE NO SUCH JUMPS. ALL JUMPS IN DISPLACEMENTS ACROSS STEPS ARE IGNORED

*boundary, amplitude=AMP-1, type=VELOCITY

*boundary

*boundary

*contactpair, interaction=FRICTION, mechanicalconstraint=KINEMATIC, cpset=INT-1

*contactpair, interaction=FRICTION, mechanicalconstraint=KINEMATIC, cpset=INT-2

*endstep

P R O B L E M   S I Z E

NUMBER OF ELEMENTS IS	6000
NUMBER OF NODES IS	6233
NUMBER OF NODES DEFINED BY THE USER	6233
TOTAL NUMBER OF VARIABLES IN THE MODEL	12468

(DEGREES OF FREEDOM PLUS MAX NO. OF ANY LAGRANGE MULTIPLIER VARIABLES. INCLUDE *PRINT,SOLVE=YES TO GET THE ACTUAL NUMBER.)

END OF USER INPUT PROCESSING

JOB TIME SUMMARY

USER TIME (SEC) = 0.80000

SYSTEM TIME (SEC) = 0.10000

TOTAL CPU TIME (SEC) = 0.90000

WALLCLOCK TIME (SEC) = 1

Appendix 5: Value from Stress-Strain Diagram for Wrought Copper.

Stress (MPa)	Strain	Stress (MPa)	Strain	Stress (MPa)	Strain	Stress (MPa)	Strain
0.000	0.000	212.145	0.156	230.708	0.469	101.993	0.566
40.797	0.003	214.185	0.188	230.912	0.500	81.594	0.566
81.594	0.006	216.225	0.219	231.116	0.531	61.196	0.566
122.391	0.013	220.305	0.250	231.319	0.544	40.797	0.566
163.189	0.016	222.344	0.281	213.165	0.556	20.399	0.566
173.388	0.025	224.384	0.313	203.986	0.559	20.399	0.566
179.507	0.044	226.424	0.344	177.468	0.563	0.000	0.575
187.667	0.063	228.464	0.375	163.189	0.564		
203.986	0.109	229.484	0.406	142.789	0.566		
208.065	0.125	230.504	0.438	122.391	0.566		

(Source: Author)

Appendix 6: Pass Schedules for Producing Various Copper Wire Sizes

	Die Sequence for Producing 0.52 mm Copper Wire																
Position	1	2	3	4	5	6	7	8	9	10	11	12	13	14	15	16	17
Die Size (mm)	2.11	1.92	1.75	1.56	1.45	1.29	1.174	1.04	0.92	0.85	0.80	0.75	0.70	0.65	0.60	0.55	0.52
Area Reduction (%)	41.6	17.2	16.9	20.5	13.6	20.9	17.2	21.5	21.7	14.6	11.4	12.1	12.9	13.8	14.8	15.9	10.6

	Die Sequence for Producing 0.68 mm Copper Wire															
Position	1	2	3	4	5	6	7	8	9	10	11	12	13	14	15	16
Die Size (mm)	2.32	2.11	1.92	1.75	1.56	1.45	1.35	1.22	1.174	1.04	0.92	0.85	0.80	0.75	0.70	0.68
Area Reduction (%)	29.3	17.3	17.2	16.9	20.5	13.6	13.3	18.3	7.4	21.5	21.7	14.6	11.4	12.1	12.9	5.6

	Die Sequence for Producing 0.85 mm Copper Wire												
Position	1	2	3	4	5	6	7	8	9	10	11	12	13
Die Size (mm)	2.55	2.32	2.11	1.92	1.75	1.56	1.45	1.38	1.22	1.174	1.04	0.92	0.85
Area Reduction (%)	14.6	17.2	17.3	17.2	16.9	20.5	13.6	9.4	21.8	7.4	21.5	21.7	14.6

Appendix 6: Pass Schedules for Producing Various Copper Wire Sizes (continued)

	Die Sequence for Producing 1.04 mm Copper Wire											
Position	1	2	3	4	5	6	7	8	9	10	11	12
Die Size (mm)	2.55	2.32	2.11	1.92	1.75	1.56	1.45	1.38	1.32	1.22	1.174	1.04
Area Reduction (%)	14.6	17.2	17.3	17.2	16.9	20.5	13.6	9.4	8.5	14.6	7.4	21.5
	Die Sequence for Producing 1.35 mm Copper Wire											
Position	1	2	3	4	5	6	7	8				
Die Size (mm)	2.55	2.32	2.11	1.92	1.75	1.56	1.45	1.35				
Area Reduction (%)	14.6	17.2	17.3	17.2	16.9	20.5	13.6	13.3				
	Die Sequence for Producing 1.38 mm Copper Wire											
Position	1	2	3	4	5	6	7	8				
Die Size (mm)	2.55	2.32	2.11	1.92	1.75	1.56	1.45	1.38				
Area Reduction (%)	14.6	17.2	17.3	17.2	16.9	20.5	13.6	9.4				
	Die Sequence for Producing 1.71 mm Copper Wire											
Position	1	2	3	4	5	6						
Die Size (mm)	2.55	2.32	2.11	1.92	1.78	1.71						
Area Reduction (%)	14.6	17.2	17.3	17.2	14.1	7.7						

(Source: Author)

Appendix 7: Die Design Drawings

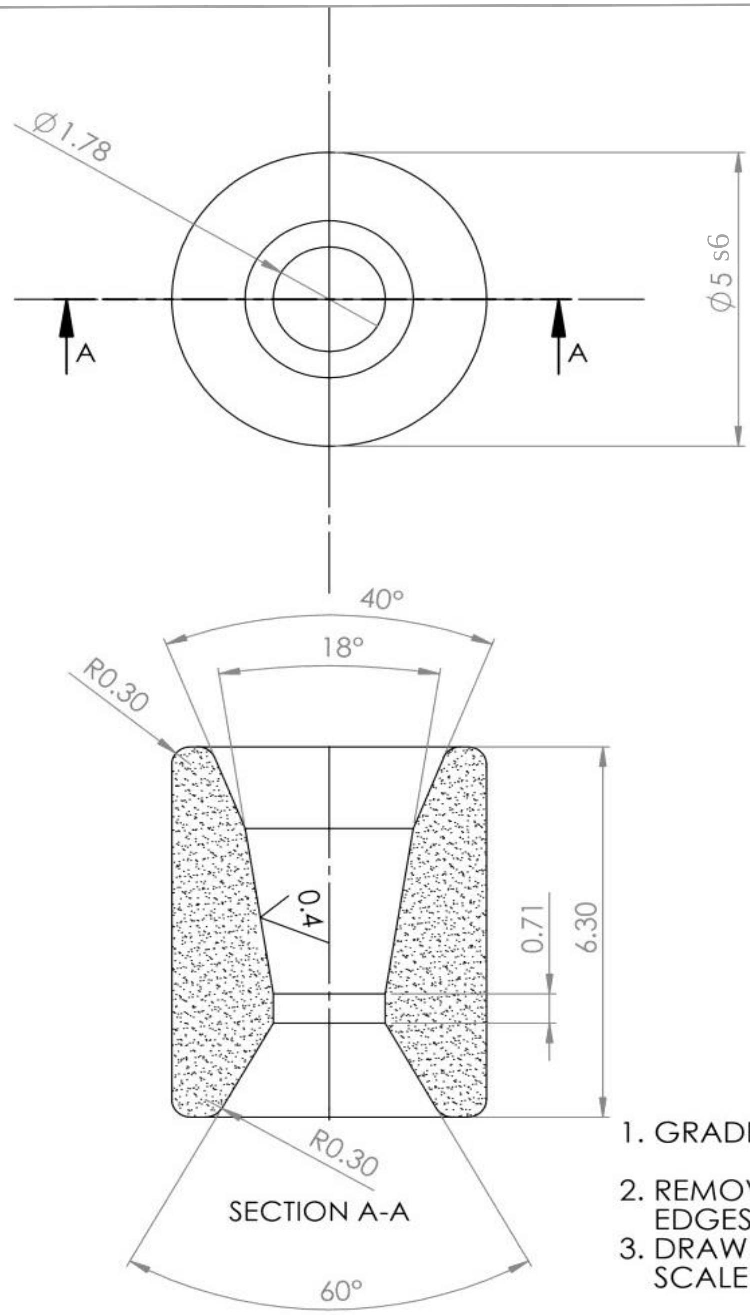

1. GRADE 94 WC- 6Co
2. REMOVE ALL SHARP EDGES
3. DRAWING NOT TO SCALE

UNLESS OTHERWISE SPECIFIED:
DIMENSIONS ARE IN MILLIMETERS
SURFACE FINISH:
TOLERANCES:
LINEAR:
ANGULAR:

FINISH:

DEBUR AND BREAK SHARP EDGES

DO NOT SCALE DRAWING

REVISION

	NAME	SIGNATURE	DATE
DRAWN			
CHK'D			
APPV'D			
MFG			
Q.A			

MATERIAL:

WEIGHT:

TITLE:

1.78 CARBIDE NIB

DWG NO. **CN 11** A4

SCALE:10:1

SHEET 1 OF 1

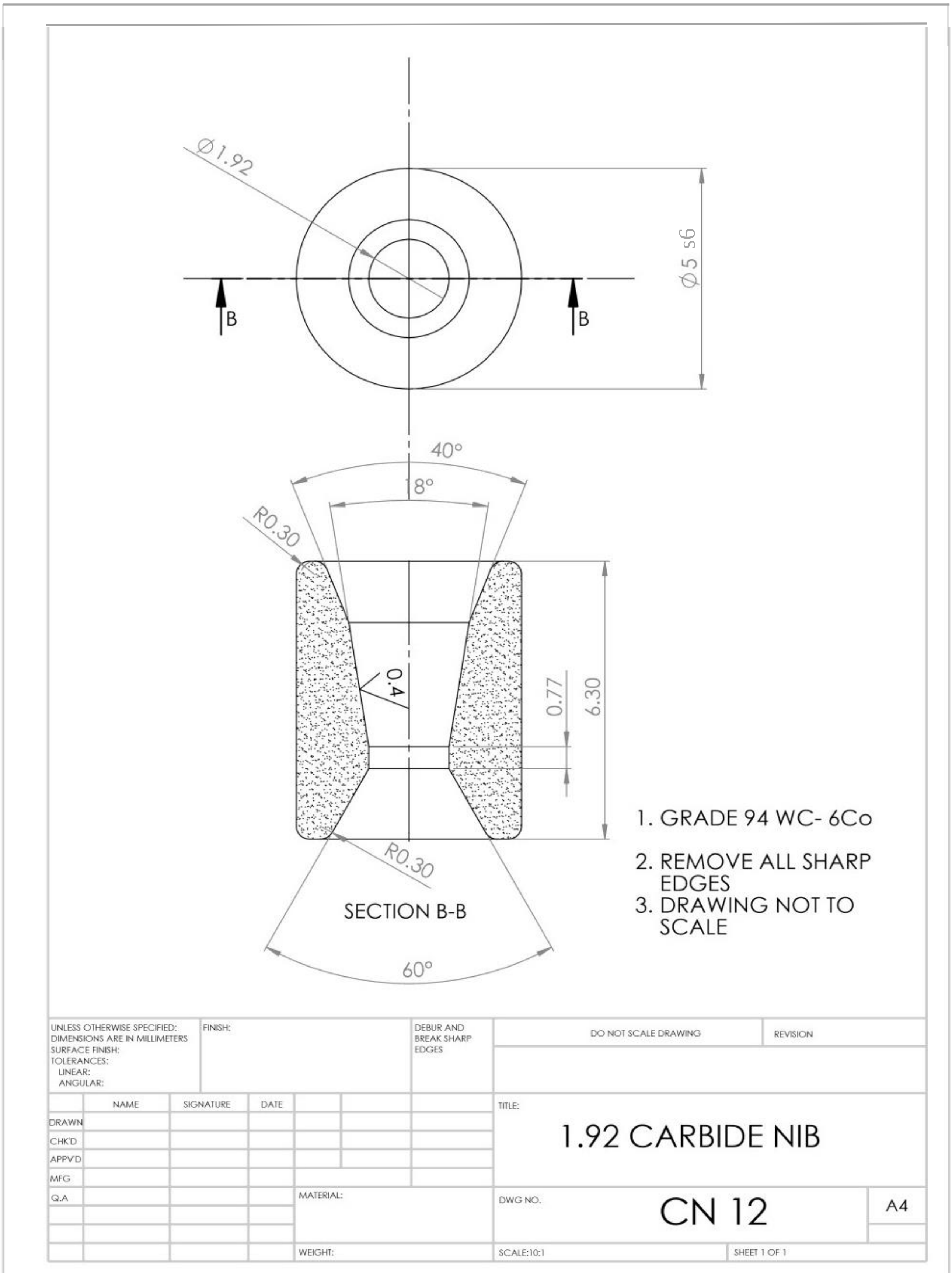

Ø1.92
Ø5 s6
B
B
40°
18°
R0.30
0.4
0.77
6.30
R0.30
SECTION B-B
60°
1. GRADE 94 WC- 6Co
2. REMOVE ALL SHARP EDGES
3. DRAWING NOT TO SCALE
UNLESS OTHERWISE SPECIFIED:
DIMENSIONS ARE IN MILLIMETERS
SURFACE FINISH:
TOLERANCES:
LINEAR:
ANGULAR:
FINISH:
DEBUR AND BREAK SHARP EDGES
DO NOT SCALE DRAWING
REVISION
NAME
SIGNATURE
DATE
DRAWN
CHK'D
APPV'D
MFG
Q.A
TITLE:
1.92 CARBIDE NIB
MATERIAL:
DWG NO.
CN 12
A4
WEIGHT:
SCALE:10:1
SHEET 1 OF 1

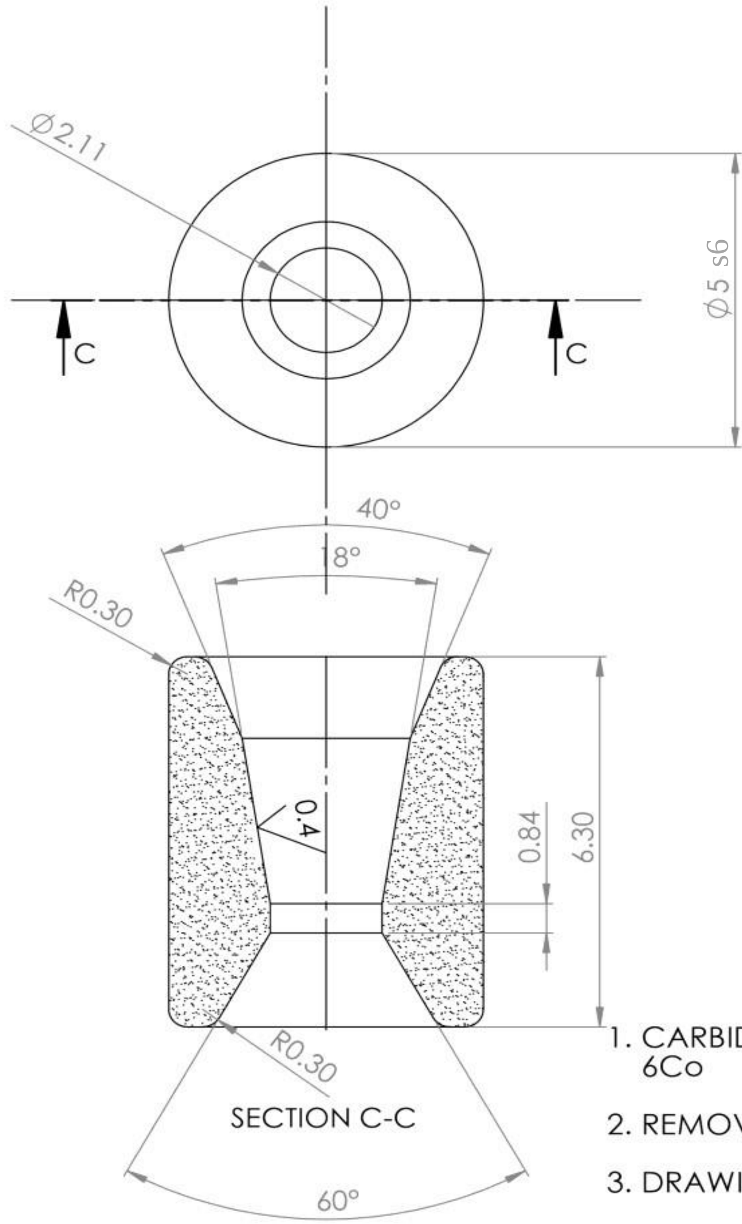

SECTION C-C

1. CARBIDE GRADE 94 WC-6Co
2. REMOVE ALL SHARP EDGES
3. DRAWING NOT TO SCALE

UNLESS OTHERWISE SPECIFIED:
DIMENSIONS ARE IN MILLIMETERS
SURFACE FINISH:
TOLERANCES:
LINEAR:
ANGULAR:

FINISH:

DEBUR AND BREAK SHARP EDGES

DO NOT SCALE DRAWING

REVISION

	NAME	SIGNATURE	DATE
DRAWN			
CHK'D			
APPV'D			
MFG			
Q.A			

TITLE:

2.11 CARBIDE NIB

MATERIAL:

WEIGHT:

DWG NO. CN 13

A4

SCALE:10:1

SHEET 1 OF 1

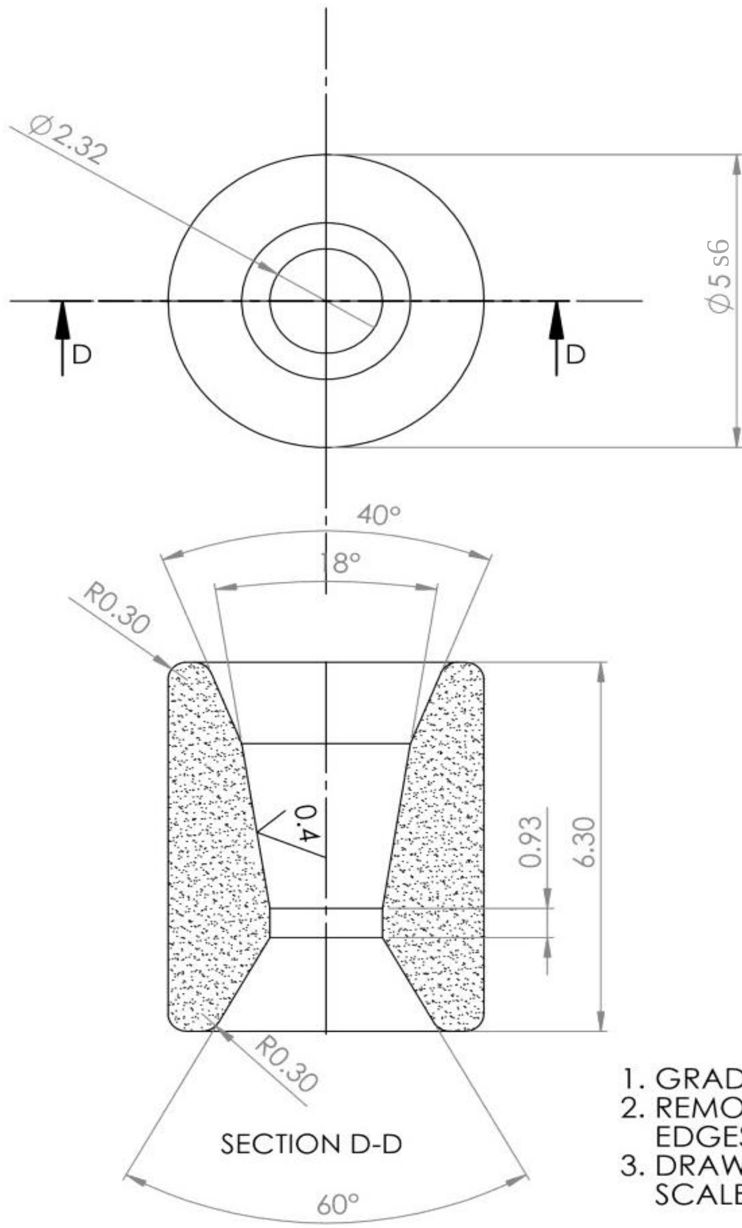

1. GRADE 94 WC- 6Co
2. REMOVE ALL SHARP EDGES
3. DRAWINGS NOT TO SCALE

UNLESS OTHERWISE SPECIFIED: DIMENSIONS ARE IN MILLIMETERS SURFACE FINISH: TOLERANCES: LINEAR: ANGULAR:	FINISH:			DEBUR AND BREAK SHARP EDGES	DO NOT SCALE DRAWING	REVISION
	NAME	SIGNATURE	DATE		TITLE: 2.32 CARBIDE NIB	
DRAWN						
CHK'D						
APPV'D						
MFG						
Q.A				MATERIAL:	DWG NO. CN 14	A4
				WEIGHT:	SCALE:10:1	SHEET 1 OF 1

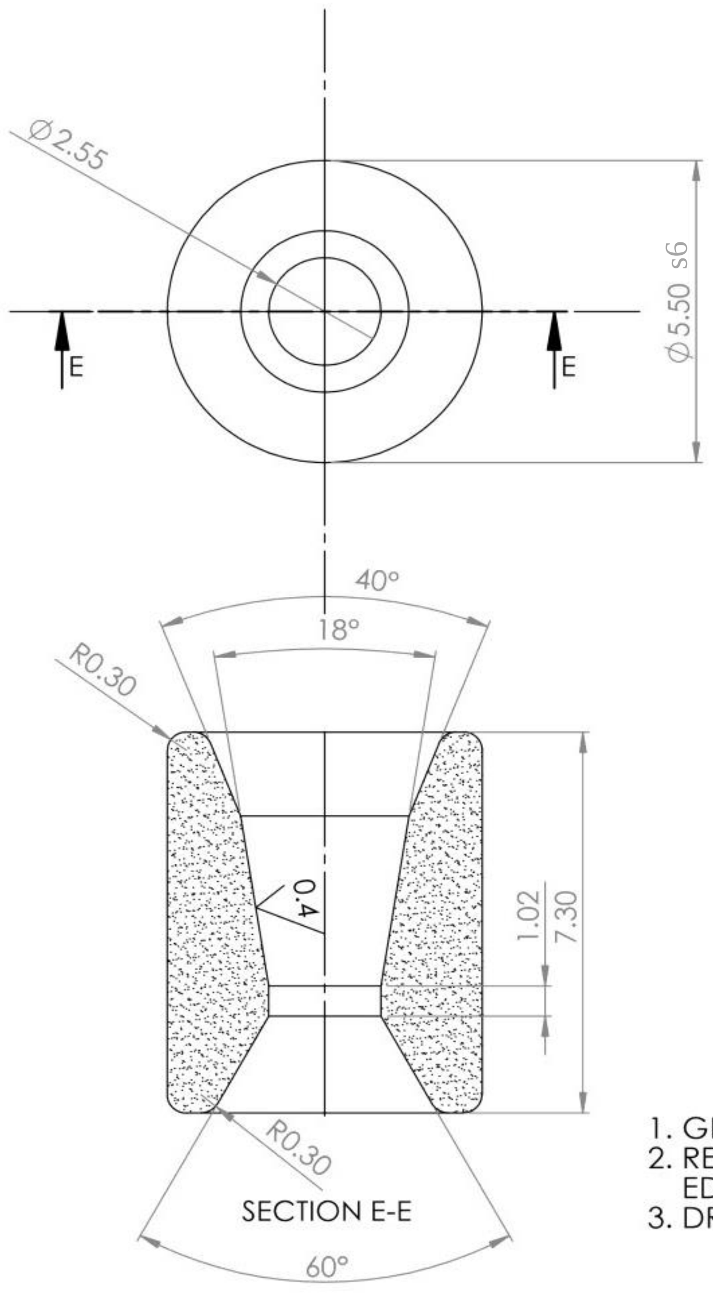

SECTION E-E

1. GRADE 94 WC- 6Co
2. REMOVE ALL SHARP EDGES
3. DRAWING NOT TO SCALE

UNLESS OTHERWISE SPECIFIED: DIMENSIONS ARE IN MILLIMETERS SURFACE FINISH: TOLERANCES: LINEAR: ANGULAR:	FINISH:		DEBUR AND BREAK SHARP EDGES	DO NOT SCALE DRAWING	REVISION
	NAME	SIGNATURE	DATE	TITLE:	
DRAWN				2.55 CARBIDE NIB	
CHK'D					
APPV'D					
MFG					
Q.A			MATERIAL:	DWG NO. CN 15	A4
			WEIGHT:	SCALE:10:1	SHEET 1 OF 1

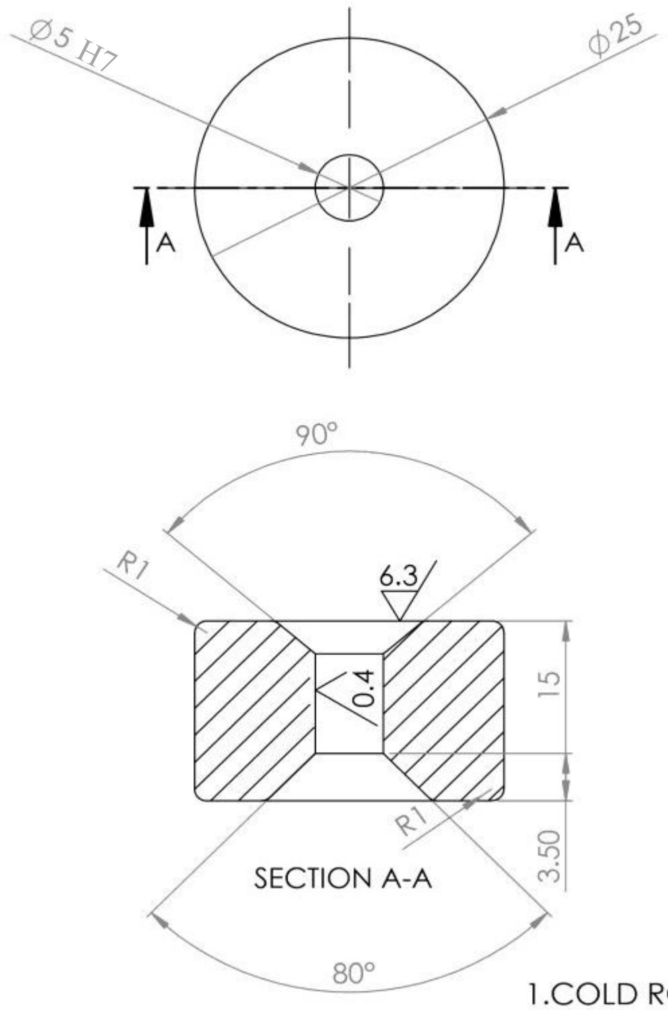

1.COLD ROLLED CARBON STEEL

2. REMOVE ALL SHARP EDGES

3. DRAWING NOT TO SCALE

UNLESS OTHERWISE SPECIFIED:
DIMENSIONS ARE IN MILLIMETERS
SURFACE FINISH:
TOLERANCES:
LINEAR:
ANGULAR:

FINISH:

DEBUR AND BREAK SHARP EDGES

DO NOT SCALE DRAWING

REVISION

	NAME	SIGNATURE	DATE
DRAWN			
CHK'D			
APPV'D			
MFG			
Q.A			

TITLE:

STEEL SHELL

MATERIAL:

WEIGHT:

DWG NO.

SS 03

A4

SCALE:2:1

SHEET 1 OF 1